Statistical tool for the array geometry optimization in the context of the sources localization

Dinh Thang Vu

THESE DE DOCTORAT

DE L'UNIVERSITÉ PARIS-SUD XI

Spécialité : Physique

Présentée par

Dinh Thang VU

pour obtenir le grade de

DOCTEUR DE L'UNIVERSITÉ PARIS-SUD 11

Sujet de la thèse :

Outils statistiques pour le positionnement optimal de capteurs dans le contexte de la localisation de sources

Thèse présentée et soutenue à Supélec le 19 Octobre 2011 devant le jury composé de :

Mr.	Pascal CHEVALIER	CNAM	Président
Mr.	Yide WANG	Université de Nantes	Rapporteur
Mr.	Philippe FORSTER	Université Paris X Nanterre	Rapporteur
Mr.	Jean Philippe OVARLEZ	ONERA	Examinateur
Mme.	Sylvie MARCOS	Université Paris-Sud XI	Directrice de thèse
Mr.	Alexandre RENAUX	Université Paris-Sud XI	Co-directeur de thèse
Mr.	Rémy BOYER	Université Paris-Sud XI	Co-directeur de thèse

Laboratoire des Signaux et Systèmes
Université Paris-Sud / SUPELEC / CNRS / UMR 8506
3 rue Joliot Curie, 91192, Gif sur Yvette, France

à mes parents.

Remerciements

Tout d'abord, je tiens à remercier mes encadrants Sylvie, Alex et Rémy d'avoir retenu ma candidature pour cette thèse. Je me souviens encore de notre premier entretien téléphonique qui m'a mené à joindre votre super équipe. Ça fait déjà trois ans, le temps coule trop vite.

Merci Sylvie d'avoir m'accueilli dans votre équipe, pour vos conseils scientifiques, pour votre responsabilité et pour vos soutiens pendant les 3 années de thèse. Je vous remercie d'avoir me fait voyager malgré le petit budget de l'équipe.

Merci Rémy pour ta générosité, pour ta disponibilité et pour tes motivations de recherche. Je pense que personne ne pourra abattre notre record d'échanger des emails. Grâce à toi, on a autant des publications.

Merci Alex. Tu es l'encadrant le plus cool que je connais. Tu m'a appris ce qui est au-delà de la thèse. J'ai toujours pleins de souvenirs de nos "vacances" à Jérusalem avec Éric et Pascal. "Ce qui s'est passé à Jérusalem va rester à Jérusalem". Désormais, je ne t'embête plus mais on pourra toujours organiser des "réunions scientifiques" dans les bistros.

Je tiens à remercier aux rapporteurs M. Yide Wang, M. Philipe Forster qui ont accepté de juger cette thèse ainsi pour leurs remarques très pertinentes sur mon manuscrit. Je remercie M. Jean Philipe Ovarlez et M. Pascal Chevalier d'avoir participé au jury de ma soutenance, et également d'avoir m'apporté leurs points de vue en pratique.

Merci à Nabil et Duy d'avoir partagé le fameux bureau B4.03 où nous avions des jours agréables à regarder les matchs de football, à surfer Youtube, facebook et à télécharger des films. Vive la vie des thésards !!!!!!!!!

Merci à tous mes amis au Laboratoire des Signaux et Systèmes (LSS) et à Supélec: José, Amadou, Mael, Véronica, Elsa, Lana, Zeina, François, Hashem, Diarra, Sofian, Ziad, Ching, Fredou, Pierre, Jean-François, Veneeth, Mélanie. Grâce à vous, je n'oublierai jamais l'ambiance amicale, souriante dans notre Labo. Je vous souhaite une réussite pour votre thèse, et pour votre vie professionnelle. Merci les personnels administratifs: Daniel, le "iron man" Franck, Maryvonne, Myriam, Helena, Fréderic, Céline, Jack. Merci capitaine Fred pour tes motivations pour le football. Merci le clan des compatriots: Xuan Thang, Duy, Ngoc, Hieu, Dung, Bien, Nam, Vy, Minh, Tuan, Minh qui ont ramené la culture vietnamienne à Supélec. Grâce à vous, le Viet Nam n'est jamais loin de la France. Je tiens à remercier pour mon ami Trinh Anh Tuan, qui m'a fait parvenir des articles IEEE que je n'ai jamais eu d'argent pour acheter.

Finalement, merci à ma famille. Je tiens à remercier profondément mes parents qui ont sacrifié beaucoup pour éduquer mon grand frère et moi, et qui nous supportent toujours. Je vous dédie cette thèse. Merci Huong, ma femme, pour ton amour, pour être toujours à mon côté. Sans toi, je ne peux jamais surmonter du stress pour faire des dizaines page de calcul. Merci mon grand frère et ma belle-soeur pour votre support et encouragement. Je vous aime.

Dinh Thang
20 Octobre 2011

Abstract

This thesis deals with the array geometry optimization problem in the context of sources localization. We have considered two approaches for the array geometry optimization: the performance estimation in terms of mean square error approach and the statistical resolution limit (SRL) approach. In the first approach, the lower bounds on the mean square error which are usually used in array processing to evaluate the estimation performance independently of the considered estimator have been considered. We have investigated two kinds of lower bounds: the well-known Cramér-Rao bound (CRB) for the deterministic model in which the parameters are assumed to be deterministic, and the Weiss-Weinstein bound (WWB) which is less studied, for the Bayesian model, in which, the parameters are assumed to be random with some *prior* distributions. We have proposed closed-form expressions of these bounds, which can be used as a statistical tool for array geometry design. Compared to the CRB, the WWB can predict the threshold effect of the MSE in the non-asymptotic area. Moreover, the closed-form expressions of the WWB proposed for a general Gaussian model with parameterized mean or parameterized covariance matrix can also be useful for other problems. Based on these closed-form expressions, the 3D array geometry and the classical planar array geometry have been investigated under (i) the conditional observation model in which the source signal is modeled as a deterministic sequence and under (ii) the unconditional observation model in which the source signal is modeled as a Gaussian random process. Conditions concerning the isotropic and uncoupling properties were then derived.

In the second approach, we have considered the statistical resolution limit which characterizes the minimal separation between the two closed spaced sources which still allows to determine correctly the number of sources. In this thesis, we are interested in the SRL in the Bayesian context which is less studied in the literature. Based on the linearized observation model with the minimum probability of error, we have introduced the two Bayesian approaches of the SRL based on the detection and information theories which could lead to some interesting tools for the system design.

Keywords : Array processing, information theory, detection theory, DOA estimation, estimation performance analysis, minimal bounds on mean-square error, statistical resolution limit.

Résumé

Cette thèse porte sur l'étude du positionnement optimal des capteurs dans un réseau ou antenne pour la localisation de sources. Nous avons étudié deux approches: l'approche basée sur les performances de l'estimation en terme d'erreur quadratique moyenne et l'approche basée sur le seuil statistique de résolution (SSR).

Pour le première approche, nous avons considéré les bornes inférieures de l'erreur quadratique moyenne qui sont utilisées généralement pour évaluer la performance d'estimation indépendamment du type d'estimateur considéré. Nous avons étudié deux types de bornes: la borne de Cramér-Rao (BCR) pour le modèle où les paramètres sont supposés déterministes et la borne de Weiss-Weinstein (BWW) pour le modèle où les paramètres sont supposés aléatoires. Nous avons établi les expressions analytiques de ces bornes pour développer des outils statistiques afin d'optimiser la géométrie des réseaux de capteurs. Par rapport à la BCR, la borne BWW peut repérer le décrochement de l'EQM des estimateurs dans la zone non-asymptotique. De plus, les expressions analytiques de la BWW pour un modèle Gaussien général à moyenne paramétrée ou à matrice de covariance paramétrée sont données explicitement. À partir de ces expressions analytiques, nous avons étudié l'impact de la géométrie des réseaux de capteurs sur les performances d'estimation en utilisant les réseaux de capteurs 2D et 3D pour deux modèles des observations concernant les signaux sources: (i) le modèle déterministe et (ii) le modèle stochastique. Nous en avons ensuite déduit des conditions concernant les propriétés d'isotropie et de découplage.

Pour la deuxième approche, nous avons considéré le seuil statistique de résolution qui caractérise la séparation minimale entre deux sources. Dans cette thèse, nous avons dérivé le SSR pour le contexte Bayésien moins étudié dans la littérature. Nous avons introduit un modèle des observations linéarisé basé sur le critère de probabilité d'erreur minimale. Ensuite, nous avons présenté deux approches Bayésiennes pour le SSR, l'une basée sur la théorie de l'information (lemme de Stein) et l'autre basée sur la théorie de la détection. Ces approches pourront être utilisées pour améliorer la capacité de résolution des systèmes. Plus particulièrement, ces approches nous ont permis de comparer plusieurs géometrie d'antenne conduisant à la résolution limite minimale.

Mots clés : Traitement d'antenne, analyse de performance, borne inférieure de l'erreur quadratique moyenne, estimation de DDA, seuil statistique de résolution.

Contents

Chapter 1

Introduction

1.1 Generality

Array processing has been a topic of interest for the last few decades. The applications of array processing expanded in many fields. In wireless communication, the sensor arrays are referred to smart antennas to identify the position of the mobile devices and then locate the antenna beam on the devices. In radio astronomy, several cooperative telescopes form an array to capture the extraterrestrial radio signals. In environmental (weather, pollution...) monitoring, the sensor array provides a better surveillance and a better knowledge of the environment. For example, the seismic warning system consists of an array of seismic sensors distributed in a region and a high speed communication system in order to collect the data and detect the strength and propagation of an eventually earthquake event. In radar, the conventional radar consists of a transmitter and a receiver to transmit the electromagnetic pulsed signal and to receive the reflect signal in order to determine the range, the position, the velocity of a target, such as an aircraft. While the passive radar has no dedicated transmitter, therefore it exploits a wide variety of urban signals such as: television signal, FM signal, GSM signal, etc. In sonar, the acoustic signal measured by an array of hydrophones towed behind a ship helps to detect and locate the appearance of a sub-marine.

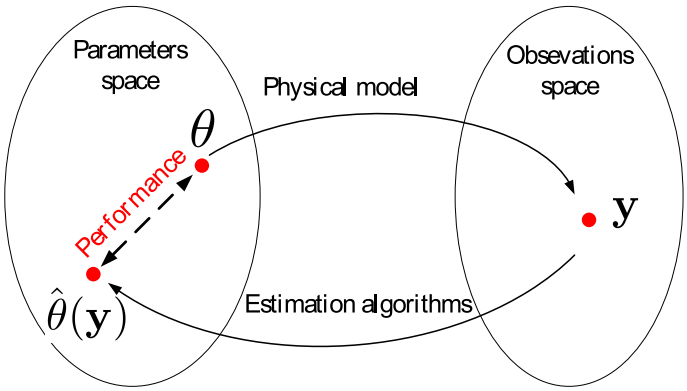

Figure 1.1: The estimation procedure.

Parametric parameter estimation generally provides solutions to array processing problems. The main aim of the parameter estimation is to extract the spatio-temporal information parameterized in the signal measured by a network of sensors spatially distributed. Since the

observations are perturbed by noise, one needs to set up some observation models. Based on the used model, one then has to apply the estimation algorithms in order to estimate the unknown parameters. The whole procedure of the parameter estimation is resumed in Fig. 1.1. A vast number of estimation algorithms exists in the literature, which can be classified into two main categories [KV96]: the spectral-based methods and the parametric methods. The spectral-based approaches such as the beamforming technique, the Capon algorithm, the MUSIC, etc., estimate the parameters by the way of forming some spectral function of the parameters of interest, then these parameters estimated are referred to the peaks in the function diagram. The parametric approaches such as the maximum likelihood estimator (MLE), the maximum a posteriori (MAP),etc., are more accurate than the formers since the data model is more exploited, and still provide a good performance in the scenarios of coherent signals. However, the laters require a high computational complexity due to the multidimensional search. This is the reason why the former approaches are preferred for the practice implementation.

The performance of any estimator can be quantified via its empirical mean square error (MSE). This quantity characterizes the "distance" between the real parameter and the estimated value of the parameter. The MSE in non-linear estimation problems is generally obtained by using Monter Carlo trials. Therefore, concerning the multi unknown parameters problem, a multidimensional search is required, leading a high difficulty to obtain the empirical MSE. Moreover, a Monte Carlo simulation is not able to give us an analytical formula which could be used to know how to improve the system. However, there is in the literature another way to evaluate the estimation performance independently of the considered estimator. This is the so-called lower bound on the MSE, *e.g.*, the well-known Cramér-Rao bound (CRB). The CRB is widely investigated in the literature due to its simplicity. For any unbiased estimator $\hat{\theta}(\mathbf{y})$, its MSE is greater than or equal to the CRB, *i.e.*, $MSE(\hat{\theta}(\mathbf{y})) \geq CRB$. The CRB is calculated by the inversion of the Fisher information matrix (FIM) in which the Fisher information represents the way to measure the information about the parameter contained in the observations via its likelihood function. An estimator which achieves the CRB is said to be efficient.

Depending on the parameter assumption, there are two categories of lower bounds: the deterministic bounds in which the parameters are assumed to be deterministic and unknown quantities, and the Bayesian bounds in which the parameters are assumed to be random with a known *prior* distribution. The deterministic bounds consider the behavior of the local (conditional) MSE, *i.e.*, $MSE_{local}(\theta) = \int_{\Omega} (\hat{\theta}(\mathbf{y}) - \theta)^2 p(\mathbf{y};\theta) d\mathbf{y}$ where Ω denotes the observations space, $p(\mathbf{y};\theta)$ denotes the conditional distribution of the observations. On the other hand, the Bayesian bounds consider the behavior of the global MSE, *i.e.*, $MSE_{global} = \int_{\Theta}\int_{\Omega} (\hat{\theta}(\mathbf{y}) - \theta)^2 p(\mathbf{y},\theta) d\mathbf{y} d\theta$, where Θ denotes the parameters space, $p(\mathbf{y},\theta)$ denotes the joint distribution of the observations. The Bayesian bound can be subdivided again into two families: the Weiss-Weinstein family, in which the bounds are derived from a covariance inequality principle, and the Ziv-Zakai family, in which the bounds are derived from a binary hypothesis test [RFL+08, VB07].

It has been shown in [Van68] that for a non-linear problem such as DOA estimation, there are three areas of operation concerning the MSE of the parametric method *w.r.t* the signal to noise ratio (SNR), and/or the number of observations (see Fig. 1.2). In the high SNR scenario and/or the large number of observations scenario, *i.e.*, in the asymptotic area, the MSE is low, *i.e.*, the estimators performance is generally close to the CRB. When the SNR and/or the number of observations decrease beyond a certain value, the MSE increases quickly, leading to the threshold effect. This is the outlier area. Finally, when the SNR and/or the number of observations are very weak, the observed signal is reduced to the noise component which leads to an estimation mainly based on the support of the parameters. Consequently, the MSE exhibits a flat behavior which

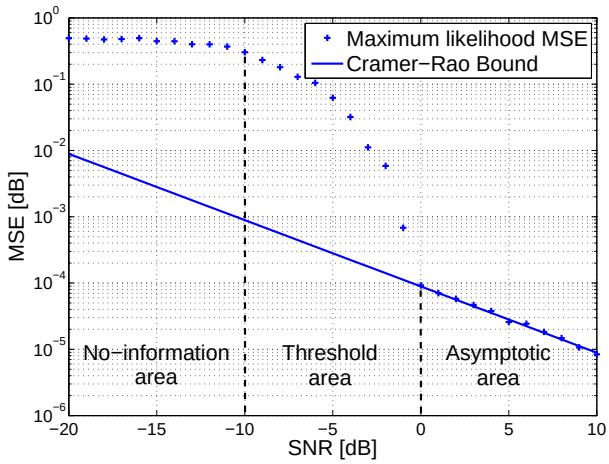

Figure 1.2: Three zones of operation of the MSE of the maximum likelihood estimator.

refers to the non-information area. All the aforementioned bounds are tight in the asymptotic area. But in the non-asymptotic area, the tightness of the bounds is different. Some bounds can capture the threshold effect while the others cannot. For example the CRB is only a tight bound in the asymptotic area but in the non-asymptotic area, the CRB is too optimistic since the CRB is a local bound. One of the main aim of the lower bound study is to enhance the tightness of the bound *w.r.t* the MSE behavior.

Compared to the deterministic bound, the Bayesian bound takes into account the support of the parameters via the *prior* distribution. Therefore, the deterministic bounds exceed the MSE in the non-asymptotic area while the Bayesian bounds which are able to capture the threshold are more or less tight in all the area. Moreover, the Bayesian bounds do not require the constraints about unbiased estimator as the deterministic bounds. Indeed, concerning the case of deterministic parameter, the local MSE can be written as $MSE_{local}(\theta) = Cov(\theta) + Bias^2(\theta)$. Where $Cov(\theta)$ and $Bias(\theta)$ denote the covariance and the bias of the estimator, respectively. If the estimator is unbiased, *i.e.*, $\int_{\Omega}(\hat{\theta}(\mathbf{y}) - \theta)p(\mathbf{y};\theta)d\mathbf{y} = 0$, one obtains $MSE_{local}(\theta) = Cov(\theta)$, and one can straightforwardly derive the deterministic bounds from the covariance inequality principle. Nevertheless, there is a circumstance where the estimator can be biased, for example outside the asymptotic area. The computation of the deterministic bounds in such case becomes really difficult because of the dependance of the MSE on the bias, which depends again on the kind of the considered estimator. Consequently, Bayesian bounds could provide a better indication of the threshold than the deterministic bounds.

Through the previous analysis, one observes that the performance bound provides a potential tool to investigate several problems in array processing by avoiding Monte Carlo simulations with a high computational cost. Thus, one of the motivations of this thesis concerns the application of the performance bound in the context of sources localization.

Beside the MSE criteria, there are in the literature other approaches to study the estimation performance. Particularly, we are here interested to investigate the statistical resolution limit problem (SRL). The SRL characterizes the minimal separation between the close spaced source signals, which still allows to determine the correct number of signals. The resolution limit varies from an algorithm to the other. Indeed, the classical beamforming method can only resolve two sinusoidal components provided that their separation is higher than the Fourier

(Rayleigh) resolution limit denoted by δ_F: $\delta \geq \delta_F = 2\pi/N$ for high SNR, where δ denotes the separation between the two sources, and N denotes the number of data samples. Compared to the beamforming, the high-resolution methods such as ESPRIT, ML, MUSIC can resolve the case of $\delta < \delta_F$. Furthermore, when the SNR tends to infinity, these high-resolution methods can always determine the source number no matter how the two sources are close. Therefore, the study of the general SRL which is not based on any specific method could lead to an array geometry design tool for improving the resolution ability of the system.

1.2 The motivations and the results of the thesis

1.2.1 Motivations

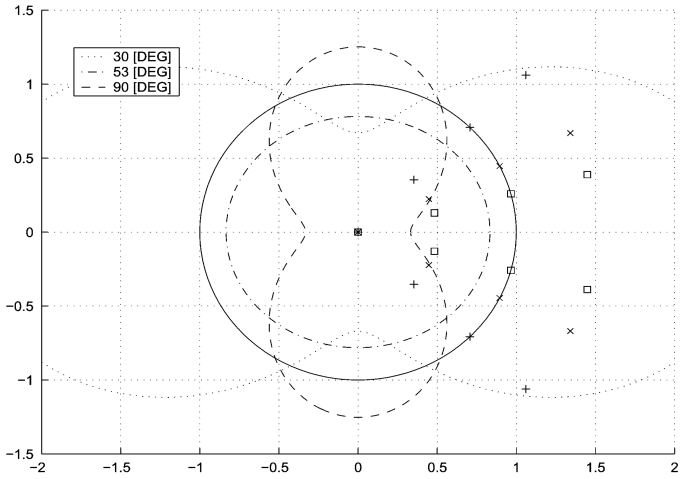

Figure 1.3: The ratio of the Cramér-Rao bound between the uniform circular array and the V-shaped array *w.r.t* the opening angle of the V-shaped array (legend shows the value of the opening angle).

The principal motivation of this thesis is based on the results presented in [GM06]. In this paper, the authors studied the impact of the planar array geometry on the estimation accuracy under the unconditional observation model, in the context of direction of arrival (DOA) estimation. They developed an analytical expression of the Cramér-Rao bound (CRB). The CRB was then used as a tool for the array geometry design. Particularly, a special type of sensor array was investigated, the so-called V-shaped sensor array. The interesting point of the V-shaped array is given by the opening angle between the two branches, which is known as a degree of freedom. By varying this opening angle, the authors can exhaustively study the impact of the planar array geometry on the estimation performance, also leading to the condition to obtain some desired properties in sensor array, such as the isotropic and decoupling properties. Surprisingly, they showed that contrarily to the intuitive condition of isotropic estimation accuracy, in which, the array has a symmetric form, the asymmetric V-shaped array can also provide the isotropic performance provided that the opening angle is equal to 53.13° (see Fig. 1.3 (given in [GM06], Fig. 4)). The advantage of the asymmetric sensor array compared to the symmetric sensor array, for the same number of sensors, is the gain of the aperture. Therefore, asymmetric sensor array can intuitively estimate more accurately than the symmetric. It is clear that the configuration of the sensor array has a strong impact on the estimation performance.

Based on the above analysis, the objectives of this thesis concern the optimization of the array geometry based on the estimation performance. Particularly:

- Almost all the previous researches about sensor array geometry are based on the unconditional observation model. However, beside the unconditional observation model, there is another model about the source signal, the so-called conditional model. The later was less exploited in the literature. This might due to the fact that under the conditional model, if the signal sequences are unknown to the observer, they are considered as parameters of interest that one has to estimate. Consequently, the computational cost increases as the dimension of the parameter vector increases *w.r.t.* the size of the signal sequences. However, one can find in practice several applications where the source signals are assumed to be known at the observer, such as in mobile telecommunication applications. Thanks to this assumption, one can consider both models with the same computational cost, which could lead to some interesting comparisons between these models.

- Although several applications require the 3D form of the sensor array, the 3D sensor array was less studied in the literature. The impact of the array geometry on the estimation has been shown in the previous analysis, as a by-product, one observes that the estimation depends on the dimension of the array. For example in the context of DOA estimation, the 1D sensor array is only able to estimate a single parameter: the elevation angle, while, the 2D sensor array can both estimate the elevation and the azimuth angles. Consequently, compared to the 2D sensor array, intuitively, one observes that the 3D sensor array could have some advantages. However, the drawback of the 3D geometry is the high computational cost. Therefore, we are highly motivated in this thesis to bring the advantages of the 3D array geometry compared to the classical 2D array geometry to light. So, one of the aims of this thesis is about the 3D sensor array geometry optimization based on the well-known CRB.

- The CRB is intensively exploited in the literature because of its simplicity. However, the CRB is only a tight bound in the asymptotic area. Therefore, we are motivated to implement a more relevant bound for the array geometry optimization. In [Ren07], a closed-form expression of the Weiss-Weinstein bound (WWB), which is known as the tightest bound in the Weiss-Weinstein family, for a simple case of spectral analysis was derived. These results encouraged us to apply the WWB [WW88] to the array geometry optimization problem, in the Bayesian context, where the parameters are assumed to be random with a *prior* distribution. It should be noted that the WWB is much more difficult to implement than the CRB. Indeed, it requires the study of the ambiguity diagram ,*i.e.*, the test points, in order to be optimized.

- One of the motivations of this thesis is based on the results of [AW08], in which the authors introduced a new approach for the SRL in the Bayesian context, the so-called Theorical resolution limit (TRL). The approach was derived by using the first order of the Taylor series expansion of the marginal probability error. This approach is general and does not depend on any specific estimation algorithms. It should be noted that there are several approaches for the SRL. However, these approaches were almost related in the deterministic parameter context, where the parameters are assumed to be deterministic. The Bayesian context has several important applications in the literature but it was less studied. Therefore, to introduce some Bayesian approaches of the SRL is an objective of this thesis.

1.2.2 Results and thesis outline

The contributions of this thesis are presented in three parts

- In Chapter 2, the impact of the 3D sensor array on the estimation performance was investigated based on the CRB. The approach is based on a type of array geometry consisting of an arbitrary planar array and an orthogonal branch array. This type of array geometry allows to characterize the contribution of the third dimension to the estimation performance. We developed the closed-form expressions of the CRB for the 3D sensor array under both the conditional and unconditional models. We showed that the 3D sensor array overcomes the ambiguity problem of the classical 2D sensor array. The conditions for isotropy and decoupling have been derived. As a by-product, several particular forms of the sensor array made by uniform linear arrays (ULA) have been considered. After several comparisons between the conditional and unconditional models, we have shown that the conditions for isotropy and decoupling for the two models are different. Again, we have shown that even with an 3D asymmetric array, one can also achieve the isotropic and decoupling properties.

- In Chapter 3, the application of the WWB in array processing is considered. The closed-form expressions of the WWB for a general Gaussian model with parameterized mean or parameterized covariance matrix were derived. They could be also useful for other problems. Moreover, compared to the other publications in the literature, the parameter s was not fixed to $1/2$ in this thesis, therefore, we can consider also the impact of the parameter s to the optimization of the WWB. The compact expressions of the WWB was derived in the context of DOA estimation, under the conditional and unconditional observation models by using the non-uniform linear array and the arbitrary planar array. By numerical simulations, we have shown that the WWB is efficient to capture the behavior of the empirical mean square error (MSE) obtained by the maximum a posteriori estimator (MAP). Furthermore, surprisingly, the WWB was optimized with $s = 1/2$, which led also to the most compact WWB expressions. Finally, the application of the WWB to the array geometry optimization was investigated.

- In Chapter 4, we consider the approach for the statistical resolution limit problem based on the binary hypothesis test. We have introduced the Bayesian context for the SRL problem. A linearized observation model based on the minimum probability error has been presented. Based on this linearized model, we have derived two SRL approaches based on the information theory and detection theory. More particularly, we have used the Stein lemma in information theory which links the relative entropy and the false alarm probability, and the Neyman Pearson decision criterion. By comparing with another Bayesian approach: the TRL approach, and a numerical approach, the so-called the Akaike information criterion (AIC), we showed that the SRL obtained from both the theoretical and empirical approaches are close.

The contributions of this thesis are published in:

International transactions

- [VRBMb] D. T. Vu, A. Renaux, R. Boyer, S. Marcos, "A Cramér-Rao bounds based analysis of 3D antenna array geometries made from ULA branches", Multidimensional systems and signal processing, Springer.

- [VRBMc] D. T. Vu, A. Renaux, R. Boyer, S. Marcos, "Some results on the Weiss-Weinstein bound in array processing", *IEEE*. Trans. on Signal Processing, in revision.

- [VEBM] D. T. Vu, M. N. El Korso, R. Boyer, S. Marcos, "Bayesian Statistical Resolution Limit based on Information and Detection theories", *IEEE*. Trans. on Signal Processing, submitted.

International and national conferences

- [VRB] D. T. Vu, A. Renaux, R. Boyer, and S. Marcos. "Analyse des performances de réseaux de capteurs 2D et 3D pour la localisation de source". In Proc. du colloque GRETSI sur le traitement du signal et des images, Dijon, France, 2009.

- [VRBM10b] D. T. Vu, A. Renaux, R. Boyer, and S. Marcos. "Performance analysis of 2D and 3D antenna arrays for source localization". In Proc. of European Signal Processing Conference (EUSIPCO), Aalborg, Denmark, August 2010.

- [VRBM10a] D. T. Vu, A. Renaux, R. Boyer, and S. Marcos. "Closed-form expression of the Weiss-Weinstein bound for 3D source localization : the conditional case". In Proc. of *IEEE* Workshop on Sensor Array and Multi-channel Processing (SAM), Kibutz Ma'ale Hahamisha, Israel, October 2010, (special session on performance bound in array processing).

- [VRBM11] D. T. Vu, A. Renaux, R. Boyer, S. Marcos, "Weiss-Weinstein bound and SNR threshold analysis for DOA estimation with a COLD array", in Proc. of *IEEE* Workshop on Statistical Signal Processing, SSP-2011, Nice, France, (special session on polarized signal processing).

- [VEB$^+$11a] D. T. Vu, M. N. El Korso, R. Boyer, A. Renaux, S. Marcos, "Angular resolution limit for vector-sensor arrays: detection and information theory approaches", in Proc. of *IEEE* Workshop on Statistical Signal Processing, SSP-2011, Nice, France, (special session on polarized signal processing).

- [VRBMa] D. T. Vu, A. Renaux, R. Boyer, S. Marcos, "Borne de Weiss-Weinstein pour la localisation de source polarisée à l'aide d'un réseau de capteurs COLD", Gretsi, 2011, Bordeaux, France.

- [VEB$^+$11b] D. T. Vu, M. N. El Korso, R. Boyer, A. Renaux, S. Marcos, "Résolution limite angulaire : Approches basées sur la théorie de l'information et sur la théorie de la détection", Gretsi, 2011, Bordeaux, France.

Chapter 2

Geometry optimization based on the Cramér-Rao Bound

2.1 Introduction

In the context of passive sources localization by an array of sensors, the Direction-Of-Arrival (DOA) estimation performance is not only linked to the kind of estimator used but also to the array geometry, *i.e.*, the sensors location in the space. For an array of sensors, the meaning of "performance" can be seen from different points of view: beampattern properties, ambiguities of the array, isotropy, localization estimation in terms of mean square error (MSE), etc. A huge amount of works is available in the literature concerning the study of array ambiguities (see, *e.g.*, [Man04, GC81, TGT96, LJ92, GW91]) the beampattern (see, *e.g.*, [Van02b, SM05]), and the isotropic properties of arrays (see, *e.g.*, [BM03]).

In this chapter, we are interested in the optimal array geometry leading to the best performance in terms of MSE. More particularly, we will focus on three dimensional (3D) array geometries less studied in the literature. Indeed, although there are already many available results on planar arrays (2D), there are other geometries such as 3D arrays. There are many applications where the sensors are scattered in space leading to an arbitrary shape of the antenna (network of telescopes on the Earth's surface, networks of electrodes on the skull of a patient, networks of sensors in a room or in a small space for robotics functions, networks of buoys on the surface of the sea, etc). Moreover, compared to the 2D antenna, the 3D antenna have some intuitive advantages, such as the 3D antenna overcomes the ambiguity of the 2D antenna in some ambiguous cases. For example, one can imagine that in the radar application problem, the targets are located in the 3D space and could be hidden by certain types of landscape (hills, forests, etc.). Therefore, the targets would be "invisible" for a simple planar antenna. However, the 3D antenna could provide a better detection in this situation. The limited number of results in 3D geometry antenna is perhaps due to its complexity leading to more complex expressions.

The analysis already provided in the literature deals with two kinds of geometries: geometries based on circular arrays [Van02b] or spherical arrays [SSL68], and geometries based on linear branches (such as the well known Uniform Linear Array (ULA), the V-shaped arrays, the cross arrays or rectangular arrays). More particular attention has been paid on uniform arrays. This chapter follows the context of arrays made with ULA branches.

In order to study the performance in terms of MSE, the most popular tool is clearly the Cramér-Rao bound (CRB) [SN89], probably because it can generally be achieved by the variance of localization estimators for a high number of snapshots [SN90b] or at high Signal-to-Noise Ratio (SNR) [RFCL06, RFBL07]. The CRB has already been widely used in the literature to describe

the fundamental properties of arrays. Through a simple form of the CRB expression, [HS91] shows the impact of the sensors location on the DOA estimation accuracy in the case of 2D arrays. Concerning DOA estimation, in [Nie94], [BM03], [MS91], some conditions on sensors positions to ensure the isotropy are studied for 2D, and 3D arrays, by way of the off-diagonal entries of the CRB, where, the arrays have the same estimation accuracy over the whole field of view. In [YS05], [LS09], the CRB for the source position estimation based on the time difference of arrival method (TDOA) is used to prove that the best geometry which minimizes the trace of the CRB matrix is the uniform angular array (UAA). A Bayesian CRB approach for the case where the source is coplanar with the antenna and the DOA is modeled as a random variable is introduced in [OM05]. In [GM06], a deep study of the CRB for 2D antenna and a source anywhere in the space has been provided, leading to interesting results concerning the so-called V-shaped array in terms of isotropy, and MSE performance. Then, based on the work of [GM06], a novel planar geometry called the optimum ambiguity-free planar antenna array with a closed-form of V-shaped array has been introduced in [GAM09]. Finally, in a recent work [FC09], the authors showed that both the conditional and unconditional CRB, jointly with the variance of the DOA obtained from MUSIC algorithm, can be expressed in the same term depending on the sensors location, and this kind of CRB expressions can be used as a tool in order to optimize the array.

Note that, in array processing, the source signal is generally modeled as a Gaussian random process or as a deterministic sequence. These models are referred to as the unconditional model, and the conditional model respectively [OVSN93]. Particularly, under the conditional model, the incoming signal waveforms can be assumed as either known or unknown parameters. Consequently, the computational cost of the estimation problem varies *w.r.t* the signal waveforms assumption. The unknown signal waveforms always lead to the increase of the parameter dimension compared to the unconditional model. On the contrary, there are in the literature several applications where the signal amplitudes are known such as in mobile telecommunications. The knowledge of the signal can improve the estimation performance and also reduce the problem complexity. We can cite here several works concerning the context of known signal waveform (see, *e.g.*, [LC93, CM97, LHSV95, LvdV99, Cho04a]).

Of course, since the observation model can change, there are two different CRB associated to each model called unconditional CRB (UCRB), and conditional CRB (CCRB). It has been proved that the UCRB can be achieved for a high number of snapshots [SN90b], however, it is not achievable at high SNR (for a fixed number of snapshots) [RFBL07]. On the other hand, the CCRB is achieved at high SNR [RFCL06] but it is not achieved for a large number of snapshots [SN90b]. Surprisingly, to the best of our knowledge, all the previously proposed results are conducted in the framework of the unconditional observation model, and consequently, in the framework of the UCRB. We will show in this chapter that in the framework of the conditional model, some results concerning the array geometry differ significantly from the unconditional observation model.

In this chapter, both conditional, and unconditional observation models are considered to study 3D geometries. First, we detail the Fisher Information Matrix (FIM) expressions concerning the azimuth and elevation in the case of a general 3D array. Secondly, closed form expressions of the CRB are provided when one adds an orthogonal branch to a planar array with any geometry. This model is the first step to analyze the contribution of the third dimension. Indeed an intuitive advantage of 3D antenna arrays *w.r.t* 2D antenna arrays is the overcoming of the ambiguity problem in the elevation estimation. Third, to analyze the impact of the array geometry on estimation, we propose several closed-form expressions of the CRB for classical array shapes made with the well known ULA branches. Note that these kinds of geometry (namely

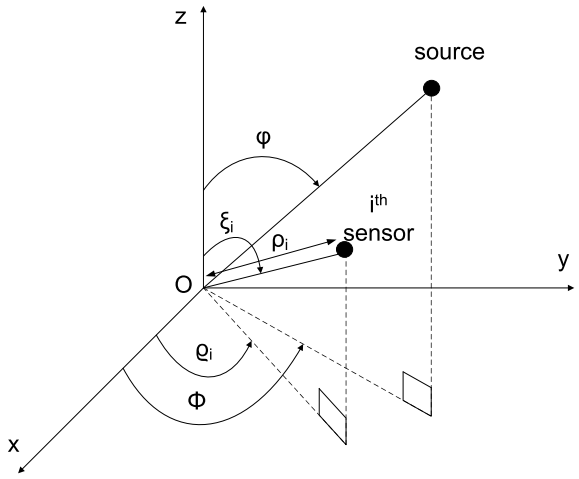

Figure 2.1: Coordinate system for the source, and the sensors

the L-shaped, and V-shaped arrays) have already been investigated in the 2D case, which are seen as particular cases of our proposed expressions. In [HSW91], the L-shaped antenna arrays have been proved to have 37% better accuracy than the cross array. In [FT08], the author introduces the isotropic conditions for the sensors positions, and for the opening angle between the two branches of the uniform/ nonuniform V-shaped planar antenna under the unconditional assumption. Our goal is to extend these geometries in the 3D case to analyze the impact of a 3D additional branch in terms of MSE. These results are then analyzed to describe the performance of these arrays in terms of MSE, isotropy and the decoupling properties. Finally, the comparison between the 3D and the 2D antenna arrays, and also the comparison between 3D and uniform circular antenna arrays (UCA), which have the same number of sensors, are analyzed to illustrate the impact of the third dimension. However, with a constant number of sensors, in order to add the third dimension to the antenna, the aperture of the antenna must be reduced. Therefore, the estimation accuracy will be affected.

2.2 Model setup

In this chapter, we are interested in using an unbiased estimator to localize a single source emitting a narrow-band signal in the far-field area by using a three dimensional array containing M identical and omnidirectional sensors. The source position is characterized by its spherical coordinates such as the bearing angle vector $\boldsymbol{\theta} = \begin{bmatrix} \phi & \varphi \end{bmatrix}^T$ where ϕ is the azimuth and φ the elevation of the source. The i^{th} sensor position is characterized by the triple parameters $(\rho_i,\ \xi_i,\ \varrho_i)$ (see Fig. 2.1). φ, and ξ_i are measured clockwise from the z axis, while ϕ, and ϱ_i are measured counter-clockwise from the x axis. Let $s(t)$, $y(t)$, $n(t)$ denote the source signal, the output signal at the array of sensors and the additive noise, respectively, for $t = 1, \ldots, T$, where T is the number of snapshots. At the t^{th} observation, the output signal at the array of sensors is then given by:

$$\mathbf{y}(t) = \begin{bmatrix} y_1(t) \\ \vdots \\ y_M(t) \end{bmatrix} = \begin{bmatrix} e^{\left(\frac{j2\pi}{\lambda}\mathbf{v}_1^T\mathbf{r}(\theta)\right)} \\ \vdots \\ e^{\left(\frac{j2\pi}{\lambda}\mathbf{v}_M^T\mathbf{r}(\theta)\right)} \end{bmatrix} s(t) + \mathbf{n}(t) = \mathbf{a}(\boldsymbol{\theta})s(t) + \mathbf{n}(t), \tag{2.1}$$

where λ denotes the wavelength. The vector $\mathbf{a}(\boldsymbol{\theta})$ is the $M \times 1$ steering vector with its i^{th} element given by $[\mathbf{a}(\boldsymbol{\theta})]_i = \exp\left(\frac{j2\pi}{\lambda}\mathbf{v}_i^T\mathbf{r}(\boldsymbol{\theta})\right)$, where $\mathbf{r}(\boldsymbol{\theta}) = \left[\begin{array}{ccc} \sin\varphi\cos\phi & \sin\varphi\sin\phi & \cos\varphi \end{array}\right]^T$ is the unit vector pointing towards the source, and $\mathbf{v}_i = \left[\begin{array}{ccc} \rho_i\sin\xi_i\cos\varrho_i & \rho_i\sin\xi_i\sin\varrho_i & \rho_i\cos\xi_i \end{array}\right]^T$ is the position of the i^{th} sensor. In the spherical coordinate system, the i^{th} element of the steering vector is given by:

$$[\mathbf{a}(\boldsymbol{\theta})]_i = e^{\left(\frac{2j\pi\rho_i}{\lambda}(\sin\varphi\sin\xi_i\cos(\phi-\varrho_i)+\cos\xi_i\cos\varphi)\right)}. \tag{2.2}$$

The noise vector $\mathbf{n}(t) \in \mathbb{C}^M$ is assumed to be Gaussian, circular, independent, and identically distributed (*i.i.d.*), zero mean with covariance matrix $\sigma_n^2\mathbf{I}_M$.

Concerning the source signals, two kinds of models have been investigated in the literature (see, *e.g.*, [SN90a] or [OVSN93]) and will be alternatively used in this thesis.

- $\mathcal{M}_1$: *Conditional or deterministic model*: $\forall t$, $\mathbf{s}(t)$ is assumed complex and deterministic known. Note that, under the conditional model assumption, the signal waveforms can be assumed either unknown or known. While the conditional observation model with unknown waveforms seems more challenging, the conditional model with known waveforms signals which will be used in this thesis can be found in several applications such as in mobile telecommunication and radar (see *e.g.* [LC93], [CM97], [LHSV95], [LvdV99], and [Cho04b])

- $\mathcal{M}_2$: *Unconditional or stochastic model*: $\mathbf{s}(t)$ is assumed to be a complex circular random vector, i.i.d., statistically independent of the noise, Gaussian with zero-mean and known covariance matrix $\mathbb{E}\left[\mathbf{s}\,(t)\,\mathbf{s}^H\,(t)\right] = \mathbf{R_s}$. Note that concerning the previous results on the Cramér-Rao bound available in the literature [SN90a], the covariance matrix $\mathbf{R_s}$ is assumed to be unknown. In this thesis, we have made the simpler assumption that the covariance matrix $\mathbf{R_s}$ is known. These assumptions have already been used for the calculus of bounds more complex than the Cramér-Rao bound (see, *e.g.*, [XBR04], [BEV96b], [RM95]). In this chapter, since we consider the single source scenario, the variance of the source signal $s(t)$ is denoted σ_s^2 for the model $\mathcal{M}_2$, *i.e.*, $s(t) \sim \mathbb{C}\mathcal{N}(0, \sigma_s^2)$.

Depending on the assumption $\mathcal{M}_1$ or $\mathcal{M}_2$ which is used, both mean or covariance matrix of the output signal may depend on $\boldsymbol{\theta}$. To be more general, let us first assume that $\mathbf{y};\boldsymbol{\theta} \sim \mathbb{C}\mathcal{N}(\boldsymbol{\mu}(\boldsymbol{\theta}), \mathbf{R_y}(\boldsymbol{\theta}))$, where $\boldsymbol{\mu}(\boldsymbol{\theta})$ is the $M \times 1$ mean vector, and $\mathbf{R_y}(\boldsymbol{\theta})$ is the $M \times M$ covariance matrix. From the Schwarz inequality, the variance of any unbiased estimator $\widehat{\boldsymbol{\theta}}$ will satisfy: $var(\widehat{\theta}_i) \geq \left[\mathbf{FIM}^{-1}(\theta)\right]_{ii}$ which is known as the CRB, where $\mathbf{FIM}(\theta)$ is the $M \times M$ Fisher Information Matrix (FIM). For *i.i.d* observations, the FIM is given by [Van02b]:

$$[\mathbf{FIM}(\boldsymbol{\theta})]_{i,j} = -\mathbb{E}\left\{\frac{\partial^2 \ln p(\mathbf{y};\boldsymbol{\theta})}{\partial\theta_i\partial\theta_j}\right\} = -\sum_{t=1}^{T}\mathbb{E}\left\{\frac{\partial^2 \ln p(\mathbf{y}(t);\boldsymbol{\theta})}{\partial\theta_i\partial\theta_j}\right\}, \tag{2.3}$$

where $\mathbf{y} = [\mathbf{y}(1) \quad \ldots \quad \mathbf{y}(T)]$. The likelihood function is given by: $p(\mathbf{y};\boldsymbol{\theta}) = \prod_{t=1}^{T} p(\mathbf{y}(t);\boldsymbol{\theta})$, where

$$p(\mathbf{y}(t);\boldsymbol{\theta}) = \frac{1}{\pi^M \det\left[\mathbf{R_y}(\boldsymbol{\theta})\right]} e^{\left(-(\mathbf{y}(t)-\boldsymbol{\mu}(\boldsymbol{\theta}))^H\mathbf{R_y^{-1}}(\boldsymbol{\theta})(\mathbf{y}(t)-\boldsymbol{\mu}(\boldsymbol{\theta}))\right)}.$$

A general expression of the FIM for circular Gaussian complex observations can be deduced from [Kay93], and [Bos94]:

$$[\mathbf{FIM}(\boldsymbol{\theta})]_{i,j} = tr\left(\mathbf{R_y}^{-1}(\theta)\frac{\partial\mathbf{R_y}(\boldsymbol{\theta})}{\partial\theta_i}\mathbf{R_y^{-1}}(\boldsymbol{\theta})\frac{\partial\mathbf{R_y}(\boldsymbol{\theta})}{\partial\theta_j}\right) + 2\Re\left(\left[\frac{\partial\boldsymbol{\mu}(\boldsymbol{\theta})}{\partial\theta_i}\right]^H\mathbf{R_y^{-1}}(\boldsymbol{\theta})\frac{\partial\boldsymbol{\mu}(\boldsymbol{\theta})}{\partial\theta_j}\right). \tag{2.4}$$

The parameters of interest are the azimuth, and elevation angles, *i.e.*, the vector $\boldsymbol{\theta}$ which are assumed deterministic. Therefore, the CRB, denoted $\mathbf{C}(\boldsymbol{\theta})$, is a 2×2 matrix which can be defined as:

$$\mathbf{C}(\boldsymbol{\theta}) = \mathbf{FIM}(\boldsymbol{\theta})^{-1} = \begin{bmatrix} C_{\varphi\varphi}(\boldsymbol{\theta}) & C_{\varphi\phi}(\boldsymbol{\theta}) \\ C_{\phi\varphi}(\boldsymbol{\theta}) & C_{\phi\phi}(\boldsymbol{\theta}) \end{bmatrix}, \tag{2.5}$$

where $C_{\varphi\varphi}$, and $C_{\phi\phi}$ represent the CRBs of elevation and azimuth, respectively. $C_{\varphi\phi} = C_{\phi\varphi}$ represents the coupling between parameters φ, and ϕ.

2.3 FIM expressions for a general 3D array

In this section, we will detail the CRB expressions under both the conditional, and unconditional observation models.

2.3.1 Conditional observation model ($\mathcal{M}_1$ assumption)

Under $\mathcal{M}_1$, since the parameters only appear in the mean $\boldsymbol{\mu}(\boldsymbol{\theta})$, *i.e.*, $\mathbf{R}_{\mathbf{y}}(\boldsymbol{\theta})$ is not a function of $\boldsymbol{\theta}$ in this case, from Eqn. (2.4), the FIM can be simplified as follows:

$$[\mathbf{FIM}(\boldsymbol{\theta})]_{i,j} = 2\Re\left(\frac{\partial\boldsymbol{\mu}(\boldsymbol{\theta})^H}{\partial\theta_i}\mathbf{R}_{\mathbf{y}}^{-\mathbf{1}}(\boldsymbol{\theta})\frac{\partial\boldsymbol{\mu}(\boldsymbol{\theta})}{\partial\theta_j}\right). \tag{2.6}$$

In this case, the mean vector is given by: $\boldsymbol{\mu}(\boldsymbol{\theta}) = (\mathbf{I}_T \otimes \mathbf{a}(\boldsymbol{\theta}))\mathbf{s}$, where $\otimes$ denotes the Kronecker product, $\mathbf{s}$ denotes the source signal vector $\boldsymbol{s} = [s(1)\dots s(T)]^T$. The covariance matrix is given by: $\mathbf{R}_{\mathbf{y}} = \sigma_n^2\mathbf{I}_{MT}$. Therefore, (2.6) becomes:

$$[\mathbf{FIM}(\boldsymbol{\theta})]_{i,j} = \frac{2\left\|\boldsymbol{s}\right\|^2}{\sigma_n^2}\Re\left(\frac{\partial\boldsymbol{a}(\boldsymbol{\theta})}{\partial\theta_i}^H\frac{\partial\boldsymbol{a}(\boldsymbol{\theta})}{\partial\theta_j}\right), \tag{2.7}$$

where $i,j \in \{1,2\}^2$, and $\theta_1 = \varphi$, and $\theta_2 = \phi$, and where $\left\|\boldsymbol{s}\right\|^2 = \boldsymbol{s}^H\boldsymbol{s}$. The derivation of the steering vector *w.r.t.* φ, and ϕ is

$$\begin{aligned}\frac{\partial[\mathbf{a}(\boldsymbol{\theta})]_i}{\partial\varphi} = \frac{2j\pi\rho_i}{\lambda}&\left(\cos\varphi\sin\xi_i\cos\left(\phi-\varrho_i\right)-\cos\xi_i\sin\varphi\right)\\ &\times e^{\left(\frac{2j\pi\rho_i}{\lambda}\left(\sin\varphi\sin\xi_i\cos\left(\phi-\varrho_i\right)+\cos\xi_i\cos\varphi\right)\right)},\end{aligned} \tag{2.8}$$

and

$$\frac{\partial[\mathbf{a}(\boldsymbol{\theta})]_i}{\partial\phi} = \frac{2j\pi\rho_i}{\lambda}\left(-\sin\varphi\sin\xi_i\sin\left(\phi-\varrho_i\right)\right)e^{\left(\frac{2j\pi\rho_i}{\lambda}\left(\sin\varphi\sin\xi_i\cos\left(\phi-\varrho_i\right)+\cos\xi_i\cos\varphi\right)\right)}. \tag{2.9}$$

Then, (2.7) becomes

$$\begin{cases}\frac{[\mathbf{FIM}]_{1,1}}{A_{SNR}} = \sum_{i=1}^{M}\rho_i^2\left(\cos\varphi\sin\xi_i\cos\left(\phi-\varrho_i\right)-\cos\xi_i\sin\varphi\right)^2,\\ \frac{[\mathbf{FIM}]_{2,2}}{A_{SNR}} = \sum_{i=1}^{M}\rho_i^2\left(\sin\varphi\sin\xi_i\sin\left(\phi-\varrho_i\right)\right)^2,\\ \frac{[\mathbf{FIM}]_{1,2}}{A_{SNR}} = -\sum_{i=1}^{M}\rho_i^2\left(\sin\varphi\sin\xi_i\sin\left(\phi-\varrho_i\right)\right)\left(\cos\varphi\sin\xi_i\cos\left(\phi-\varrho_i\right)-\cos\xi_i\sin\varphi\right),\end{cases} \tag{2.10}$$

where $A_{SNR} = \frac{8\pi^2\left\|\boldsymbol{s}\right\|^2}{\sigma_n^2\lambda^2}$. The determinant of the **FIM** is given by

$$\det\left(\mathbf{FIM}(\boldsymbol{\theta})\right) = [\mathbf{FIM}]_{1,1}[\mathbf{FIM}]_{2,2} - [\mathbf{FIM}]_{1,2}[\mathbf{FIM}]_{2,1}. \tag{2.11}$$

2.3.2 Unconditional observation model ($\mathcal{M}_2$ assumption)

Under the $\mathcal{M}_2$ assumption, since the parameters only appear in the covariance $\mathbf{R_y}(\boldsymbol{\theta})$, from Eqn. (2.4), the FIM becomes:

$$[\mathbf{FIM}(\boldsymbol{\theta})]_{i,j} = tr\left(\mathbf{R_y^{-1}}(\boldsymbol{\theta})\frac{\partial \mathbf{R_y}(\boldsymbol{\theta})}{\partial \theta_i}\mathbf{R_y^{-1}}(\boldsymbol{\theta})\frac{\partial \mathbf{R_y}(\boldsymbol{\theta})}{\partial \theta_j}\right). \tag{2.12}$$

Because $\mathbf{R_y}(\boldsymbol{\theta}) = \sigma_s^2\mathbf{I}_T \otimes (\mathbf{a}(\boldsymbol{\theta})\mathbf{a^H}(\boldsymbol{\theta})) + \sigma_n^2\mathbf{I}_{MT}$ and from [PF88, eq. (39)], (2.12) can be written as follows:

$$[\mathbf{FIM}(\boldsymbol{\theta})]_{i,j} = \frac{2TM\sigma_s^4}{\sigma_n^2(\sigma_n^2 + M\sigma_s^2)}\left(\frac{\partial \boldsymbol{a}(\boldsymbol{\theta})}{\partial \theta_i}^H\frac{\partial \boldsymbol{a}(\boldsymbol{\theta})}{\partial \theta_j} - \frac{1}{M}\frac{\partial \boldsymbol{a}(\boldsymbol{\theta})}{\partial \theta_i}^H\boldsymbol{a}(\boldsymbol{\theta})\boldsymbol{a}(\boldsymbol{\theta})^H\frac{\partial \boldsymbol{a}(\boldsymbol{\theta})}{\partial \theta_j}\right), \tag{2.13}$$

where $i,j = \{1,2\}^2$. $\frac{\partial \mathbf{a}(\boldsymbol{\theta})}{\partial \theta_1} = \frac{\partial \mathbf{a}(\boldsymbol{\theta})}{\partial \varphi}$ is given by Eqn. (2.8) and $\frac{\partial \mathbf{a}(\boldsymbol{\theta})}{\partial \theta_2} = \frac{\partial \mathbf{a}(\boldsymbol{\theta})}{\partial \phi}$ is given by Eqn. (2.9). Then, (2.13) leads to (2.14), where $B_{SNR} = \frac{8\pi^2 TM\sigma_s^4}{\sigma_n^2\lambda^2(\sigma_n^2+M\sigma_s^2)}$.

$$\begin{cases} \frac{[\mathbf{FIM}]_{1,1}}{B_{SNR}} = & \sum_{i=1}^{M}\rho_i^2\left(\cos\varphi\sin\xi_i\cos\left(\phi-\varrho_i\right)-\cos\xi_i\sin\varphi\right)^2 \\ & -\frac{1}{M}\left(\sum_{i=1}^{M}\rho_i\left(\cos\varphi\sin\xi_i\cos\left(\phi-\varrho_i\right)-\cos\xi_i\sin\varphi\right)\right)^2, \\ \frac{[\mathbf{FIM}]_{2,2}}{B_{SNR}} = & \sum_{i=1}^{M}\rho_i^2\left(\sin\varphi\sin\xi_i\sin\left(\phi-\varrho_i\right)\right)^2 - \frac{1}{M}\left(\sum_{i=1}^{M}\rho_i\sin\varphi\sin\xi_i\sin\left(\phi-\varrho_i\right)\right)^2, \\ \frac{[\mathbf{FIM}]_{1,2}}{B_{SNR}} = & -\sum_{i=1}^{M}\rho_i^2\left(\cos\varphi\sin\xi_i\cos\left(\phi-\varrho_i\right)-\cos\xi_i\sin\varphi\right)\left(\sin\varphi\sin\xi_i\sin\left(\phi-\varrho_i\right)\right) \\ & +\frac{1}{M}\sum_{i=1}^{M}\rho_i\left(\cos\varphi\sin\xi_i\cos\left(\phi-\varrho_i\right)-\cos\xi_i\sin\varphi\right)\sum_{i=1}^{M}\rho_i\sin\varphi\sin\xi_i\sin\left(\phi-\varrho_i\right), \end{cases} \tag{2.14}$$

The determinant of the **FIM** is given by (2.11). In order to simplify the analysis of the general CRBs expressions, we will consider in the following section the CRBs expressions in case of several 3D array geometries based on ULA branches.

2.4 Planar array + ULA orthogonal branch

We here consider two cases of planar antenna plus a linear antenna branch. This later either is orthogonal or not orthogonal to the planar part. In order to analyze the impact of the array branch position to the estimation performance of the antenna, let us consider a numerical simulation about the DOA estimation performance of the antenna made from a uniform circular antenna with 7 sensors and a uniform linear branch with 2 sensors (see Fig. 2.2.(a)). Let β denotes the angle between the branch and the circular antenna plane. The inter-sensors spacing is a half-wavelength. We then compare the estimation performance between the antenna with $\beta = 90°$, *i.e.*, orthogonal branch and the antenna with $\beta = 45°$. Fig. 2.2.(b) shows the polar representation of the CRB of azimuth w.r.t azimuth angle with the elevation angle, $\varphi = 45°$. Fig. 2.2.(c) represents the polar representation of the CRB of elevation w.r.t elevation angle with the azimuth angle $\phi = 90°$. The smaller the CRB the better estimation performance. One can observe that the antenna with an orthogonal branch is better in elevation estimation accuracy than the non-orthogonal branch antenna. On the contrary, the non-orthogonal branch antenna is better than the orthogonal branch antenna in terms of azimuth estimation. By several others simulations and analyses, we observe that the compromise about the DOA estimation

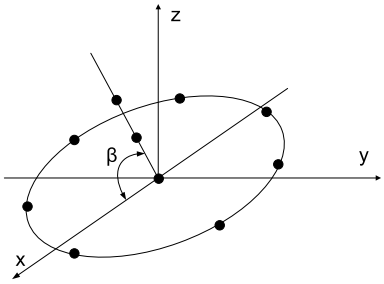

(a) Orthogonal branch antenna and non orthogonal branch antenna

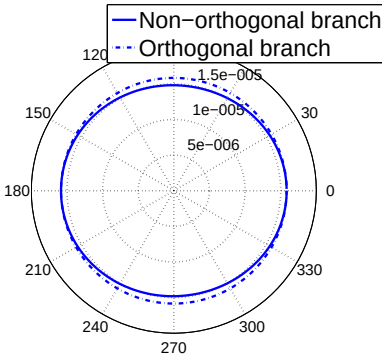

(b) $C_{\phi\phi}$ *w.r.t* ϕ, with $\varphi = 45°$

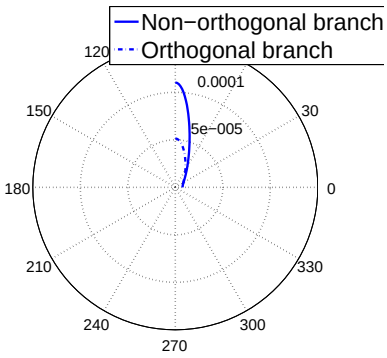

(c) $C_{\varphi\varphi}$ *w.r.t* φ, with $\phi = 90°$

Figure 2.2: Orthogonal branch versus non-orthogonal branch antenna.

performance between the orthogonal and non-orthogonal branch antenna depends to the source position, i.e., the DOA. Consequently, we cannot find the optimal branch position for the whole field of source position. However, let us remind that the estimation performance is strongly dependent on the aperture of the antenna. The larger the aperture antenna the better the estimation accuracy. Therefore, in order to improve the contribution of the 3^{rd} dimension (Oz direction), we have to find the antenna configuration maximizing the aperture of the antenna in the 3^{rd} dimension for the same aperture of the branch. It is clear that the orthogonal branch antenna is the solution. Therefore, in this chapter, we consider only the orthogonal branch antenna case. In this section, we consider an extension of an arbitrary planar array consisting of N_1 sensors when an (or two opposite) ULA orthogonal branch(es) are added. The number of sensors located on the orthogonal branch(es) is denoted by N_2. Therefore, the total number of sensors is given by $M = N_1 + N_2$. Without loss of generality, let us assume that the z axis is a ULA branch, while the xOy plane coincides with the planar array. In order to analyze the impact of the third dimension to the estimation performance, let us denote $\rho_{k,i}$ the distance of a sensor to the origin where the index $k = 1$ means that the sensor is located on the plane otherwise $k = 2$ means that the sensor is located on the orthogonal branch. For this reason, $\rho_{2,i}$ represents the distance from the origin to a sensor located on the orthogonal branch and $\rho_{1,i}$

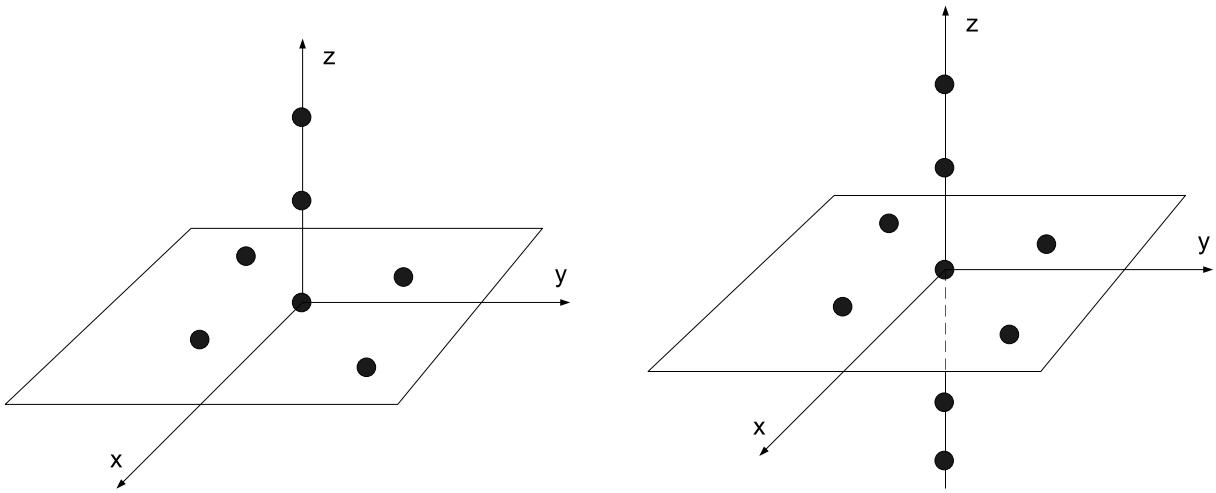

(a) Planar array with an ULA orthogonal branch

(b) Planar array with two symetric ULA orthogonal branches

Figure 2.3: Planar extension array

represents the distance from the origin to a sensor located on the plane xOy. Then, let us set:

$$\begin{aligned}
S_{12} &= \sum_{i=1}^{N_1} \rho_{1,i}^2 e^{2j\varrho_i}, \\
S_{10} &= \sum_{i=1}^{N_1} \rho_{1,i}^2, \\
S_{11} &= \sum_{i=1}^{N_1} \rho_{1,i} e^{j\varrho_i}, \\
S_{13} &= \sum_{i=1}^{N_1} \rho_{1,i}, \\
S_{20} &= \sum_{i=N_1+1}^{M} \rho_{2,i}^2, \\
S_{23} &= \sum_{i=N_1+1}^{M} \rho_{2,i}.
\end{aligned} \tag{2.15}$$

Note that the parameters $S_{k,i}$, with $k \in \{1,2\}, i \in \{0,\ldots,3\}$ depends only on the array geometry.

2.4.1 Planar array with an ULA orthogonal branch

The antenna geometry is illustrated in Fig 2.3(a).

- *Conditional observation model*

Under $\mathcal{M}_1$, the CRB has the following compact expression (see Appendix 2.8.1 for the proof):

$$
\begin{aligned}
C_{\varphi\varphi} &= \frac{2}{A_{SNR}} \frac{\left(S_{10} - \Re\{S_{12}e^{-2j\phi}\}\right)}{\left(\cos^2\varphi(S_{10}^2 - \|S_{12}\|^2) + \sin^2\varphi S_{20}\left(2S_{10} - 2\Re\{S_{12}e^{-2j\phi}\}\right)\right)}, \\
C_{\phi\phi} &= \frac{4}{A_{SNR}\sin^2\varphi} \frac{\left[\frac{1}{2}\cos^2\varphi\left(\Re\{S_{12}e^{-2j\phi}\} + S_{10}\right) + \sin^2\varphi S_{20}\right]}{\left(\cos^2\varphi(S_{10}^2 - \|S_{12}\|^2) + \sin^2\varphi S_{20}\left(2S_{10} - 2\Re\{S_{12}e^{-2j\phi}\}\right)\right)}, \\
C_{\varphi\phi} &= \frac{-\cos\varphi}{A_{SNR}\sin\varphi} \frac{\Im\{S_{12}e^{-2j\phi}\}}{\left(\cos^2\varphi(S_{10}^2 - \|S_{12}\|^2) + \sin^2\varphi S_{20}\left(2S_{10} - 2\Re\{S_{12}e^{-2j\phi}\}\right)\right)}.
\end{aligned} \tag{2.16}
$$

- *Unconditional observation model*

The elements of the CRB are given by : $C_{ij} = \frac{Num_{ij}}{Den}$ where $i, j = \{\phi, \varphi\}^2$. The denominator of CRB is given by:

$$
\begin{aligned}
\frac{Den}{(B_{SNR})^2\sin^2\varphi} = \; & \frac{\cos^2\varphi}{4}\left(\left(S_{10} - \frac{\|S_{11}\|^2}{M}\right)^2 - \left\|S_{12} - \frac{S_{11}^2}{M}\right\|^2\right) \\
& + \frac{\sin 2\varphi}{2M} S_{23}\left(S_{10}\Re\left\{e^{-j\phi}S_{11}\right\} - \Re\left\{e^{-j\phi}S_{12}S_{11}^*\right\}\right) \\
& + \sin^2\varphi\frac{S_{20}}{2}\left(S_{10} - \frac{\|S_{11}\|^2}{M} - \Re\left\{e^{-2j\phi}\left(S_{12} - \frac{S_{11}^2}{M}\right)\right\}\right) \\
& + \sin^2\varphi\frac{S_{23}^2}{2M}\left(\Re\left\{e^{-2j\phi}S_{12}\right\} - S_{10}\right).
\end{aligned} \tag{2.17}
$$

The numerators of the CRB elements are given by:

$$
\begin{aligned}
\frac{Num_{\phi\phi}}{B_{SNR}} = \; & \frac{\cos^2\varphi}{2}\left(S_{10} - \frac{\|S_{11}\|^2}{M} + \Re\left\{e^{-2j\phi}\left(S_{12} - \frac{S_{11}^2}{M}\right)\right\}\right) \\
& + \sin^2\varphi\left(S_{20} - \frac{S_{23}^2}{M}\right) + \frac{\sin 2\varphi S_{23}}{M}\Re\left\{e^{-j\phi}S_{11}\right\}, \\
\frac{Num_{\varphi\varphi}}{B_{SNR}} = \; & \frac{\sin^2\varphi}{2}\left(S_{10} - \frac{\|S_{11}\|^2}{M} - \Re\left\{e^{-2j\phi}\left(S_{12} - \frac{S_{11}^2}{M}\right)\right\}\right), \\
\frac{Num_{\varphi\phi}}{B_{SNR}} = \; & \frac{\sin 2\varphi}{4}\Im\left\{e^{-2j\phi}\left(S_{12} - \frac{S_{11}^2}{M}\right)\right\} + \frac{\sin^2\varphi S_{23}}{M}\Im\left\{e^{-j\phi}S_{11}\right\}.
\end{aligned} \tag{2.18}
$$

The proof is shown in Appendix 2.8.2.

2.4.2 Planar array with two symmetric orthogonal branches

If the antenna structure has two symmetric orthogonal branches in such a way that the orthogonal branches centroid is located on xOy plane (see Fig. 2.3(b)), then, a simpler CRB expression can be deduced for the unconditional model.

- *Conditional observation model*

In this case, the CRB has the same expressions as the previous antenna model given in Eqn. (2.16).

- *Unconditional observation model*

Let N_2' be the number of sensors located on the opposite orthogonal branch. Hence, the CRB expression can be deduced from the geometry described on Fig. 2.3(a) by letting $S_{23} = 0$. This

leads to:

$$
\begin{aligned}
C_{\phi\phi} &= \frac{\frac{\cos^2\varphi\left(S_{10}-\frac{\|S_{11}\|^2}{M}+\Re\left\{e^{-2j\phi}\left(S_{12}-\frac{S_{11}^2}{M}\right)\right\}\right)}{2B_{SNR}\sin^2\varphi}+\frac{\sin^2\varphi S_{20}}{B_{SNR}\sin^2\varphi}}{\left(\begin{array}{l}\frac{\cos^2\varphi}{4}\left(\left(S_{10}-\frac{\|S_{11}\|^2}{M}\right)^2-\left\|S_{12}-\frac{S_{11}^2}{M}\right\|^2\right)\\ +\frac{S_{20}\sin^2\varphi}{2}\left(S_{10}-\frac{\|S_{11}\|^2}{M}-\Re\left\{e^{-2j\phi}\left(S_{12}-\frac{S_{11}^2}{M}\right)\right\}\right)\end{array}\right)},\\
C_{\varphi\varphi} &= \frac{\frac{1}{2B_{SNR}}\left(S_{10}-\frac{\|S_{11}\|^2}{M}-\Re\left\{e^{-2j\phi}\left(S_{12}-\frac{S_{11}^2}{M}\right)\right\}\right)}{\left(\begin{array}{l}\frac{\cos^2\varphi}{4}\left(\left(S_{10}-\frac{\|S_{11}\|^2}{M}\right)^2-\left\|S_{12}-\frac{S_{11}^2}{M}\right\|^2\right)\\ +\frac{S_{20}\sin^2\varphi}{2}\left(S_{10}-\frac{\|S_{11}\|^2}{M}-\Re\left\{e^{-2j\phi}\left(S_{12}-\frac{S_{11}^2}{M}\right)\right\}\right)\end{array}\right)},\\
C_{\varphi\phi} &= \frac{-\frac{\cos\varphi}{2B_{SNR}\sin\varphi}\Im\left\{e^{-2j\phi}\left(S_{12}-\frac{S_{11}^2}{M}\right)\right\}}{\left(\begin{array}{l}\frac{\cos^2\varphi}{4}\left(\left(S_{10}-\frac{\|S_{11}\|^2}{M}\right)^2-\left\|S_{12}-\frac{S_{11}^2}{M}\right\|^2\right)\\ +\frac{S_{20}\sin^2\varphi}{2}\left(S_{10}-\frac{\|S_{11}\|^2}{M}-\Re\left\{e^{-2j\phi}\left(S_{12}-\frac{S_{11}^2}{M}\right)\right\}\right)\end{array}\right)}.
\end{aligned}
\tag{2.19}
$$

See Appendix 2.8.3 for the proof.

2.4.3 Planar array

Due to the fact that planar array (2D) is a particular case of a 3D array ($N_2 = 0$), the CRB for an arbitrary planar array are obtained by letting $S_{20} = S_{23} = 0$, which leads to the following equations. Under $\mathcal{M}_1$ assumption:

$$
\begin{aligned}
C_{\varphi\varphi} &= \frac{2\left(S_{10}-\Re\{S_{12}e^{-2j\phi}\}\right)}{A_{SNR}\cos^2\varphi(S_{10}^2-\|S_{12}\|^2)},\\
C_{\phi\phi} &= \frac{2\left(\Re\{S_{12}e^{-2j\phi}\}+S_{10}\right)}{A_{SNR}\sin^2\varphi(S_{10}^2-\|S_{12}\|^2)},\\
C_{\varphi\phi} &= -\frac{\Im\{S_{12}e^{-2j\phi}\}}{A_{SNR}\sin\varphi\cos\varphi(S_{10}^2-\|S_{12}\|^2)}.
\end{aligned}
\tag{2.20}
$$

and under $\mathcal{M}_2$ assumption, the CRB leads to the results of [GM06]:

$$
\begin{aligned}
C_{\phi\phi} &= \frac{S_{10}-\frac{\|S_{11}\|^2}{M}+\Re\left\{e^{-2j\phi}\left(S_{12}-\frac{S_{11}^2}{M}\right)\right\}}{B_{SNR}\frac{\sin^2\varphi}{2}\left(\left(S_{10}-\frac{\|S_{11}\|^2}{M}\right)^2-\left\|S_{12}-\frac{S_{11}^2}{M}\right\|^2\right)},\\
C_{\varphi\varphi} &= \frac{S_{10}-\frac{\|S_{11}\|^2}{M}-\Re\left\{e^{-2j\phi}\left(S_{12}-\frac{S_{11}^2}{M}\right)\right\}}{B_{SNR}\frac{\cos^2\varphi}{2}\left(\left(S_{10}-\frac{\|S_{11}\|^2}{M}\right)^2-\left\|S_{12}-\frac{S_{11}^2}{M}\right\|^2\right)},\\
C_{\varphi\phi} &= -\frac{\Im\left\{e^{-2j\phi}\left(S_{12}-\frac{S_{11}^2}{M}\right)\right\}}{B_{SNR}\frac{\sin 2\varphi}{4}\left(\left(S_{10}-\frac{\|S_{11}\|^2}{M}\right)^2-\left\|S_{12}-\frac{S_{11}^2}{M}\right\|^2\right)}.
\end{aligned}
\tag{2.21}
$$

2.4.4 Analysis

2.4.4.1 Isotropy and uncoupling properties

One of several interests from the obtained closed-form expressions of the CRB is to design the array antenna in terms of isotropy, directivity, uncoupled parameters estimation... An array antenna is called isotropic if it has an uniform estimation accuracy, *i.e.*, the CRB is not a function of the parameter of interest over the whole field of view. The uncoupled property is a desired criterion to have azimuth and elevation estimation errors mutually independent and hence, to avoid the degradation of the CRB. In [Man04, MS91, Nie94, GM06], the isotropy condition and uncoupled parameters estimation for planar antenna were introduced. It showed that we can achieve both isotropic and uncoupled properties with some particular array geometries. In the literature, considering the isotropic property, the CRB is used only for the planar array as a criterion [BM03], [GM06], while the mean square angular error (MSAE) is used for studying the 3D array [BM03]. The CRB closed-form expressions previously derived are used here to find the array's configuration where isotropic and/or uncoupled properties are attained.

- *Conditional observation model*

Because in both cases: single orthogonal branch and two symmetric orthogonal branches, we always have the same expression for the CRB under $\mathcal{M}_1$, the isotropic and uncoupling conditions in these cases are similar. From the definition of isotropy and from Eqn. (2.16), both isotropic (only in terms of azimuth) and uncoupling are obtained if

$$S_{12} = 0. \tag{2.22}$$

Since S_{12} represents the sensors located on the plane xOy, we can deduce a criterion for the sensors positioning which respect to Eqn. (2.22):

$$\begin{cases} \sum\limits_{i=1}^{N_1} \rho_{1,i}^2 \cos 2\varrho_i = 0, \\ \sum\limits_{i=1}^{N_1} \rho_{1,i}^2 \sin 2\varrho_i = 0. \end{cases} \tag{2.23}$$

The L-shaped array extension is an example that can achieve criterion (2.23) and it will be detailed in the next section.

- *Unconditional observation model*

For the planar antenna with a single symmetric orthogonal branch, from Eqn. (2.17) and (2.18), isotropy and uncoupled properties can be achieved if the following expressions are both satisfied:

$$\begin{cases} S_{12} = 0, \\ S_{11} = 0. \end{cases} \tag{2.24}$$

The expression $S_{11} = 0$ leads to:

$$\begin{cases} \sum\limits_{i=1}^{N_1} \rho_{1,i} \cos \varrho_i = 0, \\ \sum\limits_{i=1}^{N_1} \rho_{1,i} \sin \varrho_i = 0, \end{cases} \tag{2.25}$$

i.e., the line containing the ULA branch must pass through the centroid of the planar array. Some examples of the arrays satisfying condition (2.24) are shown in Fig. 2.4.

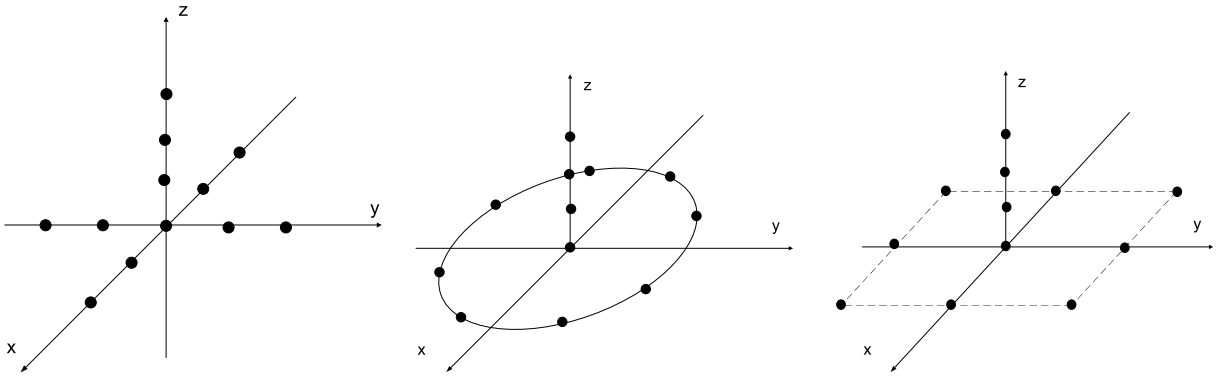

(a) Cross extension (b) Uniform circular extension (c) Square extension

Figure 2.4: Various 3D isotropic array satisfying (2.24)

Contrary to the single ULA orthogonal branch case, for the planar antenna with two symmetric orthogonal branches, from Eqn. (2.19), isotropic and uncoupling estimation are met if

$$S_{12} = \frac{S_{11}^2}{M}. \tag{2.26}$$

It leads to the same solution of the planar arrays [GM06], where (2.24) is a particular solution. Hence, the sensors positions located on the xOy plane must satisfy the following criteria:

$$\begin{cases} \sum\limits_{i=1}^{N_1} \rho_{1,i}^2 \cos 2\varrho_i = \dfrac{\left(\sum\limits_{i=1}^{N_1} \rho_{1,i} \cos \varrho_i\right)^2 - \left(\sum\limits_{i=1}^{N_1} \rho_{1,i} \sin \varrho_i\right)^2}{M}, \\ \sum\limits_{i=1}^{N_1} \rho_{1,i}^2 \sin 2\varrho_i = \frac{2}{M} \sum\limits_{i=1}^{N_1} \rho_{1,i} \cos \varrho_i \sum\limits_{i=1}^{N_1} \rho_{1,i} \sin \varrho_i. \end{cases} \tag{2.27}$$

An intuitive solution of (2.26) is given by $S_{12} = S_{11} = 0$ with some antenna models shown in Fig. 2.4 (with two symmetric orthogonal axes).

From these analysis, we can conclude here:

- Under $\mathcal{M}_1$, by adding an orthogonal branch to the planar antenna, or under $\mathcal{M}_2$ with two symmetric branches added, the conditions of isotropy and decoupling do not change.
- However under $\mathcal{M}_2$, in the case where only one orthogonal branch is added, only the particular solution $S_{11} = S_{12} = 0$ leads to the isotropy and decoupling.

2.4.4.2 Conditional versus unconditional models

Intuitively, one can observe that the CRB expressions under $\mathcal{M}_1$ are generally more compact than under $\mathcal{M}_2$. Surprisingly, by comparing Eqn. (2.16), (2.17) and (2.18) for the 3D model and Eqn. (2.20) and (2.21) for the planar antenna, it can be noted that: the CCRB and the UCRB can be expressed in the same term *w.r.t* the sensors' location, if the following condition is satisfied:

$$S_{11} = S_{23} = 0. \tag{2.28}$$

In other words, the arrays will have the same behavior under both conditional and unconditional observation models if the two ULA branches are symmetric and the line containing these branches

must pass through the centroid of the planar antenna. Moreover, by considering the ratio between CCRB and UCRB for this family of arrays:

$$\frac{UCRB}{CCRB} = \frac{A_{SNR}}{B_{SNR}} = 1 + \frac{1}{M\frac{\sigma_s^2}{\sigma_n^2}} = 1 + \frac{1}{M \times SNR}, \tag{2.29}$$

It is clear that for a large number of sensors or a high signal to noise ratio, this family of arrays has the identical estimation accuracy under both $\mathcal{M}_1$ and $\mathcal{M}_2$. This is consistent with the results presented in [SN90b].

2.4.5 Summary

From these aforementioned results , some remarks can be done:

- The analytic and compact expressions of the CRB under both the conditional and the unconditional observation models for a family of 3D antenna arrays and arbitrary 2D antenna arrays are derived.
- The CRB of azimuth and elevation of the 2D models are a cosine or a sine function of the source elevation. This has been already noticed in [GM06] for the unconditional case, but, to the best of our knowledge, was not known in the conditional observation case. They vary in opposite ways: when the azimuth CRB is minimum, the elevation CRB is maximum and conversely. Moreover, one can see that the CRB of azimuth (respectively elevation) tends to infinity when elevation tends to 0° (respectively 90°). However, the CRB of elevation of the 3D arrays is no longer a sine function of elevation and has a finite value at $\varphi = 90^\circ$. Consequently, the 3D arrays model overcomes the ambiguity problem case of the 2D arrays.
- We found the conditions on the array geometry with which we obtain the same estimation accuracy under both $\mathcal{M}_1$ and $\mathcal{M}_2$ assumptions.
- The isotropic and decoupling criteria are introduced. We find that, under $\mathcal{M}_1$, adding an orthogonal branch to the planar array does not change the conditions of isotropy and decoupling. While under $\mathcal{M}_2$, depending to the number of branches added (single branch or two symmetric branches), the conditions of isotropy and decoupling may be modified then leading to a particular solution.

2.5 Particular cases

In the previous Section, an array geometry consisting of a single orthogonal branch (or two symmetric orthogonal branches) added to an arbitrary planar array has been considered and closed-form expressions of CRB have been introduced. In this Section, we will detail these CRB expressions for several important particular cases of planar antennas and their 3D extensions in order to simplify the antenna design problem. These antenna array geometries have been widely studied in several works but almost all of them are limited to the 2D geometry arrays. In particular, the 3D extension of the V-shaped antenna array will be used here to analyze the impact of the third dimension on the estimation accuracy.

2.5.1 3D extension of the V-shaped array

First of all, we study the V-shaped array extension consisting of a 2D V-shaped array made from two ULA branches separated by an angle denoted Δ and from one or two opposite ULA

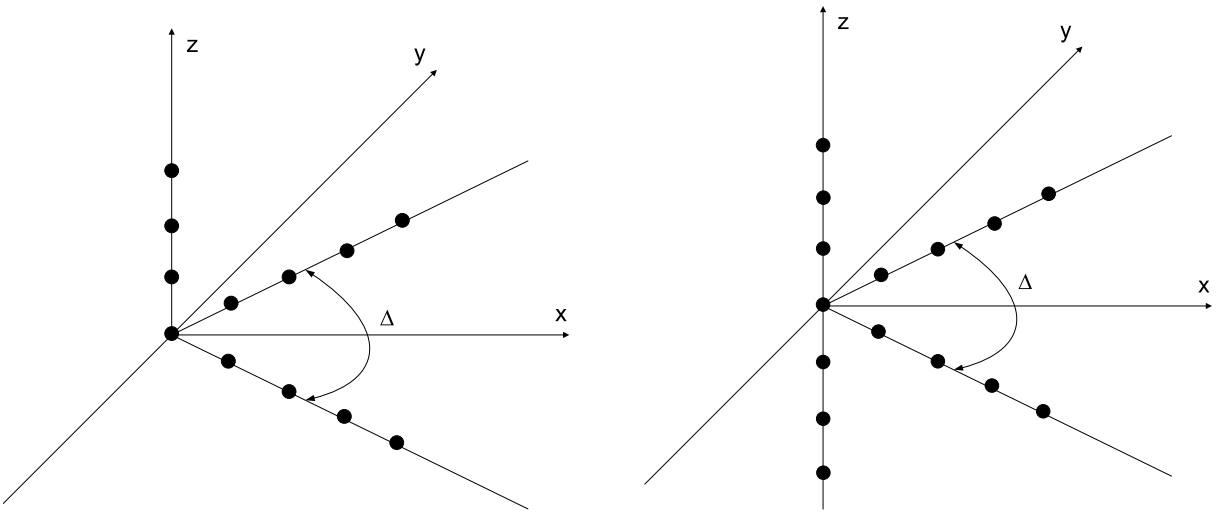

(a) V-shaped with an orthogonal branch

(b) V-shaped with two orthogonal symmetric branches

Figure 2.5: V-shaped array extension

orthogonal branches (Fig. 2.5). Without loss of generality, we assume that the V-shaped array is located on the xOy plane, while its ULA orthogonal branch(es) coincide(s) with the z axis. The opening angle Δ is used as a degree of freedom to find the optimal geometry. Note that in [GM06], the V-shaped 2D array has been studied only under the unconditional observation model. Consequently, a condition on Δ leading to an isotropic array when the number of sensors M tends to infinity was found: ($\Delta_{iso} = 2\arctan(1/2)$). The authors proved also that the V-shaped 2D array has better performance than the classical uniform circular array for the same number of sensors.

Consequently, we here extend the work of [GM06] to the 3D case under both conditional and unconditional models. For this array, under both assumptions $\mathcal{M}_1$ and $\mathcal{M}_2$, the parameters S_{12}, S_{11}, S_{10} can be expressed as (see Appendix 2.8.4 for the proof):

$$\begin{cases} S_{12} = S_{10}\cos\Delta, \\ S_{11} = S_{13}\cos\frac{\Delta}{2}, \\ \Im\{S_{12}e^{-2j\phi}\} = -S_{10}\cos\Delta\sin 2\phi, \\ \Re\{S_{12}e^{-2j\phi}\} = S_{10}\cos\Delta\cos 2\phi, \\ \Re\{S_{11}e^{-j\phi}\} = S_{13}\cos\frac{\Delta}{2}\cos\phi, \\ \Im\{S_{11}e^{-j\phi}\} = -S_{13}\cos\frac{\Delta}{2}\sin\phi, \\ \Re\left\{e^{-2j\phi}\left(S_{12} - \frac{S_{11}^2}{M}\right)\right\} = \left(S_{10}\cos\Delta - \frac{S_{13}^2\cos^2\frac{\Delta}{2}}{M}\right)\cos 2\phi, \\ \Re\{e^{-j\phi}S_{12}S_{11}^*\} = S_{10}S_{13}\cos\Delta\cos\frac{\Delta}{2}\cos\phi. \end{cases} \tag{2.30}$$

These parameters will be then applied into Eqn. (2.16), (2.17), (2.18) and (2.19) in order to find closed-form expressions of the CRB of the V-shaped 3D array extension.

2.5.1.1 V-shaped 2D array with an orthogonal branch

The geometry of this antenna model is presented in Fig. 2.5(a).

- *Conditional observation model*

The CRB is easily derived from Eqn. (2.16) and leads to

$$\begin{aligned}
C_{\varphi\varphi} &= \frac{2}{A_{SNR}} \frac{S_{10}(1-\cos\Delta\cos 2\phi)}{\left(S_{10}^2\sin^2\Delta\cos^2\varphi+\sin^2\varphi 2S_{10}S_{20}(1-\cos\Delta\cos 2\phi)\right)},\\
C_{\phi\phi} &= \frac{4}{A_{SNR}\sin^2\varphi} \frac{\left(\frac{1}{2}\cos^2\varphi S_{10}(\cos\Delta\cos 2\phi+1)+\sin^2\varphi S_{20}\right)}{\left(S_{10}^2\sin^2\Delta\cos^2\varphi+\sin^2\varphi 2S_{10}S_{20}(1-\cos\Delta\cos 2\phi)\right)},\\
C_{\varphi\phi} &= \frac{1}{A_{SNR}\tan\varphi} \frac{S_{10}\cos\Delta\sin 2\phi}{\left(S_{10}^2\sin^2\Delta\cos^2\varphi+\sin^2\varphi 2S_{10}S_{20}(1-\cos\Delta\cos 2\phi)\right)}.
\end{aligned} \tag{2.31}$$

- *Unconditional observation model*

By applying Eqn. (2.30) into Eqn. (2.17) and (2.18), the CRB is given by: $C_{ij} = \frac{Num_{ij}}{Den}$ where $(i,j) = \{\varphi,\phi\}$ and where the denominator Den is given by

$$\begin{aligned}
\frac{Den}{(B_{SNR})^2\sin^2\varphi} &= \cos^2\varphi S_{10}\left(\frac{S_{10}\sin^2\Delta}{4}+\frac{S_{13}^2\cos^2\frac{\Delta}{2}}{2M}(\cos\Delta-1)\right)\\
&\quad+\frac{\sin 2\varphi S_{23}S_{10}S_{13}}{2M}\cos\frac{\Delta}{2}(1-\cos\Delta)\cos\phi\\
&\quad+\sin^2\varphi\cos 2\phi\left(\frac{S_{23}^2S_{10}\cos\Delta}{2M}-\frac{S_{20}}{2}\left(S_{10}\cos\Delta-\frac{S_{13}^2\cos^2\frac{\Delta}{2}}{M}\right)\right)\\
&\quad+\sin^2\varphi\left(\frac{S_{20}S_{10}}{2}-\frac{S_{20}S_{13}^2\cos^2\frac{\Delta}{2}}{2M}-\frac{S_{10}S_{23}^2}{2M}\right).
\end{aligned} \tag{2.32}$$

and where the numerators are given by

$$\begin{aligned}
\frac{Num_{\phi\phi}}{B_{SNR}} &= \cos^2\varphi\left(\frac{S_{10}}{2}-\frac{S_{13}^2\cos^2\frac{\Delta}{2}}{2M}\right)+\sin^2\varphi(S_{20}-\frac{S_{23}^2}{M})\\
&\quad+\frac{\cos^2\varphi\cos 2\phi}{2}\left(S_{10}\cos\Delta-\frac{S_{13}^2\cos^2\frac{\Delta}{2}}{M}\right)\\
&\quad+\frac{1}{M}\sin 2\varphi S_{23}S_{13}\cos\frac{\Delta}{2}\cos\phi,\\
\frac{Num_{\varphi\varphi}}{B_{SNR}} &= \sin^2\varphi\left(\frac{S_{10}}{2}-\frac{S_{13}^2\cos^2\frac{\Delta}{2}}{2M}\right)-\frac{\sin^2\varphi\cos 2\phi}{2}\left(S_{10}\cos\Delta-\frac{S_{13}^2\cos^2\frac{\Delta}{2}}{M}\right),\\
\frac{Num_{\varphi\phi}}{B_{SNR}} &= -\frac{\sin 2\varphi}{4}\sin 2\phi\left(S_{10}\cos\Delta-\frac{S_{13}^2\cos^2\frac{\Delta}{2}}{M}\right)-\frac{\sin^2\varphi}{M}S_{23}S_{13}\cos\frac{\Delta}{2}\sin\phi.
\end{aligned} \tag{2.33}$$

The analysis of these expressions will be detailed in the next section.

2.5.1.2 V-shaped 2D array with two symmetric orthogonal branches

The geometry of this antenna model is presented in Fig. 2.5(b).

- *Conditional observation model*

The expressions of CRB under $\mathcal{M}_1$ are the same as Eqn. (2.31).

- *Unconditional observation model*

Similarly to the above section, if the 3D array is built from a planar array and two orthogonal symmetric branches (Fig. 2.5(b)), by applying Eqn. (2.30) into Eqn. (2.19), we have more compact CRB expressions given by:

$$
\begin{aligned}
C_{\phi\phi} &= \frac{\frac{\cos^2\varphi\left(\frac{S_{10}}{2}-\frac{S_{13}^2\cos^2\frac{\Delta}{2}}{2M}\right)+\sin^2\varphi S_{20}+\frac{1}{2}\cos^2\varphi\cos 2\phi\left(S_{10}\cos\Delta-\frac{S_{13}^2\cos^2\frac{\Delta}{2}}{M}\right)}{B_{SNR}\sin^2\varphi}}{\left(\begin{array}{l} S_{10}\cos^2\varphi\left(\frac{S_{10}\sin^2\Delta}{4}+\frac{S_{13}^2\cos^2\frac{\Delta}{2}(\cos\Delta-1)}{2M}\right) \\ -S_{20}\sin^2\varphi\left(\cos 2\phi\left(S_{10}\cos\Delta-\frac{S_{13}^2\cos^2\frac{\Delta}{2}}{M}\right)-\left(\frac{S_{10}}{2}-\frac{S_{13}^2\cos^2\frac{\Delta}{2}}{2M}\right)\right)\end{array}\right)}, \\
C_{\varphi\varphi} &= \frac{\frac{S_{10}-\frac{1}{M}S_{13}^2\cos^2\frac{\Delta}{2}-\cos 2\phi\left(S_{10}\cos\Delta-\frac{S_{13}^2\cos^2\frac{\Delta}{2}}{M}\right)}{2B_{SNR}}}{\left(\begin{array}{l} S_{10}\cos^2\varphi\left(\frac{S_{10}\sin^2\Delta}{4}+\frac{S_{13}^2\cos^2\frac{\Delta}{2}(\cos\Delta-1)}{2M}\right) \\ -S_{20}\sin^2\varphi\left(\cos 2\phi\left(S_{10}\cos\Delta-\frac{S_{13}^2\cos^2\frac{\Delta}{2}}{M}\right)-\left(\frac{S_{10}}{2}-\frac{S_{13}^2\cos^2\frac{\Delta}{2}}{2M}\right)\right)\end{array}\right)}, \\
C_{\varphi\phi} &= \frac{\frac{\sin^2\varphi\cos\varphi\sin 2\phi\left(S_{10}\cos\Delta-\frac{S_{13}^2\cos^2\frac{\Delta}{2}}{M}\right)}{2B_{SNR}}}{\left(\begin{array}{l} S_{10}\cos^2\varphi\left(\frac{S_{10}\sin^2\Delta}{4}+\frac{S_{13}^2\cos^2\frac{\Delta}{2}(\cos\Delta-1)}{2M}\right) \\ -S_{20}\sin^2\varphi\left(\cos 2\phi\left(S_{10}\cos\Delta-\frac{S_{13}^2\cos^2\frac{\Delta}{2}}{M}\right)-\left(\frac{S_{10}}{2}-\frac{S_{13}^2\cos^2\frac{\Delta}{2}}{2M}\right)\right)\end{array}\right)}.
\end{aligned}
\tag{2.34}
$$

These expressions concerning the V-shaped 3D array under conditional and unconditional observation models will be analyzed in the next section.

2.5.2 L-shaped 3D array extension

We call "L-shaped 3D array extension" a particular case of the V-shaped 3D array where the parameter Δ is fixed to be $\Delta = \frac{\pi}{2}$. The L-shaped (2D) array has already been studied in [HSW91] where it is shown that the L-shaped (2D) array is 37% better in terms of estimation accuracy than the cross array. Without loss of generality, let us suppose that the three branches of the array coincides with the coordinate system axes (see Fig. 2.6(a)).

2.5.2.1 Conditional observation model

Under $\mathcal{M}_1$, expression (2.31) leads to

$$
\begin{aligned}
C_{\varphi\varphi} &= \frac{2}{A_{SNR}(S_{10}\cos^2\varphi + 2S_{20}\sin^2\varphi)}, \\
C_{\phi\phi} &= \frac{2}{A_{SNR}S_{10}\sin^2\varphi}, \\
C_{\varphi\phi} &= 0.
\end{aligned}
\tag{2.35}
$$

We can notice that, in this case, the parameters φ and ϕ are decoupled. The CRB becomes very compact.

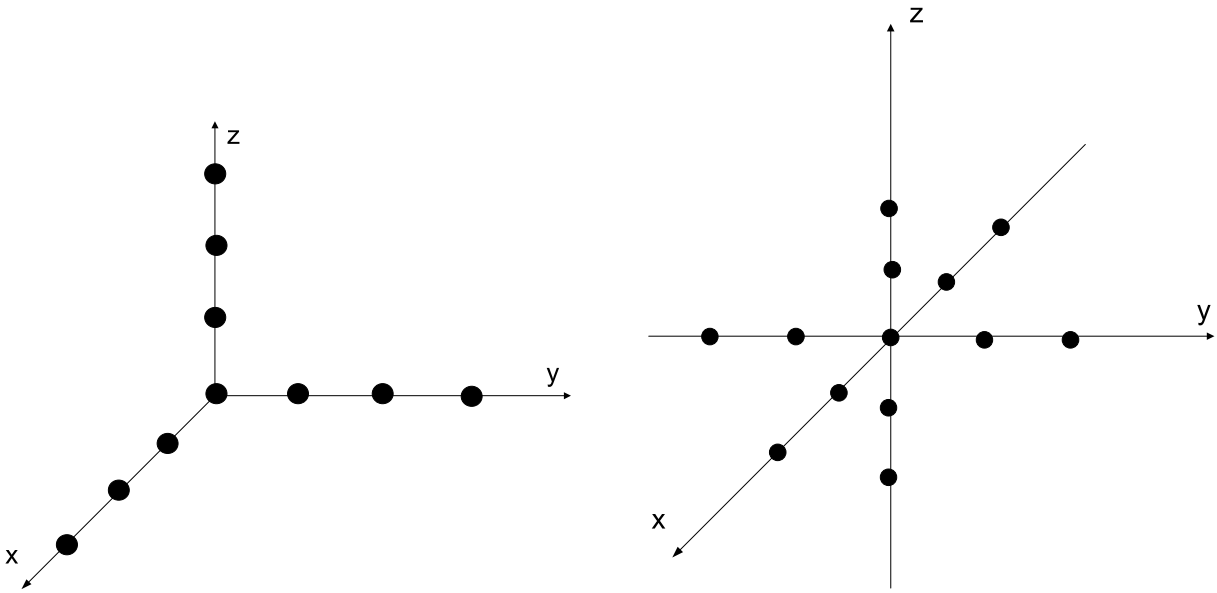

(a) L-shaped 3D array extension (b) 3D uniform angular array

Figure 2.6: Orthogonal arrays

2.5.2.2 Unconditional observation model

Under $\mathcal{M}_2$, by letting $\Delta = 90°$, Eqn. (2.32) and (2.33) become

$$
\begin{aligned}
C_{\phi\phi} &= \frac{\left(\cos^2\varphi\left(\frac{S_{10}}{2}-\frac{S_{13}^2(\cos 2\phi+1)}{4M}\right)+\sin^2\varphi(S_{20}-\frac{S_{23}^2}{M})+\frac{1}{M\sqrt{2}}\sin 2\varphi\cos\phi S_{23}S_{13}\right)}{B_{SNR}\sin^2\varphi} \\
&\quad \Bigg/ \left(\begin{array}{l} S_{10}\cos^2\varphi\left(\frac{S_{10}}{4}-\frac{S_{13}^2}{4M}\right)+\frac{S_{23}S_{10}S_{13}\cos\phi\sin 2\varphi}{2\sqrt{2}M} \\ -\frac{1}{4M}\sin^2\varphi\cos 2\phi S_{20}S_{13}^2+\sin^2\varphi\left(\frac{S_{20}S_{10}}{2}-\frac{S_{20}S_{13}^2}{4M}-\frac{S_{10}S_{23}^2}{2M}\right)\end{array}\right), \\
C_{\varphi\varphi} &= \frac{\frac{1}{2B_{SNR}}\left(S_{10}+\frac{1}{2M}S_{13}^2(\cos 2\phi-1)\right)}{\left(\begin{array}{l} S_{10}\cos^2\varphi\left(\frac{S_{10}}{4}-\frac{S_{13}^2}{4M}\right)+\frac{S_{23}S_{10}S_{13}\cos\phi\sin 2\varphi}{2\sqrt{2}M} \\ -\frac{1}{4M}\sin^2\varphi\cos 2\phi S_{20}S_{13}^2+\sin^2\varphi\left(\frac{S_{20}S_{10}}{2}-\frac{S_{20}S_{13}^2}{4M}-\frac{S_{10}S_{23}^2}{2M}\right)\end{array}\right)}, \\
C_{\varphi\phi} &= \frac{\frac{1}{\sqrt{2}MU_{SNR}\sin^2\varphi}\left(\frac{1}{4\sqrt{2}}S_{13}^2\sin 2\varphi\sin 2\phi-\sin^2\varphi\sin\phi S_{23}S_{13}\right)}{\left(\begin{array}{l} S_{10}\cos^2\varphi\left(\frac{S_{10}}{4}-\frac{S_{13}^2}{4M}\right)+\frac{S_{23}S_{10}S_{13}\cos\phi\sin 2\varphi}{2\sqrt{2}M} \\ -\frac{1}{4M}\sin^2\varphi\cos 2\phi S_{20}S_{13}^2+\sin^2\varphi\left(\frac{S_{20}S_{10}}{2}-\frac{S_{20}S_{13}^2}{4M}-\frac{S_{10}S_{23}^2}{2M}\right)\end{array}\right)}.
\end{aligned}
\tag{2.36}
$$

2.5.3 3D uniform angular array

A natural variant of "L-shaped 3D extension array", presented in Fig. 2.6(b), can be considered. This array is called 3D uniform angular antenna array (UAA). In [YS05], the UAA has been proved to minimize the CRB for the source position's estimation. Thanks to its special structure, which is totally symmetric, its CRB becomes more compact due to the fact that $S_{11} = S_{12} = S_{13} = S_{23} = 0$.

2.5.3.1 Conditional observation model

The CRB is the same as Eqn. (2.35).

2.5.3.2 Unconditional observation model

$$\begin{cases} C_{\phi\phi} &= \frac{2}{B_{SNR}S_{10}\sin^2\varphi}, \\ C_{\varphi\varphi} &= \frac{2}{B_{SNR}\left(S_{10}\cos^2\varphi+2S_{20}\sin^2\varphi\right)}, \\ C_{\varphi\phi} &= 0. \end{cases} \tag{2.37}$$

From Eqn. (2.35) and (2.37), we observe that under $\mathcal{M}_1$ and $\mathcal{M}_2$, the CRB of the UAA has identical expressions except the terms A_{SNR} under $\mathcal{M}_1$ and B_{SNR} under $\mathcal{M}_2$. Therefore, we conclude that the UAA has a similar behavior under both the conditional and unconditional observation assumptions.

Moreover, if we choose the array structure such as $S_{20} = \frac{S_{10}}{2}$, *i.e.*, the number of sensors of the six branches are equal, or $N_2 = N_2' = \frac{N_1-1}{4}$, then the CRB of elevation is independent to both the azimuth and elevation, *i.e.*, to the DOA.

2.5.4 Analysis

In this Section, the aforementioned results for the particular antenna models are analyzed in order to find the isotropy, uncoupling condition and also to compare their behavior under the conditional and unconditional assumptions.

2.5.4.1 Isotropy and uncoupling properties

In this case, our purpose is to find the value of the degree of freedom Δ_{iso} with which, the V-shaped extension arrays attain isotropy and/ or decoupling.

- *Conditional observation model*

The condition of isotropy and decoupling (2.22) leads Eqn. (2.31) to $\Delta_{iso} = 90°$ for both V-shaped with a single orthogonal branch or with two symmetric orthogonal branches antenna. It can be noted that this case is in contradiction with the results mentioned in [GM06] for the unconditional model and 2D array and with the results obtained below.

- *Unconditional observation model*

Concerning the V-shaped array with an orthogonal branch, from condition (2.24), the isotropic property is achieved if $S_{11} = 0$ is satisfied, *i.e.*, the line containing the ULA branch must pass through the centroid of the planar antenna. Given the fact that the line containing the ULA branch does not pass through the centroid of the planar part of the V-shaped 3D extension, therefore, there is no value of Δ satisfying the isotropic condition.

Concerning the V-shaped array with two symmetric orthogonal branches, from Eqn. (2.34) and (2.26), we can see that Δ_{iso} is the solution of equation $S_{12} - \frac{S_{11}^2}{M} = 0$. Consequently, depending on the method used to make the branches of the antenna array (ULA, minimum redundancy [Mof68], D-optimal [HRW91], etc.) we might obtain different values of Δ_{iso}. In the case where the antenna array is made from ULA, then (2.27) easily leads to (see Appendix 2.8.5 for the proof):

$$\Delta_{iso} = \arccos\left(\frac{3(N_1^2-1)}{8MN_1 - 3N_1^2 + 3}\right). \tag{2.38}$$

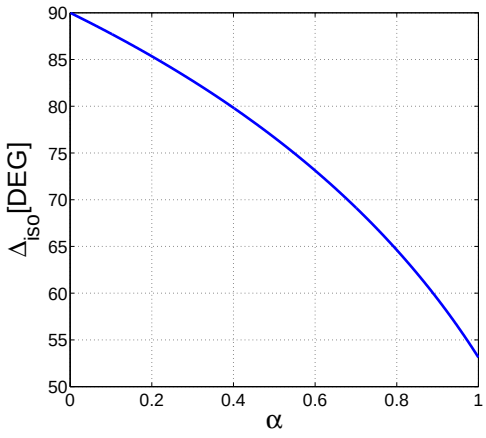

Figure 2.7: Variation of Δ_{iso} *w.r.t.* α with $M = 1000$.

Let us set the positive $\alpha = \frac{N_1}{M} \leq 1$. The value of α associated to a planar antenna will be equal to 1, while that one associated to a 3D antenna array is strictly lower than 1. Then, Δ_{iso} can be expressed as $\Delta_{iso} = \arccos\left(\frac{3(\alpha^2-1/M^2)}{8\alpha-3\alpha^2+3/M^2}\right)$. We are also interested to define the range of Δ_{iso} *w.r.t.* α in this case. It is clear that:

$$\begin{array}{l} \text{If } \alpha \to 1 \text{ and } M \gg 1 \Rightarrow \Delta_{iso} \simeq \arccos\left(\frac{3}{5}\right) = 53.13^\circ \\ \text{If } \alpha \to 0 \text{ and } M \gg 1 \Rightarrow \Delta_{iso} \simeq \arccos\left(0\right) = 90^\circ \end{array} \tag{2.39}$$

In Fig. 2.7, when α tends to 0, *i.e*, the number of sensors located on the orthogonal axis is much larger than the number of sensors located on the planar array then the value of Δ_{iso} tends to 90°. On the contrary, if α tends to 1, *i.e*, the number of sensors located on the planar array is much larger than those located on the orthogonal axis, then, the value of Δ_{iso} tends to $\arccos(3/5)$. In particular, in the case where $\alpha = 1$, we obtain exactly the same result ($\Delta_{iso} = 53.13^\circ$) for the planar antenna array as in [GM06]. Therefore, Δ_{iso} in this case will vary from 53.13° to 90°.

A remark can be done here that under $\mathcal{M}_2$, adding two symmetric orthogonal branches does not modify the conditions of isotropy and decoupling ($S_{12} = S_{11}^2/M$) *w.r.t* the planar array, but it changes the arrangement of the sensors located on the planar part because of the intervention of N_2 to S_{12} and S_{11}.

2.5.4.2 Conditional versus unconditional models

Since the V-shaped 3D extension array does not satisfy condition (2.28) because the line containing the ULA branch does not pass through the centroid of the planar part of the antenna, then it is impossible to find an optimal value of Δ, with which the CCRB and the UCRB have the same expressions. The CCRB in this case is always more compact than the UCRB. Contrary to the V-shaped 3D array extension , the 3D UAA satisfies condition (2.28). Therefore the UCRB and CCRB will have the identical compact expression at high SNR or for a large number of sensors.

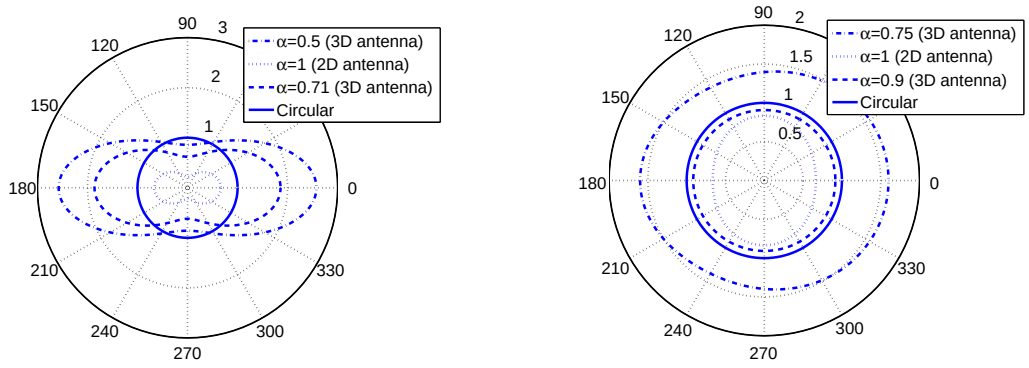

(a) Conditional observation model

(b) Unconditional observation model

Figure 2.8: Polar representation of the normalized CRB of azimuth for all values of azimuth angle, with different values of α, $\Delta = 60°$ and $\varphi = 45°$. The array has a single orthogonal branch.

2.5.5 Summary

Thanks to the degree of freedom Δ of the V-shaped family arrays, the analysis of the impact of the array geometry on the estimation performance is simplified. We here can make some remarks:

- In almost cases, CCRB has a more compact expression than UCRB.
- Under $\mathcal{M}_1$, the value of Δ_{iso} is constant ($\Delta_{iso} = 90°$), while it takes a range of values under $\mathcal{M}_2$, depending to the antenna array configuration. In particular, when $\alpha = 1$, we find the same results ($\Delta_{iso} = 53.13°$) for the V-shaped (2D) antenna as in [GM06].
- The 3D uniform angular array has several advantages: isotropy, uncoupling, minimization of the CRB in case of the source position's location using TDOA method and the same estimation accuracy under both the $\mathcal{M}_1$ or $\mathcal{M}_2$ assumptions.

2.6 Comparison of the estimation accuracy

In this section, we will use the closed form expressions of the CRB calculated in the previous section to compare the estimation performance between the above studied arrays with other classical arrays. In order to simplify the array design problem, we only consider the behavior of the CRB of the V-shaped antenna array and its 3D extension. Its closed form CRB will be analyzed *w.r.t.* the opening angle Δ. For the simulation, all branches of the antenna array being either 2D (two branches) or 3D (three branches or four branches) are made from ULAs with the inter-sensor space of half the wavelength. The simulations are performed with a signal to noise ratio equal to 10 dB and a number of snapshots $T = 100$.

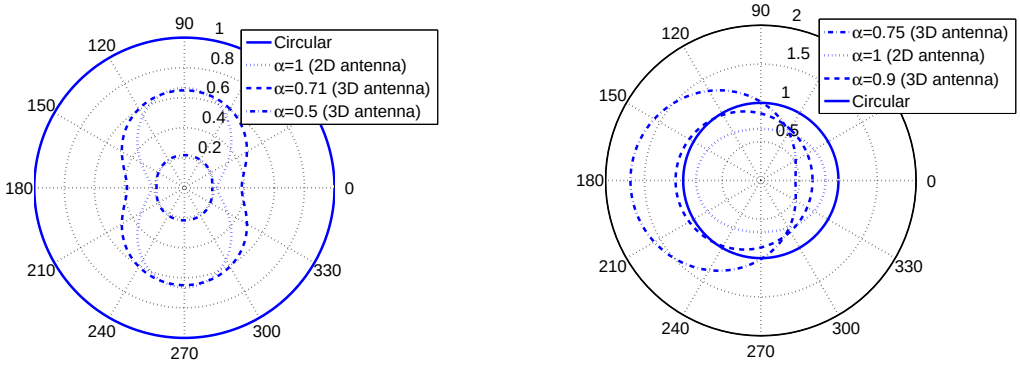

(a) Conditional observation model

(b) Unconditional observation model

Figure 2.9: Polar representation of the normalized CRB of elevation for all values of azimuth angle, with different values of α, $\Delta = 60°$ and $\varphi = 45°$. The array has a single orthogonal branch.

2.6.1 Comparison of the estimation performance between the V-shaped 3D antenna array extension and the planar circular antenna array

We here compare the estimation performance between the 3D V-shaped antenna array extension with an isotropic classic antenna: the uniform circular antenna (UCA). For this comparison, the antenna arrays will have the same number of sensors. The sensors of UCA are half-wavelength inter-element spaced, thus, the value of its radius is given by $r = \frac{\lambda}{4 \sin \frac{\pi}{M}}$. Figs. 2.8 and 2.9 represent respectively the CRB of azimuth and elevation normalized by the CRB of the UCA ($C_{\varphi\varphi}/C_{\varphi\varphi}^{(UCA)}$, $C_{\phi\phi}/C_{\phi\phi}^{(UCA)}$) *w.r.t.* the aforementioned coefficient α, at the opening angle $\Delta = 60°$ and at the elevation $\varphi = 45°$ under both conditional and unconditional observation models.

- *Conditional observation model*

In Fig 2.9(a), the accuracy concerning the elevation estimation of the V-shaped antenna is always lower, *i.e.*, better than the UCA. In Fig 2.8(a), it is shown that the performance concerning the azimuth estimation is strictly linked to the number of sensors located on the orthogonal branch, *i.e.*, on the coefficient α. We observed that when the ratio α varies, the estimation performance concerning azimuth and elevation varies differently. When the one improves, the other deteriorates. For the value of α close to 1, *i.e.*, almost all of the sensors are located on the planar antenna, the estimation accuracy in terms of both the azimuth and elevation of the V-shaped family is better than the one of the UCA.

- *Unconditional observation model*

Figs. 2.8(b) and 2.9(b) show that the performance concerning estimation of both azimuth and elevation are strongly dependent on the number of sensors located on the orthogonal branch, *i.e.*, the coefficient α. The link between α and the CRB under $\mathcal{M}_2$ is more complicated than under $\mathcal{M}_1$. When α decreases, then the CRB concerning azimuth estimation deteriorates, while the CRB concerning elevation estimation varies differently according to the DOA: it improves in some zone of DOA while worsens in the other zones. For the value of α close to 1, the V-shaped family performs better in terms of both azimuth and elevation estimation than the UCA.

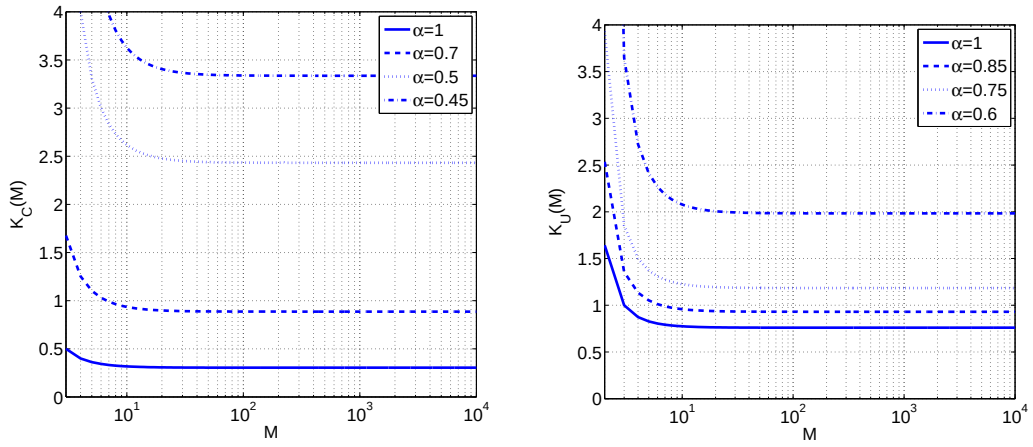

(a) Conditional observation model (b) Unconditional observation model

Figure 2.10: Fraction $K(M)$ in term of the number of sensors M

2.6.2 Comparison of the estimation performance of the isotropic antennas

We are interested in considering the case where our array attains the isotropic and uncoupling properties. We here compare the V-shaped isotropic array ($\Delta_{iso} = \frac{\pi}{2}$ under $\mathcal{M}_1$ and $\Delta_{iso} = \arccos\left(\frac{3(\alpha^2-1/M^2)}{8\alpha-3\alpha^2+3/M^2}\right)$ under $\mathcal{M}_2$) with the classical isotropic UCA. As mentioned in the previous section, under $\mathcal{M}_2$, the 3D V-shaped array extension becomes an isotropic array if there are two symmetric orthogonal branches. Therefore, under $\mathcal{M}_1$, a 3D V-shaped array with a single orthogonal branch is used while under $\mathcal{M}_2$, a 3D V-shaped array with two symmetric orthogonal branches is used. We consider the ratio $K_C(M)$ (under $\mathcal{M}_1$) or $K_U(M)$ (under $\mathcal{M}_2$) between the CRB concerning the estimation of the azimuth of a family of V-shaped isotropic arrays and the UCA array. Thus, we have $K_C(M) = K_U(M) = \frac{C^{2D}_{\phi\phi}}{C^{UCA}_{\phi\phi}}$ if $\alpha = 1$ and $K_C(M) = K_U(M) = \frac{C^{3D}_{\phi\phi}}{C^{UCA}_{\phi\phi}}$ if $\alpha < 1$. Therefore, this fraction shows the gain in estimation of the azimuth accuracy of the family of V-shaped arrays *w.r.t.* to the UCA array.

- *Conditional observation model*

From (2.35), the ratio of CRB concerning the azimuth of these antenna arrays is given by (see Appendix 2.8.6 for the proof):

$$\begin{aligned} &K_C(M) = \frac{3}{\alpha(\alpha^2M^2-1)\sin^2\frac{\pi}{M}}. \\ &\text{If } \alpha M >> 1 \rightarrow K_C(M) = \frac{3}{\pi^2\alpha^3}. \end{aligned} \tag{2.40}$$

We can say that the V-shaped antenna array is better than the UCA array in terms of the estimation of azimuth if and only if the fraction $K_C(M)$ is smaller than 1. Fig. 2.10(a) shows that the 3D V-shaped isotropic antenna array is better than the UCA array provided that the value of α satisfies: $0.76 < \alpha < 1$ and $M > 6$.

- *Unconditional observation model*

From (2.34), after some calculations, the ratio $K_U(M)$ is given by (see Appendix 2.8.6 for the proof):

$$\begin{array}{l} K_U(M) = \frac{3(8\alpha M^2 - 3\alpha^2 M^2 + 3)}{\sin^2 \frac{\pi}{M} \alpha(\alpha^2 M^2 - 1)(8\alpha M^2 - 6\alpha^2 M^2 + 6)}. \\ \text{If } \alpha M >> 1 \rightarrow K_U(M) = \frac{3(8-3\alpha)}{\alpha^3(8-6\alpha)\pi^2}. \end{array} \tag{2.41}$$

Fig. 2.10(b) shows that the 3D V-shaped isotropic antenna array is better than the UCA array if: $0.84 < \alpha < 1$ and $M > 7$.

Table 2.1: 'The azimuth estimation performance gain of the 3D V-shaped isotropic antenna according to the UCA'

α	1	0.9	0.8	0.7	0.6
$\mathcal{M}_1$ assumption	0.6959	0.5829	0.4060	0.1133	-0.4081
$\mathcal{M}_2$ assumption	0.2399	0.1498	-0.0393	-0.3765	-0.9838

Tab. 2.1 shows the value of $1 - K_U(M)$ and $1 - K_C(M)$ *w.r.t.* α. These values represent the gain concerning the azimuth estimation of the 3D V-shaped isotropic antenna array to the UCA array for a large number of sensors. We here want to find the value of α with which $1-K_C(M) > 0$ under $\mathcal{M}_1$ or $1-K_U(M) > 0$ under $\mathcal{M}_2$ *i.e.*, the 3D V-shaped antenna array has better azimuth estimation accuracy than the UCA array. Under both the $\mathcal{M}_1$ and $\mathcal{M}_2$ assumptions, it is clear that, for all $\alpha > 0.85$, the 3D V-shaped isotropic array is always better than the UCA. Moreover, if $\alpha = 1$ then the azimuth estimation accuracy of the V-shaped isotropic planar array is at least 20% better than the UCA array.

2.6.3 Comparison of the estimation performance between 2D and 3D antenna arrays

In the following, we compare the performance of estimation between the 3D and 2D arrays. The V-shaped 2D antenna array has $M = 7$ sensors (one at the origin with three other sensors on each branch). The V-shaped 3D extension antenna array consisting of a single orthogonal branch is also made from $M = 7$ sensors (one at the origin and two sensors on every three branches). It should be noted that taking some sensors from the planar array of the 2D antenna array to make the 3D antenna array will decrease the aperture and hence, reduce its performance. Therefore, using non ULA such as minimum redundancy, D-optimal, etc. instead of using ULA can maintain the aperture and also, the performance.

Fig. 2.11 shows the behaviors of $C^{3D}_{\varphi\varphi}$, $C^{3D}_{\phi\phi}$, $C^{2D}_{\varphi\varphi}$, $C^{2D}_{\phi\phi}$ in terms of the opening angle Δ varying from 0° to 90° under $\mathcal{M}_1$ and $\mathcal{M}_2$ and at $\phi = 20°$ and $\varphi = 70°$. This is the scenario where the source is close to the plane of the array. Under both two assumptions, for the estimation of elevation φ, we can see that the 3D antenna array has always the better performance compared to the 2D antenna. However, concerning the azimuth estimation, the 3D array only has better performance than the 2D array if $\Delta < 20°$ under $\mathcal{M}_1$ or $\Delta < 12°$ under $\mathcal{M}_2$.

Fig. 2.12 shows the same curves, but values of ϕ and φ are respectively equal to 50° and 30°. This is the scenario where the source is far from the plane of the antenna array. In this case, for both $\mathcal{M}_1$ and $\mathcal{M}_2$ assumptions, it should be better, contrary to intuition, to choose the 2D antenna array over a limited opening angle obtained numerically by solving $\max\left(C^{3D}_{\phi\phi} = C^{2D}_{\phi\phi}, C^{3D}_{\varphi\varphi} = C^{2D}_{\varphi\varphi}\right)$ as a function of Δ.

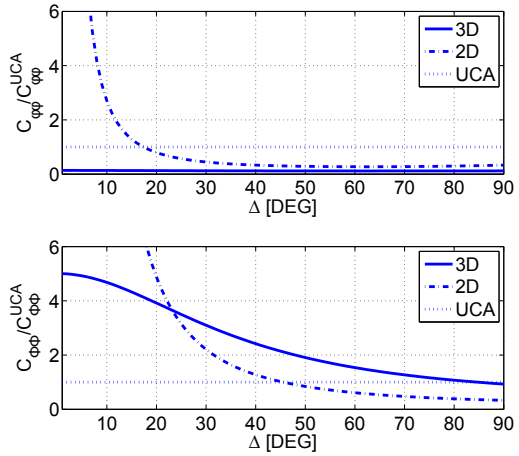

(a) Conditional observation model

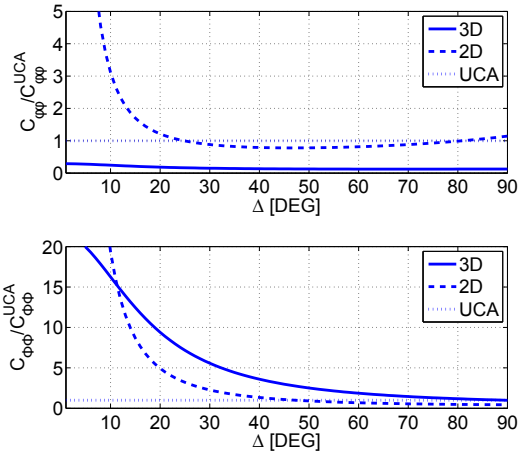

(b) Unconditional observation model

Figure 2.11: The behavior of $C^{3D}_{\varphi\varphi}$, $C^{2D}_{\varphi\varphi}$, $C^{3D}_{\phi\phi}$ and $C^{2D}_{\phi\phi}$ normalized by the CRB of the UCA according to Δ at $\phi = 20°$ and $\varphi = 70°$

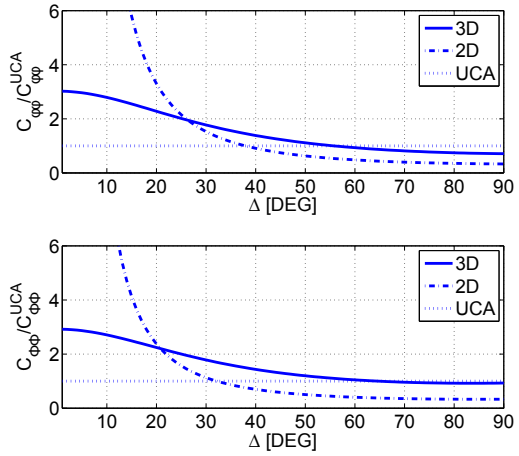

(a) Conditional observation model

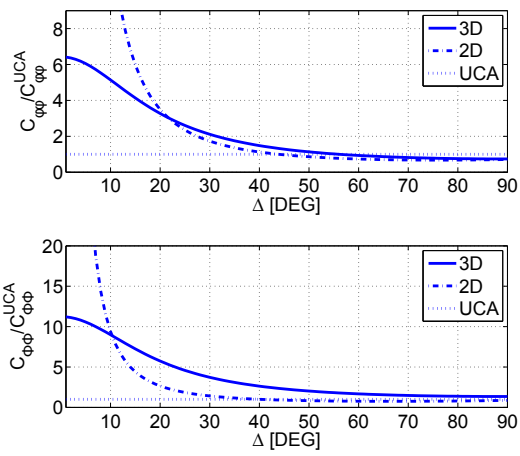

(b) Unconditional observation model

Figure 2.12: The behavior of $C^{3D}_{\varphi\varphi}$, $C^{2D}_{\varphi\varphi}$, $C^{3D}_{\phi\phi}$ and $C^{2D}_{\phi\phi}$ normalized by the CRB of the UCA according to Δ at $\phi = 50°$ and $\varphi = 30°$

Finally, by an exhaustive research over all three parameters: elevation, azimuth and opening angle, we found that concerning the elevation estimation, the 3D antenna array is always better than the 2D antenna if the elevation is larger than a certain threshold φ_0.

- *Conditional observation model*

We can prove in this case that the threshold φ_0 is about 62.2° by solving

$$\frac{C_{\varphi\varphi}^{3D}}{C_{\varphi\varphi}^{2D}} < 1 \Leftrightarrow \varphi > \arctan\sqrt{\max_{\Delta,\phi}\{\Gamma\}}, \tag{2.42}$$

where $\Gamma = \frac{\sin^2\Delta\big((M^2-1)-\alpha(\alpha^2M^2-1)\big)}{(1-\cos\Delta\cos 2\phi)4(1-\alpha)((1-\alpha)M+1)(2(1-\alpha)M+1)}$, $\alpha = \frac{N_1}{M} = \frac{5}{7}, M = 7, \varphi \in [0^\circ, 90^\circ], \Delta \in (0^\circ, 180^\circ), \phi \in [0^\circ, 360^\circ]$.

- *Unconditional observation model*

By numerical calculus, in the case where $\alpha = 5/7$ and $M = 7$, we obtain the threshold $\varphi_0 \simeq 65^\circ$.

2.7 Conclusion

In this chapter, we derived the closed form expressions of the CRB for the estimation of azimuth and elevation of a far field single source in both the conditional and unconditional observation models where a planar array or its 3D extension is used. The 3D array extension here is made by adding one or two orthogonal branches to an arbitrary planar array. These CRB closed form expressions are used here as a useful tool in order to find the isotropy, uncoupling conditions and the contribution of the third dimension to the estimation accuracy and also to introduce a comparison between conditional and unconditional observation models. Consequently, we showed that the 3D array overcomes the ambiguity problem of the planar (2D) array. Moreover, we found that there is a family of array geometries with which the CRB can be expressed in the same term under both the conditional and unconditional assumptions. Furthermore, at high signal to noise ratio or with a large number of sensors, the CRB expressions under the two assumptions become identical. In the following step, the CRB closed form expressions are then applied into several particular well-known array geometries such as: the V-shaped/ L-shaped array 3D extension, the uniform angular array. It is shown that the isotropy and uncoupling conditions of the 3D array under conditional and unconditional assumptions are different from each other. In particular, for the V-shaped arrays family, under the unconditional observation model, the opening angle Δ_{iso} depends on the number of sensors located on the orthogonal branches while $\Delta_{iso} = 90^\circ$ is the desired value under the conditional assumption. Finally, through several simulations, we conclude that the performance of estimation of the 3D array strongly depends on the rate between the number of sensors located on the orthogonal branches and the total number of sensors (α). When this rate varies, the estimation concerning azimuth and elevation varies differently. In the other hand, by choosing a suitable rate (α close to 1), the 3D array has the better performance than the classical UCA concerning both azimuth and elevation estimation for the same number of sensors. It should be noted that, for a constant number of sensors, adding the 3D branch will decrease the aperture of the antenna, therefore, deteriorate the estimation performance.

2.8 Appendix

2.8.1 Proof of Eqn. (2.16)

The derivation of the i^{th} element of the steering vector is given by

$$\begin{aligned}\frac{\partial a_i(\varphi,\phi)}{\partial \varphi} &= \frac{2j\pi\rho_i}{\lambda}\left(\cos\varphi\sin\xi_i\cos\left(\phi-\varrho_i\right)-\cos\xi_i\sin\varphi\right)e^{\left(\frac{2j\pi\rho_i}{\lambda}\sin\varphi\sin\xi_i\cos\left(\phi-\varrho_i\right)+\cos\xi_i\cos\varphi\right)},\\ \frac{\partial a_i(\varphi,\phi)}{\partial \phi} &= -\frac{2j\pi\rho_i}{\lambda}\sin\varphi\sin\xi_i\sin\left(\phi-\varrho_i\right)e^{\left(\frac{2j\pi\rho_i}{\lambda}\sin\varphi\sin\xi_i\cos\left(\phi-\varrho_i\right)+\cos\xi_i\cos\varphi\right)}.\end{aligned} \tag{2.43}$$

Let us note that the sensors located on the xOy plane are such that $\xi_i = \frac{\pi}{2}$, while the sensors located on the orthogonal axe are such that $\xi_i = 0$. After some calculation, from (2.7), it easy to obtain the elements of the Fisher Information Matrix:

$$\begin{aligned}\frac{[\mathbf{FIM}(\boldsymbol{\theta})]_{11}}{A_{SNR}} &= \sum_{i=1}^{M}\rho_i^2\left(\cos\varphi\sin\xi_i\cos\left(\phi-\varrho_i\right)-\cos\xi_i\sin\varphi\right)^2\\ &= \sum_{i=1}^{N_1}\rho_{1,i}^2\cos^2\varphi\cos^2\left(\phi-\varrho_i\right)+\sum_{i=N_1+1}^{M}\rho_{2,i}^2\sin^2\varphi\\ &= \frac{\cos^2\varphi}{4}\left(e^{2j\phi}\sum_{i=1}^{N_1}\rho_{1,i}^2e^{-2j\varrho_i}+e^{-2j\phi}\sum_{i=1}^{N_1}\rho_{1,i}^2e^{2j\varrho_i}+2\sum_{i=1}^{N_1}\rho_{1,i}^2\right)+\sin^2\varphi\sum_{i=N_1+1}^{M}\rho_{2,i}^2\\ &= \frac{\cos^2\varphi}{4}\left(e^{2j\phi}S_{12}^*+e^{-2j\phi}S_{12}+2S_{10}\right)+\sin^2\varphi S_{20}\\ &= \frac{1}{2}\cos^2\varphi\left(\Re\{e^{-2j\phi}S_{12}\}+S_{10}\right)+\sin^2\varphi S_{20},\end{aligned} \tag{2.44}$$

$$\begin{aligned}\frac{[\mathbf{FIM}(\boldsymbol{\theta})]_{22}}{A_{SNR}} &= \sum_{i=1}^{M}\rho_i^2\left(\sin\varphi\sin\xi_i\sin\left(\phi-\varrho_i\right)\right)^2\\ &= \sin^2\varphi\sum_{i=1}^{N_1}\rho_{1,i}^2\sin^2\left(\phi-\varrho_i\right)\\ &= -\frac{\sin^2\varphi}{4}\left(e^{2j\phi}\sum_{i=1}^{N_1}\rho_{1,i}^2e^{-2j\varrho_i}+e^{-2j\phi}\sum_{i=1}^{N_1}\rho_{1,i}^2e^{2j\varrho_i}-2\sum_{i=1}^{N_1}\rho_{1,i}^2\right)\\ &= -\frac{\sin^2\varphi}{4}\left(e^{2j\phi}S_{12}^*+e^{-2j\phi}S_{12}-2S_{10}\right)\\ &= -\frac{1}{2}\sin^2\varphi\left(\Re\{e^{-2j\phi}S_{12}\}-S_{10}\right),\end{aligned} \tag{2.45}$$

and

$$\begin{aligned}\frac{[\mathbf{FIM}(\boldsymbol{\theta})]_{12}}{A_{SNR}} &= -\sum_{i=1}^{M}\rho_i^2 \sin\varphi \sin\xi_i \sin\left(\phi-\varrho_i\right)\left(\cos\varphi\sin\xi_i\cos\left(\phi-\varrho_i\right)-\cos\xi_i\sin\varphi\right)\\ &= -\sin\varphi\cos\varphi\sum_{i=1}^{N_1}\rho_{1,i}^2\sin\left(\phi-\varrho_i\right)\cos\left(\phi-\varrho_i\right)\\ &= -\frac{1}{8j}\sin 2\varphi\left(e^{2j\phi}\sum_{i=1}^{N_1}\rho_{1,i}^2 e^{-2j\varrho_i}-e^{-2j\phi}\sum_{i=1}^{N_1}\rho_{1,i}^2 e^{2j\varrho_i}\right) \qquad (2.46)\\ &= -\frac{1}{8j}\sin 2\varphi\left(e^{2j\phi}S_{12}^{*}-e^{-2j\phi}S_{12}\right)\\ &= \frac{1}{4}\sin 2\varphi\Im\{e^{-2j\phi}S_{12}\}. \qquad (2.47)\end{aligned}$$

The FIM determinant is given by:

$$\begin{aligned}&\frac{\det\left[\mathbf{FIM}(\boldsymbol{\theta})\right]}{C_{SNR}^2} = \frac{[\mathbf{FIM}(\boldsymbol{\theta})]_{11}[\mathbf{FIM}(\boldsymbol{\theta})]_{22}-[\mathbf{FIM}(\boldsymbol{\theta})]_{12}[\mathbf{FIM}(\boldsymbol{\theta})]_{21}}{C_{SNR}^2}\\ &= \left(\tfrac{\cos^2\varphi}{4}\left(e^{2j\phi}S_{12}^{*}+e^{-2j\phi}S_{12}+2S_{10}\right)+\sin^2\varphi S_{20}\right)\left(-\tfrac{\sin^2\varphi}{4}\left(e^{2j\phi}S_{12}^{*}+e^{-2j\phi}S_{12}-2S_{10}\right)\right)\\ &\quad-\left(-\tfrac{1}{8j}\sin 2\varphi\left(e^{2j\phi}S_{12}^{*}-e^{-2j\phi}S_{12}\right)\right)^2\\ &= \tfrac{\sin^2 2\varphi}{64}\left(4S_{10}^2-\left(e^{2j\phi}S_{12}^{*}+e^{-2j\phi}S_{12}\right)^2\right)-\tfrac{\sin^4\varphi}{4}S_{20}\left(e^{2j\phi}S_{12}^{*}+e^{-2j\phi}S_{12}-2S_{10}\right)\\ &\quad+\tfrac{\sin^2 2\varphi}{64}\left(e^{2j\phi}S_{12}^{*}-e^{-2j\phi}S_{12}\right)^2\\ &= \tfrac{\sin^2 2\varphi}{64}\left(4S_{10}^2-4\|S_{12}\|^2\right)+\tfrac{\sin^4\varphi}{4}S_{20}\left(2S_{10}-2\Re\{e^{-2j\phi}S_{12}\}\right)\\ &= \tfrac{\sin^2\varphi}{4}\left(\cos^2\varphi(S_{10}^2-\|S_{12}\|^2)+2\sin^2\varphi S_{20}\left(S_{10}-\Re\{e^{-2j\phi}S_{12}\}\right)\right).\end{aligned} \qquad (2.48)$$

2.8.2 Proof of Eqn. (2.17) and Eqn. (2.18)

In the same way as for conditional case, from (2.13), we have

$$\begin{aligned}&\frac{[\mathbf{FIM}(\boldsymbol{\theta})]_{1,1}}{B_{SNR}} =\\ &= \sum_{i=1}^{M}\rho_i^2\left(\cos\varphi\sin\xi_i\cos\left(\phi-\varrho_i\right)-\cos\xi_i\sin\varphi\right)^2-\tfrac{1}{M}\left(\sum_{i=1}^{M}\rho_i\left(\cos\varphi\sin\xi_i\cos\left(\phi-\varrho_i\right)-\cos\xi_i\sin\varphi\right)\right)^2\\ &= \cos^2\varphi\sum_{i=1}^{N_1}\rho_{1,i}^2\cos^2\left(\phi-\varrho_i\right)+\sin^2\varphi\sum_{i=N_1+1}^{M}\rho_{2,i}^2-\tfrac{1}{M}\left(\cos\varphi\sum_{i=1}^{N_1}\rho_{1,i}\cos\left(\phi-\varrho_i\right)-\sin\varphi\sum_{i=N_1+1}^{M}\rho_{2,i}\right)^2\\ &= \tfrac{1}{4}\cos^2\varphi\sum_{i=1}^{N_1}\rho_{1,i}^2\left(e^{2j(\phi-\varrho_i)}+e^{-2j(\phi-\varrho_i)}+2\right)+\sin^2\varphi\sum_{i=N_1+1}^{M}\rho_{2,i}^2\\ &\quad-\tfrac{\cos^2\varphi}{4M}\left(\sum_{i=1}^{N_1}\rho_{1,i}(e^{j(\phi-\varrho_i)}+e^{-j(\phi-\varrho_i)})\right)^2-\tfrac{\sin^2\varphi}{M}\left(\sum_{i=N_1+1}^{M}\rho_{2,i}\right)^2\\ &\quad+\tfrac{\sin 2\varphi}{2M}\sum_{i=1}^{N_1}\rho_{1,i}(e^{j(\phi-\varrho_i)}+e^{-j(\phi-\varrho_i)})\sum_{i=N_1+1}^{M}\rho_{2,i}\\ &= \tfrac{1}{4}\cos^2\varphi\left(S_{12}e^{-2j\phi}+S_{12}^{*}e^{2j\phi}+2S_{10}\right)+\sin^2\varphi S_{20}-\tfrac{1}{M}\left(\tfrac{\cos^2\varphi}{4}\left(S_{11}^2e^{-2j\phi}+S_{11}^{2*}e^{2j\phi}+2\|S_{11}\|^2\right)\right.\\ &\qquad\left.+\sin^2\varphi S_{23}^2-\tfrac{\sin 2\varphi}{2}\left(S_{11}e^{-j\phi}+S_{11}^{*}e^{j\phi}\right)S_{23}\right)\\ &= \tfrac{1}{2}\cos^2\varphi\left(S_{10}-\tfrac{\|S_{11}\|^2}{M}+\Re\left\{e^{-2j\phi}\left(S_{12}-\tfrac{S_{11}^2}{M}\right)\right\}\right)+\sin^2\varphi\left(S_{20}-\tfrac{S_{23}^2}{M}\right)+\tfrac{\sin 2\varphi}{M}S_{23}\Re\{e^{-j\phi}S_{11}\},\end{aligned}$$

(2.49)

$$
\begin{aligned}
\frac{[\mathbf{FIM}(\boldsymbol{\theta})]_{2,2}}{B_{SNR}} &= \sum_{i=1}^{M}\rho_i^2\sin^2\varphi\sin^2\xi_i\sin^2\left(\phi-\varrho_i\right) - \tfrac{1}{M}\left(\sum_{i=1}^{M}\rho_i\sin\varphi\sin\xi_i\sin\left(\phi-\varrho_i\right)\right)^2 \\
&= \sin^2\varphi\sum_{i=1}^{N_1}\rho_{p,i}^2\sin^2\left(\phi-\varrho_i\right) - \tfrac{\sin^2\varphi}{M}\left(\sum_{i=1}^{N_1}\rho_{1,i}\sin\left(\phi-\varrho_i\right)\right)^2 \\
&= -\tfrac{1}{4}\sin^2\varphi\sum_{i=1}^{N_1}\rho_{1,i}^2\left(e^{2j(\phi-\varrho_i)}+e^{-2j(\phi-\varrho_i)}-2\right) + \tfrac{\sin^2\varphi}{4M}\left(\sum_{i=1}^{N_1}\rho_{1,i}\left(e^{j(\phi-\varrho_i)}-e^{-j(\phi-\varrho_i)}\right)\right)^2 \\
&= -\tfrac{1}{4}\sin^2\varphi\left(e^{-2j\phi}S_{12}+e^{2j\phi}S_{12}^{*}-2S_{10}\right) + \tfrac{\sin^2\varphi}{4M}\left(e^{2j\phi}S_{11}^{2*}+e^{-2j\phi}S_{11}^{2}-2\|S_{11}\|^2\right) \\
&= \tfrac{1}{2}\sin^2\varphi\left(S_{10}-\tfrac{\|S_{11}\|^2}{M}-\Re\left\{e^{-2j\phi}\left(S_{12}-\tfrac{S_{11}^2}{M}\right)\right\}\right),
\end{aligned}
\tag{2.50}
$$

and

$$
\begin{aligned}
\frac{[\mathbf{FIM}(\boldsymbol{\theta})]_{1,2}}{B_{SNR}} &= -\sum_{i=1}^{M}\rho_i\sin\varphi\sin\xi_i\sin^2\left(\phi-\varrho_i\right)\left(\cos\varphi\sin\xi_i\cos\left(\phi-\varrho_i\right)-\cos\xi_i\sin\varphi\right) \\
&\quad + \tfrac{1}{M}\sum_{i=1}^{M}\rho_i\left(\cos\varphi\sin\xi_i\cos\left(\phi-\varrho_i\right)-\cos\xi_i\sin\varphi\right)\sum_{i=1}^{M}\rho_i\sin\varphi\sin\xi_i\sin\left(\phi-\varrho_i\right) \\
&= -\sin\varphi\cos\varphi\sum_{i=1}^{N_1}\rho_{1,i}^2\sin\left(\phi-\varrho_i\right)\cos\left(\phi-\varrho_i\right) \\
&\quad + \tfrac{1}{M}\sin\varphi\left(\cos\varphi\sum_{i=1}^{N_1}\rho_{1,i}\cos\left(\phi-\varrho_i\right)-\sin\varphi\sum_{i=N_1+1}^{M}\rho_{2,i}\right)\sum_{i=1}^{N_1}\rho_{1,i}\sin\left(\phi-\varrho_i\right) \\
&= -\tfrac{\sin\varphi\cos\varphi}{4j}\sum_{i=1}^{N_1}\rho_{1,i}^2\left(e^{2j(\phi-\varrho_i)}-e^{-2j(\phi-\varrho_i)}\right) \\
&\quad + \tfrac{1}{2jM}\sin\varphi\left(\tfrac{1}{2}\cos\varphi\sum_{i=1}^{N_1}\rho_{1,i}\left(e^{j(\phi-\varrho_i)}+e^{-j(\phi-\varrho_i)}\right)-\sin\varphi\sum_{i=N_1+1}^{M}\rho_{2,i}\right) \\
&\qquad \times\left(\sum_{i=1}^{N_1}\rho_{1,i}\left(e^{j(\phi-\varrho_i)}-e^{-j(\phi-\varrho_i)}\right)\right) \\
&= -\tfrac{\sin\varphi\cos\varphi}{4j}\left(e^{2j\phi}S_{12}^{*}-e^{-2j\phi}S_{12}\right) + \tfrac{\sin\varphi}{2jM}\left(\tfrac{1}{2}\cos\varphi(e^{j\phi}S_{11}+e^{-j\phi}S_{11}^{*})-\sin\varphi S_{23}\right)\left(e^{j\phi}S_{11}^{*}-e^{-j\phi}S_{11}\right) \\
&= \tfrac{\sin\varphi\cos\varphi}{2}\Im\left\{e^{-2j\phi}\left(S_{12}-\tfrac{S_{11}^2}{M}\right)\right\} + \tfrac{\sin^2\varphi}{M}S_{23}\Im\left\{e^{-j\phi}S_{11}\right\}.
\end{aligned}
\tag{2.51}
$$

The FIM determinant is given by:

$$
\begin{aligned}
&\frac{\det\left[\mathbf{FIM}(\boldsymbol{\theta})\right]}{B_{SNR}^2} = \frac{[\mathbf{FIM}(\boldsymbol{\theta})]_{1,1}[\mathbf{FIM}(\boldsymbol{\theta})]_{2,2}-[\mathbf{FIM}(\boldsymbol{\theta})]_{1,2}[\mathbf{FIM}(\boldsymbol{\theta})]_{2,1}}{B_{SNR}^2} \\
&= \left(\tfrac{1}{2}\cos^2\varphi\left(S_{10}-\tfrac{\|S_{11}\|^2}{M}+\Re\left\{e^{-2j\phi}\left(S_{12}-\tfrac{S_{11}^2}{M}\right)\right\}\right)+\sin^2\varphi\left(S_{20}-\tfrac{S_{23}^2}{M}\right)+\tfrac{\sin 2\varphi}{M}S_{23}\Re\{e^{-j\phi}S_{11}\}\right) \\
&\quad\times\left(\tfrac{1}{2}\sin^2\varphi\left(S_{10}-\tfrac{\|S_{11}\|^2}{M}-\Re\left\{e^{-2j\phi}\left(S_{12}-\tfrac{S_{11}^2}{M}\right)\right\}\right)\right) \\
&\quad-\left(\tfrac{1}{2}\sin\varphi\cos\varphi\Im\left\{e^{-2j\phi}\left(S_{12}-\tfrac{S_{11}^2}{M}\right)\right\}+\tfrac{1}{M}\sin^2\varphi S_{23}\Im\left\{e^{-j\phi}S_{11}\right\}\right)^2 \\
&= \tfrac{1}{4}\sin^2\varphi\cos^2\varphi\left(\left(S_{10}-\tfrac{\|S_{11}\|^2}{M}\right)^2-\Re^2\left\{e^{-2j\phi}\left(S_{12}-\tfrac{S_{11}^2}{M}\right)\right\}\right) \\
&\quad+\tfrac{1}{2}\sin^2\varphi\left(S_{10}-\tfrac{\|S_{11}\|^2}{M}-\Re\left\{e^{-2j\phi}\left(S_{12}-\tfrac{S_{11}^2}{M}\right)\right\}\right)\left(\sin^2\varphi\left(S_{20}-\tfrac{S_{23}^2}{M}\right)+\tfrac{\sin 2\varphi}{M}S_{23}\Re\{e^{-j\phi}S_{11}\}\right) \\
&\quad-\tfrac{1}{4}\sin^2\varphi\cos^2\varphi\Im^2\left\{e^{-2j\phi}\left(S_{12}-\tfrac{S_{11}^2}{M}\right)\right\}-\tfrac{1}{M^2}\sin^4\varphi S_{23}^2\Im^2\left\{e^{-j\phi}S_{11}\right\} \\
&\quad-\tfrac{1}{M}\sin^3\varphi\cos\varphi\Im\left\{e^{-2j\phi}\left(S_{12}-\tfrac{S_{11}^2}{M}\right)\right\}S_{23}\Im\left\{e^{-j\phi}S_{11}\right\} \\
&= \tfrac{1}{4}\sin^2\varphi\cos^2\varphi\left(\left(S_{10}-\tfrac{\|S_{11}\|^2}{M}\right)^2-\left\|S_{12}-\tfrac{S_{11}^2}{M}\right\|^2\right) \\
&\quad+\sin^4\varphi\left(\tfrac{1}{2}\left(S_{20}-\tfrac{S_{23}^2}{M}\right)\left(S_{10}-\tfrac{\|S_{11}\|^2}{M}-\Re\left\{e^{-2j\phi}\left(S_{12}-\tfrac{S_{11}^2}{M}\right)\right\}\right)-\tfrac{1}{M^2}S_{23}^2\Im^2\left\{e^{-j\phi}S_{11}\right\}\right) \\
&\quad+\tfrac{S_{23}}{M}\sin^3\varphi\cos\varphi \\
&\quad\times\left(\Re\{e^{-j\phi}S_{11}\}\left(S_{10}-\tfrac{\|S_{11}\|^2}{M}-\Re\left\{e^{-2j\phi}\left(S_{12}-\tfrac{S_{11}^2}{M}\right)\right\}\right)-\Im\{e^{-j\phi}S_{11}\}\Im\left\{e^{-2j\phi}\left(S_{12}-\tfrac{S_{11}^2}{M}\right)\right\}\right) \\
&= \tfrac{1}{4}\sin^2\varphi\cos^2\varphi\left(\left(S_{10}-\tfrac{\|S_{11}\|^2}{M}\right)^2-\left\|S_{12}-\tfrac{S_{11}^2}{M}\right\|^2\right) \\
&\quad+\sin^4\varphi\left(\tfrac{1}{2}S_{20}\left(S_{10}-\tfrac{\|S_{11}\|^2}{M}-\Re\left\{e^{-2j\phi}\left(S_{12}-\tfrac{S_{11}^2}{M}\right)\right\}\right)\right) \\
&\quad-\tfrac{S_{23}^2\sin^4\varphi}{M} \\
&\times\left(\tfrac{1}{2}\left(S_{10}-\tfrac{\|S_{11}\|^2}{M}-\tfrac{1}{2}\left(e^{-2j\phi}S_{12}+e^{2j\phi}S_{12}^*-\tfrac{e^{-2j\phi}S_{11}^2+e^{2j\phi}S_{11}^{2*}}{M}\right)\right)-\tfrac{e^{-2j\phi}S_{11}^2+e^{2j\phi}S_{11}^{2*}-2\|S_{11}\|^2}{4M}\right) \\
&\quad+\tfrac{S_{23}\sin^2\varphi\sin 2\varphi}{2M}\left(\tfrac{e^{-j\phi}S_{11}+e^{j\phi}S_{11}^*}{2}\right)\left(S_{10}-\tfrac{S_{11}S_{11}^*}{M}-\tfrac{e^{-2j\phi}S_{12}+e^{2j\phi}S_{12}^*}{2}+\tfrac{e^{-j\phi}S_{11}^2+e^{j\phi}S_{11}^{2*}}{2M}\right) \\
&\quad-\tfrac{S_{23}\sin^2\varphi\sin 2\varphi}{2M}\left(\tfrac{e^{-j\phi}S_{11}-e^{j\phi}S_{11}^*}{2j}\right)\left(\tfrac{e^{-2j\phi}S_{12}-e^{2j\phi}S_{12}^*}{2j}-\tfrac{e^{-2j\phi}S_{11}^2-e^{2j\phi}S_{11}^{2*}}{2jM}\right) \\
&= \tfrac{1}{4}\sin^2\varphi\cos^2\varphi\left(\left(S_{10}-\tfrac{\|S_{11}\|^2}{M}\right)^2-\left\|S_{12}-\tfrac{S_{11}^2}{M}\right\|^2\right) \\
&\quad+\sin^4\varphi\left(\tfrac{1}{2}S_{20}\left(S_{10}-\tfrac{\|S_{11}\|^2}{M}-\Re\left\{e^{-2j\phi}\left(S_{12}-\tfrac{S_{11}^2}{M}\right)\right\}\right)-\tfrac{S_{23}^2}{2M}\left(S_{10}-\Re\{e^{-2j\phi}S_{12}\}\right)\right) \\
&\quad+\tfrac{S_{23}\sin^2\varphi\sin 2\varphi}{2M}\left(S_{10}\Re\{e^{-j\phi}S_{11}\}-\Re\{e^{-j\phi}S_{12}S_{11}^*\}\right).
\end{aligned}
\tag{2.52}
$$

2.8.3 Proof of Eqn. (2.19)

Note that the sensors located on the xOy plane are such that $\xi_i = \frac{\pi}{2}$, while the sensors located on the first orthogonal axe have $\xi_i = 0$ and the sensors located on the second orthogonal axe are such that $\xi_i = \pi$. In the same way as we prove Eqn. (2.17) and (2.18), with the assumption that the two orthogonal branches are symmetric, it leads to:

$$
\sum_{i=1}^{N_2}\rho_{2,i}\cos\xi_i = \sum_{i=1}^{\frac{N_2}{2}}\rho_{2,i}\cos 0+\sum_{i=\frac{N_2}{2}+1}^{N_2}\rho_{2,i}\cos\pi = \sum_{i=1}^{\frac{N_2}{2}}\rho_{2,i}-\sum_{i=\frac{N_2}{2}+1}^{N_2}\rho_{2,i}=0. \tag{2.53}
$$

Finally it is easy obtain (2.19) from Eqn. (2.17) and (2.18) by letting $S_{23}=0$.

2.8.4 Proof of Eqn. (2.30)

Suppose that N_1 is an odd number. Since the two branches of V-shaped array are symmetric, we have:

$$\begin{aligned} S_{12} = \sum_{i=1}^{N_1} \rho_{p,i}^2 e^{-2j\varrho_i} &= \sum_{i=1}^{(N_1-1)/2} \rho_{p,i}^2 e^{-2j\frac{\Delta}{2}} + \sum_{i=1}^{(N_1-1)/2} \rho_{p,i}^2 e^{2j\frac{\Delta}{2}} \\ &= \sum_{i=1}^{(N_1-1)/2} \rho_{p,i}^2 \left(e^{-j\Delta} + e^{j\Delta}\right) \\ &= 2\cos\Delta \sum_{i=1}^{(N_1-1)/2} \rho_{p,i}^2 \\ &= S_{10}\cos\Delta, \end{aligned} \tag{2.54}$$

$$\begin{aligned} S_{11} = \sum_{i=1}^{N_1} \rho_{1,i} e^{-j\varrho_i} &= \sum_{i=1}^{(N_1-1)/2} \rho_{1,i} e^{-j\frac{\Delta}{2}} + \sum_{i=1}^{(N_1-1)/2} \rho_{1,i} e^{j\frac{\Delta}{2}} \\ &= \sum_{i=1}^{(N_1-1)/2} \rho_{p,i}^2 \left(e^{-j\frac{\Delta}{2}} + e^{j\frac{\Delta}{2}}\right) \\ &= 2\cos\tfrac{\Delta}{2} \sum_{i=1}^{(N_1-1)/2} \rho_{p,i}^2 \\ &= S_{13}\cos\tfrac{\Delta}{2}, \end{aligned} \tag{2.55}$$

$$\Im\{e^{-2j\phi}S_{12}\} = \Im\{e^{-2j\phi}S_{10}\cos\Delta\} = \frac{1}{2j}S_{10}\cos\Delta\left(e^{-2j\phi} - e^{2j\phi}\right) = -S_{10}\cos\Delta\sin 2\phi, \tag{2.56}$$

$$\Re\{e^{-2j\phi}S_{12}\} = \Re\{e^{-2j\phi}S_{10}\cos\Delta\} = \frac{1}{2}S_{10}\cos\Delta\left(e^{-2j\phi} + e^{2j\phi}\right) = S_{10}\cos\Delta\cos 2\phi, \tag{2.57}$$

$$\Re\{S_{11}e^{-j\phi}\} = \Re\{e^{-j\phi}S_{13}\cos\frac{\Delta}{2}\} = \frac{1}{2}S_{13}\cos\frac{\Delta}{2}\left(e^{-j\phi} + e^{j\phi}\right) = S_{13}\cos\frac{\Delta}{2}\cos\phi, \tag{2.58}$$

$$\Im\{e^{-j\phi}S_{11}\} = \Im\{e^{-j\phi}S_{13}\cos\frac{\Delta}{2}\} = \frac{1}{2j}S_{13}\cos\frac{\Delta}{2}\left(e^{-j\phi} - e^{j\phi}\right) = -S_{13}\cos\frac{\Delta}{2}\sin\phi, \tag{2.59}$$

$$\begin{aligned} \Re\left\{e^{-2j\phi}\left(S_{12} - \tfrac{S_{11}^2}{M}\right)\right\} &= \Re\left\{e^{-2j\phi}\left(S_{10}\cos\Delta - \tfrac{S_{13}^2\cos^2\frac{\Delta}{2}}{M}\right)\right\} \\ &= \tfrac{1}{2}\left(S_{10}\cos\Delta - \tfrac{S_{13}^2\cos^2\frac{\Delta}{2}}{M}\right)\left(e^{-2j\phi} + e^{2j\phi}\right) \\ &= \left(S_{10}\cos\Delta - \tfrac{S_{13}^2\cos^2\frac{\Delta}{2}}{M}\right)\cos 2\phi, \end{aligned} \tag{2.60}$$

and

$$\begin{aligned} \Re\{e^{-j\phi}S_{12}S_{11}^*\} &= \Re\{e^{-j\phi}S_{10}S_{13}\cos\Delta\cos\frac{\Delta}{2}\} \\ &= \frac{1}{2}S_{10}S_{13}\cos\Delta\cos\frac{\Delta}{2}\left(e^{-j\phi} + e^{j\phi}\right) \\ &= S_{10}S_{13}\cos\Delta\cos\frac{\Delta}{2}\cos\phi. \end{aligned} \tag{2.61}$$

2.8.5 Proof of Eqn. (2.38)

Applying (2.30) into (2.26), we have

$$S_{12} - \frac{S_{11}^2}{M} = S_{10}\cos\Delta - \frac{S_{13}^2\cos^2\frac{\Delta}{2}}{M} = 0.$$

Since our antenna array is made from ULA branches, then $S_{10} = \frac{N_1(N_1+1)(N_1-1)}{12}$ and $S_{13} = \frac{(N_1+1)(N_1-1)}{4}$. After some simple calculus, we obtain

$$\Delta_{iso} = \arccos\left(\frac{3N_1^2-3}{8MN_1-3N_1^2+3}\right).$$

2.8.6 Proof of Eqn. (2.40) and Eqn. (2.41)

2.8.6.1 Proof of Eqn. (2.40)

From (2.35) we have

$$\begin{aligned} K_C(M) &= \frac{\frac{2}{A_{SNR}S_{10}^{L-shaped}\sin^2\varphi}}{\frac{2}{A_{SNR}S_{10}^{Cir}\sin^2\varphi}} \\ &= \frac{12Mr^2}{N_1(N_1+1)(N_1-1)\frac{\lambda^2}{4}} \\ &= \frac{12M\frac{\lambda^2}{4\sin^2\frac{\pi}{M}}}{\alpha M(\alpha^2M^2-1)\frac{\lambda^2}{4}} \\ &= \frac{3}{\alpha(\alpha^2M^2-1)\sin^2\frac{\pi}{M}}. \end{aligned} \tag{2.62}$$

2.8.6.2 Proof of Eqn. (2.41)

From Eqn. (2.34), under isotropy condition, we have

$$S_{10}\cos\Delta_{iso} = \frac{S_{13}^2\cos^2\frac{\Delta_{iso}}{2}}{M} \Rightarrow \Delta_{iso} = \arccos\left(\frac{3N_1^2-3}{8MN_1-3N_1^2+3}\right) \Rightarrow \cos\Delta_{iso} = \frac{3N_1^2-3}{8MN_1-3N_1^2+3}.$$

Therefore, the CRB concerning the azimuth estimation of the V-shaped with two symmetric orthogonal branches is given by

$$\begin{aligned} C_{\phi\phi} &= \frac{\cos^2\varphi\left(\frac{S_{10}}{2}-\frac{S_{13}^2\cos^2\frac{\Delta_{iso}}{2}}{2M}\right)+\sin^2\varphi S_{20}}{B_{SNR}\sin^2\varphi\left\{S_{10}\cos^2\varphi\left(\frac{S_{10}\sin^2\Delta_{iso}}{4}+\frac{S_{13}^2\cos^2\frac{\Delta_{iso}}{2}(\cos\Delta_{iso}-1)}{2M}\right)+S_{20}\sin^2\varphi\left(\frac{S_{10}}{2}-\frac{S_{13}^2\cos^2\frac{\Delta_{iso}}{2}}{2M}\right)\right\}} \\ &= \frac{\cos^2\varphi\left(\frac{S_{10}}{2}-\frac{S_{10}\cos\Delta_{iso}}{2}\right)+\sin^2\varphi S_{20}}{B_{SNR}\sin^2\varphi\left\{S_{10}\cos^2\varphi\left(\frac{S_{10}\sin^2\Delta_{iso}}{4}+\frac{S_{10}\cos\Delta_{iso}(\cos\Delta_{iso}-1)}{2}\right)+S_{20}\sin^2\varphi\left(\frac{S_{10}}{2}-\frac{S_{10}\cos\Delta_{iso}}{2}\right)\right\}} \\ &= \frac{\cos^2\varphi\frac{S_{10}}{2}(1-\cos\Delta_{iso})+\sin^2\varphi S_{20}}{B_{SNR}\sin^2\varphi\left\{\frac{1}{4}S_{10}^2\cos^2\varphi(1-\cos\Delta_{iso})^2+\frac{1}{2}\sin^2\varphi S_{20}S_{10}(1-\cos\Delta_{iso})\right\}} \\ &= \frac{2}{B_{SNR}\sin^2\varphi(1-\cos\Delta_{iso})S_{10}}. \end{aligned}$$

Hence

$$
\begin{aligned}
K_U(M) &= \frac{\frac{2}{B_{SNR}\sin^2\varphi(1-\cos\Delta_{iso})S_{10}^{V-shapediso}}}{\frac{2}{B_{SNR}\sin^2\varphi S_{10}^{Cir}}} \\
&= \frac{M\frac{\frac{\lambda^2}{4}}{4\sin^2\frac{\pi}{M}}}{\frac{1}{12}(1-\cos\Delta_{iso})\alpha M(\alpha^2M^2-1)\frac{\lambda^2}{4}} \\
&= \frac{3(8\alpha M^2-3\alpha^2M^2+3)}{\sin^2\frac{\pi}{M}\alpha(\alpha^2M^2-1)(8\alpha M^2-6\alpha^2M^2+6)}.
\end{aligned} \tag{2.63}
$$

Chapter 3

Array geometry optimization based on the Weiss-Weinstein bound

3.1 Introduction

In this chapter, we consider the context of source localization in the Bayesian context. In particularly, we are interested in the Weiss-Weinstein bound which is known to be one of the tightest Bayesian bound with the bound of the Ziv-Zakai family. We will study the two main source models used in the literature [OVSN93]: the unconditional (or stochastic) model where the source signals are assumed to be Gaussian and the conditional (deterministic) model where the source signals are assumed to be deterministic. Surprisingly, in the context of array processing, while closed-form expressions of the Ziv-Zakai bound (more precisizely its extension by Bell et. al. [BEV96a]) were proposed around 15 years ago for the unconditional model, the results concerning the Weiss-Weinstein bound are, most of the time, conducted by way of simulations. Concerning the unconditional model, in [NH88], the Weiss-Weinstein bound has been evaluated by way of simulations and has been compared to the mean square error of the MUSIC algorithm and classical Beamforming using a 8×8 element array antenna. In [NV94], the authors have introduced a numerical comparison between the Bayesian Cramér-Rao bound, the Ziv-Zakai bound and the Weiss-Weinstein bound for DOA estimation. In [Ath01], numerical simulations of the Weiss-Weinstein bound to optimize sensor positions for non-uniform linear arrays have been presented. Again in the unconditional model context, in [XBR04], by considering the matched-field estimation problem, the authors have derived a semi closed-form expression of a simplified version of the Weiss-Weinstein bound for the DOA estimation. Indeed, the integration over the prior probability density function was not performed. The conditional model (with known waveforms) is studied only in [Ren07], where a closed-form expression of the WWB is given in the simple case of spectral analysis and in [VRBM10b] which is a simplified version of the bound for linear arrays.

While the primary goal of this chapter is to give closed-form expressions of the Weiss-Weinstein bound for the DOA estimation of a single source with an arbitrary planar array of sensors, under both the conditional and unconditional source signal models, we also provide partial closed-form expressions of the bound which could be useful for other problems. First, we study the general Gaussian observation model with parameterized mean or parameterized covariance matrix. Indeed, one of the success of the Cramér-Rao is that, for this observation model, a closed-form expression of the Fisher information matrix is available: this is the so-called Slepian-Bang formula [Kay93]. Such formula has been less investigated in the context of bound tighter than the Cramér-Rao bound. Second, some results are given in the multiple sources con-

text without specifying the structure of the steering matrix and of the noise covariance matrix. Finally, these results are applied to the particular case of a single source for two kinds of array geometries: the non-uniform linear array (elevation only) and the planar (azimuth and elevation) array. Consequently, the aim of this chapter is also to provide a textbook of formulas which could be applied in other fields. Moreover, note that one particularity of this chapter in comparison with the previous works on the Weiss-Weinstein bound is that we do not use the assumption $s = 1/2$, $\forall i$.

This chapter is organized as follows. Section 3.2 is devoted to the array processing observation model which will be used in the chapter. In Section 3.3, a short background on the Weiss-Weinstein bound is presented and two general closed-form expressions which will be the cornerstone for our array processing problems are derived. In Section 3.4 we apply these general results to the array processing problem without specifying the structure of the steering matrix. In Section 3.5, we study the particular case of the non-uniform linear array and of the planar array for which we provide both closed-form expressions of the bound. Some simulation results are proposed in Section 3.6. Finally, Section 3.7 gives our conclusions.

3.2 Problem setup

In this section, the general observation model generally used in array signal processing is presented as well as the first different assumptions used in the remaining of the paper. Particularly, the so-called conditional and unconditional source models are emphasized.

3.2.1 Observations model

We consider the classical scenario of an array with M sensors which receives N complex bandpass signals $\mathbf{s}(t) = [s_1(t)\ \ s_2(t) \cdots s_N(t)]^T$. The output of the array is a $M \times 1$ complex vector $\mathbf{y}(t)$ which can be modelled as follows (see, *e.g.*, [Van02a] or [OVSN93])

$$\mathbf{y}(t) = \mathbf{A}(\boldsymbol{\theta})\,\mathbf{s}(t) + \mathbf{n}(t), \qquad t = 1, \ldots, T, \tag{3.1}$$

where T is the number of snapshots, where $\boldsymbol{\theta} = [\theta_1\ \theta_2 \cdots \theta_q]^T$ is an unknown parameter vector of interest[1], where $\mathbf{A}(\boldsymbol{\theta})$ is the so-called $M \times N$ steering matrix of the array response to the sources, and where the $M \times 1$ random vector $\mathbf{n}(t)$ is an additive noise.

3.2.2 Assumptions

- The unknown parameters of interest are assumed to be random with an *a priori* probability density function $p(\theta_i)$, $i = 1, \ldots, q$. These random parameters are assumed to be statistically independent such that the *a priori* joint probability density function is $p(\boldsymbol{\theta}) = \prod_{i=1}^{q} p(\theta_i)$. We also assume that the parameter space, denoted Θ, is a connected subset of $\mathbb{R}^q$ (see [BE08]).

- The noise vector is assumed to be complex Gaussian, statistically independent of the parameters, i.i.d., circular, with zero mean and a known covariance matrix $\mathbb{E}\left[\mathbf{n}(t)\,\mathbf{n}^H(t)\right] = \mathbf{R_n}$. This assumption will be cancelled in Section 3.5 where it will be assumed that $\mathbf{R_n} = \sigma_n^2\mathbf{I}$. In any case, $\mathbf{R_n}$ is assumed to be a full rank matrix.

[1] Note that one source can be described by several parameters. Consequently, $q > N$ in general.

- The steering matrix $\mathbf{A}(\boldsymbol{\theta})$ is assumed such that the observation model is identifiable. From Section 3.3 to Section 3.4, the structure of $\mathbf{A}(\boldsymbol{\theta})$ is not specified in order to obtain the more general results.

- Concerning the source signals, we consider again the two aforementioned models $\mathcal{M}_1$ and $\mathcal{M}_2$ introduced in chapter 2.

3.2.3 Likelihood of the observations

Let $\mathbf{R}_{\mathbf{y}} = \mathbb{E}\left[\mathbf{y}(t)\,\mathbf{y}^H(t)\right]$ be the covariance matrix of the observation vector $\mathbf{y}(t)$. According to the aforementioned assumptions, it is easy to see that under $\mathcal{M}_2$, the observations $\mathbf{y}(t)$ are distributed as a complex circular Gaussian random vector with zero mean and covariance matrix $\mathbf{R}_{\mathbf{y}}(\boldsymbol{\theta}) = \mathbf{A}(\boldsymbol{\theta})\mathbf{R}_{\mathbf{s}}\mathbf{A}^H(\boldsymbol{\theta}) + \mathbf{R}_{\mathbf{n}}$ while under $\mathcal{M}_1$, the observations $\mathbf{y}(t)$ are distributed as a complex circular Gaussian random vector with mean $\mathbf{A}(\boldsymbol{\theta})\mathbf{s}(t)$ and covariance matrix $\mathbf{R}_{\mathbf{y}} = \mathbf{R}_{\mathbf{n}}$. Moreover, in both cases the observations are *i.i.d.*.

Therefore, the likelihood, $p(\mathbf{y};\boldsymbol{\theta})$, of the full observations matrix $\mathbf{y} = [\mathbf{y}(1)\ \ \mathbf{y}(2)\ \ \ldots\ \ \mathbf{y}(T)]$ under $\mathcal{M}_1$ is given by

$$p(\mathbf{y};\boldsymbol{\theta}) = \frac{1}{\pi^{MT}\left|\mathbf{R}_{\mathbf{n}}\right|^T}\exp\left(-\sum_{t=1}^{T}\left(\mathbf{y}(t) - \mathbf{A}(\boldsymbol{\theta})\,\mathbf{s}(t)\right)^H\mathbf{R}_{\mathbf{n}}^{-1}\left(\mathbf{y}(t) - \mathbf{A}(\boldsymbol{\theta})\,\mathbf{s}(t)\right)\right), \tag{3.2}$$

and the likelihood under $\mathcal{M}_2$ is given by

$$p(\mathbf{y};\boldsymbol{\theta}) = \frac{1}{\pi^{MT}\left|\mathbf{R}_{\mathbf{y}}(\boldsymbol{\theta})\right|^T}\exp\left(-\sum_{t=1}^{T}\mathbf{y}(t)^H\mathbf{R}_{\mathbf{y}}^{-1}(\boldsymbol{\theta})\mathbf{y}(t)\right), \tag{3.3}$$

where $\mathbf{R}_{\mathbf{y}}(\boldsymbol{\theta}) = \mathbf{A}(\boldsymbol{\theta})\mathbf{R}_{\mathbf{s}}\mathbf{A}^H(\boldsymbol{\theta}) + \mathbf{R}_{\mathbf{n}}$.

3.3 Weiss-Weinstein bound: Generalities

In this Section, we first remind to the reader the structure of the Weiss-Weinstein bound on the mean square error and the assumptions used to compute this bound. Second, a general result about the Gaussian observation model with parameterized mean or parameterized covariance matrix which, to the best of our knowledge, does not appear in the literature is presented. This result will be useful for the study of the unconditional model $\mathcal{M}_2$ and of the conditional model $\mathcal{M}_1$ in the next Section.

3.3.1 Background

The Weiss-Weinstein bound for a $q \times 1$ real parameter vector $\boldsymbol{\theta}$ is a $q \times q$ matrix denoted **WWB** and is given as follows [WW88]

$$\mathbf{WWB} = \mathbf{H}\mathbf{G}^{-1}\mathbf{H}^T, \tag{3.4}$$

where the $q \times q$ matrix $\mathbf{H} = [\mathbf{h}_1\ \mathbf{h}_2 \ldots \mathbf{h}_q]$ contains the so-called test-points $\mathbf{h}_i$, $i = 1, \ldots, q$ such that $\boldsymbol{\theta} + \mathbf{h}_i \in \Theta\ \forall \mathbf{h}_i$. The $k,l-$element of the $q \times q$ matrix $\mathbf{G}$ is given by

$$\{\mathbf{G}\}_{k,l} = \frac{\mathbb{E}\left[\left(L^{s_k}(\mathbf{y};\boldsymbol{\theta}+\mathbf{h}_k,\boldsymbol{\theta}) - L^{1-s_k}(\mathbf{y};\boldsymbol{\theta}-\mathbf{h}_k,\boldsymbol{\theta})\right)\left(L^{s_l}(\mathbf{y};\boldsymbol{\theta}+\mathbf{h}_l,\boldsymbol{\theta}) - L^{1-s_l}(\mathbf{y};\boldsymbol{\theta}-\mathbf{h}_l,\boldsymbol{\theta})\right)\right]}{\mathbb{E}\left[L^{s_k}(\mathbf{y};\boldsymbol{\theta}+\mathbf{h}_k,\boldsymbol{\theta})\right]\mathbb{E}\left[L^{s_l}(\mathbf{y};\boldsymbol{\theta}+\mathbf{h}_l,\boldsymbol{\theta})\right]}, \tag{3.5}$$

where the expectations are taken over the joint probability density function $p(\mathbf{Y},\boldsymbol{\theta})$ and where the function $L(\mathbf{Y};\boldsymbol{\theta}+\mathbf{h}_i,\boldsymbol{\theta})$ is defined by $L(\mathbf{y};\boldsymbol{\theta}+\mathbf{h}_i,\boldsymbol{\theta})=\frac{p(\mathbf{Y},\boldsymbol{\theta}+\mathbf{h}_i)}{p(\mathbf{Y},\boldsymbol{\theta})}$. The elements s_i are such that $s_i\in[0,1]$, $i=1,\ldots,q$.

Note that we have the following order relation [WW88]

$$\mathbf{Cov}\left(\hat{\boldsymbol{\theta}}\right)=\mathbb{E}\left[\left(\hat{\boldsymbol{\theta}}-\boldsymbol{\theta}\right)\left(\hat{\boldsymbol{\theta}}-\boldsymbol{\theta}\right)^T\right]\succeq\mathbf{WWB}, \tag{3.6}$$

where $\mathbf{A}\succeq\mathbf{B}$ means that the matrix $(\mathbf{A}-\mathbf{B})$ is a semi-positive definite matrix and where $\mathbf{Cov}\left(\hat{\boldsymbol{\theta}}\right)$ is the global (the expectation is taken over the joint pdf $p(\mathbf{Y},\boldsymbol{\theta})$) mean square error of any estimator $\hat{\boldsymbol{\theta}}$ of the parameter vector $\boldsymbol{\theta}$. Finally, in order to obtain a tight bound, one has to maximize $\mathbf{WWB}$ over the test-points $\mathbf{h}_i$ and s_i $i=1,\ldots,q$. Note that this maximization can be done by using the trace of $\mathbf{HG}^{-1}\mathbf{H}^T$ or with respect to the Loewner partial ordering [LRNM10]. In this chapter we will use the trace of $\mathbf{HG}^{-1}\mathbf{H}^T$ which is enough to obtain tight results.

3.3.2 A general result on the Weiss-Weinstein bound and its application to the Gaussian observation models

An analytical result on the Weiss-Weinstein bound which will be useful in the following derivations and which could be useful for other problems is derived in this part. Note that this result is independent of the parameter vector size q and of the considered observation model.

Let us denote Ω the observation space. By rewriting the elements of matrix $\mathbf{G}$ (see Eqn. (3.5)) involved in the Weiss-Weinstein bound, one obtains for the numerator denoted $N_{\{\mathbf{G}\}_{k,l}}$,

$$\begin{aligned}
&N_{\{\mathbf{G}\}_{k,l}}=\\
&=\mathbb{E}\left[\left(L^{s_k}(\mathbf{y};\boldsymbol{\theta}+\mathbf{h}_k,\boldsymbol{\theta})-L^{1-s_k}(\mathbf{y};\boldsymbol{\theta}-\mathbf{h}_k,\boldsymbol{\theta})\right)\left(L^{s_l}(\mathbf{y};\boldsymbol{\theta}+\mathbf{h}_l,\boldsymbol{\theta})-L^{1-s_l}(\mathbf{y};\boldsymbol{\theta}-\mathbf{h}_l,\boldsymbol{\theta})\right)\right]\\
&=\int_{\Theta}\int_{\Omega}\frac{p^{s_k}(\mathbf{y},\boldsymbol{\theta}+\mathbf{h}_k)\,p^{s_l}(\mathbf{y},\boldsymbol{\theta}+\mathbf{h}_l)}{p^{s_k+s_l-1}(\mathbf{y},\boldsymbol{\theta})}d\mathbf{y}d\boldsymbol{\theta}+\int_{\Theta}\int_{\Omega}\frac{p^{1-s_k}(\mathbf{y},\boldsymbol{\theta}-\mathbf{h}_k)\,p^{1-s_l}(\mathbf{y},\boldsymbol{\theta}-\mathbf{h}_l)}{p^{1-s_k-s_l}(\mathbf{y},\boldsymbol{\theta})}d\mathbf{y}d\boldsymbol{\theta}\\
&-\int_{\Theta}\int_{\Omega}\frac{p^{s_k}(\mathbf{y},\boldsymbol{\theta}+\mathbf{h}_k)\,p^{1-s_l}(\mathbf{y},\boldsymbol{\theta}-\mathbf{h}_l)}{p^{s_k-s_l}(\mathbf{y},\boldsymbol{\theta})}d\mathbf{y}d\boldsymbol{\theta}-\int_{\Theta}\int_{\Omega}\frac{p^{1-s_k}(\mathbf{y},\boldsymbol{\theta}-\mathbf{h}_k)\,p^{s_l}(\mathbf{y},\boldsymbol{\theta}+\mathbf{h}_l)}{p^{s_l-s_k}(\mathbf{y},\boldsymbol{\theta})}d\mathbf{y}d\boldsymbol{\theta},
\end{aligned} \tag{3.7}$$

and for the denominator denoted $D_{\{\mathbf{G}\}_{k,l}}$,

$$\begin{aligned}
D_{\{\mathbf{G}\}_{k,l}}&=\mathbb{E}\left[L^{s_k}(\mathbf{y};\boldsymbol{\theta}+\mathbf{h}_k,\boldsymbol{\theta})\right]\mathbb{E}\left[L^{s_l}(\mathbf{y};\boldsymbol{\theta}+\mathbf{h}_l,\boldsymbol{\theta})\right]\\
&=\int_{\Theta}\int_{\Omega}\frac{p^{s_k}(\mathbf{y},\boldsymbol{\theta}+\mathbf{h}_k)}{p^{s_k-1}(\mathbf{y},\boldsymbol{\theta})}d\mathbf{y}d\boldsymbol{\theta}\int_{\Theta}\int_{\Omega}\frac{p^{s_l}(\mathbf{y},\boldsymbol{\theta}+\mathbf{h}_l)}{p^{s_l-1}(\mathbf{y},\boldsymbol{\theta})}d\mathbf{y}d\boldsymbol{\theta}.
\end{aligned} \tag{3.8}$$

Let us now define a function $\eta(\alpha,\beta,\mathbf{u},\mathbf{v})$ as

$$\eta(\alpha,\beta,\mathbf{u},\mathbf{v})=\int_{\Theta}\int_{\Omega}\frac{p^{\alpha}(\mathbf{y},\boldsymbol{\theta}+\mathbf{u})\,p^{\beta}(\mathbf{y},\boldsymbol{\theta}+\mathbf{v})}{p^{\alpha+\beta-1}(\mathbf{y},\boldsymbol{\theta})}d\mathbf{y}d\boldsymbol{\theta}, \tag{3.9}$$

where $(\alpha,\beta)\in[0,1]^2$ and where $(\mathbf{u},\mathbf{v})$ are two $q\times 1$ vectors such that $\boldsymbol{\theta}+\mathbf{u}\in\Theta$ and $\boldsymbol{\theta}+\mathbf{v}\in\Theta$. By identification, it is easy to see that

$$\{\mathbf{G}\}_{k,l}=\frac{\eta\left(s_k,s_l,\mathbf{h}_k,\mathbf{h}_l\right)+\eta\left(1-s_k,1-s_l,-\mathbf{h}_k,-\mathbf{h}_l\right)-\eta\left(s_k,1-s_l,\mathbf{h}_k,-\mathbf{h}_l\right)-\eta\left(1-s_k,s_l,-\mathbf{h}_k,\mathbf{h}_l\right)}{\eta\left(s_k,0,\mathbf{h}_k,\mathbf{0}\right)\eta\left(0,s_l,\mathbf{0},\mathbf{h}_l\right)}. \tag{3.10}$$

Note that we choose the arbitrary notation $D_{\{\mathbf{G}\}_{k,l}}=\eta\left(s_k,0,\mathbf{h}_k,\mathbf{0}\right)\eta\left(0,s_l,\mathbf{0},\mathbf{h}_l\right)$ for the denominator. The notation $D_{\{\mathbf{G}\}_{k,l}}=\eta\left(s_k,1,\mathbf{h}_i,\mathbf{0}\right)\eta\left(1,s_l,\mathbf{0},\mathbf{h}_l\right)$ or, even, $D_{\{\mathbf{G}\}_{k,l}}=\eta\left(s_k,0,\mathbf{h}_k,\mathbf{v}\right)\times\eta\left(0,s_l,\mathbf{u},\mathbf{h}_l\right)$ will lead to the same result.

With Eqn. (3.10), it is clear that the knowledge of $\eta\left(\alpha,\beta,\mathbf{u},\mathbf{v}\right)$ for a particular problem leads to the Weiss-Weinstein bound (without the maximization procedure over the test-points and over the parameters s_i). Surprisingly, this simple expression is given in [WW88] only for $s_i=\frac{1}{2}$, $\forall i$ and not for the general case.

Let us now detail this function $\eta\left(\alpha,\beta,\mathbf{u},\mathbf{v}\right)$. Thanks to the Bayes rule, the function $\eta\left(\alpha,\beta,\mathbf{u},\mathbf{v}\right)$ can be rewritten

$$\begin{aligned}\eta\left(\alpha,\beta,\mathbf{u},\mathbf{v}\right)&=\int_{\Theta}\frac{p^{\alpha}\left(\boldsymbol{\theta}+\mathbf{u}\right)p^{\beta}\left(\boldsymbol{\theta}+\mathbf{v}\right)}{p^{\alpha+\beta-1}\left(\boldsymbol{\theta}\right)}\int_{\Omega}\frac{p^{\alpha}\left(\mathbf{y};\boldsymbol{\theta}+\mathbf{u}\right)p^{\beta}\left(\mathbf{y};\boldsymbol{\theta}+\mathbf{v}\right)}{p^{\alpha+\beta-1}\left(\mathbf{y};\boldsymbol{\theta}\right)}d\mathbf{y}d\boldsymbol{\theta}\\&=\int_{\Theta}\acute{\eta}_{\boldsymbol{\theta}}\left(\alpha,\beta,\mathbf{u},\mathbf{v}\right)\frac{p^{\alpha}\left(\boldsymbol{\theta}+\mathbf{u}\right)p^{\beta}\left(\boldsymbol{\theta}+\mathbf{v}\right)}{p^{\alpha+\beta-1}\left(\boldsymbol{\theta}\right)}d\boldsymbol{\theta},\end{aligned} \tag{3.11}$$

where we define

$$\acute{\eta}_{\boldsymbol{\theta}}\left(\alpha,\beta,\mathbf{u},\mathbf{v},\boldsymbol{\theta}\right)=\int_{\Omega}\frac{p^{\alpha}\left(\mathbf{y};\boldsymbol{\theta}+\mathbf{u}\right)p^{\beta}\left(\mathbf{y};\boldsymbol{\theta}+\mathbf{v}\right)}{p^{\alpha+\beta-1}\left(\mathbf{y};\boldsymbol{\theta}\right)}d\mathbf{y}. \tag{3.12}$$

Our aim is to give the most general result. Consequently, we will focus only on $\acute{\eta}_{\boldsymbol{\theta}}\left(\alpha,\beta,\mathbf{u},\mathbf{v}\right)$ since the *a priori* probability density function depends on the considered problem.

3.3.2.1 Gaussian observation model with parameterized mean

One calls (circular, i.i.d.) the Gaussian observation model with a parameterized mean, a model such that the observations $\mathbf{y}\left(t\right)\sim\mathbb{C}\mathcal{N}\left(\mathbf{f}\left(\boldsymbol{\theta}\right),\mathbf{R}_{\mathbf{y}}\right)$ where $\boldsymbol{\theta}$ contains the parameters of interest. Note that $\mathcal{M}_1$ is a special case of this model since the parameters of interest appear only in the mean of the observations which has the following particular structure $\mathbf{f}\left(\boldsymbol{\theta}\right)=\mathbf{A}(\boldsymbol{\theta})\mathbf{s}\left(t\right)$ (and $\mathbf{R}_{\mathbf{y}}=\mathbf{R}_{\mathbf{n}}$). For notational convenience, we do not emphasize the dependence of $\mathbf{f}\left(\boldsymbol{\theta}\right)$ on t. The closed-form expression of $\acute{\eta}_{\boldsymbol{\theta}}\left(\alpha,\beta,\mathbf{u},\mathbf{v}\right)$ is given in this case by

$$\begin{aligned}\ln\acute{\eta}_{\boldsymbol{\theta}}\left(\alpha,\beta,\mathbf{u},\mathbf{v}\right)=-\sum_{t=1}^{T}&\alpha\left(1-\alpha\right)\mathbf{f}^{H}\left(\boldsymbol{\theta}+\mathbf{u}\right)\mathbf{R}_{\mathbf{y}}^{-1}\mathbf{f}\left(\boldsymbol{\theta}+\mathbf{u}\right)+\beta\left(1-\beta\right)\mathbf{f}^{H}\left(\boldsymbol{\theta}+\mathbf{v}\right)\mathbf{R}_{\mathbf{y}}^{-1}\mathbf{f}\left(\boldsymbol{\theta}+\mathbf{v}\right)\\&+\left(1-\alpha-\beta\right)\left(\alpha+\beta\right)\mathbf{f}^{H}\left(\boldsymbol{\theta}\right)\mathbf{R}_{\mathbf{y}}^{-1}\mathbf{f}\left(\boldsymbol{\theta}\right)-2\,\mathrm{Re}\left\{\alpha\beta\mathbf{f}^{H}\left(\boldsymbol{\theta}+\mathbf{u}\right)\mathbf{R}_{\mathbf{y}}^{-1}\mathbf{f}\left(\boldsymbol{\theta}+\mathbf{v}\right)\right.\\&\left.+\alpha\left(1-\alpha-\beta\right)\mathbf{f}^{H}\left(\boldsymbol{\theta}+\mathbf{u}\right)\mathbf{R}_{\mathbf{y}}^{-1}\mathbf{f}\left(\boldsymbol{\theta}\right)+\beta\left(1-\alpha-\beta\right)\mathbf{f}^{H}\left(\boldsymbol{\theta}+\mathbf{v}\right)\mathbf{R}_{\mathbf{y}}^{-1}\mathbf{f}\left(\boldsymbol{\theta}\right)\right\},\end{aligned} \tag{3.13}$$

or equivalently by

$$\begin{aligned}\ln \acute{\eta}_{\boldsymbol{\theta}}(\alpha,\beta,\mathbf{u},\mathbf{v}) = -\sum_{t=1}^{T} & \alpha(1-\alpha-\beta)\left\|\mathbf{R}_{\mathbf{y}}^{-1/2}(\mathbf{f}(\boldsymbol{\theta}+\mathbf{u})-\mathbf{f}(\boldsymbol{\theta}))\right\|^2 \\ & +\alpha\beta\left\|\mathbf{R}_{\mathbf{y}}^{-1/2}(\mathbf{f}(\boldsymbol{\theta}+\mathbf{u})-\mathbf{f}(\boldsymbol{\theta}+\mathbf{v}))\right\|^2 \\ & +\beta(1-\alpha-\beta)\left\|\mathbf{R}_{\mathbf{y}}^{-1/2}(\mathbf{f}(\boldsymbol{\theta}+\mathbf{v})-\mathbf{f}(\boldsymbol{\theta}))\right\|^2. \end{aligned} \tag{3.14}$$

The details are given in Appendix 3.8.1.

3.3.2.2 Gaussian observation model with parameterized covariance matrix

One calls (circular, i.i.d.) the Gaussian observation model with a parameterized covariance matrix, a model such that the observations $\mathbf{y}(t) \sim \mathbb{C}\mathcal{N}(\mathbf{0}, \mathbf{R}_{\mathbf{y}}(\boldsymbol{\theta}))$ where $\boldsymbol{\theta}$ are the parameters of interest. Note that $\mathcal{M}_2$ is a special case of this model since the parameters of interest appear only in the covariance matrix of the observations which has the following particular structure $\mathbf{R}_{\mathbf{y}}(\boldsymbol{\theta}) = \mathbf{A}(\boldsymbol{\theta})\mathbf{R}_{\mathbf{s}}\mathbf{A}^H(\boldsymbol{\theta}) + \mathbf{R}_{\mathbf{n}}$. The closed-form expression of $\acute{\eta}_{\boldsymbol{\theta}}(\alpha,\beta,\mathbf{u},\mathbf{v})$ is given by:

$$\acute{\eta}_{\boldsymbol{\theta}}(\alpha,\beta,\mathbf{u},\mathbf{v}) = \frac{|\mathbf{R}_{\mathbf{y}}(\boldsymbol{\theta})|^{T(\alpha+\beta-1)}}{|\mathbf{R}_{\mathbf{y}}(\boldsymbol{\theta}+\mathbf{u})|^{T\alpha}\,|\mathbf{R}_{\mathbf{y}}(\boldsymbol{\theta}+\mathbf{v})|^{T\beta}\left|\alpha\mathbf{R}_{\mathbf{y}}^{-1}(\boldsymbol{\theta}+\mathbf{u})+\beta\mathbf{R}_{\mathbf{y}}^{-1}(\boldsymbol{\theta}+\mathbf{v})-(\alpha+\beta-1)\mathbf{R}_{\mathbf{y}}^{-1}(\boldsymbol{\theta})\right|^{T}}. \tag{3.15}$$

The proof is given in Appendix 3.8.2.

3.4 General application to array processing

In the previous Section, it has been shown that the Weiss-Weinstein bound computation (or, at least, the matrix $\mathbf{G}$ computation) is reduced to the knowledge of the function $\eta(\alpha,\beta,\mathbf{u},\mathbf{v})$ given by Eqn. (3.9). As one can see in Eqn. (3.10), the elements of the matrix $\mathbf{G}$ depend on $\eta(\alpha,\beta,\mathbf{u},\mathbf{v})$ for particular values of α, β, $\mathbf{u}$, and $\mathbf{v}$. Consequently, the goal of this Section is to detail these particular functions for our model given by Eqn. (3.1). Since Eqn. (3.9) can be decomposed into a *deterministic part* (in the sense where $\acute{\eta}_{\boldsymbol{\theta}}(\alpha,\beta,\mathbf{u},\mathbf{v})$ (see Eqn. (3.12)) only depends on the likelihood function) and a *Bayesian part* (when we have to integrate $\acute{\eta}_{\boldsymbol{\theta}}(\alpha,\beta,\mathbf{u},\mathbf{v})$ over the *a priori* probability density function of the parameters), we will first focus on the particular functions $\acute{\eta}_{\boldsymbol{\theta}}(\alpha,\beta,\mathbf{u},\mathbf{v})$ by using the results of the previous Section on the Gaussian observation model with the parameterized mean or covariance matrix. Second, we will detail the passage from $\acute{\eta}_{\boldsymbol{\theta}}(\alpha,\beta,\mathbf{u},\mathbf{v})$ to $\eta(\alpha,\beta,\mathbf{u},\mathbf{v})$ in the particular case where $p(\theta_i)$ is a uniform probability density function $\forall i$. Another result will also be given in the case of a Gaussian prior.

3.4.1 Analysis of $\acute{\eta}_{\boldsymbol{\theta}}(\alpha,\beta,\mathbf{u},\mathbf{v})$

We will now detail the particular functions $\acute{\eta}_{\boldsymbol{\theta}}(\alpha,\beta,\mathbf{u},\mathbf{v})$ involved in the different elements of $\{\mathbf{G}\}_{k,l}$, $k,l \in \{1,q\}^2$ for both models $\mathcal{M}_2$ and $\mathcal{M}_1$.

3.4.1.1 Conditional observation model $\mathcal{M}_1$

Under the conditional model $\mathcal{M}_1$, by using Eqn. (3.14) with $\mathbf{f}(\boldsymbol{\theta}) = \mathbf{A}(\boldsymbol{\theta})\mathbf{s}(t)$ and $\mathbf{R}_{\mathbf{y}} = \mathbf{R}_{\mathbf{n}}$ one obtains straightforwardly the functions $\acute{\eta}_{\boldsymbol{\theta}}(\alpha,\beta,\mathbf{u},\mathbf{v})$ involved in the elements $\{\mathbf{G}\}_{k,l} = \{\mathbf{G}\}_{l,k}$

$$\begin{cases} \ln \acute{\eta}_{\boldsymbol{\theta}}(s_k, s_l, \mathbf{h}_k, \mathbf{h}_l) = s_k(s_k+s_l-1)\,\zeta_{\boldsymbol{\theta}}(\mathbf{h}_k, \mathbf{0}) + s_l(s_k+s_l-1)\,\zeta_{\boldsymbol{\theta}}(\mathbf{h}_l, \mathbf{0}) - s_k s_l \zeta_{\boldsymbol{\theta}}(\mathbf{h}_k, \mathbf{h}_l), \\ \ln \acute{\eta}_{\boldsymbol{\theta}}(1-s_k, 1-s_l, -\mathbf{h}_k, -\mathbf{h}_l) = (s_k-1)(s_k+s_l-1)\,\zeta_{\boldsymbol{\theta}}(-\mathbf{h}_k, \mathbf{0}) \\ \qquad + (s_l-1)(s_k+s_l-1)\,\zeta_{\boldsymbol{\theta}}(-\mathbf{h}_l, \mathbf{0}) - (1-s_k)(1-s_l)\,\zeta_{\boldsymbol{\theta}}(-\mathbf{h}_k, -\mathbf{h}_l), \\ \ln \acute{\eta}_{\boldsymbol{\theta}}(s_k, 1-s_l, \mathbf{h}_k, -\mathbf{h}_l) = s_k(s_k-s_l)\,\zeta_{\boldsymbol{\theta}}(\mathbf{h}_k, \mathbf{0}) + (1-s_l)(s_k-s_l)\,\zeta_{\boldsymbol{\theta}}(-\mathbf{h}_l, \mathbf{0}) \\ \qquad + s_k(s_l-1)\,\zeta_{\boldsymbol{\theta}}(\mathbf{h}_k, -\mathbf{h}_l), \\ \ln \acute{\eta}_{\boldsymbol{\theta}}(1-s_k, s_l, -\mathbf{h}_k, \mathbf{h}_l) = (s_k-1)(s_k-s_l)\,\zeta_{\boldsymbol{\theta}}(-\mathbf{h}_k, \mathbf{0}) + s_l(s_l-s_k)\,\zeta_{\boldsymbol{\theta}}(\mathbf{h}_l, \mathbf{0}) \\ \qquad + (s_k-1)\,s_l \zeta_{\boldsymbol{\theta}}(-\mathbf{h}_k, \mathbf{h}_l), \\ \ln \acute{\eta}_{\boldsymbol{\theta}}(s_k, 0, \mathbf{h}_k, \mathbf{0}) = s_k(s_k-1)\,\zeta_{\boldsymbol{\theta}}(\mathbf{h}_k, \mathbf{0}), \\ \ln \acute{\eta}_{\boldsymbol{\theta}}(0, s_l, \mathbf{0}, \mathbf{h}_l) = s_l(s_l-1)\,\zeta_{\boldsymbol{\theta}}(\mathbf{h}_l, \mathbf{0}), \end{cases} \tag{3.16}$$

where we define

$$\zeta_{\boldsymbol{\theta}}(\boldsymbol{\mu}, \boldsymbol{\rho}) = \sum_{t=1}^{T} \left\| \mathbf{R}_{\mathbf{n}}^{-1/2} \left(\mathbf{A}(\boldsymbol{\theta}+\boldsymbol{\mu}) - \mathbf{A}(\boldsymbol{\theta}+\boldsymbol{\rho}) \right) \mathbf{s}(t) \right\|^2. \tag{3.17}$$

The diagonal elements of $\mathbf{G}$ are obtained by letting $k = l$ in the above equations. Note that, since we are working on matrix $\mathbf{G}$, all the previously proposed results are made whatever the number of test-points.

3.4.1.2 Unconditional observation model $\mathcal{M}_2$

Under the unconditional model $\mathcal{M}_2$, by using Eqn. (3.15), one obtains straightforwardly the functions $\acute{\eta}_{\boldsymbol{\theta}}(\alpha, \beta, \mathbf{u}, \mathbf{v})$ involved in the elements $\{\mathbf{G}\}_{k,l} = \{\mathbf{G}\}_{l,k}$

$$\begin{cases} \acute{\eta}_{\boldsymbol{\theta}}(s_k, s_l, \mathbf{h}_k, \mathbf{h}_l) = \dfrac{|\mathbf{R}_{\mathbf{y}}(\boldsymbol{\theta})|^{T(s_k+s_l-1)}}{|\mathbf{R}_{\mathbf{y}}(\boldsymbol{\theta}+\mathbf{h}_k)|^{Ts_k} |\mathbf{R}_{\mathbf{y}}(\boldsymbol{\theta}+\mathbf{h}_l)|^{Ts_l} \left| s_k \mathbf{R}_{\mathbf{y}}^{-1}(\boldsymbol{\theta}+\mathbf{h}_k) + s_l \mathbf{R}_{\mathbf{y}}^{-1}(\boldsymbol{\theta}+\mathbf{h}_l) - (s_k+s_l-1)\mathbf{R}_{\mathbf{y}}^{-1}(\boldsymbol{\theta}) \right|^T}, \\ \acute{\eta}_{\boldsymbol{\theta}}(1-s_k, 1-s_l, -\mathbf{h}_k, -\mathbf{h}_l) = \dfrac{|\mathbf{R}_{\mathbf{y}}(\boldsymbol{\theta})|^{T(1-s_k-s_l)} |\mathbf{R}_{\mathbf{y}}(\boldsymbol{\theta}-\mathbf{h}_k)|^{T(s_k-1)} |\mathbf{R}_{\mathbf{y}}(\boldsymbol{\theta}-\mathbf{h}_l)|^{T(s_l-1)}}{\left| (1-s_k)\mathbf{R}_{\mathbf{y}}^{-1}(\boldsymbol{\theta}-\mathbf{h}_k) + (1-s_l)\mathbf{R}_{\mathbf{y}}^{-1}(\boldsymbol{\theta}-\mathbf{h}_l) - (1-s_k-s_l)\mathbf{R}_{\mathbf{y}}^{-1}(\boldsymbol{\theta}) \right|^T}, \\ \acute{\eta}_{\boldsymbol{\theta}}(s_k, 1-s_l, \mathbf{h}_k, -\mathbf{h}_l) = \dfrac{|\mathbf{R}_{\mathbf{y}}(\boldsymbol{\theta})|^{T(s_k-s_l)} |\mathbf{R}_{\mathbf{y}}(\boldsymbol{\theta}-\mathbf{h}_l)|^{T(s_l-1)}}{|\mathbf{R}_{\mathbf{y}}(\boldsymbol{\theta}+\mathbf{h}_k)|^{Ts_k} \left| s_k \mathbf{R}_{\mathbf{y}}^{-1}(\boldsymbol{\theta}+\mathbf{h}_k) + (1-s_l)\mathbf{R}_{\mathbf{y}}^{-1}(\boldsymbol{\theta}-\mathbf{h}_l) - (s_k-s_l)\mathbf{R}_{\mathbf{y}}^{-1}(\boldsymbol{\theta}) \right|^T}, \\ \acute{\eta}_{\boldsymbol{\theta}}(1-s_k, s_l, -\mathbf{h}_k, \mathbf{h}_l) = \dfrac{|\mathbf{R}_{\mathbf{y}}(\boldsymbol{\theta})|^{T(s_l-s_k)} |\mathbf{R}_{\mathbf{y}}(\boldsymbol{\theta}-\mathbf{h}_k)|^{T(s_k-1)}}{|\mathbf{R}_{\mathbf{y}}(\boldsymbol{\theta}+\mathbf{h}_l)|^{Ts_l} \left| (1-s_k)\mathbf{R}_{\mathbf{y}}^{-1}(\boldsymbol{\theta}-\mathbf{h}_k) + s_l \mathbf{R}_{\mathbf{y}}^{-1}(\boldsymbol{\theta}+\mathbf{h}_l) - (s_l-s_k)\mathbf{R}_{\mathbf{y}}^{-1}(\boldsymbol{\theta}) \right|^T}, \\ \acute{\eta}_{\boldsymbol{\theta}}(s_k, 0, \mathbf{h}_k, \mathbf{0}) = \dfrac{|\mathbf{R}_{\mathbf{y}}(\boldsymbol{\theta})|^{T(s_k-1)}}{|\mathbf{R}_{\mathbf{y}}(\boldsymbol{\theta}+\mathbf{h}_k)|^{Ts_k} \left| s_k \mathbf{R}_{\mathbf{y}}^{-1}(\boldsymbol{\theta}+\mathbf{h}_k) - (s_k-1)\mathbf{R}_{\mathbf{y}}^{-1}(\boldsymbol{\theta}) \right|^T}, \\ \acute{\eta}_{\boldsymbol{\theta}}(0, s_l, \mathbf{0}, \mathbf{h}_l) = \dfrac{|\mathbf{R}_{\mathbf{y}}(\boldsymbol{\theta})|^{T(s_l-1)}}{|\mathbf{R}_{\mathbf{y}}(\boldsymbol{\theta}+\mathbf{h}_l)|^{Ts_l} \left| s_l \mathbf{R}_{\mathbf{y}}^{-1}(\boldsymbol{\theta}+\mathbf{h}_l) - (s_l-1)\mathbf{R}_{\mathbf{y}}^{-1}(\boldsymbol{\theta}) \right|^T}. \end{cases} \tag{3.18}$$

The diagonal elements of $\mathbf{G}$ are obtained by letting $k = l$ in the above equations.

3.4.2 Analysis of $\eta(\alpha, \beta, \mathbf{u}, \mathbf{v})$ with a uniform prior

Of course, the analysis of $\eta(\alpha, \beta, \mathbf{u}, \mathbf{v})$ given by Eqn. (3.11) can only be conducted by specifying the *a priori* probability density functions of the parameters. Consequently, the results provided here are very specific. However, note that, in general, this aspect is less emphasized in the literature where most of the authors give results without specifying the prior probability density functions and compute numerically the "remain" of the bound (see e.g., [XBR04] [BEV96a]).

We assume that all the parameters θ_i have a uniform prior distribution over the interval $[a_i, b_i]$ and are statistically independent. We will also assume one test-point per parameter, otherwise there is no possibility to obtain (pseudo) closed-form expressions. Consequently, the matrix $\mathbf{H}$ is such that

$$\mathbf{H} = Diag([h_1\ h_2 \cdots h_q]), \tag{3.19}$$

and vector $\mathbf{h}_i$, $i = 1, \ldots, q$, takes the value h_i at the i^{th} row and zero elsewhere. So, in this analysis, vector $\mathbf{u}$ takes the value u_i at the i^{th} row and zero elsewhere and vector $\mathbf{v}$ takes the value v_j at the j^{th} row and zero elsewhere (of course, we can have $i = j$). Under these assumptions, $\eta(\alpha, \beta, \mathbf{u}, \mathbf{v})$ can be rewritten for $i \neq j$

$$\begin{aligned}\eta(\alpha,\beta,\mathbf{u},\mathbf{v}) &= \int_{\Theta} \acute{\eta}_{\boldsymbol{\theta}}(\alpha,\beta,\mathbf{u},\mathbf{v}) \frac{p^{\alpha}(\theta_i+u_i)\, p^{\beta}(\theta_j+v_j)\, p^{\beta}(\theta_i)\, p^{\alpha}(\theta_j)}{p^{\alpha+\beta-1}(\theta_i)\, p^{\alpha+\beta-1}(\theta_j)} \prod_{\substack{k=1 \\ k\neq i, k\neq j}}^{q} p(\theta_k)\, d\boldsymbol{\theta} \\ &= \frac{1}{\prod_{k=1}^{q}(b_k-a_k)} \int_{\Theta^{q-2}} \int_{\Theta_j} \int_{\Theta_i} \acute{\eta}_{\boldsymbol{\theta}}(\alpha,\beta,\mathbf{u},\mathbf{v})\, d\theta_i d\theta_j d(\boldsymbol{\theta}/\{\theta_i,\theta_j\}), \end{aligned} \tag{3.20}$$

where $\Theta_i = \begin{cases} [a_i, b_i - u_i] & \text{if } u_i > 0, \\ [a_i - u_i, b_i] & \text{if } u_i < 0, \end{cases}$ and $\Theta_j = \begin{cases} [a_j, b_j - v_j] & \text{if } v_j > 0, \\ [a_j - v_j, b_j] & \text{if } v_j < 0, \end{cases}$. For $i = j$, one can have $\mathbf{v} = \pm\mathbf{u}$, then one obtains

$$\begin{aligned}\eta(\alpha,\beta,\mathbf{u},\mathbf{v}=\pm\mathbf{u}) &= \int_{\Theta} \acute{\eta}_{\boldsymbol{\theta}}(\alpha,\beta,\mathbf{u},\mathbf{v}) \frac{p^{\alpha}(\theta_i+u_i)\, p^{\beta}(\theta_i \pm u_i)}{p^{\alpha+\beta-1}(\theta_i)} \prod_{\substack{k=1 \\ k\neq i}}^{q} p(\theta_k)\, d\boldsymbol{\theta} \\ &= \frac{1}{\prod_{k=1}^{q}(b_k-a_k)} \int_{\Theta^{q-1}} \int_{\Theta_i} \acute{\eta}_{\boldsymbol{\theta}}(\alpha,\beta,\mathbf{u},\mathbf{v}=\pm\mathbf{u})\, d\theta_i d(\boldsymbol{\theta}/\{\theta_i\}). \end{aligned} \tag{3.21}$$

In the last equation, if $\mathbf{v} = -\mathbf{u}$ then $\Theta_i = \begin{cases} [a_i + u_i, b_i - u_i] & \text{if } u_i > 0, \\ [a_i - u_i, b_i + u_i] & \text{if } u_i < 0, \end{cases}$, while, if $\mathbf{v} = \mathbf{u}$ then $\Theta_i = \begin{cases} [a_i, b_i - u_i] & \text{if } u_i > 0, \\ [a_i - u_i, b_i] & \text{if } u_i < 0, \end{cases}$.

Depending on the structure of $\acute{\eta}_{\boldsymbol{\theta}}(\alpha, \beta, \mathbf{u}, \mathbf{v})$, $\eta(\alpha, \beta, \mathbf{u}, \mathbf{v})$ has to be computed numerically or a closed-form expression can be found.

Another particular case which appears sometimes is when the function $\acute{\eta}_{\boldsymbol{\theta}}(\alpha, \beta, \mathbf{u}, \mathbf{v})$ does not depend on $\boldsymbol{\theta}$ (see, e.g., [Ren07] and Section 3.5). In this case, $\acute{\eta}_{\boldsymbol{\theta}}(\alpha, \beta, \mathbf{u}, \mathbf{v})$ is denoted $\acute{\eta}(\alpha, \beta, \mathbf{u}, \mathbf{v})$ and one obtains from Eqn. (3.20)

$$\begin{aligned}\eta(\alpha,\beta,\mathbf{u},\mathbf{v}) &= \frac{\acute{\eta}(\alpha,\beta,\mathbf{u},\mathbf{v})}{\prod_{k=1}^{q}(b_k-a_k)} \left(\prod_{\substack{k=1 \\ k\neq i, k\neq j}}^{q} \int_{a_k}^{b_k} d\theta_k \right) \int_{\Theta_i} d\theta_i \int_{\Theta_j} d\theta_j \\ &= \frac{(b_i - a_i - |u_i|)(b_j - a_j - |v_j|)}{(b_i - a_i)(b_j - a_j)} \acute{\eta}(\alpha,\beta,\mathbf{u},\mathbf{v}), \end{aligned} \tag{3.22}$$

and from Eqn. (3.21)

$$\eta(\alpha,\beta,\mathbf{u},\mathbf{v}=\mathbf{u}) = \frac{(b_i - a_i - |u_i|)}{(b_i - a_i)} \acute{\eta}(\alpha,\beta,\mathbf{u},\mathbf{v}), \tag{3.23}$$

and

$$\eta(\alpha,\beta,\mathbf{u},\mathbf{v}=-\mathbf{u}) = \frac{(b_i - a_i - 2|u_i|)}{(b_i - a_i)} \acute{\eta}(\alpha,\beta,\mathbf{u},\mathbf{v}). \tag{3.24}$$

3.4.3 Analysis of $\eta(\alpha,\beta,\mathbf{u},\mathbf{v})$ with a Gaussian prior

Finally, one can mention that if the prior is now assumed to be Gaussian, *i.e.*, $\theta_i \sim \mathcal{N}\left(\mu_i,\sigma_i^2\right)$ and $\acute{\eta}_{\boldsymbol{\theta}}(\alpha,\beta,\mathbf{u},\mathbf{v})$ does not depend on $\boldsymbol{\theta}$ one obtains after a straightforward calculus

$$\begin{aligned}\eta(\alpha,\beta,\mathbf{u},\mathbf{v}) &= \acute{\eta}(\alpha,\beta,\mathbf{u},\mathbf{v})\int_{\mathbb{R}}\frac{p^{\alpha}(\theta_i+u_i)}{p^{\alpha-1}(\theta_i)}d\theta_i\int_{\mathbb{R}}\frac{p^{\beta}(\theta_j+v_j)}{p^{\beta-1}(\theta_j)}d\theta_j \\ &= \acute{\eta}(\alpha,\beta,\mathbf{u},\mathbf{v})\exp\left(-\frac{1}{2}\left(\frac{\alpha(1-\alpha)u_i^2}{\sigma_i^2}+\frac{\beta(1-\beta)v_j^2}{\sigma_j^2}\right)\right),\end{aligned} \tag{3.25}$$

$$\begin{aligned}\eta(\alpha,\beta,\mathbf{u},\mathbf{v}=\mathbf{u}) &= \acute{\eta}(\alpha,\beta,\mathbf{u},\mathbf{v})\int_{\mathbb{R}}\frac{p^{\alpha+\beta}(\theta_i+u_i)}{p^{\alpha+\beta-1}(\theta_i)}d\theta_i \\ &= \acute{\eta}(\alpha,\beta,\mathbf{u},\mathbf{v})\exp\left(-\frac{(\alpha+\beta)(1-\alpha-\beta)u_i^2}{2\sigma_i^2}\right),\end{aligned} \tag{3.26}$$

and

$$\begin{aligned}\eta(\alpha,\beta,\mathbf{u},\mathbf{v}=-\mathbf{u}) &= \acute{\eta}(\alpha,\beta,\mathbf{u},\mathbf{v})\int_{\mathbb{R}}\frac{p^{\alpha}(\theta_i+u_i)\,p^{\beta}(\theta_i-u_i)}{p^{\alpha+\beta-1}(\theta_i)}d\theta_i \\ &= \acute{\eta}(\alpha,\beta,\mathbf{u},\mathbf{v})\exp\left(-\frac{\left(\alpha+\beta-\alpha^2-\beta^2+2\alpha\beta\right)u_i^2}{2\sigma_i^2}\right).\end{aligned} \tag{3.27}$$

3.5 Specific applications to array processing: DOA estimation

We now consider the application of the Weiss-Weinstein bound in the particular context of source localization. Indeed, until now the structure of the steering matrix $\mathbf{A}(\boldsymbol{\theta})$ for a particular problem has not been used in the proposed (semi) closed-form expressions. Consequently, these previous results can be applied to a large class of estimation problems such as far-field and near-field sources localization, passive localization with polarized array of sensors, or radar (known waveforms).

Here, we want to focus on the direction-of-arrival estimation of a single source in the far-field area with narrow-band signal. In this case, the steering matrix $\mathbf{A}(\boldsymbol{\theta})$ becomes a steering vector denoted $\mathbf{a}(\boldsymbol{\theta})$ (except for one preliminary result concerning the conditional model which will be given whatever the number of sources in Section 3.5.1.1). The structure of this vector will be specified by the analysis of two kinds of array geometry: the non-uniform linear array from which only one angle-of-arrival can be estimated ($\boldsymbol{\theta}$ becomes a scalar) and the arbitrary planar array from which both azimuth and elevation can be estimated ($\boldsymbol{\theta}$ becomes a 2×1 vector). In any case, the array always consists of M identical, omnidirectional sensors. Both model $\mathcal{M}_2$ and $\mathcal{M}_1$ will be considered and the noise will be assumed spatially uncorrelated: $\mathbf{R}_{\mathbf{n}}=\sigma_n^2\mathbf{I}$. Since we focus on the single source scenario, the variance of the source signal $s(t)$ is denoted σ_s^2 for model $\mathcal{M}_1$.

The general structure of the i^{th} element of the steering vector is as follows

$$\{\mathbf{a}(\boldsymbol{\theta})\}_i = \exp\left(j\frac{2\pi}{\lambda}\mathbf{r}_i^T\boldsymbol{\theta}\right),\ i=1,\ldots,M \tag{3.28}$$

where $\boldsymbol{\theta}$ represents the parameter vector, λ denotes the wavelength and $\mathbf{r}_i$ denotes the coordinate of the i^{th} sensor position with respect to a given referential. In the following, $\mathbf{r}_i$ will be a scalar or a 2×1 vector depending on the context (linear array or planar array).

3.5.1 Preliminary results

Since our analysis is now reduced to the single source case, we here give some other closed-form expressions which will be useful when we will detail the specific linear and planar arrays.

3.5.1.1 Conditional observation model $\mathcal{M}_1$

Note that the results proposed here are in the context of any number of sources. Under the conditional model, the set of functions $\acute{\eta}_\theta$ given by Eqn. (3.16) is linked to the function $\zeta_{\boldsymbol{\theta}}(\boldsymbol{\mu},\boldsymbol{\rho})$ given by Eqn. (3.17). In this analysis, vector $\boldsymbol{\mu}$ takes the value μ_i at the i^{th} row and zero elsewhere and vector $\boldsymbol{\rho}$ takes the value ρ_j at the j^{th} row and zero elsewhere (of course, we can have $i=j$). In Appendix 3.8.3, the calculus of the following closed-form expressions for $\zeta_{\boldsymbol{\theta}}(\boldsymbol{\mu},\boldsymbol{\rho})$ are detailed.

- If $(m-1)\,p+1 \leq i,j \leq mp$, where p denotes the number of parameters per source, then, we have

$$\begin{aligned}\zeta_{\boldsymbol{\theta}}(\boldsymbol{\mu},\boldsymbol{\rho}) = &\sum_{t=1}^{T} \left\|\{\mathbf{s}(t)\}_m\right\|^2 \sum_{i=1}^{M}\sum_{j=1}^{M} \left\{\mathbf{R}_{\mathbf{n}}^{-1}\right\}_{i,j} e^{\left(j\frac{2\pi}{\lambda}\left(\mathbf{r}_j^T-\mathbf{r}_i^T\right)\boldsymbol{\theta}_m\right)} \\ &\times\left(e^{\left(-j\frac{2\pi}{\lambda}\mathbf{r}_i^T\boldsymbol{\mu}_m\right)}-e^{\left(-j\frac{2\pi}{\lambda}\mathbf{r}_i^T\boldsymbol{\rho}_m\right)}\right)\left(e^{\left(j\frac{2\pi}{\lambda}\mathbf{r}_j^T\boldsymbol{\mu}_m\right)}-e^{\left(j\frac{2\pi}{\lambda}\mathbf{r}_j^T\boldsymbol{\rho}_m\right)}\right). \end{aligned} \tag{3.29}$$

- Otherwise, if $(m-1)\,p+1 \leq i \leq mp$ and $(n-1)\,p+1 \leq j \leq np$, we have

$$\begin{aligned}\zeta_{\boldsymbol{\theta}}(\boldsymbol{\mu},\boldsymbol{\rho}) = &\sum_{t=1}^{T} \left\|\{\mathbf{s}(t)\}_m\right\|^2 \sum_{i=1}^{M}\sum_{j=1}^{M} \left\{\mathbf{R}_{\mathbf{n}}^{-1}\right\}_{i,j} e^{\left(j\frac{2\pi}{\lambda}\left(\mathbf{r}_j^T-\mathbf{r}_i^T\right)\boldsymbol{\theta}_m\right)} e^{\left(-j\frac{2\pi}{\lambda}\mathbf{r}_i^T\boldsymbol{\mu}_m\right)} e^{\left(j\frac{2\pi}{\lambda}\mathbf{r}_j^T\boldsymbol{\mu}_m\right)} \\ &+\sum_{t=1}^{T} \left\|\{\mathbf{s}(t)\}_n\right\|^2 \sum_{i=1}^{M}\sum_{j=1}^{M} \left\{\mathbf{R}_{\mathbf{n}}^{-1}\right\}_{i,j} e^{\left(j\frac{2\pi}{\lambda}\left(\mathbf{r}_j^T-\mathbf{r}_i^T\right)\boldsymbol{\theta}_n\right)} e^{\left(-j\frac{2\pi}{\lambda}\mathbf{r}_i^T\boldsymbol{\rho}_n\right)} e^{\left(j\frac{2\pi}{\lambda}\mathbf{r}_j^T\boldsymbol{\rho}_n\right)} \\ &-2\,\mathrm{Re}\left(\sum_{t=1}^{T}\{\mathbf{s}(t)\}_m^*\{\mathbf{s}(t)\}_n \sum_{i=1}^{M}\sum_{j=1}^{M}\left\{\mathbf{R}_{\mathbf{n}}^{-1}\right\}_{i,j} e^{\left(j\frac{2\pi}{\lambda}\left(\mathbf{r}_j^T\boldsymbol{\theta}_n-\mathbf{r}_i^T\boldsymbol{\theta}_m\right)\right)} e^{\left(-j\frac{2\pi}{\lambda}\mathbf{r}_i^T\boldsymbol{\mu}_m\right)} e^{\left(j\frac{2\pi}{\lambda}\mathbf{r}_j^T\boldsymbol{\rho}_n\right)}\right). \end{aligned} \tag{3.30}$$

In particular, if one assumes $\mathbf{R}_n = \sigma_n^2\mathbf{I}$, then, several simplifications can be done.

- If $(m-1)\,p+1 \leq i,j \leq mp$, then

$$\zeta_{\boldsymbol{\theta}}(\boldsymbol{\mu},\boldsymbol{\rho}) = \frac{1}{\sigma_n^2}\sum_{i=1}^{M}\left\|e^{\left(-j\frac{2\pi}{\lambda}\mathbf{r}_i^T\boldsymbol{\mu}_m\right)}-e^{\left(-j\frac{2\pi}{\lambda}\mathbf{r}_i^T\boldsymbol{\rho}_m\right)}\right\|^2 \sum_{t=1}^{T}\left\|\{\mathbf{s}(t)\}_m\right\|^2, \tag{3.31}$$

  where we note that the function $\zeta_{\boldsymbol{\theta}}(\boldsymbol{\mu},\boldsymbol{\rho})$ does not depend on the parameter $\boldsymbol{\theta}$.

- Otherwise, if $(m-1)\,p+1 \leq i \leq mp$ and $(n-1)\,p+1 \leq j \leq np$, then

$$\begin{aligned}\zeta_{\boldsymbol{\theta}}(\boldsymbol{\mu},\boldsymbol{\rho}) = &\frac{1}{\sigma_n^2}\sum_{i=1}^{M}\left\|e^{\left(-j\frac{2\pi}{\lambda}\mathbf{r}_i^T\boldsymbol{\mu}_m\right)}\right\|^2 \sum_{t=1}^{T}\left\|\{\mathbf{s}(t)\}_m\right\|^2 + \frac{1}{\sigma_n^2}\sum_{i=1}^{M}\left\|e^{\left(-j\frac{2\pi}{\lambda}\mathbf{r}_i^T\boldsymbol{\rho}_n\right)}\right\|^2 \sum_{t=1}^{T}\left\|\{\mathbf{s}(t)\}_n\right\|^2 \\ &-2\,\mathrm{Re}\left(\frac{1}{\sigma_n^2}\sum_{i=1}^{M} e^{\left(j\frac{2\pi}{\lambda}\mathbf{r}_i^T\left(\boldsymbol{\theta}_n-\boldsymbol{\theta}_m\right)\right)} e^{\left(-j\frac{2\pi}{\lambda}\mathbf{r}_i^T\boldsymbol{\mu}_m\right)} e^{\left(j\frac{2\pi}{\lambda}\mathbf{r}_i^T\boldsymbol{\rho}_n\right)} \sum_{t=1}^{T}\{\mathbf{s}(t)\}_m^*\{\mathbf{s}(t)\}_n\right) \end{aligned} \tag{3.32}$$

3.5.1.2 Unconditional observation model $\mathcal{M}_2$

In order to detail the set of functions $\acute{\eta}_\theta$ given by Eqn. (3.18), one has to find closed-form expressions of the determinant $|\mathbf{R}_\mathbf{y}(\boldsymbol{\theta}+\mathbf{u})|$ and of determinants having the following structure: $\left|m_1\mathbf{R}_\mathbf{y}^{-1}(\boldsymbol{\theta}_1)+m_2\mathbf{R}_\mathbf{y}^{-1}(\boldsymbol{\theta}_2)\right|$ with $m_1+m_2=1$ or $\left|m_1\mathbf{R}_\mathbf{y}^{-1}(\boldsymbol{\theta}_1)+m_2\mathbf{R}_\mathbf{y}^{-1}(\boldsymbol{\theta}_2)+m_3\mathbf{R}_\mathbf{y}^{-1}(\boldsymbol{\theta}_3)\right|$ with $m_1+m_2+m_3=1$. Under $\mathcal{M}_2$, the observation covariance matrix is now given by

$$\mathbf{R}_\mathbf{y}(\boldsymbol{\theta})=\sigma_s^2\mathbf{a}(\boldsymbol{\theta})\mathbf{a}^H(\boldsymbol{\theta})+\sigma_n^2\mathbf{I}_M. \tag{3.33}$$

Concerning the calculus of $|\mathbf{R}_\mathbf{y}(\boldsymbol{\theta}+\mathbf{u})|$, it is easy to find

$$|\mathbf{R}_\mathbf{y}(\boldsymbol{\theta}+\mathbf{u})|=\sigma_n^{2M}\left(1+\frac{\sigma_s^2}{\sigma_n^2}\left\|\mathbf{a}(\boldsymbol{\theta}+\mathbf{u})\right\|^2\right) \tag{3.34}$$

Moreover, after calculus detailed in Appendix 3.8.4, one obtains for the other determinants

$$\begin{aligned}\left|m_1\mathbf{R}_\mathbf{y}^{-1}(\boldsymbol{\theta}_1)+m_2\mathbf{R}_\mathbf{y}^{-1}(\boldsymbol{\theta}_2)\right|=\frac{1}{(\sigma_n^2)^M}\Big(&1-\varphi_1 m_1\left\|\mathbf{a}(\boldsymbol{\theta}_1)\right\|^2+m_2\varphi_2\left\|\mathbf{a}(\boldsymbol{\theta}_2)\right\|^2\\&-\varphi_1 m_1\varphi_2 m_2\left(\left|\mathbf{a}^H(\boldsymbol{\theta}_1)\mathbf{a}(\boldsymbol{\theta}_2)\right|^2-\left\|\mathbf{a}(\boldsymbol{\theta}_1)\right\|^2\left\|\mathbf{a}(\boldsymbol{\theta}_2)\right\|^2\right)\Big)\end{aligned} \tag{3.35}$$

and

$$\begin{aligned}&\left|m_1\mathbf{R}^{-1}(\boldsymbol{\theta}_1)+m_2\mathbf{R}^{-1}(\boldsymbol{\theta}_2)+m_3\mathbf{R}^{-1}(\boldsymbol{\theta}_3)\right|=\\&\frac{1}{(\sigma_n^2)^M}\left(1-\sum_{k=1}^{3}m_k\varphi_k\left\|\mathbf{a}(\boldsymbol{\theta}_k)\right\|^2-\frac{1}{2}\sum_{k=1}^{3}\sum_{\substack{k'=1\\k'\neq k}}^{3}m_k\varphi_k m_{k'}\varphi_{k'}\left(\left|\mathbf{a}^H(\boldsymbol{\theta}_k)\mathbf{a}(\boldsymbol{\theta}_{k'})\right|^2-\left\|\mathbf{a}(\boldsymbol{\theta}_k)\right\|^2\left\|\mathbf{a}(\boldsymbol{\theta}_{k'})\right\|^2\right)\right.\\&-\left(\prod_{k=1}^{3}m_k\varphi_k\right)\left(\prod_{k=1}^{3}\left\|\mathbf{a}(\boldsymbol{\theta}_k)\right\|^2-\frac{1}{2}\sum_{k=1}^{3}\sum_{\substack{k'=1\\k'\neq k}}^{3}\sum_{\substack{k''=1\\k''\neq k'\neq k}}^{3}\left|\mathbf{a}^H(\boldsymbol{\theta}_k)\mathbf{a}(\boldsymbol{\theta}_{k'})\right|^2\left\|\mathbf{a}(\boldsymbol{\theta}_{k''})\right\|^2\right.\\&\left.\left.+\mathbf{a}^H(\boldsymbol{\theta}_3)\mathbf{a}(\boldsymbol{\theta}_2)\mathbf{a}^H(\boldsymbol{\theta}_1)\mathbf{a}(\boldsymbol{\theta}_3)\mathbf{a}^H(\boldsymbol{\theta}_2)\mathbf{a}(\boldsymbol{\theta}_1)+\mathbf{a}^H(\boldsymbol{\theta}_3)\mathbf{a}(\boldsymbol{\theta}_1)\mathbf{a}^H(\boldsymbol{\theta}_1)\mathbf{a}(\boldsymbol{\theta}_2)\mathbf{a}^H(\boldsymbol{\theta}_2)\mathbf{a}(\boldsymbol{\theta}_3)\right)\right),\end{aligned} \tag{3.36}$$

where

$$\varphi_k=\frac{\sigma_s^2}{\sigma_s^2\left\|\mathbf{a}(\boldsymbol{\theta}_k)\right\|^2+\sigma_n^2},\quad k=1,2,3. \tag{3.37}$$

It is clear that the above proposed formulae for both the unconditional and the conditional models can be applied to any kind of array geometry and whatever the number of sources. However, they generally depend on the parameter vector $\boldsymbol{\theta}$. This means that, in general, the calculus of the set of functions η will have to be performed numerically (except if one is able to find a closed-form expression of Eqn. (3.11)). In the following, we present a kind of array geometry where, fortunately, the set of functions $\acute{\eta}_\theta$ will not depend on $\boldsymbol{\theta}$ leading to a straightforward calculus of the bound.

3.5.2 3D Source localization with a planar array

We first consider the problem of DOA estimation of a single narrow band source in the far field area by using an arbitrary planar array. In fact, we start by this general setting because the non-uniform linear array is clearly a particular case of this array. Without loss of generality, we assume that the sensors of this array lay on the xOy plan with Cartesian coordinates (see Fig.

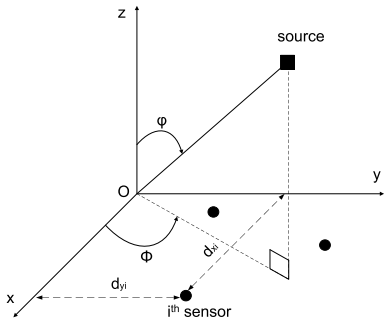

Figure 3.1: 3D source localization using a planar array antenna.

3.1). Therefore, the vector $\mathbf{r}_i$ contains the coordinate of the i^{th} sensor position with respect to this referential, *i.e.*, $\mathbf{r}_i = [d_{x_i} \; d_{y_i}]^T$, $i = 1, \ldots, M$. From (3.28), the steering vector is given by

$$\mathbf{a}(\boldsymbol{\theta}) = \left[\exp\left(j\frac{2\pi}{\lambda}(d_{x_1}u + d_{y_1}v) \right) \ldots \exp\left(j\frac{2\pi}{\lambda}(d_{x_M}u + d_{y_M}v) \right) \right]^T, \tag{3.38}$$

where, as in [BEV96a], the parameter vector of interest is $\boldsymbol{\theta} = [u \quad v]^T$ where

$$\begin{cases} u = \sin\varphi\cos\phi, \\ v = \sin\varphi\sin\phi, \end{cases} \tag{3.39}$$

and where φ and ϕ represent the elevation and azimuth angles of the source, respectively. The parameters space is such that $u \in [-1, 1]$ and $v \in [-1, 1]$. Therefore, we assume that they both follow a uniform distribution over $[-1, 1]$. Note that from a physical point of view, it should be more tempting to choose a uniform prior for φ and ϕ. This will lead to a probability density functions for u and v not uniform. To the best of our knowledge, this assumption has only been used in the context of lower bounds in [NV94]. Unfortunately, such prior leads to an untrackable expression of the bound (see Eqn. (21) of [NV94]). Consequently, other authors have generally not specified the prior leading to semi closed-form expressions of bounds (*i.e.* that it remains a numerical integration to perform over the parameters) [BEV96a] [XBR04]. On the other hand, in order to obtain a closed-form expression, authors have generally used a simplified assumption, i.e. a uniform prior directly on u and v, see, for example, [XBB04] [Ath01]). In this chapter, we have followed the same way by expecting a slight modification of performance with respect to a more physical model and in order to be able to get closed-form expressions of the bound.

We choose the matrix of test points such that

$$\mathbf{H} = [\mathbf{h}_u \quad \mathbf{h}_v] = \begin{bmatrix} h_u & 0 \\ 0 & h_v \end{bmatrix}. \tag{3.40}$$

Then, we have: $\boldsymbol{\theta}+\mathbf{h_u} = [u + h_u \quad v]^T$ and $\boldsymbol{\theta}+\mathbf{h_v} = [u \quad v + h_v]^T$. Moreover, we now have two elements $s_i \in [0, 1]$, $i = 1, 2$ for which we will prefer the notation s_u and s_v, respectively.

3.5.2.1 Conditional observation model $\mathcal{M}_1$

Under $\mathcal{M}_1$, let us set $C_{SNR} = \frac{1}{\sigma_n^2}\sum_{t=1}^{T}\|s(t)\|^2$. The closed-form expressions of the elements of matrix $\mathbf{G}$ are given by (see Appendix 3.8.5 for the proof):

$$\{\mathbf{G}\}_{uu} = \frac{\left(\begin{array}{l}\left(1-\frac{|h_u|}{2}\right)\exp\left(4s_u(2s_u-1)C_{SNR}\left(M-\sum_{k=1}^{M}\cos\left(\frac{2\pi}{\lambda}d_{x_k}h_u\right)\right)\right)\\ +\left(1-\frac{|h_u|}{2}\right)\exp\left(4(2s_u-1)(s_u-1)C_{SNR}\left(M-\sum_{k=1}^{M}\cos\left(\frac{2\pi}{\lambda}d_{x_k}h_u\right)\right)\right)\\ -2(1-|h_u|)\exp\left(2s_u(s_u-1)C_{SNR}\left(M-\sum_{k=1}^{M}\cos\left(\frac{4\pi}{\lambda}d_{x_k}h_u\right)\right)\right)\end{array}\right)}{\left(1-\frac{|h_u|}{2}\right)^2\exp\left(4s_u(s_u-1)C_{SNR}\left(M-\sum_{k=1}^{M}\cos\left(\frac{2\pi}{\lambda}d_{x_k}h_u\right)\right)\right)}, \tag{3.41}$$

$$\{\mathbf{G}\}_{vv} = \frac{\left(\begin{array}{l}\left(1-\frac{|h_v|}{2}\right)\exp\left(4s_v(2s_v-1)C_{SNR}\left(M-\sum_{k=1}^{M}\cos\left(\frac{2\pi}{\lambda}d_{y_k}h_v\right)\right)\right)\\ +\left(1-\frac{|h_v|}{2}\right)\exp\left(4(2s_v-1)(s_v-1)C_{SNR}\left(M-\sum_{k=1}^{M}\cos\left(\frac{2\pi}{\lambda}d_{y_k}h_v\right)\right)\right)\\ -2(1-|h_v|)\exp\left(2s_v(s_v-1)C_{SNR}\left(M-\sum_{k=1}^{M}\cos\left(\frac{4\pi}{\lambda}d_{y_k}h_v\right)\right)\right)\end{array}\right)}{\left(1-\frac{|h_v|}{2}\right)^2\exp\left(4s_v(s_v-1)C_{SNR}\left(M-\sum_{k=1}^{M}\cos\left(\frac{2\pi}{\lambda}d_{y_k}h_v\right)\right)\right)}, \tag{3.42}$$

$$\{\mathbf{G}\}_{uv} = \frac{\left(\begin{array}{l}\exp\left(\begin{array}{l}2s_u(s_u+s_v-1)C_{SNR}\left(M-\sum_{k=1}^{M}\cos\left(\frac{2\pi}{\lambda}d_{x_k}h_u\right)\right)\\ +2s_v(s_u+s_v-1)C_{SNR}\left(M-\sum_{k=1}^{M}\cos\left(\frac{2\pi}{\lambda}d_{y_k}h_v\right)\right)\\ -2s_us_vC_{SNR}\left(M-\sum_{k=1}^{M}\cos\left(\frac{2\pi}{\lambda}(d_{x_k}h_u-d_{y_k}h_v)\right)\right)\end{array}\right)\\ +\exp\left(\begin{array}{l}2(s_u-1)(s_u+s_v-1)C_{SNR}\left(M-\sum_{k=1}^{M}\cos\left(\frac{2\pi}{\lambda}d_{x_k}h_u\right)\right)\\ +2(s_v-1)(s_u+s_v-1)C_{SNR}\left(M-\sum_{k=1}^{M}\cos\left(\frac{2\pi}{\lambda}d_{y_k}h_v\right)\right)\\ -2(1-s_u)(1-s_v)C_{SNR}\left(M-\sum_{k=1}^{M}\cos\left(\frac{2\pi}{\lambda}(d_{x_k}h_u-d_{y_k}h_v)\right)\right)\end{array}\right)\\ -\exp\left(\begin{array}{l}2s_u(s_u-s_v)C_{SNR}\left(M-\sum_{k=1}^{M}\cos\left(\frac{2\pi}{\lambda}d_{x_k}h_u\right)\right)\\ +2(1-s_v)(s_u-s_v)C_{SNR}\left(M-\sum_{k=1}^{M}\cos\left(\frac{2\pi}{\lambda}d_{y_k}h_v\right)\right)\\ +2s_u(s_v-1)C_{SNR}\left(M-\sum_{k=1}^{M}\cos\left(\frac{2\pi}{\lambda}(d_{x_k}h_u+d_{y_k}h_v)\right)\right)\end{array}\right)\\ -\exp\left(\begin{array}{l}2(s_u-1)(s_u-s_v)C_{SNR}\left(M-\sum_{k=1}^{M}\cos\left(\frac{2\pi}{\lambda}d_{x_k}h_u\right)\right)\\ +2s_v(s_v-s_u)C_{SNR}\left(M-\sum_{k=1}^{M}\cos\left(\frac{2\pi}{\lambda}d_{y_k}h_v\right)\right)\\ +2(s_u-1)s_vC_{SNR}\left(M-\sum_{k=1}^{M}\cos\left(\frac{2\pi}{\lambda}(d_{x_k}h_u+d_{y_k}h_v)\right)\right)\end{array}\right)\end{array}\right)}{\left(\begin{array}{l}\exp\left(2s_u(s_u-1)C_{SNR}\left(M-\sum_{k=1}^{M}\cos\left(\frac{2\pi}{\lambda}d_{x_k}h_u\right)\right)\right)\\ \times\exp\left(2s_v(s_v-1)C_{SNR}\left(M-\sum_{k=1}^{M}\cos\left(\frac{2\pi}{\lambda}d_{y_k}h_v\right)\right)\right)\end{array}\right)}, \tag{3.43}$$

and $\{\mathbf{G}\}_{uv} = \{\mathbf{G}\}_{vu}$. Consequently, the conditional Weiss-Weinstein bound is a 2×2 matrix given by:

$$\begin{aligned}\mathbf{WWB} &= \mathbf{H}\mathbf{G}^{-1}\mathbf{H}^T \\ &= \frac{1}{\{\mathbf{G}\}_{uu}\{\mathbf{G}\}_{vv} - \{\mathbf{G}\}_{uv}^2} \begin{bmatrix} h_u^2\{\mathbf{G}\}_{vv} & -h_u h_v\{\mathbf{G}\}_{uv} \\ -h_u h_v\{\mathbf{G}\}_{uv} & h_v^2\{\mathbf{G}\}_{uu} \end{bmatrix},\end{aligned} \tag{3.44}$$

which has to be optimized over s_u, s_v, h_u, and h_v. Concerning the optimization over s_u and s_v, several other works in the literature have suggested to simply use $s_u = s_v = 1/2$. Most of the time, numerical simulations of this simplified bound compared with the bound obtained after optimization over s_u and s_v leads to the same results while there is no formal proof of this fact (see [VB07] page 41 footnote 17). Note that, thanks to the expressions obtained in the next Section concerning the linear array, we will be able to prove that $s = 1/2$ is a (maybe not unique) correct choice for the linear array. In the case of the planar array treated in this Section, we will only check this property by simulation.

In the particular case where $s_u = s_v = 1/2$ one obtains the following simplified expressions

$$\{\mathbf{G}\}_{uu} = \frac{2\left(1 - \frac{|h_u|}{2}\right) - 2(1 - |h_u|)\exp\left(-\frac{C_{SNR}}{2}\left(M - \sum_{k=1}^{M}\cos\left(\frac{4\pi}{\lambda}d_{x_k}h_u\right)\right)\right)}{\left(1 - \frac{|h_u|}{2}\right)^2\exp\left(-C_{SNR}\left(M - \sum_{k=1}^{M}\cos\left(\frac{2\pi}{\lambda}d_{x_k}h_u\right)\right)\right)}, \tag{3.45}$$

$$\{\mathbf{G}\}_{vv} = \frac{2\left(1 - \frac{|h_v|}{2}\right) - 2(1 - |h_v|)\exp\left(-\frac{C_{SNR}}{2}\left(M - \sum_{k=1}^{M}\cos\left(\frac{4\pi}{\lambda}d_{y_k}h_v\right)\right)\right)}{\left(1 - \frac{|h_v|}{2}\right)^2\exp\left(-C_{SNR}\left(M - \sum_{k=1}^{M}\cos\left(\frac{2\pi}{\lambda}d_{y_k}h_v\right)\right)\right)}, \tag{3.46}$$

$$\{\mathbf{G}\}_{uv} = \frac{\begin{pmatrix} 2\exp\left(-\frac{C_{SNR}}{2}\left(M - \sum_{k=1}^{M}\cos\left(\frac{2\pi}{\lambda}(d_{x_k}h_u - d_{y_k}h_v)\right)\right)\right) \\ -2\exp\left(-\frac{C_{SNR}}{2}\left(M - \sum_{k=1}^{M}\cos\left(\frac{2\pi}{\lambda}(d_{x_k}h_u + d_{y_k}h_v)\right)\right)\right) \end{pmatrix}}{\exp\left(-\frac{C_{SNR}}{2}\left(2M - \sum_{k=1}^{M}\cos\left(\frac{2\pi}{\lambda}d_{x_k}h_u\right) - \sum_{k=1}^{M}\cos\left(\frac{2\pi}{\lambda}d_{y_k}h_v\right)\right)\right)}. \tag{3.47}$$

By using the above expressions in Eqn. (3.44) and after an optimization over the test points, one obtains the Weiss-Weinstein bound.

3.5.2.2 Unconditional observation model $\mathcal{M}_2$

Under $\mathcal{M}_2$, let us set $U_{SNR} = \frac{\sigma_s^4}{\sigma_n^2(M\sigma_s^2+\sigma_n^2)}$. The closed-form expressions of the elements of matrix $\mathbf{G} = \begin{bmatrix} \{\mathbf{G}\}_{uu} & \{\mathbf{G}\}_{uv} \\ \{\mathbf{G}\}_{vu} & \{\mathbf{G}\}_{vv} \end{bmatrix}$ are given by (see Appendix 3.8.6 for the proof):

$$\{\mathbf{G}\}_{uu} = \frac{\begin{pmatrix} \left(1-\frac{|h_u|}{2}\right)\left(1+2s_u(1-2s_u)U_{SNR}\left(M^2-\left\|\sum_{k=1}^{M}\exp\left(-j\frac{2\pi}{\lambda}d_{x_k}h_u\right)\right\|^2\right)\right)^{-T} \\ +\left(1-\frac{|h_u|}{2}\right)\left(1+2(1-s_u)(2s_u-1)U_{SNR}\left(M^2-\left\|\sum_{k=1}^{M}\exp\left(-j\frac{2\pi}{\lambda}d_{x_k}h_u\right)\right\|^2\right)\right)^{-T} \\ -2\left(1-|h_u|\right)\left(1+s_u(1-s_u)U_{SNR}\left(M^2-\left\|\sum_{k=1}^{M}\exp\left(-j\frac{4\pi}{\lambda}d_{x_k}h_u\right)\right\|^2\right)\right)^{-T} \end{pmatrix}}{\left(1-\frac{|h_u|}{2}\right)^2\left(1+s_u(1-s_u)U_{SNR}\left(M^2-\left\|\sum_{k=1}^{M}\exp\left(-j\frac{2\pi}{\lambda}d_{x_k}h_u\right)\right\|^2\right)\right)^{-2T}}, \tag{3.48}$$

$$\{\mathbf{G}\}_{vv} = \frac{\begin{pmatrix} \left(1-\frac{|h_v|}{2}\right)\left(1+2s_v(1-2s_v)U_{SNR}\left(M^2-\left\|\sum_{k=1}^{M}\exp\left(-j\frac{2\pi}{\lambda}d_{y_k}h_v\right)\right\|^2\right)\right)^{-T} \\ +\left(1-\frac{|h_v|}{2}\right)\left(1+2(1-s_v)(2s_v-1)U_{SNR}\left(M^2-\left\|\sum_{k=1}^{M}\exp\left(-j\frac{2\pi}{\lambda}d_{y_k}h_v\right)\right\|^2\right)\right)^{-T} \\ -2\left(1-|h_v|\right)\left(1+s_v(1-s_v)U_{SNR}\left(M^2-\left\|\sum_{k=1}^{M}\exp\left(-j\frac{4\pi}{\lambda}d_{y_k}h_v\right)\right\|^2\right)\right)^{-T} \end{pmatrix}}{\left(1-\frac{|h_v|}{2}\right)^2\left(1+s_v(1-s_v)U_{SNR}\left(M^2-\left\|\sum_{k=1}^{M}\exp\left(-j\frac{2\pi}{\lambda}d_{y_k}h_v\right)\right\|^2\right)\right)^{-2T}}, \tag{3.49}$$

and

$$\{\mathbf{G}\}_{uv} =$$

$$\frac{\left(\begin{array}{l}\left(\begin{array}{l}1-U_{SNR}\left(\begin{array}{l}s_u s_v\left(\left\|\sum_{k=1}^{M}\exp\left(-j\frac{2\pi}{\lambda}(d_{x_k}h_u-d_{y_k}h_v)\right)\right\|^2-M^2\right)\\+s_u(1-s_u-s_v)\left(\left\|\sum_{k=1}^{M}\exp\left(-j\frac{2\pi}{\lambda}d_{x_k}h_u\right)\right\|^2-M^2\right)\\+s_v(1-s_u-s_v)\left(\left\|\sum_{k=1}^{M}\exp\left(-j\frac{2\pi}{\lambda}d_{y_k}h_v\right)\right\|^2-M^2\right)\end{array}\right)\\-s_u s_v(1-s_u-s_v)\frac{U_{SNR}^2\sigma_n^2}{\sigma_s^2}\times\\\times\left(\begin{array}{l}\sum_{k=1}^{M}\exp\left(j\frac{2\pi d_{y_k}h_v}{\lambda}\right)\sum_{k=1}^{M}\exp\left(-j\frac{2\pi d_{x_k}h_u}{\lambda}\right)\sum_{k=1}^{M}\exp\left(j\frac{2\pi(d_{x_k}h_u-d_{y_k}h_v)}{\lambda}\right)\\+\sum_{k=1}^{M}\exp\left(-j\frac{2\pi d_{y_k}h_v}{\lambda}\right)\sum_{k=1}^{M}\exp\left(j\frac{2\pi d_{x_k}h_u}{\lambda}\right)\sum_{k=1}^{M}\exp\left(-j\frac{2\pi(d_{x_k}h_u-d_{y_k}h_v)}{\lambda}\right)\\-M\left\|\sum_{k=1}^{M}\exp\left(-j\frac{2\pi}{\lambda}d_{y_k}h_v\right)\right\|^2-M\left\|\sum_{k=1}^{M}\exp\left(-j\frac{2\pi}{\lambda}d_{x_k}h_u\right)\right\|^2\\-M\left\|\sum_{k=1}^{M}\exp\left(-j\frac{2\pi}{\lambda}(d_{x_k}h_u-d_{y_k}h_v)\right)\right\|^2+M^3\end{array}\right)\end{array}\right)^{-T}\\+\left(\begin{array}{l}1-U_{SNR}\left(\begin{array}{l}(1-s_u)(1-s_v)\left(\left\|\sum_{k=1}^{M}\exp\left(j\frac{2\pi}{\lambda}(d_{x_k}h_u-d_{y_k}h_v)\right)\right\|^2-M^2\right)\\+(1-s_u)(s_u+s_v-1)\left(\left\|\sum_{k=1}^{M}\exp\left(j\frac{2\pi}{\lambda}d_{x_k}h_u\right)\right\|^2-M^2\right)\\+(1-s_v)(s_u+s_v-1)\left(\left\|\sum_{k=1}^{M}\exp\left(j\frac{2\pi}{\lambda}d_{y_k}h_v\right)\right\|^2-M^2\right)\end{array}\right)\\-(1-s_u)(1-s_v)(s_u+s_v-1)\frac{U_{SNR}^2\sigma_n^2}{\sigma_s^2}\times\\\times\left(\begin{array}{l}\sum_{k=1}^{M}\exp\left(j\frac{2\pi d_{y_k}h_v}{\lambda}\right)\sum_{k=1}^{M}\exp\left(-j\frac{2\pi d_{x_k}h_u}{\lambda}\right)\sum_{k=1}^{M}\exp\left(j\frac{2\pi(d_{x_k}h_u-d_{y_k}h_v)}{\lambda}\right)\\+\sum_{k=1}^{M}\exp\left(-j\frac{2\pi d_{y_k}h_v}{\lambda}\right)\sum_{k=1}^{M}\exp\left(j\frac{2\pi d_{x_k}h_u}{\lambda}\right)\sum_{k=1}^{M}\exp\left(-j\frac{2\pi(d_{x_k}h_u-d_{y_k}h_v)}{\lambda}\right)\\-M\left\|\sum_{k=1}^{M}\exp\left(-j\frac{2\pi}{\lambda}d_{y_k}h_v\right)\right\|^2-M\left\|\sum_{k=1}^{M}\exp\left(-j\frac{2\pi}{\lambda}d_{x_k}h_u\right)\right\|^2\\-M\left\|\sum_{k=1}^{M}\exp\left(-j\frac{2\pi}{\lambda}(d_{x_k}h_u-d_{y_k}h_v)\right)\right\|^2+M^3\end{array}\right)\end{array}\right)^{-T}\end{array}\right)}{\left(1+s_u(1-s_u)U_{SNR}\left(M^2-\left\|\sum_{k=1}^{M}\exp\left(-j\frac{2\pi}{\lambda}d_{x_k}h_u\right)\right\|^2\right)\right)^{-T}\left(1+s_v(1-s_v)U_{SNR}\left(M^2-\left\|\sum_{k=1}^{M}\exp\left(-j\frac{2\pi}{\lambda}d_{y_k}h_v\right)\right\|^2\right)\right)^{-T}}$$

$$-\left(\begin{array}{l}\left(\begin{array}{l}1-U_{SNR}\left(\begin{array}{l}s_u(1-s_v)\left(\left\|\sum_{k=1}^{M}\exp\left(-j\frac{2\pi}{\lambda}(d_{x_k}h_u+d_{y_k}h_v)\right)\right\|^2-M^2\right)\\+s_u(s_v-s_u)\left(\left\|\sum_{k=1}^{M}\exp\left(-j\frac{2\pi}{\lambda}d_{x_k}h_u\right)\right\|^2-M^2\right)\\+(1-s_v)(s_v-s_u)\left(\left\|\sum_{k=1}^{M}\exp\left(j\frac{2\pi}{\lambda}d_{y_k}h_v\right)\right\|^2-M^2\right)\end{array}\right)\\-s_u(1-s_v)(s_v-s_u)\frac{U_{SNR}^2\sigma_n^2}{\sigma_s^2}\times\\\times\left(\begin{array}{l}\sum_{k=1}^{M}\exp\left(j\frac{2\pi d_{y_k}h_v}{\lambda}\right)\sum_{k=1}^{M}\exp\left(j\frac{2\pi d_{x_k}h_u}{\lambda}\right)\sum_{k=1}^{M}\exp\left(-j\frac{2\pi(d_{x_k}h_u+d_{y_k}h_v)}{\lambda}\right)\\+\sum_{k=1}^{M}\exp\left(-j\frac{2\pi d_{y_k}h_v}{\lambda}\right)\sum_{k=1}^{M}\exp\left(-j\frac{2\pi d_{x_k}h_u}{\lambda}\right)\sum_{k=1}^{M}\exp\left(j\frac{2\pi(d_{x_k}h_u+d_{y_k}h_v)}{\lambda}\right)\\-M\left\|\sum_{k=1}^{M}\exp\left(j\frac{2\pi}{\lambda}d_{y_k}h_v\right)\right\|^2-M\left\|\sum_{k=1}^{M}\exp\left(-j\frac{2\pi}{\lambda}d_{x_k}h_u\right)\right\|^2\\-M\left\|\sum_{k=1}^{M}\exp\left(-j\frac{2\pi}{\lambda}(d_{x_k}h_u+d_{y_k}h_v)\right)\right\|^2+M^3\end{array}\right)\end{array}\right)^{-T}\\-\left(\begin{array}{l}1-U_{SNR}\left(\begin{array}{l}s_v(1-s_u)\left(\left\|\sum_{k=1}^{M}\exp\left(-j\frac{2\pi}{\lambda}(d_{x_k}h_u+d_{y_k}h_v)\right)\right\|^2-M^2\right)\\+s_v(s_u-s_v)\left(\left\|\sum_{k=1}^{M}\exp\left(-j\frac{2\pi}{\lambda}d_{x_k}h_u\right)\right\|^2-M^2\right)\\+(1-s_u)(s_u-s_v)\left(\left\|\sum_{k=1}^{M}\exp\left(-j\frac{2\pi}{\lambda}d_{y_k}h_v\right)\right\|^2-M^2\right)\end{array}\right)\\-s_v(1-s_u)(s_u-s_v)\frac{U_{SNR}^2\sigma_n^2}{\sigma_s^2}\times\\\times\left(\begin{array}{l}\sum_{k=1}^{M}\exp\left(j\frac{2\pi d_{y_k}h_v}{\lambda}\right)\sum_{k=1}^{M}\exp\left(j\frac{2\pi d_{x_k}h_u}{\lambda}\right)\sum_{k=1}^{M}\exp\left(-j\frac{2\pi(d_{x_k}h_u+d_{y_k}h_v)}{\lambda}\right)\\+\sum_{k=1}^{M}\exp\left(-j\frac{2\pi d_{y_k}h_v}{\lambda}\right)\sum_{k=1}^{M}\exp\left(-j\frac{2\pi d_{x_k}h_u}{\lambda}\right)\sum_{k=1}^{M}\exp\left(j\frac{2\pi(d_{x_k}h_u+d_{y_k}h_v)}{\lambda}\right)\\-M\left\|\sum_{k=1}^{M}\exp\left(-j\frac{2\pi}{\lambda}d_{y_k}h_v\right)\right\|^2-M\left\|\sum_{k=1}^{M}\exp\left(-j\frac{2\pi}{\lambda}d_{x_k}h_u\right)\right\|^2\\-M\left\|\sum_{k=1}^{M}\exp\left(-j\frac{2\pi}{\lambda}(d_{x_k}h_u+d_{y_k}h_v)\right)\right\|^2+M^3\end{array}\right)\end{array}\right)^{-T}\end{array}\right)$$

(3.50)

and, of course, $\{\mathbf{G}\}_{uv} = \{\mathbf{G}\}_{vu}$. Consequently, the unconditional Weiss-Weinstein bound is a 2×2 matrix given by using the above equations in Eqn. (3.44). As for the conditional case, if we set $s_u = s_v = 1/2$, one obtains the following simplified expressions

$$\{\mathbf{G}\}_{uu} = \frac{2\left(1-\frac{|h_u|}{2}\right) - 2\left(1-|h_u|\right)\left(1+\frac{U_{SNR}}{4}\left(M^2 - \left\|\sum_{k=1}^{M}\exp\left(-j\frac{4\pi}{\lambda}d_{x_k}h_u\right)\right\|^2\right)\right)^{-T}}{\left(1-\frac{|h_u|}{2}\right)^2\left(1+\frac{U_{SNR}}{4}\left(M^2 - \left\|\sum_{k=1}^{M}\exp\left(-j\frac{2\pi}{\lambda}d_{x_k}h_u\right)\right\|^2\right)\right)^{-2T}} \tag{3.51}$$

$$\{\mathbf{G}\}_{vv} = \frac{2\left(1-\frac{|h_v|}{2}\right) - 2\left(1-|h_v|\right)\left(1+\frac{U_{SNR}}{4}\left(M^2 - \left\|\sum_{k=1}^{M}\exp\left(-j\frac{4\pi}{\lambda}d_{y_k}h_v\right)\right\|^2\right)\right)^{-T}}{\left(1-\frac{|h_v|}{2}\right)^2\left(1+\frac{U_{SNR}}{4}\left(M^2 - \left\|\sum_{k=1}^{M}\exp\left(-j\frac{2\pi}{\lambda}d_{y_k}h_v\right)\right\|^2\right)\right)^{-2T}} \tag{3.52}$$

and

$$\{\mathbf{G}\}_{uv} = \frac{\begin{pmatrix} 2\left(1+\frac{U_{SNR}}{4}\left(M^2 - \left\|\sum_{k=1}^{M}\exp\left(-j\frac{2\pi}{\lambda}(d_{x_k}h_u - d_{y_k}h_v)\right)\right\|^2\right)\right)^{-T} \\ -2\left(1+\frac{U_{SNR}}{4}\left(M^2 - \left\|\sum_{k=1}^{M}\exp\left(-j\frac{2\pi}{\lambda}(d_{x_k}h_u + d_{y_k}h_v)\right)\right\|^2\right)\right)^{-T} \end{pmatrix}}{\begin{pmatrix} \left(1+\frac{U_{SNR}}{4}\left(M^2 - \left\|\sum_{k=1}^{M}\exp\left(-j\frac{2\pi}{\lambda}d_{x_k}h_u\right)\right\|^2\right)\right)^{-T} \\ \times\left(1+\frac{U_{SNR}}{4}\left(M^2 - \left\|\sum_{k=1}^{M}\exp\left(-j\frac{2\pi}{\lambda}d_{y_k}h_v\right)\right\|^2\right)\right)^{-T} \end{pmatrix}}. \tag{3.53}$$

Again, the Weiss-Weinstein bound is obtained by using the above expressions in Eqn. (3.44) and after an optimization over the test points. The optimization over the test points can be done over a search grid or by using the ambiguity diagram of the array in order to reduce significantly the computational cost (see [RM97], [XBR04], [RM95], [TK99], [RAFL07]).

3.5.3 Source localization with a non-uniform linear array

We now briefly consider the DOA estimation of a single narrow band source in the far area by using a non-uniform linear array antenna. Without loss of generality, let us suppose that the linear array antenna lays on the Ox axis of the coordinate system (see Fig. 3.1), consequently, $d_{y_i} = 0$, $\forall i$. The vector of the sensor positions is denoted $[d_{x_1} \dots d_{x_M}]$. By letting $\theta = \sin\varphi$, where φ denotes the elevation angle of the source, the steering vector is then given by

$$\mathbf{a}(\theta) = \left[\exp\left(j\frac{2\pi}{\lambda}d_{x_1}\theta\right)\dots\exp\left(j\frac{2\pi}{\lambda}d_{x_M}\theta\right)\right]^T. \tag{3.54}$$

We assume that the parameter θ follows a uniform distribution over $[0,1]$. As in Section 3.4.2 and since the parameter of interest is a scalar, matrix $\mathbf{H}$ of the test points becomes a scalar denoted h_θ. In the same way, there is only one element $s_i \in [0,1]$ which will be simply denoted s. The closed-form expressions given here are straightforwardly obtained from the aforementioned results on the planar array about the element denoted $\{\mathbf{G}\}_{uu}$. We will continue to use the previously introduced notations $U_{SNR} = \frac{\sigma_s^4}{\sigma_n^2(M\sigma_s^2+\sigma_n^2)}$ and $C_{SNR} = \frac{1}{\sigma_n^2}\sum_{t=1}^{T}\|s(t)\|^2$.

3.5.3.1 Conditional observation model $\mathcal{M}_1$

The closed-form expression of the conditional Weiss-Weinstein bound $CWWB$ is given by

$$CWWB = \frac{h_\theta^2 \left(1-\frac{|h_\theta|}{2}\right)^2 \exp\left(4s(s-1)C_{SNR}\left(M-\sum_{k=1}^{M}\cos\left(\frac{2\pi}{\lambda}d_{x_k}h_\theta\right)\right)\right)}{\left(\begin{array}{l}\left(1-\frac{|h_\theta|}{2}\right)\left(\begin{array}{l}\exp\left(4s(2s-1)C_{SNR}\left(M-\sum_{k=1}^{M}\cos\left(\frac{2\pi}{\lambda}d_{x_k}h_\theta\right)\right)\right)\\ +\exp\left(4(2s-1)(s-1)C_{SNR}\left(M-\sum_{k=1}^{M}\cos\left(\frac{2\pi}{\lambda}d_{x_k}h_\theta\right)\right)\right)\end{array}\right)\\ -2\left(1-|h_\theta|\right)\exp\left(2s(s-1)C_{SNR}\left(M-\sum_{k=1}^{M}\cos\left(\frac{4\pi}{\lambda}d_{x_k}h_\theta\right)\right)\right)\end{array}\right)}. \tag{3.55}$$

Again, it is easy to see that $\left.\frac{\partial \mathbf{H}\mathbf{G}^{-1}\mathbf{H}^T}{\partial s}\right|_{s=\frac{1}{2}} = 0$. Consequently, one optimal value of s that maximizes $\mathbf{H}\mathbf{G}^{-1}\mathbf{H}^T$, $\forall h_\theta$ is $s=\frac{1}{2}$. The Weiss-Weinstein bound is then simplified as follows

$$CWWB = \sup_{h_\theta} \frac{h_\theta^2 \left(1-\frac{|h_\theta|}{2}\right)^2 \exp\left(-C_{SNR}\left(M-\sum_{k=1}^{M}\cos\left(\frac{2\pi}{\lambda}d_{x_k}h_\theta\right)\right)\right)}{2\left(1-\frac{|h_\theta|}{2}\right)-2\left(1-|h_\theta|\right)\exp\left(-\frac{1}{2}C_{SNR}\left(M-\sum_{k=1}^{M}\cos\left(\frac{4\pi}{\lambda}d_{x_k}h_\theta\right)\right)\right)}. \tag{3.56}$$

In the classical case of a uniform linear array (*i.e.*, $d_{x_k}=(k-1)d$), this expression can be still simplified by noticing that $\sum_{k=1}^{M}\cos\left(\frac{2\pi}{\lambda}d_{x_k}h_\theta\right) = M\cos\left(\frac{2\pi d}{\lambda}h_\theta\right)$.

3.5.3.2 Unconditional observation model $\mathcal{M}_2$

The closed-form expression of the unconditional Weiss-Weinstein bound, denoted $UWWB$, is given by

$$UWWB = \frac{h_\theta^2 \left(1-\frac{|h_\theta|}{2}\right)^2 \left(1+s(1-s)U_{SNR}\left(M^2-\left\|\sum_{k=1}^{M}\exp\left(-j\frac{2\pi}{\lambda}d_{x_k}h_\theta\right)\right\|^2\right)\right)^{-2T}}{\left(\begin{array}{l}\left(1-\frac{|h_\theta|}{2}\right)\left(\begin{array}{l}\left(1+2s(1-2s)U_{SNR}\left(M^2-\left\|\sum_{k=1}^{M}\exp\left(-j\frac{2\pi}{\lambda}d_{x_k}h_\theta\right)\right\|^2\right)\right)^{-T}\\ +\left(1+2(1-s)(2s-1)U_{SNR}\left(M^2-\left\|\sum_{k=1}^{M}\exp\left(-j\frac{2\pi}{\lambda}d_{x_k}h_\theta\right)\right\|^2\right)\right)^{-T}\end{array}\right)\\ -2\left(1-|h_\theta|\right)\left(1+s(1-s)U_{SNR}\left(M^2-\left\|\sum_{k=1}^{M}\exp\left(-j\frac{4\pi}{\lambda}d_{x_k}h_\theta\right)\right\|^2\right)\right)^{-T}\end{array}\right)}. \tag{3.57}$$

In order to find one optimal value of s that maximizes $\mathbf{H}\mathbf{G}^{-1}\mathbf{H}^T$, $\forall h_\theta$ we have considered the derivative of $\mathbf{H}\mathbf{G}^{-1}\mathbf{H}^T$ *w.r.t.* s. The calculus (not reported here) is straightforward and it is easy to see that $\left.\frac{\partial \mathbf{H}\mathbf{G}^{-1}\mathbf{H}^T}{\partial s}\right|_{s=\frac{1}{2}} = 0$. Consequently, the Weiss-Weinstein bound has just to be

optimized over h_θ and is simplified leading to

$$UWWB = \sup_{h_\theta} \frac{h_\theta^2 \left(1 - \frac{|h_\theta|}{2}\right)^2 \left(1 + \frac{U_{SNR}}{4}\left(M^2 - \left\|\sum_{k=1}^{M} \exp\left(-j\frac{2\pi}{\lambda} d_{x_k} h_\theta\right)\right\|^2\right)\right)^{-2T}}{2\left(1 - \frac{|h_\theta|}{2}\right) - 2\left(1 - |h_\theta|\right)\left(1 + \frac{U_{SNR}}{4}\left(M^2 - \left\|\sum_{k=1}^{M} \exp\left(-j\frac{4\pi}{\lambda} d_{x_k} h_\theta\right)\right\|^2\right)\right)^{-T}}. \tag{3.58}$$

In the classical case of a uniform linear array (*i.e.*, $d_{x_k} = (k-1)d$), this expression can be still simplified by noticing that $\sum_{k=1}^{M} \exp\left(-j\frac{2\pi}{\lambda} d_{x_k} h_\theta\right) = M \exp\left(-j\frac{2\pi d}{\lambda} h_\theta\right)$.

3.6 Simulation results and analysis

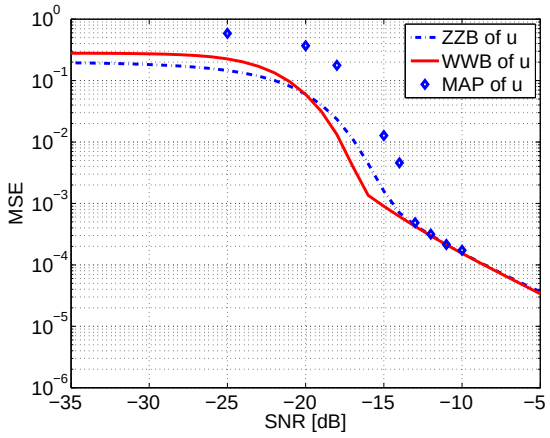

Figure 3.2: Ziv-Zakai bound, Weiss-Weinstein bound and empirical MSE of the MAP estimator: unconditional case.

As an illustration of the previously derived results, we first consider the scenario proposed in [BEV96a] Fig. 5, *i.e.*, the DOA estimation under the unconditional model using an uniform circular array consisting of $M = 16$ sensors with a half-wavelength inter-sensors spacing. The numbers of snapshots is $T = 100$. Since the array is symmetric, the performance estimation concerning parameter u and v are the same, this is why only the performance with respect to the parameters u is given in Fig. 3.2. The Weiss-Weinstein bound is computed using Eqn. (3.51), (3.52) and (3.53). The Ziv-Zakai bound is computed using Eqn. (24) in [BEV96a]. The empirical global MSE (MSE) of the maximum *a posteriori* (MAP) estimator is obtained over 2000 Monte Carlo trials. As in [BEV96a] Fig. (1b), one observes that both the Weiss-Weinstein bound and the Ziv-Zakai bound are tight w.r.t. the MSE of the MAP and capture the SNR threshold. Note that, in [BEV96a] Fig. (1b), the Weiss-Weinstein bound was computed numerically only.

To the best of our knowledge, their are no closed-form expressions of the Ziv-Zakai bound for the conditional model available in the literature. In this case, we consider 3D source localization using a V-shaped array. Indeed, it has been shown that this kind of array is able to outperform other classical planar arrays, more particularly the uniform circular array [GM06]. This array is made from two branches of uniform linear arrays with 6 sensors located on each branches and one

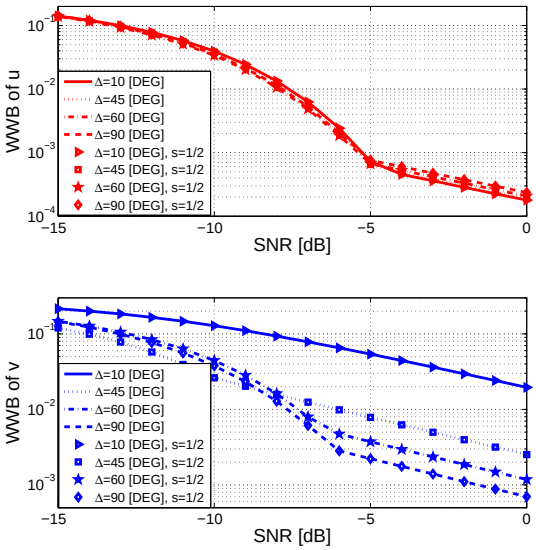

Figure 3.3: Weiss-Weinstein bounds of the V-shaped array w.r.t. the opening angle Δ.

sensor located at the origin. We denote Δ the angle between these two branches. The sensors are equally spaced with a half-wavelength. The number of snapshots is $T = 20$. Fig. 3.3 shows the behavior of the Weiss-Weinstein bound with respect to the opening angle Δ. One can observe that when Δ varies, the estimation performance concerning the estimation of parameter u varies slightly. On the contrary, the estimation performance concerning the estimation of parameter v is strongly dependent on Δ. When Δ increases from $0°$ to $90°$, the Weiss-Weinstein bound of v decreases, as well as the SNR threshold. Fig. 3.3 also shows that $\Delta = 90°$ is the optimal value, which is different with the optimal value $\Delta = 53.13°$ in [GM06] since the assumptions concerning the source signal are not the same.

3.7 Conclusion

In this chapter, the Weiss-Weinstein bound on the mean square error has been studied in the array processing context. In order to analyze the unconditional and conditional signal source models, the structure of the bound has been detailed for both Gaussian observation models with a parameterized mean or a parameterized covariance matrix.

3.8 Appendix

3.8.1 Closed-form expression of $\acute{\eta}_{\boldsymbol{\theta}}(\alpha, \beta, \mathbf{u}, \mathbf{v})$ under the Gaussian observation model with parameterized mean

Since $\mathbf{y}(t) \sim \mathbb{C}\mathcal{N}(\mathbf{f}(\boldsymbol{\theta}), \mathbf{R}_{\mathbf{y}})$, one has

$$\acute{\eta}_{\boldsymbol{\theta}}(\alpha, \beta, \mathbf{u}, \mathbf{v}) = \frac{1}{\pi^{MT} |\mathbf{R}_{\mathbf{y}}|^T} \int_{\Omega} \exp\left(-\sum_{t=1}^{T} \xi(t)\right) d\mathbf{y}, \tag{3.59}$$

with[2]

$$\begin{aligned}
\xi(t) &= \alpha (\mathbf{y}(t) - \mathbf{f}(\boldsymbol{\theta} + \mathbf{u}))^H \mathbf{R}_{\mathbf{y}}^{-1} (\mathbf{y}(t) - \mathbf{f}(\boldsymbol{\theta} + \mathbf{u})) + \beta (\mathbf{y}(t) - \mathbf{f}(\boldsymbol{\theta} + \mathbf{v}))^H \mathbf{R}_{\mathbf{y}}^{-1} (\mathbf{y}(t) - \mathbf{f}(\boldsymbol{\theta} + \mathbf{v})) \\
&\quad + (1 - \alpha - \beta) (\mathbf{y}(t) - \mathbf{f}(\boldsymbol{\theta}))^H \mathbf{R}_{\mathbf{y}}^{-1} (\mathbf{y}(t) - \mathbf{f}(\boldsymbol{\theta})) \\
&= \mathbf{y}(t)^H \mathbf{R}_{\mathbf{y}}^{-1} \mathbf{y}(t) + \alpha \mathbf{f}^H(\boldsymbol{\theta} + \mathbf{u}) \mathbf{R}_{\mathbf{y}}^{-1} \mathbf{f}(\boldsymbol{\theta} + \mathbf{u}) + \beta \mathbf{f}^H(\boldsymbol{\theta} + \mathbf{v}) \mathbf{R}_{\mathbf{y}}^{-1} \mathbf{f}(\boldsymbol{\theta} + \mathbf{v}) \\
&\quad + (1 - \alpha - \beta) \mathbf{f}^H(\boldsymbol{\theta}) \mathbf{R}_{\mathbf{y}}^{-1} \mathbf{f}(\boldsymbol{\theta}) - 2 \operatorname{Re}\left\{\mathbf{y}(t)^H \mathbf{R}_{\mathbf{y}}^{-1} (\alpha \mathbf{f}(\boldsymbol{\theta} + \mathbf{u}) + \beta \mathbf{f}(\boldsymbol{\theta} + \mathbf{v}) + (1 - \alpha - \beta) \mathbf{f}(\boldsymbol{\theta}))\right\}.
\end{aligned} \tag{3.60}$$

Let us set $\mathbf{x}(t) = \mathbf{y}(t) - (\alpha \mathbf{f}(\boldsymbol{\theta} + \mathbf{u}) + \beta \mathbf{f}(\boldsymbol{\theta} + \mathbf{v}) + (1 - \alpha - \beta) \mathbf{f}(\boldsymbol{\theta}))$. Consequently,

$$\begin{aligned}
\mathbf{x}(t)^H \mathbf{R}_{\mathbf{y}}^{-1} \mathbf{x}(t) &= \mathbf{y}(t)^H \mathbf{R}_{\mathbf{y}}^{-1} \mathbf{y}(t) - 2 \operatorname{Re}\left\{\mathbf{y}(t)^H \mathbf{R}_{\mathbf{y}}^{-1} (\alpha \mathbf{f}(\boldsymbol{\theta} + \mathbf{u}) + \beta \mathbf{f}(\boldsymbol{\theta} + \mathbf{v}) + (1 - \alpha - \beta) \mathbf{f}(\boldsymbol{\theta}))\right\} \\
&\quad + \left(\alpha \mathbf{f}^H(\boldsymbol{\theta} + \mathbf{u}) + \beta \mathbf{f}^H(\boldsymbol{\theta} + \mathbf{v}) + (1 - \alpha - \beta) \mathbf{f}^H(\boldsymbol{\theta})\right) \mathbf{R}_{\mathbf{y}}^{-1} (\alpha \mathbf{f}(\boldsymbol{\theta} + \mathbf{u}) + \beta \mathbf{f}(\boldsymbol{\theta} + \mathbf{v}) + (1 - \alpha - \beta) \mathbf{f}(\boldsymbol{\theta})).
\end{aligned} \tag{3.61}$$

And $\xi(t)$ can be rewritten as

$$\xi(t) = \mathbf{x}(t)^H \mathbf{R}_{\mathbf{y}}^{-1} \mathbf{x}(t) + \acute{\xi}(t), \tag{3.62}$$

where

$$\begin{aligned}
\acute{\xi}(t) &= \alpha (1 - \alpha) \mathbf{f}^H(\boldsymbol{\theta} + \mathbf{u}) \mathbf{R}_{\mathbf{y}}^{-1} \mathbf{f}(\boldsymbol{\theta} + \mathbf{u}) + \beta (1 - \beta) \mathbf{f}^H(\boldsymbol{\theta} + \mathbf{v}) \mathbf{R}_{\mathbf{y}}^{-1} \mathbf{f}(\boldsymbol{\theta} + \mathbf{v}) \\
&\quad + (1 - \alpha - \beta)(\alpha + \beta) \mathbf{f}^H(\boldsymbol{\theta}) \mathbf{R}_{\mathbf{y}}^{-1} \mathbf{f}(\boldsymbol{\theta}) - 2 \operatorname{Re}\left\{\alpha \beta \mathbf{f}^H(\boldsymbol{\theta} + \mathbf{u}) \mathbf{R}_{\mathbf{y}}^{-1} \mathbf{f}(\boldsymbol{\theta} + \mathbf{v}) \right. \\
&\quad \left. + \alpha (1 - \alpha - \beta) \mathbf{f}^H(\boldsymbol{\theta} + \mathbf{u}) \mathbf{R}_{\mathbf{y}}^{-1} \mathbf{f}(\boldsymbol{\theta}) + \beta (1 - \alpha - \beta) \mathbf{f}^H(\boldsymbol{\theta} + \mathbf{v}) \mathbf{R}_{\mathbf{y}}^{-1} \mathbf{f}(\boldsymbol{\theta})\right\}.
\end{aligned} \tag{3.63}$$

Note that $\acute{\xi}(t)$ is independent of $\mathbf{x}(t)$. By defining $\mathbf{x} = [\mathbf{x}(1), \mathbf{x}(2), \ldots, \mathbf{x}(T)]$, the function $\acute{\eta}_{\boldsymbol{\theta}}(\alpha, \beta, \mathbf{u}, \mathbf{v})$ becomes

$$\acute{\eta}_{\boldsymbol{\theta}}(\alpha, \beta, \mathbf{u}, \mathbf{v}) = \frac{1}{\pi^{MT} |\mathbf{R}_{\mathbf{y}}|^T} \int_{\Omega} \exp\left(-\sum_{t=1}^{T} \mathbf{x}(t)^H \mathbf{R}_{\mathbf{y}}^{-1} \mathbf{x}(t) + \acute{\xi}(t)\right) d\mathbf{x} = \exp\left(-\sum_{t=1}^{T} \acute{\xi}(t)\right), \tag{3.64}$$

since $\frac{1}{\pi^{MT} |\mathbf{R}_{\mathbf{y}}|^T} \int_{\Omega} \exp\left(-\sum_{t=1}^{T} \mathbf{x}(t)^H \mathbf{R}_{\mathbf{y}}^{-1} \mathbf{x}(t)\right) d\mathbf{x} = 1$.

[2] For simplicity, the dependance on t of $\mathbf{f}$ and $\mathbf{y}$ is not emphasized.

3.8.2 Closed-form expression of $\acute{\eta}_{\boldsymbol{\theta}}(\alpha,\beta,\mathbf{u},\mathbf{v})$ under the Gaussian observation model with parameterized covariance

Since $\mathbf{y}(t) \sim \mathbb{C}\mathcal{N}(\mathbf{0}, \mathbf{R}_{\mathbf{y}}(\boldsymbol{\theta}))$, one has,

$$\acute{\eta}_{\boldsymbol{\theta}}(\alpha,\beta,\mathbf{u},\mathbf{v}) = \frac{|\mathbf{R}_{\mathbf{y}}(\boldsymbol{\theta})|^{T(\alpha+\beta-1)}}{\pi^{MT}\,|\mathbf{R}_{\mathbf{y}}(\boldsymbol{\theta}+\mathbf{u})|^{T\alpha}\,|\mathbf{R}_{\mathbf{y}}(\boldsymbol{\theta}+\mathbf{v})|^{T\beta}} \int\limits_{\Omega} \exp\left(-\sum_{t=1}^{T}\mathbf{y}^H(t)\boldsymbol{\Gamma}^{-1}\mathbf{y}(t)\right)d\mathbf{y}, \quad (3.65)$$

where $\boldsymbol{\Gamma}^{-1} = \alpha\mathbf{R}_{\mathbf{y}}^{-1}(\boldsymbol{\theta}+\mathbf{u}) + \beta\mathbf{R}_{\mathbf{y}}^{-1}(\boldsymbol{\theta}+\mathbf{v}) - (\alpha+\beta-1)\mathbf{R}_{\mathbf{y}}^{-1}(\boldsymbol{\theta})$. Then, since

$$\int\limits_{\Omega} \exp\left\{-\sum_{t=1}^{T}\mathbf{y}^H(t)\boldsymbol{\Gamma}^{-1}\mathbf{y}(t)\right\}d\mathbf{y} = \pi^{MT}\,|\boldsymbol{\Gamma}|^T, \quad (3.66)$$

one has

$$\acute{\eta}_{\boldsymbol{\theta}}(\alpha,\beta,\mathbf{u},\mathbf{v}) = \frac{|\mathbf{R}_{\mathbf{y}}(\boldsymbol{\theta})|^{T(\alpha+\beta-1)}\,|\boldsymbol{\Gamma}|^T}{|\mathbf{R}_{\mathbf{y}}(\boldsymbol{\theta}+\mathbf{u})|^{T\alpha}\,|\mathbf{R}_{\mathbf{y}}(\boldsymbol{\theta}+\mathbf{v})|^{T\beta}} = \frac{|\mathbf{R}_{\mathbf{y}}(\boldsymbol{\theta})|^{T(\alpha+\beta-1)}}{|\mathbf{R}_{\mathbf{y}}(\boldsymbol{\theta}+\mathbf{u})|^{T\alpha}\,|\mathbf{R}_{\mathbf{y}}(\boldsymbol{\theta}+\mathbf{v})|^{T\beta}\,|\boldsymbol{\Gamma}^{-1}|^T}. \quad (3.67)$$

3.8.3 Closed-form expressions of $\zeta_{\boldsymbol{\theta}}(\boldsymbol{\mu},\boldsymbol{\rho})$

Remind that the function $\zeta_{\boldsymbol{\theta}}(\boldsymbol{\mu},\boldsymbol{\rho})$ is defined by Eqn. (3.17). Let us define p as the number of parameters per sources (assumed to be constant for each sources). Then, without loss of generality, the full parameter vector $\boldsymbol{\theta}$ can be decomposed as $\boldsymbol{\theta} = \left[\boldsymbol{\theta}_1^T \dots \boldsymbol{\theta}_N^T\right]^T$ where $\boldsymbol{\theta}_i = \left[\theta_{i,1} \dots \theta_{i,p}\right]^T$, $i = 1,\dots,N$ with $q = Np$. Remind that $\boldsymbol{\mu} = [0 \dots \mu_i \dots 0]^T$ and $\boldsymbol{\rho} = \left[0 \dots \rho_j \dots 0\right]^T$. It exists two distinct cases to study: when both index i and j are such that $(m-1)p+1 \leq i \leq mp$, $m = 1,\dots,N$ and $(m-1)p+1 \leq j \leq mp$ or when $(m-1)p+1 \leq i \leq mp$, $m = 1,\dots,N$ and $(n-1)p+1 \leq j \leq np$, $n = 1,\dots,N$ with $m \neq n$. Therefore let us denote:

$$\left\{\begin{array}{l} \boldsymbol{\mu}_m = [0 \cdots 0 \quad h_i \quad 0 \cdots 0]^T \in \mathbb{R}^p \\ \boldsymbol{\rho}_m = [0 \cdots 0 \quad h_j \quad 0 \cdots 0]^T \in \mathbb{R}^p \end{array}\right. \text{ if } (m-1)\,p+1 \leq i,j \leq mp \quad (3.68)$$

and

$$\left\{\begin{array}{l} \boldsymbol{\mu}_m = [0 \cdots 0 \quad h_i \quad 0 \cdots 0]^T \in \mathbb{R}^p, \\ \boldsymbol{\rho}_n = [0 \cdots 0 \quad h_j \quad 0 \cdots 0]^T \in \mathbb{R}^p, \end{array}\right. \text{ if } \left\{\begin{array}{l} (m-1)\,p+1 \leq i \leq mp \\ (n-1)\,p+1 \leq j \leq np \end{array}\right. , \text{ with } m \neq n. \quad (3.69)$$

3.8.3.1 The case where $(m-1)\,p+1 \leq i,j \leq mp$

In this case, one has:

$$\mathbf{A}(\boldsymbol{\theta}+\boldsymbol{\mu}) - \mathbf{A}(\boldsymbol{\theta}+\boldsymbol{\rho}) = [\mathbf{0} \cdots \mathbf{0} \quad \mathbf{a}(\boldsymbol{\theta}_m+\boldsymbol{\mu}_m) - \mathbf{a}(\boldsymbol{\theta}_m+\boldsymbol{\rho}_m) \quad \mathbf{0} \cdots \mathbf{0}] \in \mathbb{C}^{p\times N}, \quad (3.70)$$

and consequently,

$$\zeta_{\boldsymbol{\theta}}(\boldsymbol{\mu},\boldsymbol{\rho}) = \left\|\mathbf{R}_{\mathbf{n}}^{-1/2}\left(\mathbf{a}(\boldsymbol{\theta}_m+\boldsymbol{\mu}_m) - \mathbf{a}(\boldsymbol{\theta}_m+\boldsymbol{\rho}_m)\right)\right\|^2 \sum_{t=1}^{T}\left\|\{\mathbf{s}(t)\}_m\right\|^2. \quad (3.71)$$

Due to Eqn. (3.28), one has

$\left\|\mathbf{R}_{\mathbf{n}}^{-1/2}\left(\mathbf{a}(\boldsymbol{\theta}_m+\boldsymbol{\mu}_m) - \mathbf{a}(\boldsymbol{\theta}_m+\boldsymbol{\rho}_m)\right)\right\|^2 =$

$$\sum_{i=1}^{M}\sum_{j=1}^{M}\left\{\mathbf{R}_{\mathbf{n}}^{-1}\right\}_{i,j}\exp\left(j\frac{2\pi}{\lambda}\left(\mathbf{r}_j^T-\mathbf{r}_i^T\right)\boldsymbol{\theta}_m\right)\left(\exp\left(-j\frac{2\pi}{\lambda}\mathbf{r}_i^T\boldsymbol{\mu}_m\right)-\exp\left(-j\frac{2\pi}{\lambda}\mathbf{r}_i^T\boldsymbol{\rho}_m\right)\right)$$
$$\times\left(\exp\left(j\frac{2\pi}{\lambda}\mathbf{r}_j^T\boldsymbol{\mu}_m\right)-\exp\left(j\frac{2\pi}{\lambda}\mathbf{r}_j^T\boldsymbol{\rho}_m\right)\right). \tag{3.72}$$

In particular, in the case where $\mathbf{R}_{\mathbf{n}}=\sigma_n^2\mathbf{I}$ one obtains

$$\left\|\mathbf{R}_{\mathbf{n}}^{-1/2}\left(\mathbf{a}\left(\boldsymbol{\theta}_m+\boldsymbol{\mu}_m\right)-\mathbf{a}\left(\boldsymbol{\theta}_m+\boldsymbol{\rho}_m\right)\right)\right\|^2=\frac{1}{\sigma_n^2}\sum_{i=1}^{M}\left\|\exp\left(-j\frac{2\pi}{\lambda}\mathbf{r}_i^T\boldsymbol{\mu}_m\right)-\exp\left(-j\frac{2\pi}{\lambda}\mathbf{r}_i^T\boldsymbol{\rho}_m\right)\right\|^2. \tag{3.73}$$

3.8.3.2 The case where $(m-1)\,p+1\leq i\leq mp$ and where $(n-1)\,p+1\leq j\leq np$

Without loss generality, we assume that $n>m$. Then,

$$\begin{aligned}&\mathbf{A}\left(\boldsymbol{\theta}+\boldsymbol{\mu}\right)-\mathbf{A}\left(\boldsymbol{\theta}+\boldsymbol{\rho}\right)=\\&=\left[\mathbf{a}\left(\boldsymbol{\theta}_1\right)-\mathbf{a}\left(\boldsymbol{\theta}_1\right)\cdots\mathbf{a}\left(\boldsymbol{\theta}_m+\boldsymbol{\mu}_m\right)-\mathbf{a}\left(\boldsymbol{\theta}_m\right)\cdots\mathbf{a}\left(\boldsymbol{\theta}_n\right)-\mathbf{a}\left(\boldsymbol{\theta}_n+\boldsymbol{\rho}_n\right)\cdots\mathbf{a}\left(\boldsymbol{\theta}_N\right)-\mathbf{a}\left(\boldsymbol{\theta}_N\right)\right]\\&=\left[\mathbf{0}\cdots\mathbf{0}\quad\mathbf{a}\left(\boldsymbol{\theta}_m+\boldsymbol{\mu}_m\right)-\mathbf{a}\left(\boldsymbol{\theta}_m\right)\quad\mathbf{0}\cdots\mathbf{0}\quad\mathbf{a}\left(\boldsymbol{\theta}_m\right)-\mathbf{a}\left(\boldsymbol{\theta}_n+\boldsymbol{\rho}_n\right)\quad\mathbf{0}\cdots\mathbf{0}\right],\end{aligned} \tag{3.74}$$

and consequently,

$$\zeta_{\boldsymbol{\theta}}\left(\boldsymbol{\mu},\boldsymbol{\rho}\right)=\sum_{t=1}^{T}\left\|\mathbf{R}_{\mathbf{n}}^{-1/2}\left(\mathbf{a}\left(\boldsymbol{\theta}_m+\boldsymbol{\mu}_m\right)-\mathbf{a}\left(\boldsymbol{\theta}_m\right)\right)\left\{\mathbf{s}\left(t\right)\right\}_m+\left(\mathbf{a}\left(\boldsymbol{\theta}_n\right)-\mathbf{a}\left(\boldsymbol{\theta}_n+\boldsymbol{\rho}_n\right)\right)\left\{\mathbf{s}\left(t\right)\right\}_n\right\|^2. \tag{3.75}$$

Let us set $\varkappa=\mathbf{R}_{\mathbf{n}}^{-1/2}\left(\mathbf{a}\left(\boldsymbol{\theta}_m+\boldsymbol{\mu}_m\right)-\mathbf{a}\left(\boldsymbol{\theta}_m\right)\right)$and $\varrho=\mathbf{R}_{\mathbf{n}}^{-1/2}\left(\mathbf{a}\left(\boldsymbol{\theta}_n\right)-\mathbf{a}\left(\boldsymbol{\theta}_n+\boldsymbol{\rho}_n\right)\right)$. Then, $\zeta_{\boldsymbol{\theta}}\left(\boldsymbol{\mu},\boldsymbol{\rho}\right)$ can be rewritten

$$\begin{aligned}\zeta_{\boldsymbol{\theta}}\left(\boldsymbol{\mu},\boldsymbol{\rho}\right)&=\sum_{t=1}^{T}\left\|\varkappa\left\{\mathbf{s}\left(t\right)\right\}_m+\varrho\left\{\mathbf{s}\left(t\right)\right\}_n\right\|^2\\&=\sum_{t=1}^{T}\left(\varkappa^H\varkappa\left\|\left\{\mathbf{s}\left(t\right)\right\}_m\right\|^2+\varkappa^H\varrho\left\{\mathbf{s}\left(t\right)\right\}_m^*\left\{\mathbf{s}\left(t\right)\right\}_n+\varrho^H\varkappa\left\{\mathbf{s}\left(t\right)\right\}_m\left\{\mathbf{s}\left(t\right)\right\}_n^*+\varrho^H\varrho\left\|\left\{\mathbf{s}\left(t\right)\right\}_n\right\|^2\right)\\&=\varkappa^H\varkappa\sum_{t=1}^{T}\left\|\left\{\mathbf{s}\left(t\right)\right\}_m\right\|^2+\varrho^H\varrho\sum_{t=1}^{T}\left\|\left\{\mathbf{s}\left(t\right)\right\}_n\right\|^2+2\,\mathrm{Re}\left(\varkappa^H\varrho\sum_{t=1}^{T}\left\{\mathbf{s}\left(t\right)\right\}_m^*\left\{\mathbf{s}\left(t\right)\right\}_n\right).\end{aligned} \tag{3.76}$$

By using the structure of the steering matrix $\mathbf{A}$, it leads to

$$\begin{cases}\varkappa^H\varkappa=\sum\limits_{i=1}^{M}\sum\limits_{j=1}^{M}\left\{\mathbf{R}_{\mathbf{n}}^{-1}\right\}_{i,j}\exp\left(j\frac{2\pi}{\lambda}\left(\mathbf{r}_j^T-\mathbf{r}_i^T\right)\boldsymbol{\theta}_m\right)\exp\left(-j\frac{2\pi}{\lambda}\mathbf{r}_i^T\boldsymbol{\mu}_m\right)\exp\left(j\frac{2\pi}{\lambda}\mathbf{r}_j^T\boldsymbol{\mu}_m\right),\\\varrho^H\varrho=\sum\limits_{i=1}^{M}\sum\limits_{j=1}^{M}\left\{\mathbf{R}_{\mathbf{n}}^{-1}\right\}_{i,j}\exp\left(j\frac{2\pi}{\lambda}\left(\mathbf{r}_j^T-\mathbf{r}_i^T\right)\boldsymbol{\theta}_n\right)\exp\left(-j\frac{2\pi}{\lambda}\mathbf{r}_i^T\boldsymbol{\rho}_n\right)\exp\left(j\frac{2\pi}{\lambda}\mathbf{r}_j^T\boldsymbol{\rho}_n\right),\\\varkappa^H\varrho=-\sum\limits_{i=1}^{M}\sum\limits_{j=1}^{M}\left\{\mathbf{R}_{\mathbf{n}}^{-1}\right\}_{i,j}\exp\left(j\frac{2\pi}{\lambda}\left(\mathbf{r}_j^T\boldsymbol{\theta}_n-\mathbf{r}_i^T\boldsymbol{\theta}_m\right)\right)\exp\left(-j\frac{2\pi}{\lambda}\mathbf{r}_i^T\boldsymbol{\mu}_m\right)\exp\left(j\frac{2\pi}{\lambda}\mathbf{r}_j^T\boldsymbol{\rho}_n\right).\end{cases} \tag{3.77}$$

3.8.4 Closed-form expressions of $\left|m_1\mathbf{R}_{\mathbf{y}}^{-1}(\boldsymbol{\theta}_1)+m_2\mathbf{R}_{\mathbf{y}}^{-1}(\boldsymbol{\theta}_2)\right|$ and $\left|m_1\mathbf{R}_{\mathbf{y}}^{-1}(\boldsymbol{\theta}_1)+m_2\mathbf{R}_{\mathbf{y}}^{-1}(\boldsymbol{\theta}_2)+m_3\mathbf{R}_{\mathbf{y}}^{-1}(\boldsymbol{\theta}_3)\right|$

Note that this calculus is actually an extension of the result obtained in [XBR04] Appendix A in which $m_1 = m_2 = \frac{1}{2}$ and $m_3 = 0$, but follows the same method. The inverse of $\mathbf{R}_{\mathbf{y}}$ can be deduced from the Woodbury formula

$$\mathbf{R}_{\mathbf{y}}^{-1}(\boldsymbol{\theta}) = \frac{1}{\sigma_n^2}\left(\mathbf{I}_M - \frac{\sigma_s^2\mathbf{a}(\boldsymbol{\theta})\mathbf{a}^H(\boldsymbol{\theta})}{\sigma_s^2\left\|\mathbf{a}(\boldsymbol{\theta})\right\|^2+\sigma_n^2}\right).$$

Then,

$$\sum_{k=1}^{3} m_k\mathbf{R}_{\mathbf{y}}^{-1}(\boldsymbol{\theta}_k) = \frac{1}{\sigma_n^2}\sum_{k=1}^{3} m_k\left(\mathbf{I} - \frac{\sigma_s^2\mathbf{a}(\boldsymbol{\theta}_k)\mathbf{a}^H(\boldsymbol{\theta}_k)}{\sigma_s^2\left\|\mathbf{a}(\boldsymbol{\theta}_k)\right\|^2+\sigma_n^2}\right). \tag{3.78}$$

Since the rank of $\mathbf{a}(\boldsymbol{\theta}_k)\mathbf{a}^H(\boldsymbol{\theta}_k)$ is equal to 1 and since $\boldsymbol{\theta}_1 \neq \boldsymbol{\theta}_2 \neq \boldsymbol{\theta}_3$ (except for $\mathbf{h}_k = \mathbf{h}_l = \mathbf{0}$), the above matrix has $M-3$ eigenvalues equal to $\frac{1}{\sigma_n^2}\sum_{k=1}^{3} m_k$ and 3 eigenvalues corresponding to the eigenvectors made from the linear combination of $\mathbf{a}(\boldsymbol{\theta}_1)$, $\mathbf{a}(\boldsymbol{\theta}_2)$, and $\mathbf{a}(\boldsymbol{\theta}_3)$: $\mathbf{a}(\boldsymbol{\theta}_1)+p\mathbf{a}(\boldsymbol{\theta}_2)+q\mathbf{a}(\boldsymbol{\theta}_3)$. The determinant will then be the product of these M eigenvalues[3]. Let us set

$$\varphi_k = \frac{\sigma_s^2}{\sigma_s^2\left\|\mathbf{a}(\boldsymbol{\theta}_k)\right\|^2+\sigma_n^2}, \quad k = 1,2,3. \tag{3.79}$$

Then, the three aforementioned eigenvalues denoted λ must satisfy:

$$\left(\sum_{k=1}^{3} m_k\mathbf{R}_{\mathbf{y}}^{-1}(\boldsymbol{\theta}_k)\right)\left(\mathbf{a}(\boldsymbol{\theta}_1)+p\mathbf{a}(\boldsymbol{\theta}_2)+q\mathbf{a}(\boldsymbol{\theta}_3)\right) = \lambda\left(\mathbf{a}(\boldsymbol{\theta}_1)+p\mathbf{a}(\boldsymbol{\theta}_2)+q\mathbf{a}(\boldsymbol{\theta}_3)\right). \tag{3.80}$$

By using Eqn. (3.78) in the above equation and after a factorization with respect to $\mathbf{a}(\boldsymbol{\theta}_1)$, $\mathbf{a}(\boldsymbol{\theta}_2)$, and $\mathbf{a}(\boldsymbol{\theta}_3)$ one obtains

$$\begin{aligned}
&\left(x - m_1\varphi_1\left\|\mathbf{a}(\boldsymbol{\theta}_1)\right\|^2 - pm_1\varphi_1\mathbf{a}^H(\boldsymbol{\theta}_1)\mathbf{a}(\boldsymbol{\theta}_2) - qm_1\varphi_1\mathbf{a}^H(\boldsymbol{\theta}_1)\mathbf{a}(\boldsymbol{\theta}_3)\right)\mathbf{a}(\boldsymbol{\theta}_1)\\
&+\left(-m_2\varphi_2\mathbf{a}^H(\boldsymbol{\theta}_2)\mathbf{a}(\boldsymbol{\theta}_1) + p\left(x - m_2\varphi_2\left\|\mathbf{a}(\boldsymbol{\theta}_2)\right\|^2\right) - qm_2\varphi_2\mathbf{a}^H(\boldsymbol{\theta}_2)\mathbf{a}(\boldsymbol{\theta}_3)\right)\mathbf{a}(\boldsymbol{\theta}_2)\\
&+\left(-m_3\varphi_3\mathbf{a}^H(\boldsymbol{\theta}_3)\mathbf{a}(\boldsymbol{\theta}_1) - m_3\varphi_3p\mathbf{a}^H(\boldsymbol{\theta}_3)\mathbf{a}(\boldsymbol{\theta}_2) + q\left(x - m_3\varphi_3\left\|\mathbf{a}(\boldsymbol{\theta}_3)\right\|^2\right)\right)\mathbf{a}(\boldsymbol{\theta}_3) = 0,
\end{aligned} \tag{3.81}$$

where[4]

$$x = 1 - \sigma_n^2\lambda. \tag{3.82}$$

Consequently, the coefficients of $\mathbf{a}(\boldsymbol{\theta}_1)$, $\mathbf{a}(\boldsymbol{\theta}_2)$, and $\mathbf{a}(\boldsymbol{\theta}_3)$ are equals to zero leading to a system of three equations with two unknown (p and q). Solving the two first equations to find[5] p and q,

[3]Note that we are only interested by the eigenvalues. Consequently, the linear combination of of $\mathbf{a}(\boldsymbol{\theta}_1)$, $\mathbf{a}(\boldsymbol{\theta}_2)$, and $\mathbf{a}(\boldsymbol{\theta}_3)$ can be written $\mathbf{a}(\boldsymbol{\theta}_1)+p\mathbf{a}(\boldsymbol{\theta}_2)+q\mathbf{a}(\boldsymbol{\theta}_3)$ instead of $r\mathbf{a}(\boldsymbol{\theta}_1)+p\mathbf{a}(\boldsymbol{\theta}_2)+q\mathbf{a}(\boldsymbol{\theta}_3)$

[4]Note that, from Eqn. (3.18), $\sum_{k=1}^{3} m_k = 1$.

[5]p and q are given by

$$p = \frac{m_2\varphi_2\mathbf{a}^H(\boldsymbol{\theta}_2)\left(m_1\varphi_1\mathbf{a}(\boldsymbol{\theta}_1)\mathbf{a}^H(\boldsymbol{\theta}_1) + \left(x - m_1\varphi_1\left\|\mathbf{a}(\boldsymbol{\theta}_1)\right\|^2\right)\mathbf{I}\right)\mathbf{a}(\boldsymbol{\theta}_3)}{m_1\varphi_1\mathbf{a}^H(\boldsymbol{\theta}_1)\left(m_2\varphi_2\mathbf{a}(\boldsymbol{\theta}_2)\mathbf{a}^H(\boldsymbol{\theta}_2) + \left(x - m_2\varphi_2\left\|\mathbf{a}(\boldsymbol{\theta}_2)\right\|^2\right)\mathbf{I}\right)\mathbf{a}(\boldsymbol{\theta}_3)}, \tag{3.83}$$

and

$$q = \frac{\left(x - m_1\varphi_1\left\|\mathbf{a}(\boldsymbol{\theta}_1)\right\|^2\right)\left(x - m_2\varphi_2\left\|\mathbf{a}(\boldsymbol{\theta}_2)\right\|^2\right) - m_1\varphi_1m_2\varphi_2\mathbf{a}^H(\boldsymbol{\theta}_1)\mathbf{a}(\boldsymbol{\theta}_2)\mathbf{a}^H(\boldsymbol{\theta}_2)\mathbf{a}(\boldsymbol{\theta}_1)}{m_1\varphi_1\mathbf{a}^H(\boldsymbol{\theta}_1)\left(m_2\varphi_2\mathbf{a}(\boldsymbol{\theta}_2)\mathbf{a}^H(\boldsymbol{\theta}_2) + \left(x - m_2\varphi_2\left\|\mathbf{a}(\boldsymbol{\theta}_2)\right\|^2\right)\mathbf{I}\right)\mathbf{a}(\boldsymbol{\theta}_3)}. \tag{3.84}$$

and applying the solution into the last equation, one obtains the following polynomial equation of x

$$x^3 - x^2\sum_{k=1}^{3} m_k\varphi_k \left\|\mathbf{a}(\boldsymbol{\theta}_k)\right\|^2 - \frac{x}{2}\sum_{k=1}^{3}\sum_{\substack{k'=1\\k'\neq k}}^{3} m_k\varphi_k m_{k'}\varphi_{k'}\left(\left\|\mathbf{a}^H(\boldsymbol{\theta}_k)\mathbf{a}(\boldsymbol{\theta}_{k'})\right\|^2 - \left\|\mathbf{a}(\boldsymbol{\theta}_k)\right\|^2\left\|\mathbf{a}(\boldsymbol{\theta}_{k'})\right\|^2\right)$$
$$-m_1m_2m_3\varphi_1\varphi_2\varphi_3\left(\left\|\mathbf{a}(\boldsymbol{\theta}_1)\right\|^2\left\|\mathbf{a}(\boldsymbol{\theta}_2)\right\|^2\left\|\mathbf{a}(\boldsymbol{\theta}_3)\right\|^2 - \left\|\mathbf{a}^H(\boldsymbol{\theta}_2)\mathbf{a}(\boldsymbol{\theta}_3)\right\|^2\left\|\mathbf{a}(\boldsymbol{\theta}_1)\right\|^2\right.$$
$$- \left\|\mathbf{a}^H(\boldsymbol{\theta}_1)\mathbf{a}(\boldsymbol{\theta}_2)\right\|^2\left\|\mathbf{a}(\boldsymbol{\theta}_3)\right\|^2 - \left\|\mathbf{a}^H(\boldsymbol{\theta}_3)\mathbf{a}(\boldsymbol{\theta}_1)\right\|^2\left\|\mathbf{a}^H(\boldsymbol{\theta}_2)\right\|^2 + \mathbf{a}^H(\boldsymbol{\theta}_3)\mathbf{a}(\boldsymbol{\theta}_2)\mathbf{a}^H(\boldsymbol{\theta}_1)\mathbf{a}(\boldsymbol{\theta}_3)\mathbf{a}^H(\boldsymbol{\theta}_2)\mathbf{a}(\boldsymbol{\theta}_1)$$
$$\left.+\mathbf{a}^H(\boldsymbol{\theta}_3)\mathbf{a}(\boldsymbol{\theta}_1)\mathbf{a}^H(\boldsymbol{\theta}_1)\mathbf{a}(\boldsymbol{\theta}_2)\mathbf{a}^H(\boldsymbol{\theta}_2)\mathbf{a}(\boldsymbol{\theta}_3)\right) = 0$$

Since we are only interested by the product of the three eigenvalues, we do not have to solve this polynomial in λ and only the opposite of the last term is required. This leads to Eqn. (3.35) with $\sum_{k=1}^{3} m_k = 1$. Of course, the closed-form expression of $\left|m_1\mathbf{R}_{\mathbf{y}}^{-1}(\boldsymbol{\theta}_1) + m_2\mathbf{R}_{\mathbf{y}}^{-1}(\boldsymbol{\theta}_2)\right|$ is obtained by letting $m_3 = 0$ and $\sum_{k=1}^{2} m_k = 1$ in Eqn. (3.36).

3.8.5 Proof of Eqn. (3.41), (3.42) and (3.43)

By considering the following expressions

$$\mathbf{a}^H(\mathbf{u}\pm\mathbf{h}_u)\mathbf{a}(\mathbf{u}) = \sum_{i=1}^{M}\exp\left(\mp j\frac{2\pi}{\lambda}d_{xi}h_u\right),$$
$$\mathbf{a}^H(\mathbf{u}\pm\mathbf{h}_v)\mathbf{a}(\mathbf{u}) = \sum_{i=1}^{M}\exp\left(\mp j\frac{2\pi}{\lambda}d_{yi}h_v\right),$$
$$\mathbf{a}^H(\mathbf{u}+\mathbf{h}_u)\mathbf{a}(\mathbf{u}+\mathbf{h}_v) = \sum_{i=1}^{M}\exp\left(j\frac{2\pi}{\lambda}(d_{yi}h_v - d_{xi}h_u)\right),$$
$$\mathbf{a}^H(\mathbf{u}+\mathbf{h}_v)\mathbf{a}(\mathbf{u}+\mathbf{h}_u) = \sum_{i=1}^{M}\exp\left(j\frac{2\pi}{\lambda}(d_{xi}h_u - d_{yi}h_v)\right),$$
$$\mathbf{a}^H(\mathbf{u}+\mathbf{h}_u)\mathbf{a}(\mathbf{u}-\mathbf{h}_u) = \sum_{i=1}^{M}\exp\left(-j\frac{4\pi}{\lambda}d_{xi}h_u\right),$$
$$\mathbf{a}^H(\mathbf{u}+\mathbf{h}_v)\mathbf{a}(\mathbf{u}-\mathbf{h}_v) = \sum_{i=1}^{M}\exp\left(-j\frac{4\pi}{\lambda}d_{yi}h_v\right),$$

since $\mathbf{R}_{\mathbf{n}} = \sigma_n^2\mathbf{I}$, one obtains

$$\left\{\begin{array}{lcll}
\zeta_{\boldsymbol{\theta}}(\mathbf{h}_u,\mathbf{0}) & = & \zeta_{\boldsymbol{\theta}}(-\mathbf{h}_u,\mathbf{0}) & = 2C_{SNR}\left(M-\sum_{k=1}^{M}\cos\left(\frac{2\pi}{\lambda}d_{xk}h_u\right)\right),\\
\zeta_{\boldsymbol{\theta}}(\mathbf{h}_v,\mathbf{0}) & = & \zeta_{\boldsymbol{\theta}}(-\mathbf{h}_v,\mathbf{0}) & = 2C_{SNR}\left(M-\sum_{k=1}^{M}\cos\left(\frac{2\pi}{\lambda}d_{yk}h_v\right)\right),\\
\zeta_{\boldsymbol{\theta}}(\mathbf{h}_u,-\mathbf{h}_u) & = & \zeta_{\boldsymbol{\theta}}(-\mathbf{h}_u,\mathbf{h}_u) & = 2C_{SNR}\left(M-\sum_{k=1}^{M}\cos\left(\frac{4\pi}{\lambda}d_{xk}h_u\right)\right),\\
\zeta_{\boldsymbol{\theta}}(\mathbf{h}_v,-\mathbf{h}_v) & = & \zeta_{\boldsymbol{\theta}}(-\mathbf{h}_v,\mathbf{h}_v) & = 2C_{SNR}\left(M-\sum_{k=1}^{M}\cos\left(\frac{4\pi}{\lambda}d_{yk}h_v\right)\right),\\
\zeta_{\boldsymbol{\theta}}(\mathbf{h}_u,\mathbf{h}_v) & = & \zeta_{\boldsymbol{\theta}}(\mathbf{h}_v,\mathbf{h}_u) & = \zeta_{\boldsymbol{\theta}}(-\mathbf{h}_u,-\mathbf{h}_v)\\
 & = & \zeta_{\boldsymbol{\theta}}(-\mathbf{h}_v,-\mathbf{h}_u) & = 2C_{SNR}\left(M-\sum_{k=1}^{M}\cos\left(\frac{2\pi}{\lambda}(d_{xk}h_u-d_{yk}h_v)\right)\right),\\
\zeta_{\boldsymbol{\theta}}(-\mathbf{h}_u,\mathbf{h}_v) & = & \zeta_{\boldsymbol{\theta}}(\mathbf{h}_u,-\mathbf{h}_v) & = \zeta_{\boldsymbol{\theta}}(\mathbf{h}_v,-\mathbf{h}_u)\\
 & = & \zeta_{\boldsymbol{\theta}}(-\mathbf{h}_v,\mathbf{h}_u) & = 2C_{SNR}\left(M-\sum_{k=1}^{M}\cos\left(\frac{2\pi}{\lambda}(d_{xk}h_u+d_{yk}h_v)\right)\right),\\
\zeta_{\boldsymbol{\theta}}(\mathbf{h}_u,\mathbf{h}_u) & = & \zeta_{\boldsymbol{\theta}}(\mathbf{h}_v,\mathbf{h}_v) & = 0,\\
\zeta_{\boldsymbol{\theta}}(-\mathbf{h}_u,-\mathbf{h}_u) & = & \zeta_{\boldsymbol{\theta}}(-\mathbf{h}_v,-\mathbf{h}_v) & = 0.
\end{array}\right. \tag{3.85}$$

The set of function $\acute{\eta}_C$ involving $\{\mathbf{G}\}_{u,u}$ is given by plugging the above equations into Eqn. (3.16):

$$\left\{\begin{array}{lcl}
\acute{\eta}_{\boldsymbol{\theta}}(s_u,s_u,\mathbf{h}_u,\mathbf{h}_u) & = & \exp\left(4s_u(2s_u-1)C_{SNR}\left(M-\sum_{k=1}^{M}\cos\left(\frac{2\pi}{\lambda}d_{xk}h_u\right)\right)\right),\\
\acute{\eta}_{\boldsymbol{\theta}}(1-s_u,1-s_u,-\mathbf{h}_u,-\mathbf{h}_u) & = & \exp\left(4(2s_u-1)(s_u-1)C_{SNR}\left(M-\sum_{k=1}^{M}\cos\left(\frac{2\pi}{\lambda}d_{xk}h_u\right)\right)\right),\\
\acute{\eta}_{\boldsymbol{\theta}}(s_u,1-s_u,\mathbf{h}_u,-\mathbf{h}_u) & = & \acute{\eta}_{\boldsymbol{\theta}}(1-s_u,s_u,-\mathbf{h}_u,\mathbf{h}_u)\\
 & = & \exp\left(2s_u(s_u-1)C_{SNR}\left(M-\sum_{k=1}^{M}\cos\left(\frac{4\pi}{\lambda}d_{xk}h_u\right)\right)\right),\\
\acute{\eta}_{\boldsymbol{\theta}}(s_u,0,\mathbf{h}_u,\mathbf{0}) & = & \acute{\eta}_{\boldsymbol{\theta}}(0,s_u,\mathbf{0},\mathbf{h}_u)\\
 & = & \exp\left(2s_u(s_u-1)C_{SNR}\left(M-\sum_{k=1}^{M}\cos\left(\frac{2\pi}{\lambda}d_{xk}h_u\right)\right)\right),
\end{array}\right. \tag{3.86}$$

The set of function $\acute{\eta}_C$ involving $\{\mathbf{G}\}_{v,v}$ are given by

$$\left\{\begin{array}{lcl}
\acute{\eta}_{\boldsymbol{\theta}}(s_v,s_v,\mathbf{h}_v,\mathbf{h}_v) & = & \exp\left(4s_v(2s_v-1)C_{SNR}\left(M-\sum_{k=1}^{M}\cos\left(\frac{2\pi}{\lambda}d_{yk}h_v\right)\right)\right),\\
\acute{\eta}_{\boldsymbol{\theta}}(1-s_v,1-s_v,-\mathbf{h}_v,-\mathbf{h}_v) & = & \exp\left(4(2s_v-1)(s_v-1)C_{SNR}\left(M-\sum_{k=1}^{M}\cos\left(\frac{2\pi}{\lambda}d_{yk}h_v\right)\right)\right),\\
\acute{\eta}_{\boldsymbol{\theta}}(s_v,1-s_v,\mathbf{h}_v,-\mathbf{h}_v) & = & \acute{\eta}_{\boldsymbol{\theta}}(1-s_v,s_v,-\mathbf{h}_v,\mathbf{h}_v)\\
 & = & \exp\left(2s_v(s_v-1)C_{SNR}\left(M-\sum_{k=1}^{M}\cos\left(\frac{4\pi}{\lambda}d_{yk}h_v\right)\right)\right),\\
\acute{\eta}_{\boldsymbol{\theta}}(s_v,0,\mathbf{h}_v,\mathbf{0}) & = & \acute{\eta}_{\boldsymbol{\theta}}(0,s_v,\mathbf{0},\mathbf{h}_v)\\
 & = & \exp\left(2s_v(s_v-1)C_{SNR}\left(M-\sum_{k=1}^{M}\cos\left(\frac{2\pi}{\lambda}d_{yk}h_v\right)\right)\right),
\end{array}\right. \tag{3.87}$$

The set of function $\acute{\eta}_C$ involving $\{\mathbf{G}\}_{u,v}$ are given by

$$\begin{cases}
\acute{\eta}_{\boldsymbol{\theta}}(s_u, s_v, \mathbf{h}_u, \mathbf{h}_v) = \exp\left(\begin{array}{l} 2s_u(s_u+s_v-1)C_{SNR}\left(M-\sum_{k=1}^{M}\cos\left(\frac{2\pi}{\lambda}d_{xk}h_u\right)\right) \\ +2s_v(s_u+s_v-1)C_{SNR}\left(M-\sum_{k=1}^{M}\cos\left(\frac{2\pi}{\lambda}d_{yk}h_v\right)\right) \\ -2s_us_vC_{SNR}\left(M-\sum_{k=1}^{M}\cos\left(\frac{2\pi}{\lambda}(d_{xk}h_u-d_{yk}h_v)\right)\right)\end{array}\right), \\
\acute{\eta}_{\boldsymbol{\theta}}(1-s_u, 1-s_v, -\mathbf{h}_u, -\mathbf{h}_v) = \\
\qquad = \exp\left(\begin{array}{l} 2(s_u-1)(s_u+s_v-1)C_{SNR}\left(M-\sum_{k=1}^{M}\cos\left(\frac{2\pi}{\lambda}d_{xk}h_u\right)\right) \\ +2(s_v-1)(s_u+s_v-1)C_{SNR}\left(M-\sum_{k=1}^{M}\cos\left(\frac{2\pi}{\lambda}d_{yk}h_v\right)\right) \\ -2(1-s_u)(1-s_v)C_{SNR}\left(M-\sum_{k=1}^{M}\cos\left(\frac{2\pi}{\lambda}(d_{xk}h_u-d_{yk}h_v)\right)\right)\end{array}\right), \\
\acute{\eta}_{\boldsymbol{\theta}}(s_u, 1-s_v, \mathbf{h}_u, -\mathbf{h}_v) = \exp\left(\begin{array}{l} 2s_u(s_u-s_v)C_{SNR}\left(M-\sum_{k=1}^{M}\cos\left(\frac{2\pi}{\lambda}d_{xk}h_u\right)\right) \\ +2(1-s_v)(s_u-s_v)C_{SNR}\left(M-\sum_{k=1}^{M}\cos\left(\frac{2\pi}{\lambda}d_{yk}h_v\right)\right) \\ +2s_u(s_v-1)C_{SNR}\left(M-\sum_{k=1}^{M}\cos\left(\frac{2\pi}{\lambda}(d_{xk}h_u+d_{yk}h_v)\right)\right)\end{array}\right), \\
\acute{\eta}_{\boldsymbol{\theta}}(1-s_u, s_v, -\mathbf{h}_u, \mathbf{h}_v) = \exp\left(\begin{array}{l} 2(s_u-1)(s_u-s_v)C_{SNR}\left(M-\sum_{k=1}^{M}\cos\left(\frac{2\pi}{\lambda}d_{xk}h_u\right)\right) \\ +2s_v(s_v-s_u)C_{SNR}\left(M-\sum_{k=1}^{M}\cos\left(\frac{2\pi}{\lambda}d_{yk}h_v\right)\right) \\ +2(s_u-1)s_vC_{SNR}\left(M-\sum_{k=1}^{M}\cos\left(\frac{2\pi}{\lambda}(d_{xk}h_u+d_{yk}h_v)\right)\right)\end{array}\right), \\
\acute{\eta}_{\boldsymbol{\theta}}(s_u, 0, \mathbf{h}_u, \mathbf{0}) = \exp\left(2s_u(s_u-1)C_{SNR}\left(M-\sum_{k=1}^{M}\cos\left(\frac{2\pi}{\lambda}d_{xk}h_u\right)\right)\right), \\
\acute{\eta}_{\boldsymbol{\theta}}(0, s_v, \mathbf{0}, \mathbf{h}_v) = \exp\left(2s_v(s_v-1)C_{SNR}\left(M-\sum_{k=1}^{M}\cos\left(\frac{2\pi}{\lambda}d_{yk}h_v\right)\right)\right).
\end{cases} \tag{3.88}$$

One notices that the set of functions $\zeta_{\boldsymbol{\theta}}(\boldsymbol{\mu}, \boldsymbol{\rho})$ and $\acute{\eta}_{\boldsymbol{\theta}}(\alpha, \beta, \mathbf{u}, \mathbf{v})$ does not depend on $\boldsymbol{\theta}$. Consequently, as in unconditional case, the set of functions $\eta(\alpha, \beta, \mathbf{u}, \mathbf{v})$ is obtained by using the results of Section 3.4.2 whatever the considered prior on θ. In our case of a uniform prior, the set of function η involving $\{\mathbf{G}\}_{u,u}$ are given by:

$$\begin{cases}
\eta(s_u, s_u, \mathbf{h}_u, \mathbf{h}_u) = \left(1-\frac{|h_u|}{2}\right)\acute{\eta}_{\boldsymbol{\theta}}(s_u, s_u, \mathbf{h}_u, \mathbf{h}_u), \\
\eta(1-s_u, 1-s_u, -\mathbf{h}_u, -\mathbf{h}_u) = \left(1-\frac{|h_u|}{2}\right)\acute{\eta}_{\boldsymbol{\theta}}(1-s_u, 1-s_u, -\mathbf{h}_u, -\mathbf{h}_u), \\
\eta(s_u, 1-s_u, \mathbf{h}_u, -\mathbf{h}_u) = \eta_C(1-s_u, s_u, -\mathbf{h}_u, \mathbf{h}_u) = (1-|h_u|)\acute{\eta}_{\boldsymbol{\theta}}(1-s_u, s_u, -\mathbf{h}_u, \mathbf{h}_u), \\
\eta(s_u, 0, \mathbf{h}_u, \mathbf{0}) = \eta_C(0, s_u, \mathbf{0}, \mathbf{h}_u) = \left(1-\frac{|h_u|}{2}\right)\acute{\eta}_{\boldsymbol{\theta}}(0, s_u, \mathbf{0}, \mathbf{h}_u),
\end{cases} \tag{3.89}$$

The set of function η involving $\{\mathbf{G}\}_{v,v}$ are given by:

$$\begin{cases} \eta(s_v, s_v, \mathbf{h}_v, \mathbf{h}_v) = \left(1 - \frac{|h_v|}{2}\right) \acute{\eta}_{\boldsymbol{\theta}}(s_v, s_v, \mathbf{h}_v, \mathbf{h}_v), \\ \eta(1-s_v, 1-s_v, -\mathbf{h}_v, -\mathbf{h}_v) = \left(1 - \frac{|h_v|}{2}\right) \acute{\eta}_{\boldsymbol{\theta}}(1-s_v, 1-s_v, -\mathbf{h}_v, -\mathbf{h}_v), \\ \eta(s_v, 1-s_v, \mathbf{h}_v, -\mathbf{h}_v) = \eta(1-s_v, s_v, -\mathbf{h}_v, \mathbf{h}_v) = (1-|h_v|)\acute{\eta}_{\boldsymbol{\theta}}(s_v, 1-s_v, \mathbf{h}_v, -\mathbf{h}_v), \\ \eta(s_v, 0, \mathbf{h}_v, \mathbf{0}) = \eta(0, s_v, \mathbf{0}, \mathbf{h}_v) = \left(1 - \frac{|h_v|}{2}\right) \acute{\eta}_{\boldsymbol{\theta}}(s_v, 0, \mathbf{h}_v, \mathbf{0}), \end{cases} \tag{3.90}$$

And the set of function η involving $\{\mathbf{G}\}_{u,v} = \{\mathbf{G}\}_{v,u}$ are given by:

$$\begin{cases} \eta(s_u, s_v, \mathbf{h}_u, \mathbf{h}_v) = \left(1 - \frac{|h_u|}{2}\right)\left(1 - \frac{|h_v|}{2}\right) \acute{\eta}_{\boldsymbol{\theta}}(s_u, s_v, \mathbf{h}_u, \mathbf{h}_v), \\ \eta(1-s_u, 1-s_v, -\mathbf{h}_u, -\mathbf{h}_v) = \left(1 - \frac{|h_u|}{2}\right)\left(1 - \frac{|h_v|}{2}\right) \acute{\eta}_{\boldsymbol{\theta}}(1-s_u, 1-s_v, -\mathbf{h}_u, -\mathbf{h}_v), \\ \eta(s_u, 1-s_v, \mathbf{h}_u, -\mathbf{h}_v) = \left(1 - \frac{|h_u|}{2}\right)\left(1 - \frac{|h_v|}{2}\right) \acute{\eta}_{\boldsymbol{\theta}}(s_u, 1-s_v, \mathbf{h}_u, -\mathbf{h}_v), \\ \eta(1-s_u, s_v, -\mathbf{h}_u, \mathbf{h}_v) = \left(1 - \frac{|h_u|}{2}\right)\left(1 - \frac{|h_v|}{2}\right) \acute{\eta}_{\boldsymbol{\theta}}(1-s_u, s_v, -\mathbf{h}_u, \mathbf{h}_v), \\ \eta(s_u, 0, \mathbf{h}_u, \mathbf{0}) = \left(1 - \frac{|h_u|}{2}\right) \acute{\eta}_{\boldsymbol{\theta}}(s_u, 0, \mathbf{h}_u, \mathbf{0}), \\ \eta(0, s_v, \mathbf{0}, \mathbf{h}_v) = \left(1 - \frac{|h_v|}{2}\right) \acute{\eta}_{\boldsymbol{\theta}}(0, s_v, \mathbf{0}, \mathbf{h}_v). \end{cases} \tag{3.91}$$

Finally, the results are straightforward and leads to Eqn. (3.41), (3.42) and (3.43).

3.8.6 Proof of Eqn. (3.48), (3.49) and (3.50)

In fact, one only has to prove Eqn. (3.50) since Eqn. (3.48) and (3.49) can be obtained by letting $h_u = h_v$ and $s_u = s_v$ in Eqn. (3.50) and by using (h_u, s_u) for Eqn. (3.48) and (h_v, s_v) for Eqn. (3.49). By plugging Eqn. (3.35) and (3.36) into Eqn. (3.18), one obtains the closed-form expressions for the set of functions $\acute{\eta}_{\boldsymbol{\theta}}(\alpha, \beta, \mathbf{u}, \mathbf{v})$

$$\begin{cases} \acute{\eta}_{\boldsymbol{\theta}}(s_u, s_u, \mathbf{h}_u, \mathbf{h}_u, \mathbf{u}) = \left(1 + 2s_u(1-2s_u)U_{SNR}\left(M^2 - \left\|\sum_{k=1}^{M} \exp\left(-j\frac{2\pi}{\lambda}d_{xk}h_u\right)\right\|^2\right)\right)^{-T}, \\ \acute{\eta}_{\boldsymbol{\theta}}(1-s_u, 1-s_u, -\mathbf{h}_u, -\mathbf{h}_u, \mathbf{u}) = \\ \qquad = \left(1 + 2(1-s_u)(2s_u-1)U_{SNR}\left(M^2 - \left\|\sum_{k=1}^{M} \exp\left(-j\frac{2\pi}{\lambda}d_{xk}h_u\right)\right\|^2\right)\right)^{-T}, \\ \acute{\eta}_{\boldsymbol{\theta}}(s_u, 1-s_u, \mathbf{h}_u, -\mathbf{h}_u, \mathbf{u}) = \acute{\eta}_U(1-s_u, s_u, -\mathbf{h}_u, \mathbf{h}_u, \mathbf{u}) = \\ \qquad = \left(1 + s_u(1-s_u)U_{SNR}\left(M^2 - \left\|\sum_{k=1}^{M} \exp\left(-j\frac{4\pi}{\lambda}d_{xk}h_u\right)\right\|^2\right)\right)^{-T}, \\ \acute{\eta}_{\boldsymbol{\theta}}(s_u, 0, \mathbf{h}_u, \mathbf{0}, \mathbf{u}) = \acute{\eta}_U(0, s_u, \mathbf{0}, \mathbf{h}_u, \mathbf{u}) = \\ \qquad = \left(1 + s_u(1-s_u)U_{SNR}\left(M^2 - \left\|\sum_{k=1}^{M} \exp\left(-j\frac{2\pi}{\lambda}d_{xk}h_u\right)\right\|^2\right)\right)^{-T}. \end{cases} \tag{3.92}$$

$$\begin{cases} \acute{\eta}_{\boldsymbol{\theta}}(s_v, s_v, \mathbf{h}_v, \mathbf{h}_v, \mathbf{u}) = \left(1 + 2s_v(1-2s_v)U_{SNR}\left(M^2 - \left\|\sum_{k=1}^{M} \exp\left(-j\frac{2\pi}{\lambda}d_{yk}h_v\right)\right\|^2\right)\right)^{-T}, \\ \acute{\eta}_{\boldsymbol{\theta}}(1-s_v, 1-s_v, -\mathbf{h}_v, -\mathbf{h}_v, \mathbf{u}) = \\ \qquad = \left(1 + 2(1-s_v)(2s_v-1)U_{SNR}\left(M^2 - \left\|\sum_{k=1}^{M} \exp\left(-j\frac{2\pi}{\lambda}d_{yk}h_v\right)\right\|^2\right)\right)^{-T}, \\ \acute{\eta}_{\boldsymbol{\theta}}(s_v, 1-s_v, \mathbf{h}_v, -\mathbf{h}_v, \mathbf{u}) = \acute{\eta}_U(1-s_v, s_v, -\mathbf{h}_v, \mathbf{h}_v, \mathbf{u}) = \\ \qquad = \left(1 + s_v(1-s_v)U_{SNR}\left(M^2 - \left\|\sum_{k=1}^{M} \exp\left(-j\frac{4\pi}{\lambda}d_{yk}h_v\right)\right\|^2\right)\right)^{-T}, \\ \acute{\eta}_{\boldsymbol{\theta}}(s_v, 0, \mathbf{h}_v, \mathbf{0}, \mathbf{u}) = \acute{\eta}_U(0, s_v, \mathbf{0}, \mathbf{h}_v, \mathbf{u}) = \\ \qquad = \left(1 + s_v(1-s_v)U_{SNR}\left(M^2 - \left\|\sum_{k=1}^{M} \exp\left(-j\frac{2\pi}{\lambda}d_{yk}h_v\right)\right\|^2\right)\right)^{-T}. \end{cases} \tag{3.93}$$

and

$$\begin{aligned} &\acute{\eta}_{\boldsymbol{\theta}}(s_u, s_v, \mathbf{h}_u, \mathbf{h}_v, \mathbf{u}) = \\ &= \left(\begin{array}{l} 1 - U_{SNR}\left(\begin{array}{l} s_u s_v \left(\left\|\sum_{k=1}^{M} \exp\left(-j\frac{2\pi}{\lambda}(d_{xk}h_u - d_{yk}h_v)\right)\right\|^2 - M^2 \right) \\ +s_u(1-s_u-s_v)\left(\left\|\sum_{k=1}^{M} \exp\left(-j\frac{2\pi}{\lambda}d_{xk}h_u\right)\right\|^2 - M^2 \right) \\ +s_v(1-s_u-s_v)\left(\left\|\sum_{k=1}^{M} \exp\left(-j\frac{2\pi}{\lambda}d_{yk}h_v\right)\right\|^2 - M^2 \right) \end{array} \right) \\ -s_u s_v(1-s_u-s_v)\frac{U_{SNR}^2\sigma_n^2}{\sigma_s^2}\times \\ \times \left(\begin{array}{l} \sum_{k=1}^{M} \exp\left(j\frac{2\pi d_{yk}h_v}{\lambda}\right)\sum_{k=1}^{M} \exp\left(-j\frac{2\pi d_{xk}h_u}{\lambda}\right)\sum_{k=1}^{M} \exp\left(j\frac{2\pi(d_{xk}h_u - d_{yk}h_v)}{\lambda}\right) \\ +\sum_{k=1}^{M} \exp\left(-j\frac{2\pi d_{yk}h_v}{\lambda}\right)\sum_{k=1}^{M} \exp\left(j\frac{2\pi d_{xk}h_u}{\lambda}\right)\sum_{k=1}^{M} \exp\left(-j\frac{2\pi(d_{xk}h_u - d_{yk}h_v)}{\lambda}\right) \\ -M\left\|\sum_{k=1}^{M} \exp\left(-j\frac{2\pi}{\lambda}d_{yk}h_v\right)\right\|^2 - M\left\|\sum_{k=1}^{M} \exp\left(-j\frac{2\pi}{\lambda}d_{xk}h_u\right)\right\|^2 \\ -M\left\|\sum_{k=1}^{M} \exp\left(-j\frac{2\pi}{\lambda}(d_{xk}h_u - d_{yk}h_v)\right)\right\|^2 + M^3 \end{array} \right) \end{array} \right)^{-T} \end{aligned} \tag{3.94}$$

$$
\begin{aligned}
&\acute{\eta}_{\boldsymbol{\theta}}(1-s_u, 1-s_v, -\mathbf{h}_u, -\mathbf{h}_v, \mathbf{u}) = \\
&= \left(\begin{array}{l}
1 - U_{SNR} \left(\begin{array}{l}
(1-s_u)(1-s_v) \left(\left\| \sum_{k=1}^{M} \exp\left(j\frac{2\pi}{\lambda}(d_{xk}h_u - d_{yk}h_v)\right) \right\|^2 - M^2 \right) \\
+(1-s_u)(s_u+s_v-1) \left(\left\| \sum_{k=1}^{M} \exp\left(j\frac{2\pi}{\lambda}d_{xk}h_u\right) \right\|^2 - M^2 \right) \\
+(1-s_v)(s_u+s_v-1) \left(\left\| \sum_{k=1}^{M} \exp\left(j\frac{2\pi}{\lambda}d_{yk}h_v\right) \right\|^2 - M^2 \right)
\end{array} \right) \\
-(1-s_u)(1-s_v)(s_u+s_v-1)\frac{U_{SNR}^2\sigma_n^2}{\sigma_s^2} \times \\
\times \left(\begin{array}{l}
\sum_{k=1}^{M} \exp\left(j\frac{2\pi d_{yk}h_v}{\lambda}\right) \sum_{k=1}^{M} \exp\left(-j\frac{2\pi d_{xk}h_u}{\lambda}\right) \sum_{k=1}^{M} \exp\left(j\frac{2\pi(d_{xk}h_u - d_{yk}h_v)}{\lambda}\right) \\
+\sum_{k=1}^{M} \exp\left(-j\frac{2\pi d_{yk}h_v}{\lambda}\right) \sum_{k=1}^{M} \exp\left(j\frac{2\pi d_{xk}h_u}{\lambda}\right) \sum_{k=1}^{M} \exp\left(-j\frac{2\pi(d_{xk}h_u - d_{yk}h_v)}{\lambda}\right) \\
-M \left\| \sum_{k=1}^{M} \exp\left(-j\frac{2\pi}{\lambda}d_{yk}h_v\right) \right\|^2 - M \left\| \sum_{k=1}^{M} \exp\left(-j\frac{2\pi}{\lambda}d_{xk}h_u\right) \right\|^2 \\
-M \left\| \sum_{k=1}^{M} \exp\left(-j\frac{2\pi}{\lambda}(d_{xk}h_u - d_{yk}h_v)\right) \right\|^2 + M^3
\end{array} \right)
\end{array} \right)^{-T}
\end{aligned}
\tag{3.95}
$$

$$
\begin{aligned}
&\acute{\eta}_{\boldsymbol{\theta}}(s_u, 1-s_v, \mathbf{h}_u, -\mathbf{h}_v, \mathbf{u}) = \\
&= \left(\begin{array}{l}
1 - U_{SNR} \left(\begin{array}{l}
s_u(1-s_v) \left(\left\| \sum_{k=1}^{M} \exp\left(-j\frac{2\pi}{\lambda}(d_{xk}h_u + d_{yk}h_v)\right) \right\|^2 - M^2 \right) \\
+s_u(s_v-s_u) \left(\left\| \sum_{k=1}^{M} \exp\left(-j\frac{2\pi}{\lambda}d_{xk}h_u\right) \right\|^2 - M^2 \right) \\
+(1-s_v)(s_v-s_u) \left(\left\| \sum_{k=1}^{M} \exp\left(j\frac{2\pi}{\lambda}d_{yk}h_v\right) \right\|^2 - M^2 \right)
\end{array} \right) \\
-s_u(1-s_v)(s_v-s_u)\frac{U_{SNR}^2\sigma_n^2}{\sigma_s^2} \times \\
\times \left(\begin{array}{l}
\sum_{k=1}^{M} \exp\left(j\frac{2\pi d_{yk}h_v}{\lambda}\right) \sum_{k=1}^{M} \exp\left(j\frac{2\pi d_{xk}h_u}{\lambda}\right) \sum_{k=1}^{M} \exp\left(-j\frac{2\pi(d_{xk}h_u + d_{yk}h_v)}{\lambda}\right) \\
+\sum_{k=1}^{M} \exp\left(-j\frac{2\pi d_{yk}h_v}{\lambda}\right) \sum_{k=1}^{M} \exp\left(-j\frac{2\pi d_{xk}h_u}{\lambda}\right) \sum_{k=1}^{M} \exp\left(j\frac{2\pi(d_{xk}h_u + d_{yk}h_v)}{\lambda}\right) \\
-M \left\| \sum_{k=1}^{M} \exp\left(j\frac{2\pi}{\lambda}d_{yk}h_v\right) \right\|^2 - M \left\| \sum_{k=1}^{M} \exp\left(-j\frac{2\pi}{\lambda}d_{xk}h_u\right) \right\|^2 \\
-M \left\| \sum_{k=1}^{M} \exp\left(-j\frac{2\pi}{\lambda}(d_{xk}h_u + d_{yk}h_v)\right) \right\|^2 + M^3
\end{array} \right)
\end{array} \right)^{-T}
\end{aligned}
\tag{3.96}
$$

$$\acute{\eta}_{\boldsymbol{\theta}}(1-s_u,s_v,-\mathbf{h}_u,\mathbf{h}_v,\mathbf{u}) =$$
$$= \left(\begin{array}{l} 1-U_{SNR}\left(\begin{array}{l} s_v(1-s_u)\left(\left\|\sum_{k=1}^{M}\exp\left(-j\frac{2\pi}{\lambda}(d_{xk}h_u+d_{yk}h_v)\right)\right\|^2-M^2\right) \\ +s_v(s_u-s_v)\left(\left\|\sum_{k=1}^{M}\exp\left(-j\frac{2\pi}{\lambda}d_{xk}h_u\right)\right\|^2-M^2\right) \\ +(1-s_u)(s_u-s_v)\left(\left\|\sum_{k=1}^{M}\exp\left(-j\frac{2\pi}{\lambda}d_{yk}h_v\right)\right\|^2-M^2\right) \end{array}\right) \\ -s_v(1-s_u)(s_u-s_v)\frac{U_{SNR}^2\sigma_n^2}{\sigma_s^2}\times \\ \times\left(\begin{array}{l} \sum_{k=1}^{M}\exp\left(j\frac{2\pi d_{yk}h_v}{\lambda}\right)\sum_{k=1}^{M}\exp\left(j\frac{2\pi d_{xk}h_u}{\lambda}\right)\sum_{k=1}^{M}\exp\left(-j\frac{2\pi(d_{xk}h_u+d_{yk}h_v)}{\lambda}\right) \\ +\sum_{k=1}^{M}\exp\left(-j\frac{2\pi d_{yk}h_v}{\lambda}\right)\sum_{k=1}^{M}\exp\left(-j\frac{2\pi d_{xk}h_u}{\lambda}\right)\sum_{k=1}^{M}\exp\left(j\frac{2\pi(d_{xk}h_u+d_{yk}h_v)}{\lambda}\right) \\ -M\left\|\sum_{k=1}^{M}\exp\left(-j\frac{2\pi}{\lambda}d_{yk}h_v\right)\right\|^2-M\left\|\sum_{k=1}^{M}\exp\left(-j\frac{2\pi}{\lambda}d_{xk}h_u\right)\right\|^2 \\ -M\left\|\sum_{k=1}^{M}\exp\left(-j\frac{2\pi}{\lambda}(d_{xk}h_u+d_{yk}h_v)\right)\right\|^2+M^3 \end{array}\right) \end{array}\right)^{-T} \tag{3.97}$$

$$\acute{\eta}_{\boldsymbol{\theta}}(s_u,0,\mathbf{h}_u,\mathbf{0},\mathbf{u}) = \left(1+s_u(1-s_u)U_{SNR}\left(M^2-\left\|\sum_{k=1}^{M}\exp\left(-j\frac{2\pi}{\lambda}d_{xk}h_u\right)\right\|^2\right)\right)^{-T}, \tag{3.98}$$

$$\acute{\eta}_{\boldsymbol{\theta}}(0,s_v,\mathbf{0},\mathbf{h}_v,\mathbf{u}) = \left(1+s_v(1-s_v)U_{SNR}\left(M^2-\left\|\sum_{k=1}^{M}\exp\left(-j\frac{2\pi}{\lambda}d_{yk}h_v\right)\right\|^2\right)\right)^{-T}, \tag{3.99}$$

Again, since the set of functions $\acute{\eta}_{\boldsymbol{\theta}}(\alpha,\beta,\mathbf{u},\mathbf{v})$ does not depend on $\boldsymbol{\theta}$. Consequently, it is also easy to obtain the Weiss-Weinstein bound (throughout the set of functions $\eta(\alpha,\beta,\mathbf{u},\mathbf{v})$) by using the results of Section 3.4.2 whatever the considered prior on θ (only the integral $\int_{\Theta}\frac{p^{\alpha+\beta}(\theta+u)}{p^{\alpha+\beta-1}(\theta)}d\theta$ has to be calculated or computed numerically). In our case of a uniform prior, the set of function η involving $\{\mathbf{G}\}_{u,u}$ are given by:

$$\left\{ \begin{array}{l} \eta(s_u,s_u,\mathbf{h}_u,\mathbf{h}_u) = \left(1-\frac{|h_u|}{2}\right)\acute{\eta}_{\boldsymbol{\theta}}(s_u,s_u,\mathbf{h}_u,\mathbf{h}_u), \\ \eta(1-s_u,1-s_u,-\mathbf{h}_u,-\mathbf{h}_u) = \left(1-\frac{|h_u|}{2}\right)\acute{\eta}_{\boldsymbol{\theta}}(1-s_u,1-s_u,-\mathbf{h}_u,-\mathbf{h}_u), \\ \eta(s_u,1-s_u,\mathbf{h}_u,-\mathbf{h}_u) = \eta_{\boldsymbol{\theta}}(1-s_u,s_u,-\mathbf{h}_u,\mathbf{h}_u) = (1-|h_u|)\acute{\eta}_{\boldsymbol{\theta}}(1-s_u,s_u,-\mathbf{h}_u,\mathbf{h}_u), \\ \eta(s_u,0,\mathbf{h}_u,\mathbf{0}) = \eta_{\boldsymbol{\theta}}(0,s_u,\mathbf{0},\mathbf{h}_u) = \left(1-\frac{|h_u|}{2}\right)\acute{\eta}_{\boldsymbol{\theta}}(0,s_u,\mathbf{0},\mathbf{h}_u), \end{array}\right. \tag{3.100}$$

The set of function η involving $\{\mathbf{G}\}_{v,v}$ are given by:

$$\left\{ \begin{array}{l} \eta(s_v,s_v,\mathbf{h}_v,\mathbf{h}_v) = \left(1-\frac{|h_v|}{2}\right)\acute{\eta}_{\boldsymbol{\theta}}(s_v,s_v,\mathbf{h}_v,\mathbf{h}_v), \\ \eta(1-s_v,1-s_v,-\mathbf{h}_v,-\mathbf{h}_v) = \left(1-\frac{|h_v|}{2}\right)\acute{\eta}_{\boldsymbol{\theta}}(1-s_v,1-s_v,-\mathbf{h}_v,-\mathbf{h}_v), \\ \eta(s_v,1-s_v,\mathbf{h}_v,-\mathbf{h}_v) = \eta(1-s_v,s_v,-\mathbf{h}_v,\mathbf{h}_v) = (1-|h_v|)\acute{\eta}_{\boldsymbol{\theta}}(s_v,1-s_v,\mathbf{h}_v,-\mathbf{h}_v), \\ \eta(s_v,0,\mathbf{h}_v,\mathbf{0}) = \eta(0,s_v,\mathbf{0},\mathbf{h}_v) = \left(1-\frac{|h_v|}{2}\right)\acute{\eta}_{\boldsymbol{\theta}}(s_v,0,\mathbf{h}_v,\mathbf{0}), \end{array}\right. \tag{3.101}$$

And the set of function η involving $\{\mathbf{G}\}_{u,v} = \{\mathbf{G}\}_{v,u}$ are given by:

$$\begin{cases} \eta(s_u, s_v, \mathbf{h}_u, \mathbf{h}_v) = \left(1 - \frac{|h_u|}{2}\right)\left(1 - \frac{|h_v|}{2}\right)\acute{\eta}_{\boldsymbol{\theta}}(s_u, s_v, \mathbf{h}_u, \mathbf{h}_v), \\ \eta(1-s_u, 1-s_v, -\mathbf{h}_u, -\mathbf{h}_v) = \left(1 - \frac{|h_u|}{2}\right)\left(1 - \frac{|h_v|}{2}\right)\acute{\eta}_{\boldsymbol{\theta}}(1-s_u, 1-s_v, -\mathbf{h}_u, -\mathbf{h}_v), \\ \eta(s_u, 1-s_v, \mathbf{h}_u, -\mathbf{h}_v) = \left(1 - \frac{|h_u|}{2}\right)\left(1 - \frac{|h_v|}{2}\right)\acute{\eta}_{\boldsymbol{\theta}}(s_u, 1-s_v, \mathbf{h}_u, -\mathbf{h}_v), \\ \eta(1-s_u, s_v, -\mathbf{h}_u, \mathbf{h}_v) = \left(1 - \frac{|h_u|}{2}\right)\left(1 - \frac{|h_v|}{2}\right)\acute{\eta}_{\boldsymbol{\theta}}(1-s_u, s_v, -\mathbf{h}_u, \mathbf{h}_v), \\ \eta(s_u, 0, \mathbf{h}_u, \mathbf{0}) = \left(1 - \frac{|h_u|}{2}\right)\acute{\eta}_{\boldsymbol{\theta}}(s_u, 0, \mathbf{h}_u, \mathbf{0}), \\ \eta(0, s_v, \mathbf{0}, \mathbf{h}_v) = \left(1 - \frac{|h_v|}{2}\right)\acute{\eta}_{\boldsymbol{\theta}}(0, s_v, \mathbf{0}, \mathbf{h}_v). \end{cases} \tag{3.102}$$

Finally, the results are straightforward and leads to Eqn. (3.48), (3.49) and (3.50).

Chapter 4

Statistical resolution limit approach based on distance measure

4.1 Introduction

In array signal processing, the Statistical Resolution Limit (SRL) characterizes the minimum parameter separation which allows to resolve two closely spaced sources. The applications of the SRL are involved in many fields as: image processing, radar, astronomy etc.

In the literature, there are three main approaches to obtain the SRL.

(i) The first approach is based on the estimation accuracy. In this issue, one can distinguish two main criteria. The first one was introduced by Lee in [Lee92]. This latter, states that *two signals are resolvable, with respect to (w.r.t.) their location parameters of interest, θ_1 and θ_2, if the maximum standard deviation of θ_1 and θ_2 is less than half the difference between θ_1 and θ_2.* One can note that the Lee criterion ignores the coupling between the parameters of interest. To take into account this effect, Smith proposed the following criterion [Smi05]: *two signals are resolvable if the separation between the two parameters of interest θ_1 and θ_2 is less than the standard deviation of the separation estimation.* Consequently, the SRL in the Smith sense is defined as the separation between the parameters of interest, θ_1 and θ_2, that is equal to the standard deviation of the parameter separation. In [EBRM12], the extension of the SRL based on the Smith criterion is presented for multiple parameters per signal.

(ii) The second approach is based on the concept of the mean null spectrum [Cox73, SD95, AD08] and is only relevant to the choice of a specific high-resolution algorithm. In this context, the Cox criterion [Cox73] states *that two sources are resolved (w.r.t. a given high-resolution estimation algorithm) if the mean null spectrum at each parameter of interest θ_1 and θ_2 is lower than the mean of the null spectrum at the midpoint $\frac{\theta_1+\theta_2}{2}$.*

(iii) The third approach is based on a binary hypothesis test [AW08, LN07, SM04, SM06]. More precisely, we consider the hypothesis $\mathcal{H}_0$ which represents the case where two emitted signal sources are combined into a single signal (*i.e.,* $\theta_1 - \theta_2 = 0$) whereas the hypothesis $\mathcal{H}_1$ represents the situation where the two signals are resolvable (*i.e.,* $\theta_1 - \theta_2 \neq 0$). In this way, Amar & Weiss [AW08] derived the SRL based on the Minimal Probability of Error (MPE) for deterministic signals in a Bayesian context. The authors used the first order Taylor expansion of the probability of error to derive the SRL. Whereas in [LN07] Liu and Nehorai have defined the statistical resolution limit using some asymptotic properties of the Generalized Likelihood Ratio Test (GLRT). On the other hand, Sharman and Milanfar [SM04] derived the frequency resolution limit in the spectral analysis using the GLRT by linearizing directly the observation model. Furthermore, one should note that the Stein's lemma [CT91] provides a link between a

binary hypothesis test and the relative entropy (also called Kullback-Leiber Divergence) between the probability density function of the observations under $\mathcal{H}_1$ and $\mathcal{H}_0$. In this spirit, Sharman and Milanfar [SM06], derived the theoretical SNR in the context of image processing using this approach.

In array signal processing, there are two alternative assumptions to describe the parameter of interest: the deterministic assumption assumes that the parameters are deterministic and the Bayesian assumption assumes that the parameters are random with a known *prior* distribution. The deterministic approach provides the SRL at a given value of the parameter, meaning that it considers only the local SRL *w.r.t.* the parameter of interest. Meanwhile the Bayesian approach considers the SRL over the whole parameters space. Nevertheless, the Bayesian context has been less studied in the literature. We consider here the approach of the SRL in this context. Consequently, the parameters of the two sources are assumed to be random with some known *prior* distribution. Without loss of generality, we assume that the central parameter of interest (i.e., $\theta_c = \frac{\theta_1+\theta_2}{2}$ is a random parameter with a known *prior* distribution where the deterministic separation $\theta_2-\theta_1$ is very small (this assumption can be argued by the fact that the high-resolution algorithm have an infinite resolution power). One should note that this assumption is commonly used (see for example [AW08]).

To derive the SRL in the Bayesian context, we first introduce the Taylor expansion of the observation model based on the binary hypothesis test and based on the minimum probability of error criterion. Secondly, we derive the Bayesian approaches for the SRL based on the information and the detection theories, *i.e.,* based on the relative entropy and on a binary hypothesis test, respectively, more specifically, based on the Stein's lemma [CT91] and based on the Neyman-Pearson criteria. In information theory, the Stein's lemma links the false alarm probability (P_{fa}) resulted from the Neyman-Pearson decision criterion to the relative entropy. As the relative entropy can be approximated by a quadratic function in the SRL, it is possible to determine the SRL by this way. Finally, we compare these approaches to the Bayesian one presented by Amar and Weiss [AW08], we can note that, to the best of our knowledge, this is the only one concurrent approach to the Akaike information criterion (AIC) method [SSS95].

4.2 Problem statement

We consider the problem of the derivation of the statistical resolution limit based on a binary hypothesis test approach, in which, under $\mathcal{H}_0$, the observer detects only a single source, which is the combination of the two sources, and under $\mathcal{H}_1$, the observer detects two sources [AW08]:

$$\begin{cases} \mathcal{H}_0: & \mathbf{z}(t) = \mathbf{a}(\hat{\theta}(t))\hat{s}(t) + \mathbf{n}(t), \\ \mathcal{H}_1: & \mathbf{z}(t) = \mathbf{a}(\theta_1)s_1(t) + \mathbf{a}(\theta_2)s_2(t) + \mathbf{n}(t), \end{cases} \tag{4.1}$$

where $t = 1 \dots T$, in which T denotes the observations number, $\mathbf{z}(t)$ denotes the observations vector. $\mathbf{a}(\theta)$ denotes the signal waveforms with N samples, and without loss of generality, we assume that: $\|\mathbf{a}(\theta)\|^2 = N$. Let θ_i denote the parameter of interest of the i^{th} source such as the angle of arrival, the frequency, etc. $s_i(t)$ denotes the signal amplitude of the i^{th} source under $\mathcal{H}_1$. We denote $\hat{s}(t)$ and $\hat{\theta}(t)$ the signal amplitude and the parameter of interest under $\mathcal{H}_0$. The source signals are assumed to be deterministic with a known sequence. Without loss of generality, we assume that the prior distributions $p(\mathcal{H}_0) = p(\mathcal{H}_1) = 1/2$. The vector $\mathbf{n}$ denotes the additive white Gaussian noise with zero mean and covariance matrix $\sigma^2\mathbf{I}$.

4.2.1 Binary hypothesis test based on the MPE

Denoting the central parameter $\theta_c = \frac{\theta_2+\theta_1}{2}$ and the resolution $\delta = \theta_2 - \theta_1$, we adopt the Bayesian approach by the way that θ_c has a known *prior* distribution $p(\theta_c)$. Based on the MPE criteria, one obtains the closed-form expressions of $\hat{\theta}(t)$ and $\hat{s}(t)$ as in [AW08]:

$$\hat{\theta}(t) = \theta_c + \gamma(t)\delta, \tag{4.2}$$

$$\hat{s}(t) = \frac{1}{N}\mathbf{a}^H(\hat{\theta}(t))\left(\mathbf{a}(\theta_c - \frac{\delta}{2})s_1(t) + \mathbf{a}(\theta_c + \frac{\delta}{2})s_2(t)\right), \tag{4.3}$$

in which

$$\gamma(t) = \frac{|s_2(t)|^2 - |s_1(t)|^2}{2\left(|s_2(t)|^2 + |s_1(t)|^2 + 2\Re\left\{s_1^*(t)s_2(t)\right\}\right)}. \tag{4.4}$$

It is clear that

$$\mathbf{z}(t)|\theta_c \sim \begin{cases} \mathcal{H}_0 : \mathbb{C}\mathcal{N}(\boldsymbol{\mu}_0(t), \sigma^2\mathbf{I}), \\ \mathcal{H}_1 : \mathbb{C}\mathcal{N}(\boldsymbol{\mu}_1(t), \sigma^2\mathbf{I}), \end{cases} \tag{4.5}$$

where $\mathbb{C}\mathcal{N}()$ stands for Complex Normal and

$$\begin{aligned} \boldsymbol{\mu}_0(t) &= \mathbf{a}(\hat{\theta}(t))\hat{s}(t), \\ \boldsymbol{\mu}_1(t) &= \mathbf{a}(\theta_1(t))s_1(t) + \mathbf{a}(\theta_2(t))s_2(t). \end{aligned} \tag{4.6}$$

Therefore, the probability density function (pdf) of the full observation vector is given by:

$$p(\mathbf{z}; \mathcal{H}_0, \theta_c) = \frac{1}{(\pi\sigma^2)^{NT}} \exp\left(-\frac{1}{\sigma^2}\sum_{t=1}^{T}\left\|\mathbf{z}(t) - \boldsymbol{\mu}_0(t)\right\|^2\right), \tag{4.7}$$

$$p(\mathbf{z}; \mathcal{H}_1, \theta_c) = \frac{1}{(\pi\sigma^2)^{NT}} \exp\left(-\frac{1}{\sigma^2}\sum_{t=1}^{T}\left\|\mathbf{z}(t) - \boldsymbol{\mu}_1(t)\right\|^2\right). \tag{4.8}$$

where $\mathbf{z} = \left[\mathbf{z}(1)^T \dots \mathbf{z}(T)^T\right]^T$.

4.2.2 Linearized binary hypothesis test

Using the fact that θ_1, θ_2, $\hat{\theta}(t)$ are in the vicinity of θ_c, the first-order Taylor expansions of the steering vectors are given as follows:

$$\mathbf{a}(\theta_1) \cong \mathbf{a}(\theta_c) - \frac{\delta}{2}\dot{\mathbf{a}}(\theta_c) \;\text{ at } (\theta_1 = \theta_c - \tfrac{\delta}{2}), \tag{4.9}$$

$$\mathbf{a}(\theta_2) \cong \mathbf{a}(\theta_c) + \frac{\delta}{2}\dot{\mathbf{a}}(\theta_c) \;\text{ at } (\theta_2 = \theta_c + \tfrac{\delta}{2}), \tag{4.10}$$

$$\mathbf{a}(\hat{\theta}(t)) \cong \mathbf{a}(\theta_c) + \gamma(t)\delta\dot{\mathbf{a}}(\theta_c) \;\text{ at } (\hat{\theta}(t) = \theta_c + \gamma(t)\delta), \tag{4.11}$$

in which the first-order derivative *w.r.t.* θ_c of vector $\mathbf{a}(\theta_c)$ is defined as $\dot{\mathbf{a}}(\theta_c)$. Substituting (4.9), (4.10), (4.11) into (4.3), and since $\left\|\mathbf{a}(\theta_c)\right\|^2 = N$, one obtains:

$$\begin{aligned} \hat{s}(t) &\cong \frac{1}{N}\left(\mathbf{a}(\theta_c) + \gamma(t)\delta\dot{\mathbf{a}}(\theta_c)\right)^H \left(\left(\mathbf{a}(\theta_c) - \frac{\delta}{2}\dot{\mathbf{a}}(\theta_c)\right)s_1(t) + \left(\mathbf{a}(\theta_c) + \frac{\delta}{2}\dot{\mathbf{a}}(\theta_c)\right)s_2(t)\right) \\ &= s_1(t) + s_2(t) + \frac{\delta}{N}\mathbf{a}^H(\theta_c)\dot{\mathbf{a}}(\theta_c)\left(\frac{s_2(t) - s_1(t)}{2} - \gamma(t)(s_1(t) + s_2(t))\right) + \frac{\delta^2\gamma(t)}{2N}\left\|\dot{\mathbf{a}}(\theta_c)\right\|^2(s_2(t) - s_1(t)). \end{aligned} \tag{4.12}$$

By omitting the term concerning δ^2, the optimal value of $\hat{s}(t)$, can be expressed as:

$$\hat{s}(t) \cong s^+(t) + \frac{\delta}{N}\kappa_c m(t), \tag{4.13}$$

in which we set

$$s^+(t) = s_1(t) + s_2(t), \tag{4.14}$$
$$\kappa_c = \mathbf{a}^H(\theta_c)\dot{\mathbf{a}}(\theta_c), \tag{4.15}$$
$$\mathbf{m} = [m(1)\dots m(T)]^T = \mathbf{V}^T\mathbf{s}, \tag{4.16}$$

where $\mathbf{s} = [s_1(1)\ s_2(1)\dots s_1(T)\ s_2(T)]^T$ and $\mathbf{V} = \text{Bdiag}\{\mathbf{v}(1),\dots,\mathbf{v}(T)\}$ with $\mathbf{v}(t) = [\gamma(t) + \frac{1}{2}\ \ \gamma(t) - \frac{1}{2}]^T$, and where Bdiag(.) denotes the bloc-diagonal operator. According to the previous expressions, we can see that the optimal source $\hat{s}(t)$ is approximated by a linear combination of the sources $s_1(t)$ and $s_2(t)$.

The first order of the Taylor expansions of $\boldsymbol{\mu}_0(t)$ and $\boldsymbol{\mu}_1(t)$ are given by substituting (4.11) and (4.13) into the expression of $\boldsymbol{\mu}_0(t)$, and by substituting (4.9) and (4.10) into the expression of $\boldsymbol{\mu}_1(t)$. Thus, one obtains:

$$\begin{aligned}\boldsymbol{\mu}_0(t) &\cong \mathbf{a}(\hat{\theta}(t))\hat{s}(t)\\ &= (\mathbf{a}(\theta_c) + \gamma(t)\delta\dot{\mathbf{a}}(\theta_c))\left(s^+(t) + \frac{\delta}{N}\kappa_c m(t)\right)\\ &= \mathbf{a}(\theta_c)s^+(t) + \delta\left(s^+(t)\gamma(t)\dot{\mathbf{a}}(\theta_c) + \left(\frac{\kappa_c m(t)}{N}\right)\mathbf{a}(\theta_c)\right) + \frac{\delta^2}{N}\dot{\mathbf{a}}(\theta_c)\gamma(t)\kappa_c m(t),\end{aligned} \tag{4.17}$$

and

$$\begin{aligned}\boldsymbol{\mu}_1(t) &\cong \sum_{k=1}^{2}\mathbf{a}(\theta_k)s_k(t)\\ &= \left(\mathbf{a}(\theta_c) - \frac{\delta}{2}\dot{\mathbf{a}}(\theta_c)\right)s_1(t) + \left(\mathbf{a}(\theta_c) + \frac{\delta}{2}\dot{\mathbf{a}}(\theta_c)\right)s_2(t)\\ &= \mathbf{a}(\theta_c)s^+(t) + \delta\frac{s^-(t)}{2}\dot{\mathbf{a}}(\theta_c),\end{aligned} \tag{4.18}$$

where $s^-(t) = s_2(t) - s_1(t)$. Again, by omitting the term δ^2 and since the source signals are assumed to be known at the observer, by performing a change of variable $\mathbf{y}(t) = \mathbf{z}(t) - \mathbf{a}(\theta_c)s^+(t)$, the linearized hypothesis test is given by:

$$\begin{cases}\mathcal{H}_0: & \mathbf{y}(t) \cong \delta\boldsymbol{\nu}_0(t) + \mathbf{n}(t),\\ \mathcal{H}_1: & \mathbf{y}(t) \cong \delta\boldsymbol{\nu}_1(t) + \mathbf{n}(t),\end{cases} \tag{4.19}$$

where

$$\boldsymbol{\nu}_0(t) = s^+(t)\gamma(t)\dot{\mathbf{a}}(\theta_c) + \left(\frac{\kappa_c m(t)}{N}\right)\mathbf{a}(\theta_c), \tag{4.20}$$

$$\boldsymbol{\nu}_1(t) = \frac{s^-(t)}{2}\dot{\mathbf{a}}(\theta_c), \tag{4.21}$$

in which $\mathbf{y} = [\mathbf{y}(1)^T\dots\mathbf{y}(T)^T]^T$, $\mathbf{n} = [\mathbf{n}(1)^T\dots\mathbf{n}(T)^T]^T$, $\boldsymbol{\nu}_0 = \left[\boldsymbol{\nu}_0^T(1)\dots\boldsymbol{\nu}_0^T(T)\right]^T$ and $\boldsymbol{\nu}_1 = \left[\boldsymbol{\nu}_1^T(1)\dots\boldsymbol{\nu}_1^T(T)\right]^T$. Based on this linearized observation model, we will introduce the Bayesian approaches for the SRL in the following sections.

4.3 Bayesian SRL based on information theory

By maximizing the probability of detection (*i.e.*, $P_d \approx 1$) for $P_{fa} \leq \epsilon$ with ϵ goes to zero slowly, the best error exponent resulting from using the Neyman-Pearson test is given by the Stein's lemma [CT91] as follows:

$$\lim_{TN\to\infty} \ln P_{fa} = -\mathcal{D}(p(\mathbf{y},\theta_c;\mathcal{H}_1)\|p(\mathbf{y},\theta_c;\mathcal{H}_0)), \tag{4.22}$$

where $\mathcal{D}(p(\mathbf{y},\theta_c;\mathcal{H}_1)\|p(\mathbf{y},\theta_c;\mathcal{H}_0))$ denotes the relative entropy. Let Ω be the observation space, Θ denotes the parameter space. After some calculations, the relative entropy between two Gaussian distributions with parameterized means is straightforwardly given by:

$$\begin{aligned}
\mathcal{D}(p(\mathbf{y},\theta_c;\mathcal{H}_1)\|p(\mathbf{y},\theta_c;\mathcal{H}_0)) &= \int_\Theta\int_\Omega p(\mathbf{y},\theta_c;\mathcal{H}_1)\ln\left(\frac{p(\mathbf{y},\theta_c;\mathcal{H}_1)}{p(\mathbf{y},\theta_c;\mathcal{H}_0)}\right)d\mathbf{y}d\theta_c \\
&= \int_\Theta \frac{\delta^2}{\sigma^2}\sum_{t=1}^{T}\|\boldsymbol{\nu}_0(t)-\boldsymbol{\nu}_1(t)\|^2 p(\theta_c)d\theta_c \\
&= \int_\Theta \frac{\delta^2||\mathbf{m}||^2}{\sigma^2}\left\|\frac{\kappa_c}{N}\mathbf{a}(\theta_c)-\dot{\mathbf{a}}(\theta_c)\right\|^2 p(\theta_c)d\theta_c \\
&= \int_\Theta \frac{\delta^2||\mathbf{m}||^2||\dot{\mathbf{a}}(\boldsymbol{\theta}_\mathbf{c})||^2}{\sigma^2}\cos^2(\Upsilon)p(\theta_c)d\theta_c \\
&= \frac{\delta^2}{\sigma^2}\mathbb{E}\left\{||\mathbf{m}||^2||\dot{\mathbf{a}}(\boldsymbol{\theta}_\mathbf{c})||^2\cos^2(\Upsilon)\right\},
\end{aligned} \tag{4.23}$$

using the fact that $||\mathbf{a}(\theta_c)||^2 = N$ and $p(\mathcal{H}_0) = p(\mathcal{H}_1) = 1/2$. Υ is the largest canonical angle between vectors $\mathbf{a}(\theta_c)$ and $\dot{\mathbf{a}}(\theta_c)$ with $\cos^2\Upsilon = 1 - \frac{\left\|\mathbf{a}^H(\theta_c)\dot{\mathbf{a}}(\theta_c)\right\|^2}{\|\mathbf{a}(\theta_c)\|^2\|\dot{\mathbf{a}}(\theta_c)\|^2}$, and where $\mathbb{E}$ denotes the expectation *w.r.t.* the prior distribution. The important point is that the relative entropy can be approximated by a quadratic expression *w.r.t.* δ. In addition, the relative entropy is a function of the source waveforms, of the array distribution, of the noise variance and of the useful geometrical quantity which is the "angle" between the steering vector and its first-order derivative. A geometrical interpretation is the following: the more orthogonal the two vectors, the smaller the relative entropy. This means that it could be more and more difficult to discriminate the two hypothesis. According to the expression of the relative entropy, we can see that to ensure a "good" discrimination of the two hypothesis, we must have a large SRL or/and a large array distribution and/or a small noise variance.

Consequently, using (4.22) and (4.23) and the fact that for maximal P_d (close to one), $P_{fa} \approx 2P_e = 2(1-\varpi)$, where ϖ denotes the success rate, the SRL based on the Stein's lemma is given by:

$$\delta_{Stein} \cong \frac{\sigma\sqrt{-(\ln(2)+\ln(1-\varpi))}}{\mathbb{E}\left\{\|\mathbf{m}\|\,\|\dot{\mathbf{a}}(\theta_c)\|\cos\Upsilon\right\}}. \tag{4.24}$$

4.4 Detection theory approach

In this Section, we derive the SRL using the detection theory approach, particularly, using the well-known Neyman-Pearson (NP) criterion in the Bayesian context, denoted by BNP. The BNP will minimize the probability of error P_e. Even if the proposed approach is Bayesian as the

one presented by Amar and Weiss [AW08], our approach is different. Indeed, Amar and Weiss derive the SRL, denoted Theoretical Resolution Limit (TRL), based on the linearization of the error probability. In our method, we choose to linearize directly the observation signal as done by Sharman and Milanfar [SM04] (the linearisation was done *w.r.t.* δ, this can be argued by the fact that the high resolution algorithms have asymptotically an infinite resolution power [Van02b]).

In order to simplify the calculation, we perform the following change of variable formula:

$$\mathbf{z}' = \frac{\mathbf{z}}{\delta} - \boldsymbol{\nu}_0. \tag{4.25}$$

Consequently, plugging (4.25) into (4.19), one obtains

$$\begin{cases} \mathcal{H}_0 : & \mathbf{z}'; \theta_c \cong \mathbf{n}', \\ \mathcal{H}_1 : & \mathbf{z}'; \theta_c \cong \boldsymbol{\zeta} + \mathbf{n}', \end{cases} \tag{4.26}$$

where $\boldsymbol{\zeta} = \boldsymbol{\nu}_1 - \boldsymbol{\nu}_0$ and $\mathbf{n}' \sim \mathbb{C}\mathcal{N}(\mathbf{0}, \frac{\sigma^2}{\delta^2}\mathbf{I})$. Consequently, one has

$$G_{NP}(\mathbf{z}'; \theta_c) = \frac{p(\mathbf{z}'; \mathcal{H}_1, \theta_c)}{p(\mathbf{z}'; \mathcal{H}_0, \theta_c)} \underset{\mathcal{H}_0}{\overset{\mathcal{H}_1}{\gtrless}} \vartheta' = \frac{p(\mathcal{H}_0)}{p(\mathcal{H}_1)}, \tag{4.27}$$

denoting $T_{NP}(\mathbf{z}'; \theta_c) = \ln\left(G_{NP}(\mathbf{z}'; \theta_c)\right)$ and $\vartheta = \ln\left(\vartheta'\right)$, the statistics test can be given by

$$\begin{aligned} T_{NP}(\mathbf{z}'; \theta_c) &= \ln\left(\frac{p(\mathbf{z}'; \mathcal{H}_1, \theta_c)}{p(\mathbf{z}'; \mathcal{H}_0, \theta_c)}\right) = \frac{\delta^2}{\sigma^2}\left(\left\|\mathbf{z}' - \boldsymbol{\zeta}\right\|^2 - \left\|\mathbf{z}'\right\|^2\right) \\ &= \frac{\delta^2}{\sigma^2}\left(\left\|\boldsymbol{\zeta}\right\|^2 - 2\Re\left\{\boldsymbol{\zeta}^H \mathbf{z}'\right\}\right) \underset{\mathcal{H}_0}{\overset{\mathcal{H}_1}{\gtrless}} \vartheta. \end{aligned} \tag{4.28}$$

Since we have assumed that $p(\mathcal{H}_0) = p(\mathcal{H}_1) = 1/2$, one obtains

$$\begin{cases} \mathcal{H}_0 : & T_{NP}(\mathbf{z}'; \theta_c) > 0, \\ \mathcal{H}_1 : & T_{NP}(\mathbf{z}'; \theta_c) < 0. \end{cases} \tag{4.29}$$

Let $L(\mathbf{z}'; \theta_c) = \Re\left\{\boldsymbol{\zeta}^H \mathbf{z}'\right\}$, one can easily obtain

$$\begin{cases} \mathcal{H}_0 : & L(\mathbf{z}'; \theta_c) \sim \mathcal{N}(0, \varrho^2) \\ \mathcal{H}_1 : & L(\mathbf{z}'; \theta_c) \sim \mathcal{N}(\left\|\boldsymbol{\zeta}\right\|^2, \varrho^2) \end{cases} \tag{4.30}$$

where

$$\varrho^2 = \frac{\sigma^2 \left\|\boldsymbol{\zeta}\right\|^2}{2\delta^2}.$$

Thus the conditional probability of error in given by [Kay98]:

$$P_e(\delta; \theta_c) = \frac{1}{2}\left(\left(1 - Q\left(\frac{-\left\|\boldsymbol{\zeta}\right\|^2}{2\sqrt{\varrho^2}}\right)\right) + Q\left(\frac{\left\|\boldsymbol{\zeta}\right\|^2}{2\sqrt{\varrho^2}}\right)\right), \tag{4.31}$$

in which $Q(.)$ denotes the right-tail function of the probability function for a Gaussian random variable with zero mean and unit variance. Since $Q\left(\frac{-\left\|\boldsymbol{\zeta}\right\|^2}{2\sqrt{\varrho^2}}\right) = 1 - Q\left(\frac{\left\|\boldsymbol{\zeta}\right\|^2}{2\sqrt{\varrho^2}}\right)$, thus, one obtains

$$P_e(\delta; \theta_c) = Q\left(\frac{\left\|\boldsymbol{\zeta}\right\|^2}{\sqrt{4\varrho^2}}\right). \tag{4.32}$$

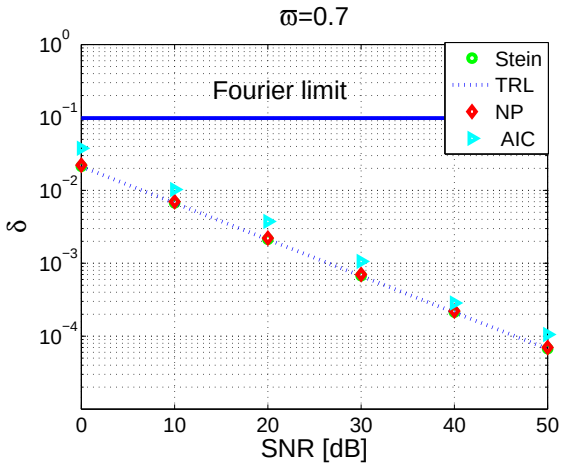

Figure 4.1: SRL vs. SNR. The considered SRLs are based on the Information Theory, on the Bayesian Neyman-Pearson (BNP), on the TRL, and on the numerical AIC, for $\varpi = 0.7$.

Since the marginal $P_e(\delta)$ is given by:

$$P_e(\delta) = \int_{\Theta} P_e(\delta;\theta_c)p(\theta_c)d\theta_c = \mathbb{E}\left\{P_e(\delta;\theta_c)\right\}. \tag{4.33}$$

Consequently, the SRL based on the BNP criteria is given by

$$\delta_{NP} \cong \frac{\sqrt{2}\sigma Q^{-1}(1-\varpi)}{\mathbb{E}\left\{\|\mathbf{m}\|\,\|\dot{\mathbf{a}}(\theta_c)\|\cos(\Upsilon)\right\}} \tag{4.34}$$

where $Q^{-1}(.)$ is the inverse of the right-tail function of the probability function for a Gaussian random variable with zero mean and unit variance.

4.5 Analysis and simulations results

In this section, we consider the performance analysis of the above SRL approaches.

4.5.1 Frequency estimation application

We consider now the context of frequency estimation in the single snapshot $T = 1$ case. The vector $\mathbf{a}(\theta)$ has the exponential form:

$$\mathbf{a}(\theta) = \left[1, e^{j\theta}, \ldots, e^{j(N-1)\theta}\right]^T. \tag{4.35}$$

We have then the more compact expressions since $\|\dot{\mathbf{a}}\|^2 = \sum_{k=1}^{N-1} k^2 = N(2N-1)(N-1)/6$ and $\cos^2\Upsilon = \frac{5N-4}{3(2N-1)}$. Furthermore, one observes that the denominator of the SRL is no longer

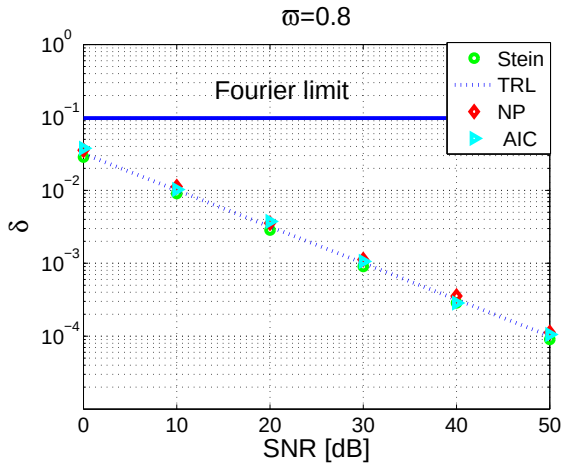

Figure 4.2: SRL vs. SNR. The considered SRLs are based on the Information Theory, on the Bayesian Neyman-Pearson (BNP), on the TRL, and on the numerical AIC, for $\varpi = 0.8$.

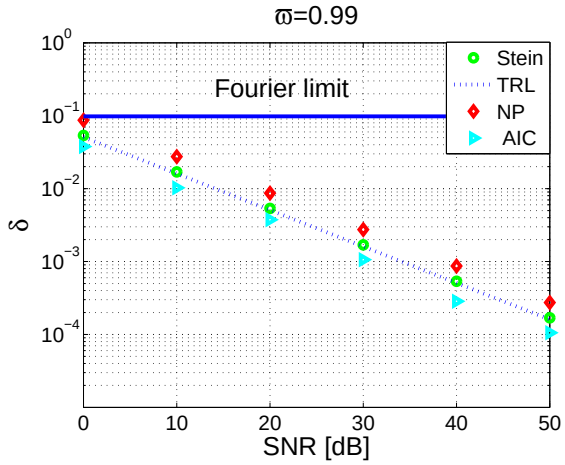

Figure 4.3: SRL vs. SNR. The considered SRLs are based on the Information Theory, on the Bayesian Neyman-Pearson (BNP), on the TRL, and on the numerical AIC, for $\varpi = 0.99$.

depended on the parameter. Therefore, the SRL can be expressed as:

$$\delta_{Stein} = \frac{\sigma\sqrt{-(\ln(2)+\ln(1-\varpi))}}{\|\mathbf{m}\|\sqrt{N(N-1)(5N-4)/18}}, \tag{4.36}$$

$$\delta_{NP} = \frac{2\sigma Q^{-1}(1-\varpi)}{\|\mathbf{m}\|\sqrt{N(N-1)(5N-4)/18}}, \tag{4.37}$$

$$\delta_{TRL} = \frac{2\sigma\sqrt{\pi}(\varpi-0.5)}{\|\mathbf{m}\|\sqrt{N(N-1)(5N-4)/18}}. \tag{4.38}$$

The observation vector length equals to $N = 64$. The signal to noise ratio SNR is defined by

$$SNR = \left(\sum_{k=1}^{2}\|\mathbf{s}_k\|^2\right) / \left(2T\sigma^2\right). \tag{4.39}$$

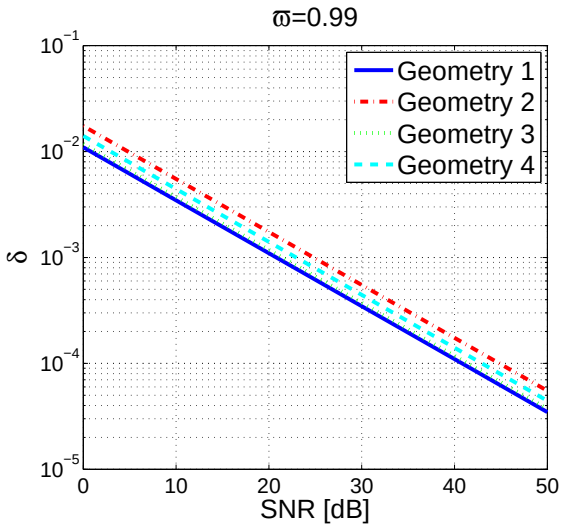

Figure 4.4: The SRL of different linear geometry array for $\varpi = 0.99$.

We compare here the SRL of the three methods *w.r.t.* the SNR. It is interesting to consider also a numerical approach for the SRL, the so-called Akaike Information Criterion (AIC) approach [SSS95]. The empirical SRL of the AIC is obtained over 200 Monte Carlo trials. We assume that the central parameter has a uniform prior distribution. Therefore the normalized central parameter is chosen randomly in the interval $[0; 1]$. Fig. 4.1 to Fig. 4.3, show the behavior of the SRL versus the SNR for different values of the success rate: $\varpi = 0.7,\ 0.8$ and 0.99, respectively. It should be noted that AIC is independent of the success rate ϖ. The Fourier limit, given by $\delta_F = 2\pi/(TN)$ represents the limit separation, given by the classical periodogram approach [Kay88]. One observes that for $\varpi = 0.7$ (see Fig. 4.1), the SRL based on the BNP, on the information theory and the TRL are very close and lower than the empirical SRL of the AIC. For $\varpi = 0.8$ (Fig. 4.2), all of the four approaches have very close SRL. And for $\varpi = 0.99$ (Fig. 4.3), the SRL of the AIC is the lowest, while the SRL of the TRL and of the information theory are always close and while the SRL of the BNP is the highest.

4.5.2 Analysis of the array geometry in the context of DOA estimation

We now consider the impact of the array geometry to the SRL in the context of DOA estimation using the linear array. We here use only the SRL based on the Stein lemma. For mathematical convenience, we consider the angle electric estimation $\theta = \sin\varphi$, where φ denotes the elevation angle. The central parameter is assumed uniformly distributed in $[-1, 1]$. The steering vector has the exponential form $[\mathbf{a}(\theta)]_k = e^{j\frac{2\pi}{\lambda}d_k\theta}$, where d_k denotes the position of the k^{th} sensor in the array. The SRL based on the Stein lemma can be simplified by

$$\delta_{Stein} = \frac{\sigma\sqrt{-(\ln(2) + \ln(1-\varpi))}}{\|\mathbf{m}\|\sqrt{\sum_{k=1}^{N} d_k^2 - \frac{\left(\sum_{k=1}^{N} d_k\right)^2}{N}}}. \tag{4.40}$$

We consider four kinds of array with the same aperture $10\frac{\lambda}{2}$, which are called the geometry 1 to the geometry 4 respectively: (1) the uniform linear array with 10 sensors and with the

inter-sensor spacing $\lambda/2$, (2) the lacunar array with 7 sensors, there is no sensor at the positions $k = 7, 8, 9$, (3) the lacunar array with 7 sensors, there is no sensor at the positions $k = 2, 3, 4$, (4) the lacunar array with 7 sensors, there is no sensor at the positions $k = 5, 6, 7$.

Figure 4.4 shows the SRL based on the Stein lemma of the four types of geometry array where $T = 100$ and $\varpi = 0.99$. The lower SRL is the better parameter estimation the array provides. One observes that the uniform linear array has the lowest SRL. While three lacunar array have different SRL even they have the same number of sensors and the same aperture. The SRL of the geometry 3 and the uniform linear array (geometry 1) are close, meanwhile the SRL of the geometry 2 is the highest. One can conclude that the nearer the sensors to the extremity, the lower the SRL.

4.6 Conclusion

In this chapter, we have investigated the SRL in the Bayesian context. Thanks to a linearized form of the observation model and based on the MPE criteria, two approaches to derive the SRL have been proposed. The two methods are based on the binary hypothesis test. The first one, which is the main contribution of this chapter, exploits the Stein's lemma which stipulates that the Probability of false alarm can be linked to the relative entropy. In addition, we show that this quantity can be approximated by a function of the square of the SRL. This result allows us to give a closed-form (analytic) expression of the SRL. Unlike to the first approach, which is based on information theory tools, the second one is based on the detection theory and derives the SRL thanks to the Neyman-Pearson decision criterion. Finally, we compare these two methods with the Theoretical Resolution Limit (TRL) of Amar and Weiss derived recently in the Bayesian context and to a numerical implementation of the Akaike information criterion (AIC). We have shown that the SRL of all Bayesian approaches obtained from either theoretical or numerical methods are very close.

Chapter 5

Conclusion and perspective

The primary goal of this thesis concerns the array geometry optimization in the context of far field source localization. We studied two approaches to evaluate the impact of the array geometry on the estimation: the performance estimation approach and the resolution limit ability approach. In the first approach, two kinds of lower bounds: the CRB and the WWB, were investigated. In the second approach, we considered the binary hypotheses test to characterize the statistical resolution limit. Moreover, we have considered several scenarios concerning the parameters and the observations. Particularly, the Bayesian model assumes that the parameters of interest are random with known *prior* distribution, while the deterministic model assumes that these parameters are deterministic with unknown quantity. Concerning the observations assumptions, the conditional observation model assumes that the observations are deterministic with a known or an unknown sequence, while the unconditional observation model assumes that the observations are random processes.

The contributions of this thesis were presented in three chapters.

In chapter 2, we considered the array geometry optimization based on the performance estimation criteria, under the deterministic parameters assumptions. We have introduced the closed-forms expressions of the Cramér-Rao lower bound under both conditional and unconditional observation models. These closed-form expressions were then used as a tool to study the impact of the array geometry on the performance estimation. Particularly, we have investigated in this chapter the 3D array geometry, which was less studied in the literature since, compared to the conventional planar array, the drawback of the 3D array geometry is the complexity to obtain closed-form expressions. Several kinds of 3D array geometries made from ULA branches were studied. The derivation of the conditions about isotropy and uncoupling arrays was conducted. We showed that these conditions under conditional and unconditional observations models are not the same.

In chapter 3, the array geometry optimization under a Bayesian scenario and based on performance estimation was considered. The Weiss-Weinstein lower bound, known as the tightest bound in the Weiss-Weinstein family, was investigated under both the conditional and unconditional observations models. In the literature, due to the high computational cost, the WWB was derived only by way of simulation and by setting the parameter s equal to $1/2$. Therefore, the optimal WWB might not be achieved. We have derived in this thesis a closed-form expression of the WWB for a general Gaussian model with a parameterized mean or a parameterized covariance matrix. Although the main aim of this thesis was to derive the WWB as a statistical tool for investigating the array processing, these closed-form expressions of the WWB could be also applied for other problems.

In chapter 4, we considered the statistical resolution limit problem. Several approaches

existed in the literature but almost all of these approaches were involved in the deterministic parameters context. We have introduced the Bayesian model for the SRL problem in which the average of the parameters was assumed to be random with *prior* distribution. We derived then some Bayesian methods based on the information theory, more particularly, based on the Stein lemma, and based on the Neyman-Pearson criterion in detection theory. The results were then compared to another Bayesian method existing in literature: the TRL. The analytical and simulation analysis showed that the performance of these Bayesian approaches are close.

Based on the above contributions, the perspective of this thesis are:

- The closed-form expression of the CRB for the 3D array can be used to study the 3D lacunar array. Compared to the classical array, the advantage of the lacunar array is that it can achieve the same performance estimation with a smaller number of sensors.
- The impact of the array geometry on the ambiguity problem can be studied by using the differential geometry approach.
- Beside the binary hypothesis test approach of the SRL, one usually considers the SRL by the performance estimation approach based on the CRB. However, the CRB is only valid in the asymptotic area. Therefore, the closed form-expressions of the WWB would be useful to investigate the SRL problem in the non-asymptotic area.
- The tightest value of the WWB is obtained by optimization over the set of the parameter s. In chapter 3, we have shown that the value $s = 1/2$, which is usually used in literature to simplify the computation, can lead to the optimal value of WWB. Therefore, finding the condition for which $s = 1/2$ is the optimal value will be a perspective of this thesis.
- This thesis considered only the Gaussian process. It is interesting to extend these contributions into non-Gaussian scenario such as the compound Gaussian distribution.

Appendix A

Résumé

A.1 Introduction

A.1.1 Généralité

Le traitement d'antenne est un sujet d'intérêt en traitement du signal avec de nombreuses applications. Dans les nouveaux systèmes de télécommunication, on utilise des réseaux de capteurs, ou antennes intelligentes, pour repérer la position des dispositifs portables. En radio astronomie, les signaux extraterrestres sont capturés grâce à des systèmes de télescopes coopératifs. Concernant la surveillance de l'environnement (climat, pollution, ...), les réseaux de capteurs permettent désormais de fournir une meilleure surveillance et une meilleure connaissance de l'environnement. Par exemple, le système d'alerte sismique est constitué d'un réseau des capteurs sismiques répartis dans une région et d'un système de communication haut débit afin de recueillir les données et de détecter éventuellement la puissance et la propagation d'un tremblement de terre. En radar, le radar classique se compose d'un émetteur et d'un récepteur pour transmettre des impulsions électromagnétiques et pour recevoir la reflection pour mesurer la distance, la position, la vitesse d'une cible, tel qu'un avion. Contrairement au système de radar classique, les radars passifs n'ont pas d'émetteur dédié, donc, ils exploitent une grande variété de signaux urbains, tels que: les signaux de télévision, les signaux FM, les signaux GSM, etc. En sonar, les signaux acoustiques mesurés par un réseau d'hydrophones remorqués par un navire sont utilisés pour détecter et localiser l'apparition d'un sous-marin.

L'estimation des paramètres d'intérêt est un problème important en traitement d'antenne. L'objectif de l'estimation des paramètres est de retirer des informations spatio-temporelles concernant des signaux à partir d'un signal mesuré sur un réseau de capteurs éparpillés dans l'espace. Vu que les observations mesurées sont normalement perturbées par le bruit, il est nécessaire d'établir un modèle des observations afin d'appliquer des algorithmes d'estimation. Concernant la localisation de sources, il y a plusieurs algorithmes d'estimation dans la littérature et ils peuvent être classifiés en deux catégories [KV96] : les méthodes basées sur l'analyse spectrale et les méthodes paramétriques. Les méthodes spectrales telles que MUSIC, Capon, la formation des voies, etc, estiment les paramètres en établissant des fonctions spectrales des paramètres d'intérêt dont les maxima donnent l'estimation des paramètres. Les méthodes paramétriques telles que l'estimateur du maximum vraisemblance, maximum a posteriori, etc. sont normalement plus précises que les méthodes spectrales parce qu'elles exploitent mieux le modèle des données, et en plus, elles ont de bonnes performances dans le cas de signaux cohérents. Pourtant, comparées aux méthodes spectrales, les méthodes paramétriques requièrent une charge de calcul importante. Pour cette raison, les méthodes spectrales sont plus utilisées dans la pratique.

Les performances des estimateurs sont qualifiées à travers leurs erreurs quadratiques moyennes (EQM) empiriques. Cette quantité représente la "distance" entre le vrai paramètre et sa valeur estimée et elle est obtenue par des tirages de Monte Carlo. L'inconvénient du tirage de Monte Carlo est sa charge de calcul. En effet, concernant des problèmes où il y a plusieurs paramètres inconnus, il nécessite des recherches multidimensionelles. De plus, le tirage Monte Carlo ne peut pas nous donner des formules analytiques afin d'optimiser le système. Toutefois, il existe dans la littérature une autre manière d'évaluer les performances d'estimation indépendamment du type d'estimateur considéré. C'est ce que l'on appelle les bornes inférieures de l'erreur quadratique moyenne, par exemple la borne de Cramér-Rao (BCR). La BCR est largement étudiée dans la littérature en raison de sa simplicité. En effet, l'EQM des estimateurs non biaisés $\hat{\theta}(\mathbf{y})$ est supérieure ou égale à la BCR, c'est-à-dire que $EQM(\hat{\theta}(\mathbf{y})) \geq BCR$. La BCR est obtenue par l'inversion de la matrice d'information de Fisher qui représente la façon de mesurer les informations du paramètre contenues dans les observations par sa fonction de vraisemblance. Un estimateur qui atteint la BCR est dit efficace.

Selon les hypothèses concernant des paramètres, les bornes inférieures sont classifiées en deux catégories : les bornes déterministes qui supposent que les paramètres sont déterministes et inconnus, et les bornes Bayésiennes qui supposent que les paramètres sont aléatoires avec une distribution *a priori* connue par l'observateur. Les bornes déterministes considèrent le comportement de l'EQM locale, c'est à dire $EQM_{locale}(\theta) = \int_{\Omega}(\hat{\theta}(\mathbf{y}) - \theta)^2 p(\mathbf{y};\theta)d\mathbf{y}$ où Ω représente l'espace des observations, et où $p(\mathbf{y};\theta)$ représente la vraisemblance des observations. Alors que les bornes Bayésiennes considèrent le comportement de l'EQM globale, c'est à dire $EQM_{globale} = \int_{\Theta}\int_{\Omega}(\hat{\theta}(\mathbf{y}) - \theta)^2 p(\mathbf{y},\theta)d\mathbf{y}d\theta$, où Θ représente l'espace des paramètres, et où $p(\mathbf{y},\theta)$ représente la distribution jointe des observations et du paramètre. Les bornes Bayésiennes peuvent être subdivisées encore en deux familles. La famille des bornes de Weiss-Weinstein qui est dérivée à partir d'une inégalité de covariance, et la famille des bornes de Ziv-Zakai qui est dérivée à partir d'un test d'hypothèses binaire [RFL+08, VB07].

Dans [Van68], il a été montré que concernant les problèmes non-linéaires tels que l'estimation de la direction d'arrivée (DDA), l'EQM obtenue par des méthodes paramétriques a trois zones d'opération en fonction du rapport signal sur bruit (RSB), et/ou du nombre des observations. Dans le scénario où le RSB ou/et le nombre des observation est élevé, l'EQM est petite et les performances des estimateurs sont normalement proches de la BCR. Cette zone est appelée la zone asymptotique. Lorsque le RSB et/ou le nombre des observations diminue au-delà d'une certaine valeur, l'EQM augmente rapidement, menant à l'effet du décrochement. Enfin, lorsque le RSB et/ou le nombre des observations est très faible, le signal observé se réduit à la composante du bruit. Pour cette raison, l'estimation se base seulement sur le support des paramètres. Par conséquent, l'EQM a un comportement plat dans cette zone appelée la zone de non-information. Toutes les bornes susmentionnées sont précises dans la zone asymptotique. Mais dans la zone non-asymptotique, la précision des bornes n'est pas la même. Certaines bornes peuvent capturer l'effet du décrochement, tandis que les autres ne peuvent pas. Par exemple, la borne BCR ne donne qu'une prédiction précise dans la zone asymptotique, mais dans la zone non-asymptotique, la BCR est trop optimiste car la BCR n'est qu'une borne locale. Un des objectifs principaux de l'étude des bornes inférieures est d'améliorer la précision des bornes par rapport au comportement de l'EQM.

Par rapport aux bornes déterministes, les bornes Bayésiennes prennent en compte le support des paramètres via la distribution *a priori*. Donc, les bornes déterministes dépassent le comportement de l'EQM dans la zone non-asymptotique, tandis que les bornes Bayésiennes sont plus ou moins précises dans toutes les zones. En outre, les bornes Bayésiennes ne nécessitent pas

que les estimateurs soient non-biaisés. En effet, concernant le cas des paramètres déterministes, l'EQM locale peut être exprimée en $EQM_{locale}(\theta) = Cov(\theta) + Biais^2(\theta)$. Pour les estimateurs non-biaisés, c'est à dire $\int_{\Omega}(\hat{\theta}(\mathbf{y}) - \theta)p(\mathbf{y};\theta)d\mathbf{y} = 0$, on obtient $EQM_{locale}(\theta) = Cov(\theta)$, et on peut dériver directement les bornes déterministes à partir de l'inégalité de la covariance. Cependant, les estimateurs peuvent-être biaisés dans certaines circonstances telles que dans la zone non-asymptotique. Le calcul des bornes déterministes des estimateurs biaisés est un problème difficile en raison de la dépendance de l'EQM au biais, ce qui dépend du type d'estimateur considéré.

À partir des analyses précédentes, il apparaît que les bornes inférieures de l'EQM constituent un outil potentiel pour étudier plusieurs problèmes en traitement d'antenne en évitant des tirages de Monte Carlo. Pour cette raison, l'une des motivations de cette thèse concerne la mise en oeuvre des applications des bornes inférieures au contexte de la localisation de sources.

Dans cette thèse, on s'intéresse non seulement à l'approche basée sur les performances d'estimation, mais également à l'approche basée sur le seuil de résolution. Dans la littérature, le seuil de résolution caractérise la séparation minimale entre deux sources proches qui permet une bonne estimation des paramètres. Le seuil de résolution dépend de l'algorithme étudié. En effet, pour un RSB grand, la méthode du périodogramme classique ne peut résoudre deux composantes à condition que leur séparation, notée δ, soit plus grande que la limite de Fourier (Rayleigh), notée δ_F: $\delta \geq \delta_F = 2\pi/N$, où N représente le nombre d'observations. Par rapport à la méthode du périodogramme, les méthodes dites à haute résolution telles que ESPRIT, MUSIC permettent d'obtenir $\delta < \delta_F$. Donc, l'étude générale du seuil de résolution qui n'est basée sur aucune méthode spécifique pourrait mener à un outil de conception de géométrie des réseaux de capteurs afin d'améliorer la capacité de résolution du système.

A.1.2 Motivations et résultats de la thèse

A.1.2.1 Motivations

La motivation de cette thèse est basée sur les résultats présentés dans [GM06]. Dans ce papier, les auteurs ont étudié l'impact de la géométrie des réseaux de capteurs planaires sur la précision des estimateurs (pour le modèle stochastique) dans le contexte de l'estimation de la direction d'arrivée d'une source (DDA). Ils ont développé des expressions analytiques de la BCR, puis, utilisé ces expressions comme un outil pour la conception de la géométrie des réseaux de capteurs. En particulier, le réseau de capteurs en V a été étudié. L'avantage de ce type de réseau est donné par l'angle d'ouverture entre ses deux branches, qui nous donne un degré de liberté. En faisant varier la valeur de l'angle d'ouverture, les auteurs peuvent étudier exhaustivement l'impact de la géométrie des réseaux de capteurs sur les performances d'estimation, ce qui conduit également aux conditions pour obtenir des propriétés désirées en traitement d'antenne telles que l'isotropie et le découplage. De manière étonnante, ils ont montré que le réseau asymétrique en V peut également être isotrope à condition que l'angle d'ouverture soit égal à 53.13°. À partir des analyses précédentes, on trouve que la configuration de la géométrie des réseaux de capteurs a un impact important sur les performances d'estimation.

L'objectif de cette thèse concerne le positionnement optimal des capteurs dans un réseau. En particulier :

- La plupart des études concernant la géométrie des réseaux de capteurs ont utilisé le modèle de signaux stochastiques. Cependant, il existe un autre modèle dans la littérature appelé le modèle déterministe. Ce modèle n'a pas beaucoup été utilisé dans la littérature peut-être parce que si la séquence des signaux est supposée inconnue au récepteur, ces signaux

seront considérés comme des paramètres d'intérêt qu'il faut estimer. Par conséquent, la charge des calculs va augmenter en fonction de la dimension du vecteur des paramètres. Cependant, on peut trouver des scénarios où la séquence des signaux est supposée connue par le récepteur, tels que dans les systèmes de télécommunication. Donc, on peut considérer les deux modèles pour le même coût de calcul et en déduire des comparaisons entre ces deux modèles.

- Bien que plusieurs applications nécessitent une forme 3D des réseaux de capteurs, les réseaux de capteurs 3D ont été moins étudiés dans la littérature. Les analyses précédentes ont démontré l'impact de la géométrie des réseaux de capteurs sur les performances d'estimation. En effet, concernant le problème de l'estimation de la DDA, les réseaux de capteurs 1D ne peuvent estimer qu'un seul paramètre : l'angle d'élévation, tandis que les réseaux de capteurs 2D et 3D peuvent estimer l'angle d'élévation et l'angle d'azimut. Pour cette raison, nous avons étudié les avantages de la géométrie 3D par rapport à la géométrie planaire classique à l'aide de l'étude de la BCR.

- La BCR est largement utilisée dans la littérature en raison de sa simplicité. Cependant, la BCR n'est précise que dans la zone asymptotique. Pour cette raison, nous avons mis en oeuvre une autre borne plus pertinente afin d'optimiser la géométrie des réseaux de capteurs. Dans [Ren07], l'expression analytique de la borne de Weiss-Weinstein (BWW) qui est une des bornes les plus précises dans la famille de Weiss-Weinstein, est dérivée pour le cas de l'analyse spectrale. Ce résultat nous a motivé pour étudier la BWW [WW88] pour le problème du positionnement optimal des capteurs, dans le contexte Bayésien (ce qui suppose que les paramètres sont aléatoires avec une distribution *a priori*).

- Une des motivation de cette thèse est basée sur les résultats de [AW08], où les auteurs ont introduit une nouvelle approche pour le SSR dans le contexte Bayésien appelé: La résolution limite théorique (RLT). Cette approche est obtenue par un développement en série Taylor au premier ordre de la probabilité d'erreur marginale. Cette approche est générale et indépendante des algorithmes d'estimation. Il faut noter qu'il y a beaucoup d'approches du SSR dans la littérature. Cependant, la plupart des approches se situent dans le contexte des paramètres déterministes qui suppose que les paramètres sont déterministe. Bien que le contexte Bayésien concerne des applications importantes dans la littérature, il est beaucoup moins étudié. Pour cette raison, notre objectif est d'introduire des approches Bayésiennes pour la SSR.

A.1.2.2 Résultats et plan de la thèse

Les contributions de cette thèse sont :

- Dans le chapitre 2, nous avons étudié l'impact de la géométrie d'un réseau de capteurs 3D sur les performances d'estimation à l'aide de l'étude de la BCR. Nous avons utilisé un type de géométrie particulier constitué par un réseau planaire quelconque et un réseau linéaire orthogonal à ce réseau planaire. Ce type de réseau nous a permis de caractériser les contributions de la troisième dimension aux performances d'estimation. Les expressions analytiques de la BCR pour la géométrie 3D ont été calculées pour les modèles de signaux déterministe et stochastique. Nous avons déduit les conditions pour l'isotropie et le découplage. Puis, plusieurs types de géométries constitués par des réseaux linéaires ont été étudiés. Nous avons montré que la condition pour obtenir les propriétés d'isotropie et de découplage pour les modèles déterministe et stochastique ne sont pas les même.

- Dans le chapitre 3, nous avons considéré les applications de la BWW en traitement d'antenne. Nous avons calculé les expression analytiques de la BWW pour le modèle Gaussien général à moyenne paramétrée ou à matrice de covariance paramétrée. Ces expressions peuvent être utiles pour une large classe de problèmes. En outre, par rapport aux autres travaux concernant la BWW dans la littérature, la valeur du paramètre s n'a pas été fixée à $1/2$, ce qui permet d'analyser l'impact du paramètre s sur la valeur optimale de la BWW. Ensuite, nous avons présenté les expressions compact de la BWW pour le contexte d'estimation de la DDA pour les modèles stochastique et déterministe en utilisant les réseaux de capteurs linéaires non-uniformes et les réseaux de capteurs planaires quelconques. Grâce aux simulations numériques, nous avons montré que la BWW est un outil efficace pour capturer le comportement de l'EQM obtenue par l'estimateur du Maximum A Posteriori. Finalement, l'application de la BWW pour le positionnement optimal des capteurs dans un réseau a été également étudié.

- Dans le chapitre 4, nous avons étudié l'approche du SSR basé sur un test d'hypothèses binaire. Nous avons introduit le contexte Bayésien pour le problème du SSR. Ensuite, nous avons proposé le modèle des observations linéarisé basé sur le critère de la probabilité d'erreur minimale. À partir de ce modèle, les deux méthodes Bayésiennes basées sur la théorie de l'information et de la détection sont présentées. Plus particulièrement, nous avons utilisé le lemme de Stein en théorie de l'information qui relie l'entropie relative avec la probabilité de fausse alarme, et le critère de décision de Neyman-Pearson. Par des comparaisons avec une autre méthode Bayésienne appelée RLT et avec la méthode numérique appelée critère de l'information Akaike (CIA), nous avons montré que le SSR obtenu par les méthodes théoriques et les méthodes numériques sont très proches.

Les contributions présentées dans cette thèse ont été publiées dans :

Revues

- [VRBMb] D. T. Vu, A. Renaux, R. Boyer, S. Marcos, "A Cramér Rao bounds based analysis of 3D antenna array geometries made from ULA branches", Multidimensional systems and signal processing, Springer.

- [VRBMc] D. T. Vu, A. Renaux, R. Boyer, S. Marcos, "Some results on the Weiss-Weinstein bound in array processing", IEEE. Trans. on Signal Processing, en révision.

- [VEBM] D. T. Vu, M. N. El Korso, R. Boyer, S. Marcos, "Bayesian Statistical Resolution Limit based on Information and Detection theories", *IEEE*. Trans. on Signal Processing, soumis.

Conférences

- [VRB] D. T. Vu, A. Renaux, R. Boyer, and S. Marcos. Analyse des performances de réseaux de capteurs 2D et 3D pour la localisation de source. In Proc. du colloque GRETSI sur le traitement du signal et des images, Dijon, France, 2009.

- [VRBM10b] D. T. Vu, A. Renaux, R. Boyer, and S. Marcos. Performance analysis of 2D and 3D antenna arrays for source localization. In Proc. of European Signal Processing Conference (EUSIPCO), Aalborg, Denmark, Août 2010.

- [VRBM10a] D. T. Vu, A. Renaux, R. Boyer, and S. Marcos. Closed-form expression of the Weiss-Weinstein bound for 3D source localization : the conditional case. In Proc. of IEEE Workshop on Sensor Array and Multi-channel Processing (SAM), Kibutz Ma'ale Hahamisha, Israel, Octobre 2010 (special session on performance bound for array processing).

- [VRBM11] D. T. Vu, A. Renaux, R. Boyer, S. Marcos, Wess-Weinstein bound and SNR threshold analysis for DOA estimation with a COLD array, to appear in Proc. of IEEE Workshop on Statistical Signal Processing, SSP-2011, Nice, France, (special session on polarized signal processing).

- [VEB+11a] D. T. Vu, M. N. El Korso, R. Boyer, A. Renaux, S. Marcos, Angular resolution limit for vector-sensor arrays: detection and information theory approaches", to appear in Proc. of IEEE Workshop on Statistical Signal Processing, SSP-2011, Nice, France, (special session on polarized signal processing).

- [VRBMa] D. T. Vu, A. Renaux, R. Boyer, S. Marcos, "Borne de Weiss-Weinstein pour la localisation de source polarise l'aide d'un réseau de capteurs COLD", Gretsi, 2011, Bordeaux, France.

- [VEB+11b] D. T. Vu, M. N. El Korso, R. Boyer, A. Renaux, S. Marcos, "Résolution limite angulaire : Approches basées sur la théorie de l'information et sur la théorie de la détection", Gretsi, 2011, Bordeaux, France.

A.2 Optimisation de la géométrie des réseaux de capteurs basée sur la borne de Cramér-Rao

Dans le contexte de la localisation passive de sources utilisant un réseau de capteurs, les performances d'estimation de la direction d'arrivée (DDA) ne sont pas seulement liées au type d'estimateur considéré, mais aussi à la géométrie du réseau de capteurs, c'est à dire à la position des capteurs dans l'espace. Pour un réseau de capteurs, les "performances" peuvent être considérées de différents points de vue: les propriétés du faisceau de rayonnement, l'ambiguïté du réseau, l'isotropie, l'estimation en terme d'EQM, etc. Une pléthore de publications concernant l'étude de l'ambiguïté des réseaux (*e.g.*, [Man04, GC81, TGT96, LJ92, GW91]), du faisceau de rayonnement (*e.g.*, [Van02b,SM05]) et des propriétés isotropique des réseaux (*e.g.*, [BM03]), sont disponibles dans la littérature.

Dans ce chapitre, nous nous sommes intéressés à la géométrie optimale des réseaux de capteurs qui mène aux meilleures performances en terme d'EQM. Plus particulièrement, nous nous sommes concentrés sur les géométries 3D des réseaux de capteurs qui ont été moins étudiées dans la littérature. En effet, malgré la richesse des résultats concernant les antennes planaires, les antennes 3D ont été peu étudiées. Par contre il existe des applications où les capteurs sont éparpillés dans l'espace ce qui fait que l'antenne est de forme arbitraire (réseau de télescopes sur la surface de la terre, réseaux d'électrodes sur le crâne d'un patient, réseaux de capteurs dans une pièce ou dans un espace réduit pour des fonctions de robotique, réseau de bouées à la surface de la mer, etc). En outre, par rapport à l'antenne 2D, les antennes 3D ont certains avantages intuitifs, tels que lever l'ambiguïté de l'antenne 2D dans certains cas.

Les analyses fournies dans la littérature traitent de deux types de géométries: les géométries basées sur les réseaux circulaires [Van02b] ou bien les réseaux sphériques [SSL68], et les géométries basées sur les réseaux linéaires tels que les réseaux linéaires uniformes, les réseaux en V, les

réseaux en croix ou en rectangle. Plus particulièrement, nous nous sommes intéressés ici au deuxième type de géométrie.

La BCR [SN89] est l'outil le plus populaire pour étudier les performances d'estimation en terme d'EQM. Ceci est du au fait que la BCR peut être atteinte généralement par la variance de l'estimateur pour un grand nombre d'observations [SN90b] ou pour un RSB élevé [RFCL06, RFBL07]. La BCR a largement été utilisée dans la littérature pour décrire les propriétés fondamentales des réseaux. Par une forme simple des expressions de la BCR, [HS91] a montré l'impact de la position des capteurs sur la précision de l'estimation de la DDA dans le cas des réseaux de capteurs 2D. Concernant l'estimation de la DDA, dans [Nie94], [BM03], [MS91], des conditions sur la position des capteurs pour assurer la propriété d'isotropie pour laquelle, les réseaux de capteurs ont la même précision d'estimation sur l'ensemble des DDA, ont été calculées par l'étude des éléments de la BCR. Dans [YS05], [LS09], la BCR pour l'estimation de la position des sources basée sur la méthode TDOA est utilisée afin de montrer que la meilleure géométrie qui minimise la trace de la BCR contient des réseaux angulaires uniformes. L'application de la BCR Bayésienne pour le cas où les sources sont dans le même plan que le réseau et pour le contexte Bayésien où les paramètres (DDA) sont supposés aléatoires est disponible dans [OM05]. Dans [GM06], une étude approfondie de la BCR pour les réseaux de capteurs 2D a été proposée et a mené à des résultats intéressants concernant un type de réseau particulier appelé le réseau en V, en terme d'EQM et d'isotropie. Basé sur les résultats présentés dans [GM06], un nouveau type de géométrie des réseaux appelé antenne optimale sans ambiguïté basée sur antenne en V a été présenté dans [GAM09]. Finalement, dans [FC09], les auteurs ont montré que la BCR pour les modèles déterministe et stochastique, liée à la variance de l'estimation de la DDA obtenue par l'algorithme MUSIC, peut être exprimée avec la même expression qui est une fonction de la position des capteurs.

En traitement d'antenne, les signaux des sources sont généralement modélisés comme un processus aléatoire ou une séquence déterministe appelés modèle stochastique et modèle déterministe, respectivement [OVSN93]. Plus particulièrement, pour le modèle déterministe, la forme d'onde des signaux peut être supposée connue ou inconnue par le récepteur. Par conséquent, la charge de calcul varie en fonction de l'hypothèse sur la séquence des signaux utilisée. Si la séquence des signaux est supposée inconnue par le récepteur, ces signaux seront considérés comme des paramètres d'intérêt à estimer, ce qui augmente la dimension du vecteur des paramètres. Cependant, il y a des applications où l'amplitude des signaux est connue par le récepteur telles que dans les télécommunications. La connaissance du signal peut améliorer les performances d'estimation, et réduire également la complexité du problème. Les travaux concernant le contexte des signaux connus sont *e.g.*, [LC93, CM97, LHSV95, LvdV99, Cho04a].

En fonction du modèle des signaux utilisé, il y a bien sûr deux types de BCR associés : la BCR stochastique et la BCR déterministe. Il a été montré que la BCR stochastique peut être atteinte pour un grand nombre des observations [SN90b], cependant, elle n'est pas atteinte pour un RSB élevé où le nombre des observations est faible [RFBL07]. D'autre part, la BCR déterministe est atteinte pour un RSB élevé [RFCL06] mais elle n'est pas atteinte pour un grand nombre des observations [SN90b]. De manière surprenante, tous les résultats proposés précédemment sont menés dans le cadre du modèle stochastique, c'est-à-dire que seule la BCR stochastique est utilisée. Dans ce chapitre, nous allons montrer que les résultat basés sur le modèle déterministe diffèrent considérablement de ceux basés sur le modèle stochastique.

Dans ce chapitre, nous avons considéré les deux modèles déterministe et stochastique pour l'étude de la géométrie 3D.

- Tout d'abord, nous avons détaillé les expressions de la matrice des information de Fisher (FIM) concernant l'estimation de l'azimut et de l'élévation dans le cas d'un réseau de cap-

teurs 3D général. Dans la littérature, l'information de Fisher représente la façon de mesurer l'information contenue dans les observations à travers leur fonction de vraisemblance.

- Deuxièmement, nous avons calculé les expressions analytiques de la BCR pour un réseau de capteurs quelconque constitué par un réseau planaire et une branche orthogonale. Ce modèle est la première étape pour analyser la contribution de la troisième dimension sur les performances d'estimation.

- Troisièmement, nous avons proposé plusieurs expressions analytiques de la BCR pour des réseaux de capteurs constitués par des branches ULA afin d'analyser l'impact de la géométrie d'antenne sur les performances d'estimation. Il faut noter que les types de géométries qui ont été étudiés dans le cas 2D et appelés antenne en V, antenne en L, ne sont que des cas particuliers dans notre approche. Dans [HSW91], les auteurs montrent que l'antenne en L permet d'améliorer de 37% la précision par rapport à l'antenne en croix. Dans [FT08], les auteurs ont introduit les conditions d'isotropie pour la position des capteurs, et pour l'angle d'ouverture entre les 2 branches de l'antenne en V uniforme/non-uniforme. Notre objectif était d'étendre ces géométries au cas 3D pour analyser l'impact de la branche 3D supplémentaire.

- Finalement, l'impact de la troisième dimension a été illustré à partir de comparaisons entre l'antenne 3D et l'antenne 2D, mais également entre l'antenne 3D et l'antenne circulaire uniforme (de même nombre de capteurs). Cependant, il faut noter que pour le même nombre de capteurs, afin de former la troisième dimension des réseaux, l'ouverture des réseaux sera diminuée. Par conséquent, la précision de l'estimation des réseaux de capteurs sera affectée.

Modèle

On considère le problème classique où l'on cherche à localiser une source émettant un signal $s(t)$ déterministe (le cas stochastique est détaillé dans le chapitre 2 du manuscript) et à bande étroite à l'aide d'un réseau de capteurs. Les capteurs sont supposés identiques et omni-directionnels. La source et le $i^{ème}$ capteur du réseau sont représentés dans l'espace à l'aide de leurs coordonnées sphériques, c'est-à-dire le couple (ϕ, φ) pour la source (supposée en champ lointain) et le triplet $(\rho_i, \varrho_i, \xi_i)$ pour le $i^{ème}$ capteur (voir figure 1(a)). Dans cette étude, nous considérons deux types de géométrie d'antenne. La première concerne une antenne planaire en V où les deux branches, séparées par un angle noté Δ, sont constituées par des antennes linéaires non obligatoirement uniformes. La deuxième géométrie considérée consiste simplement en une extension de l'antenne planaire où une branche (antenne linéaire non obligatoirement uniforme) orthogonale au plan est ajoutée (voir figure 1(b)). A partir des hypothèses susmentionnées, une simple analyse du retard inter-capteur conduit au modèle d'observation à la sortie du réseau suivant

$$\mathbf{y}(t) = [y_1(t) \dots y_M(t)]^T = \mathbf{a}(\varphi,\phi)s(t) + \mathbf{b}(t) \tag{A.1}$$

où $t = 1, \dots, T$. T est le nombre d'observations, et le vecteur directionnel est donné par :

$$\mathbf{a}(\varphi,\phi) = \begin{bmatrix} e^{\frac{2j\pi\rho_1}{\lambda}(\sin\varphi\sin\xi_1\cos(\phi-\varrho_1)+\cos\xi_1\cos\varphi)} \\ \vdots \\ e^{\frac{2j\pi\rho_M}{\lambda}(\sin\varphi\sin\xi_M\cos(\phi-\varrho_M)+\cos\xi_M\cos\varphi)} \end{bmatrix}. \tag{A.2}$$

Le vecteur de bruit $\mathbf{b}(t) \in \mathbb{C}^M$ est supposé gaussien, circulaire, i.i.d., de moyenne nulle et de matrice de covariance $\sigma^2\mathbf{I}$. Le nombre de capteurs dans le plan est noté N_1 et le nombre de

capteurs pour la branche orthogonale dans le cas de l'antenne 3D est noté N_2. Le nombre total de capteurs $M = N_1 + N_2$ sera constant lors de la comparaison des deux géométries.

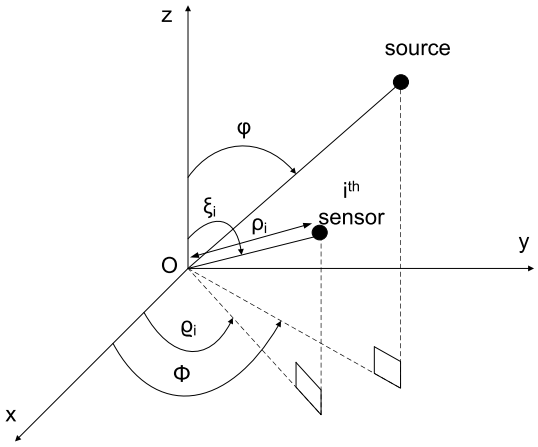

(a) Système de coordonnées pour la source et les capteurs du réseau

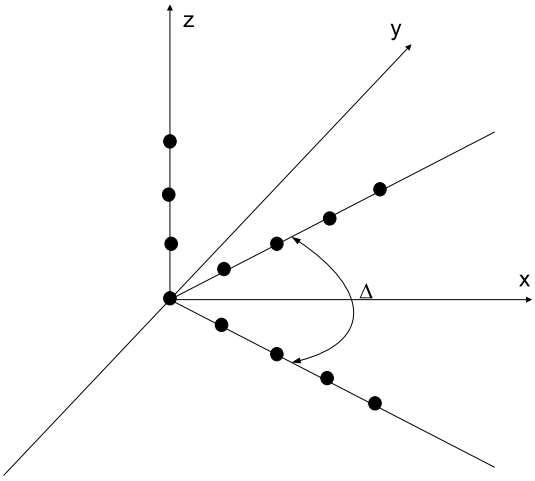

(b) Géométrie du réseau de capteurs 3D (Dans le cas du réseau 2D, seuls les capteurs dans le plan xOy sont présents)

Figure A.1: Géométrie du problème

Bornes de Cramér-Rao

L'analyse des performances ultimes, en terme de variance, qu'un estimateur (non biaisé) peut espérer atteindre est généralement conduite à l'aide des BCR. Dans le cas du modèle d'observation (A.1), il est clair que $\mathbf{y}(t)$ est distribué selon une loi gaussienne multivariée de moyenne $\mathbf{a}(\varphi,\phi)s(t)$ et de variance $\sigma^2\mathbf{I}$. Les paramètres d'intérêt pour cette étude étant l'azimut et l'élévation, c'est-à-dire ϕ et φ (puisque la variance du bruit est découplée par rapport aux autres paramètres, cette dernière est omise du vecteur de paramètres). Seule la moyenne de $\mathbf{y}(t)$ est paramétrée. Dans ce cas, après concaténation de tous les vecteurs d'observation ($t = 1, \ldots, T$), la BCR, notée $\mathbf{C}$, est donnée par [SN89]

$$\mathbf{C} = \begin{bmatrix} C_{\varphi\varphi} & C_{\varphi\phi} \\ C_{\phi\varphi} & C_{\phi\phi} \end{bmatrix} = \frac{\sigma^2}{2\mathbf{s}^H\mathbf{s}} \begin{bmatrix} \mathrm{Re}\left(\frac{\partial \mathbf{a}^H(\varphi,\phi)}{\partial\varphi}\frac{\partial \mathbf{a}(\varphi,\phi)}{\partial\varphi}\right) & \mathrm{Re}\left(\frac{\partial \mathbf{a}^H(\varphi,\phi)}{\partial\varphi}\frac{\partial \mathbf{a}(\varphi,\phi)}{\partial\phi}\right) \\ \mathrm{Re}\left(\frac{\partial \mathbf{a}^H(\varphi,\phi)}{\partial\phi}\frac{\partial \mathbf{a}(\varphi,\phi)}{\partial\varphi}\right) & \mathrm{Re}\left(\frac{\partial \mathbf{a}^H(\varphi,\phi)}{\partial\phi}\frac{\partial \mathbf{a}(\varphi,\phi)}{\partial\phi}\right) \end{bmatrix}^{-1}. \quad \text{(A.3)}$$

où l'on définit $\mathbf{s} = [s(1) \ldots s(T)]^T$ et, où $C_{\varphi\varphi}$ et $C_{\phi\phi}$ représentent, respectivement, la BCR concernant l'élévation et la BCR concernant l'azimut. $C_{\varphi\phi}$ et $C_{\phi\varphi}$ représentent le couplage des paramètres φ et ϕ.

Grâce à la structure du vecteur directionnel donné par le modèle d'observation (A.1) et après quelques efforts calculatoires qui sont détaillés dans l'annexe, en posant : $\|\mathbf{s}\|^2 = \mathbf{s}^H\mathbf{s}$, $C_{RSB} = \frac{8\pi^2\|\mathbf{s}\|^2}{\sigma^2\lambda^2}$, $S_1 = \sum_{i=1}^{N_1}\rho_i^2$, et $S_2 = \sum_{i=N_1+1}^{N_1+N_2}\rho_i^2$, on obtient les expressions analytiques des BCR dans le cas de l'antenne 3D :

$$C_{\varphi\varphi}^{3D} = \frac{2}{C_{RSB}} \frac{1 - \cos\Delta\cos 2\phi}{S_1 \sin^2\Delta\cos^2\varphi + 2S_2\sin^2\varphi(1-\cos\Delta\cos 2\phi)}, \tag{A.4}$$

$$C_{\phi\phi}^{3D} = \frac{4}{C_{RSB}\sin^2\varphi} \frac{\frac{1}{2}S_1\cos^2\varphi(1+\cos\Delta\cos 2\phi) + S_2\sin^2\varphi}{S_1^2\sin^2\Delta\cos^2\varphi + 2S_1S_2\sin^2\varphi(1-\cos\Delta\cos 2\phi)}, \tag{A.5}$$

$$C_{\varphi\phi}^{3D} = \frac{1}{C_{RSB}\tan\varphi} \frac{S_1\cos\Delta\sin 2\phi}{S_1^2\sin^2\Delta\cos^2\varphi + 2S_1S_2\sin^2\varphi(1-\cos\Delta\cos 2\phi)}. \tag{A.6}$$

Puisque l'antenne 2D n'est qu'un cas particulier de l'antenne 3D ($N_2 = 0$), les BCR sont obtenues en posant $S_2 = 0$ dans les équations ci-dessus

$$C_{\varphi\varphi}^{2D} = \frac{2}{C_{RSB}} \frac{1 - \cos\Delta\cos 2\phi}{S_1\sin^2\Delta\cos^2\varphi}, \tag{A.7}$$

$$C_{\phi\phi}^{2D} = \frac{2}{C_{RSB}} \frac{1 + \cos\Delta\cos 2\phi}{S_1\sin^2\Delta\sin^2\varphi}, \tag{A.8}$$

$$C_{\varphi\phi}^{2D} = \frac{1}{C_{RSB}} \frac{\cos\Delta\sin 2\phi}{S_1\sin^2\Delta\cos\varphi\sin\varphi}. \tag{A.9}$$

De plus, dans le cas particulier où l'on travaille avec $\Delta = \frac{\pi}{2}$, c'est-à-dire lorsque l'antenne 2D et l'antenne 3D représentent, respectivement, la base canonique de $\mathbb{R}^2$ et de $\mathbb{R}^3$, on obtient des formules compactes :

$$C_{\varphi\varphi}^{3D\perp} = \frac{1}{C_{RSB}} \frac{2}{S_1\cos^2\varphi + 2S_2\sin^2\varphi}, \tag{A.10}$$

$$C_{\phi\phi}^{3D\perp} = \frac{2}{C_{RSB}S_1\sin^2\varphi}, \tag{A.11}$$

$$C_{\varphi\phi}^{3D\perp} = 0. \tag{A.12}$$

et

$$C_{\varphi\varphi}^{2D\perp} = \frac{2}{C_{RSB}S_1\cos^2\varphi}, \tag{A.13}$$

$$C_{\phi\phi}^{2D\perp} = \frac{2}{C_{RSB}S_1\sin^2\varphi}, \tag{A.14}$$

$$C_{\varphi\phi}^{2D\perp} = 0. \tag{A.15}$$

A partir de ces expressions, on peut remarquer que :

- lorsque la source se situe dans le plan, c'est-à-dire lorsque $\varphi = \frac{\pi}{2}$, $C_{\varphi\varphi}^{2D}$ tend vers l'infini tandis que $C_{\varphi\varphi}^{3D}$ reste fini. L'antenne 3D permet donc de lever l'ambiguïté.
- Dans le cas où $\Delta = \frac{\pi}{2}$, il y a découplage entre ϕ et φ ce qui confirme l'intuition. De plus, $C_{\phi\phi}^{3D\perp}$ et $C_{\phi\phi}^{2D\perp}$ ne dépendent plus de ϕ (propriété d'isotropie par rapport à ϕ). Si de plus $S_1 = 2S_2$, c'est-à-dire lorsque les trois branches de l'antenne 3D sont constituées par des antennes linéaires uniformes avec le même nombre de capteurs, l'estimation de φ ne depend plus de la position de la source (propriété d'isotropie par rapport à φ et ϕ) pour l'antenne 3D.

Analyses et simulations

On considère dans cette partie des résultats de simulation concernant le comportement des BCR calculées précédemment en fonction du degré de liberté Δ. Toutes les branches, que le réseau

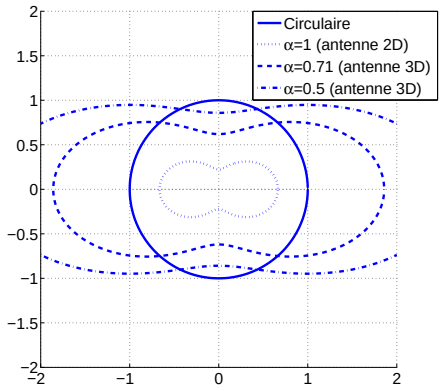

(a) BCR d'azimut normalisée en fonction de α à $\Delta = 60°$ et $\varphi = 45°$

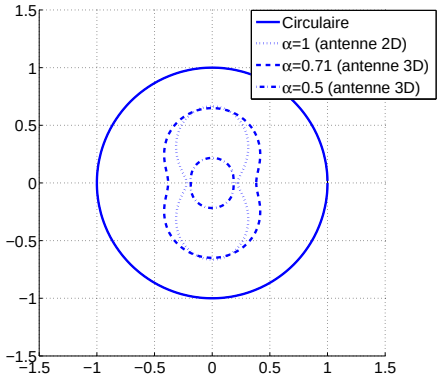

(b) BCR d'élévation normalisée en fonction de α à $\Delta = 60°$ et $\varphi = 45°$

Figure A.2: Comparaison de performance des antennes en V avec une antenne circulaire

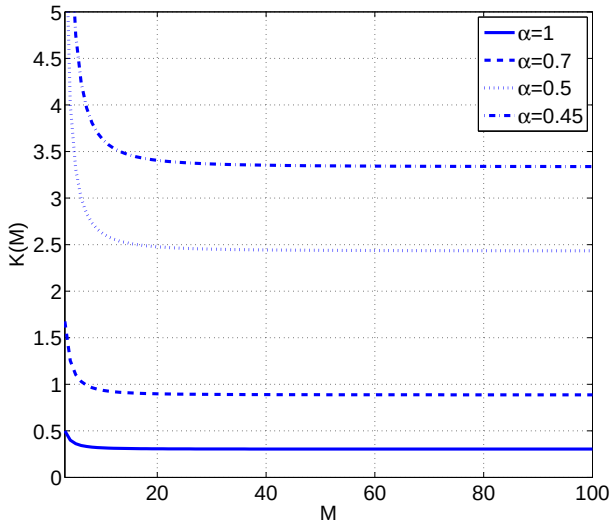

Figure A.3: Fraction $K(M)$ en fonction du nombre de capteurs M

soit 2D (deux branches) ou 3D (trois branches), sont des antennes linéaires uniformes avec un espacement inter-capteur d'une demi longueur d'onde. Pour toutes les simulations, le rapport signal sur bruit est de $10dB$ et le nombre d'observations est de $T = 50$.

Il est intéressant de comparer les performances de l'antenne en V avec une antenne isotrope classique telle que l'antenne circulaire. Ces antennes ont le même nombre de capteurs. L'antenne circulaire ayant des capteurs séparés de manière équidistante $\frac{\lambda}{2}$, la valeur de son rayon est donc $r = \frac{\lambda}{4 \sin \frac{\pi}{M}}$. En posant $\alpha = \frac{N_1}{M} \leq 1$, il vient que la valeur de α associée à l'antenne planaire est égale à 1 tandis que celle associée à l'antenne 3D est strictement inférieure à 1. Les figures A.2(a) et A.2(b) montrent respectivement les BCR concernant l'azimut et l'élévation normalisées par la borne de l'antenne circulaire pour un angle d'ouverture $\Delta = 60°$ et pour une élévation $\varphi = 45°$.

Les performances d'estimation concernant l'élévation des antennes en V sont toujours meilleures par rapport à l'antenne circulaire, alors que celles concernant l'estimation d'azimut sont liées au nombre de capteurs que l'on place sur l'axe orthogonal, c'est-à dire au coefficient α. Pour des valeurs de α proches de 1, l'estimation de l'élévation des antennes en V est meilleure que celle de l'antenne circulaire.

En particulier, si l'antenne en V et son extension 3D sont isotropes ($\Delta = \frac{\pi}{2}$), le rapport de la BCR sur l'azimut de ces antennes est donné par :

$$\begin{array}{l} K(M) = \frac{C_{\phi\phi}^{2D,3D\perp}}{C_{\phi\phi}^{Circulaire}} = \frac{3}{\alpha(\alpha^2M^2-1)\sin^2\frac{\pi}{M}}. \\ \text{Si } \alpha = 1 \text{ et } M >> 1 \rightarrow K(M) = \frac{1}{3}. \\ \text{Si } \alpha < 1 \text{ et } \alpha M >> 1 \rightarrow K(M) = \frac{1}{3\alpha^2}. \end{array} \tag{A.16}$$

On peut dire que l'antenne en V a de meilleures performances en terme d'estimation d'azimut par rapport à l'antenne circulaire si et seulement si la fraction $K(M)$ est inférieure à 1. La figure A.3 montre que l'antenne isotrope en V est meilleure que l'antenne circulaire à condition que la valeur de α satisfasse : $0.76 < \alpha < 1$.

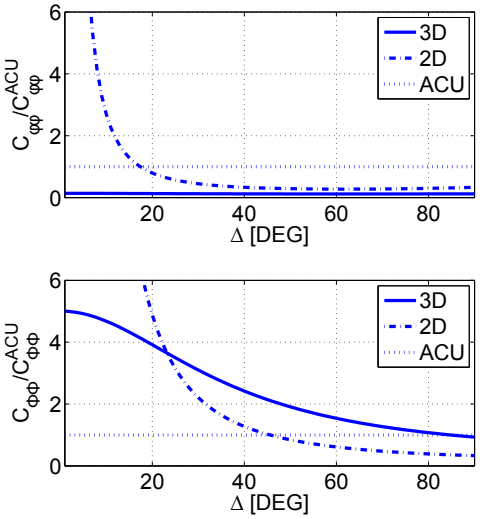

(a) Comportement de $C_{\varphi\varphi}^{3D}$, $C_{\varphi\varphi}^{2D}$, $C_{\phi\phi}^{3D}$ et $C_{\phi\phi}^{2D}$ normalisées par la valeur de la BCR de l'antenne circulaire par rapport à Δ avec $\phi = 20°$ et $\varphi = 70°$

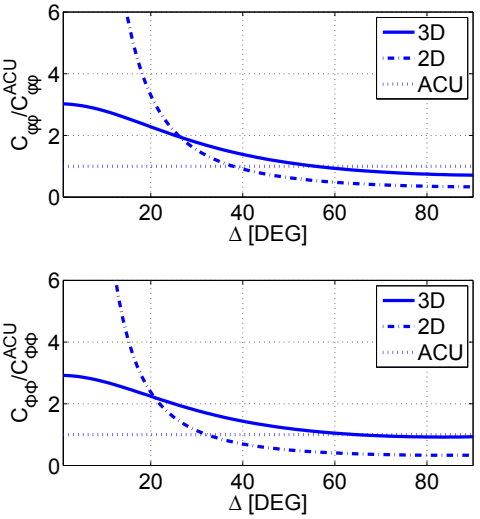

(b) Comportement de $C_{\varphi\varphi}^{3D}$, $C_{\varphi\varphi}^{2D}$, $C_{\phi\phi}^{3D}$ et $C_{\phi\phi}^{2D}$ normalisées par la valeur de la BCR de l'antenne circulaire par rapport à Δ avec $\phi = 50°$ et$\varphi = 30°$

Figure A.4: BCR normalisée en fonction de l'angle d'ouverture

Dans la suite, on compare les performances d'estimation entre le modèle 2D et 3D. Dans cette simulation, le réseau 2D est composé de $M = 7$ capteurs (un à l'origine plus trois sur chacune des deux branches). Le réseau 3D est également composé de $M = 7$ capteurs (un à l'origine plus deux sur chacune des trois branches). La figure A.4(a) montre le comportement de $C_{\varphi\varphi}^{3D}$, $C_{\varphi\varphi}^{2D}$, $C_{\phi\phi}^{3D}$ et $C_{\phi\phi}^{2D}$ par rapport à l'angle d'ouverture Δ variant de 0 à $\frac{\pi}{2}$. Pour cette simulation, les valeurs de ϕ et φ sont respectivement de 20° et 70°. Nous qualifierons ce scénario de source rasante par rapport au plan de l'antenne. On observe que pour l'estimation de l'élévation, φ, le réseau 3D permet toujours d'obtenir de meilleures performances par rapport au réseau 2D. Ceci est toujours vrai pour une valeur d'élévation de $\varphi \geq 62.2°$ dans ce cas, car on montre facilement que :

$$\frac{C_{\varphi\varphi}^{3D}}{C_{\varphi\varphi}^{2D}} < 1 \Leftrightarrow \varphi > \arctan\sqrt{\max_{\Delta,\phi}\{\Gamma\}}. \tag{A.17}$$

avec $\Gamma = \frac{\sin^2\Delta\left((M^2-1)-\alpha(\alpha^2M^2-1)\right)}{(1-\cos\Delta\cos 2\phi)4(1-\alpha)((1-\alpha)M+1)(2(1-\alpha)M+1)}$, $\alpha = \frac{N_1}{M} = \frac{5}{7}, M = 7, \varphi \in [0°, 90°], \Delta \in (0°, 180°), \phi \in [0°, 360°]$.

Au contraire, il existe une valeur de Δ (environ 23° dans ce cas) en dessous de laquelle le réseau 3D permet de meilleures performances par rapport au réseau 2D pour l'estimation de l'azimut. Cette valeur critique peut être obtenue en résolvant numériquement l'équation $C_{\phi\phi}^{3D} = C_{\phi\phi}^{2D}$ en Δ. La figure A.4(b) montre les mêmes courbes, mais pour des valeurs de ϕ et φ respectivement égales à 50° et 30°. Nous qualifierons ce scénario de source haute par rapport au plan de l'antenne. Dans ce cas, il convient, contrairement à l'intuition, de choisir le réseau 2D au dessus d'une certaine limite d'angle d'ouverture obtenue en résolvant numériquement $\max\left(C_{\phi\phi}^{3D} = C_{\phi\phi}^{2D}, C_{\varphi\varphi}^{3D} = C_{\varphi\varphi}^{2D}\right)$.

Annexe: démonstration de (A.4), (A.5) et (A.6)

Les dérivées du $i^{ième}$ élément du vecteur directionnel sont données par :

$$\frac{\partial a_i(\varphi,\phi)}{\partial\varphi} = \frac{2j\pi\rho_i}{\lambda}\left(\cos\varphi\sin\xi_i\cos\left(\phi-\varrho_i\right)-\cos\xi_i\sin\varphi\right)e^{\left(\frac{2j\pi\rho_i}{\lambda}\sin\varphi\sin\xi_i\cos\left(\phi-\varrho_i\right)+\cos\xi_i\cos\varphi\right)}, \tag{A.18}$$

et

$$\frac{\partial a_i(\varphi,\phi)}{\partial\phi} = -\frac{2j\pi\rho_i}{\lambda}\sin\varphi\sin\xi_i\sin\left(\phi-\varrho_i\right)\times e^{\left(\frac{2j\pi\rho_i}{\lambda}\sin\varphi\sin\xi_i\cos\left(\phi-\varrho_i\right)+\cos\xi_i\cos\varphi\right)}. \tag{A.19}$$

Supposons que N_1 est un nombre impair. Comme les 2 branches du V sont symétriques, on obtient :

$$\sum_{i=1}^{N_1}\rho_i^2e^{-2j\varrho_i} = \sum_{i=1}^{\frac{N_1-1}{2}}\rho_i^2e^{-2j\frac{\Delta}{2}} + \sum_{i=1}^{\frac{N_1-1}{2}}\rho_i^2e^{2j\frac{\Delta}{2}} = \sum_{i=1}^{\frac{N_1-1}{2}}\rho_i^2\left(e^{-j\Delta}+e^{j\Delta}\right) = 2\cos\Delta\sum_{i=1}^{\frac{N_1-1}{2}}\rho_i^2 = S_1\cos\Delta. \tag{A.20}$$

En notant que les capteurs qui se situent sur le plan xOy ont pour paramètre $\xi_i = \frac{\pi}{2}$, alors que les capteurs appartenant à l'axe orthogonal ont pour paramètre $\xi_i = 0$. Après quelques calculs, en appliquant (A.18) et (A.19) dans (A.3) et en sachant (A.20), les éléments de la matrice d'information de Fisher sont donnés par:

$$\begin{aligned}
\frac{[\mathbf{C}^{-1}]_{11}}{C_{RSB}} &= \sum_{i=1}^{M}\rho_i^2\left(\cos\varphi\sin\xi_i\cos\left(\phi-\varrho_i\right)-\cos\xi_i\sin\varphi\right)^2 \\
&= \sum_{i=1}^{N_1}\rho_i^2\cos^2\varphi\cos^2\left(\phi-\varrho_i\right) + \sum_{i=N_1+1}^{N_1+N_2}\rho_i^2\sin^2\varphi \\
&= \frac{\cos^2\varphi}{4}\left(e^{2j\phi}\sum_{i=1}^{N_1}\rho_i^2e^{-2j\varrho_i} + e^{-2j\phi}\sum_{i=1}^{N_1}\rho_i^2e^{2j\varrho_i} + 2\sum_{i=1}^{N_1}\rho_i^2\right) + \sin^2\varphi\sum_{i=N_1+1}^{N_1+N_2}\rho_i^2 \\
&= \frac{1}{4}\cos^2\varphi\left(S_1\cos\Delta(e^{2j\phi}+e^{-2j\phi}) + 2S_1\right) + \sin^2\varphi S_2 \\
&= \frac{1}{2}S_1\cos^2\varphi\left(\cos\Delta\cos 2\phi + 1\right) + S_2\sin^2\varphi.
\end{aligned} \tag{A.21}$$

$$\begin{aligned}
\frac{[\mathbf{C}^{-1}]_{22}}{C_{RSB}} &= \sum_{i=1}^{M} \rho_i^2 \left(\sin\varphi \sin\xi_i \sin\left(\phi - \varrho_i\right)\right)^2 \\
&= \sin^2\varphi \sum_{i=1}^{N_1} \rho_i^2 \sin^2\left(\phi - \varrho_i\right) \\
&= -\frac{1}{4}\sin^2\varphi \left(e^{2j\phi} \sum_{i=1}^{N_1} \rho_i^2 e^{-2j\varrho_i} + e^{-2j\phi} \sum_{i=1}^{N_1} \rho_i^2 e^{2j\varrho_i} - 2\sum_{i=1}^{N_1} \rho_i^2 \right) \\
&= -\frac{1}{4}\sin^2\varphi \left(S_1 \cos\Delta (e^{2j\phi} + e^{-2j\phi}) - 2S_1 \right) \\
&= -\frac{1}{2} S_1 \sin^2\varphi \left(\cos\Delta \cos 2\phi - 1\right). \qquad \text{(A.22)}
\end{aligned}$$

$$\begin{aligned}
\frac{[\mathbf{C}^{-1}]_{12}}{C_{RSB}} &= -\sum_{i=1}^{M} \left(\rho_i^2 \sin\varphi \sin\xi_i \sin\left(\phi - \varrho_i\right) \left(\cos\varphi \sin\xi_i \cos\left(\phi - \varrho_i\right) - \cos\xi_i \sin\varphi\right) \right) \\
&= -\sin\varphi\cos\varphi \sum_{i=1}^{N_1} \rho_i^2 \sin\left(\phi - \varrho_i\right)\cos\left(\phi - \varrho_i\right) \\
&= -\frac{1}{8j}\sin 2\varphi \left(e^{2j\phi} \sum_{i=1}^{N_1} \rho_i^2 e^{-2j\varrho_i} - e^{-2j\phi} \sum_{i=1}^{N_1} \rho_i^2 e^{2j\varrho_i} \right) \\
&= -\frac{1}{8j} S_1 \sin 2\varphi \cos\Delta (e^{2j\phi} - e^{-2j\phi}) \\
&= -\frac{1}{4} S_1 \sin 2\varphi \cos\Delta \sin 2\phi. \qquad \text{(A.23)}
\end{aligned}$$

Le déterminant de la matrice d'information de Fisher est donné par :

$$\begin{aligned}
\frac{\det\left[\mathbf{C}^{-\mathbf{1}}\right]}{C_{RSB}^2} &= \frac{[\mathbf{C}^{-1}]_{11}[\mathbf{C}^{-1}]_{22} - [\mathbf{C}^{-1}]_{12}[\mathbf{C}^{-1}]_{21}}{C_{RSB}^2} \\
&= \left(\frac{1}{2} S_1 \cos^2\varphi \left(\cos\Delta \cos 2\phi + 1\right) + S_2 \sin^2\varphi \right) \left(-\frac{1}{2} S_1 \sin^2\varphi \left(\cos\Delta \cos 2\phi - 1\right) \right) \\
&\quad - \left(\frac{1}{2} S_1 \sin\varphi \cos\varphi \cos\Delta \sin 2\phi \right)^2 \\
&= -\frac{1}{4} S_1^2 \sin^2\varphi \cos^2\varphi \cos^2\Delta \cos^2 2\phi + \frac{1}{4} S_1^2 \sin^2\varphi \cos^2\varphi \\
&\quad -\frac{1}{2} S_1 S_2 \sin^4\varphi (\cos\Delta \cos 2\phi - 1) - \frac{1}{4} S_1^2 \sin^2\varphi \cos^2\varphi \cos^2\Delta \sin^2 2\phi \\
&= \frac{\sin^2\varphi}{4} \left(S_1^2 \cos^2\varphi \sin^2\Delta + 2 S_1 S_2 \sin^2\varphi (1 - \cos\Delta \cos 2\phi) \right). \qquad \text{(A.24)}
\end{aligned}$$

A.3 Optimisation de la géométrie des réseaux de capteurs basée sur la borne de Weiss-Weinstein

Dans la partie précédente, la BCR était utilisée pour étudier l'impact de la géométrie du réseau sur les performances d'estimation dans le contexte où les paramètres sont supposés déterministes. Dans cette partie, nous nous sommes intéressés au développement d'un outil pour étudier cet impact dans le contexte Bayésien. La borne de Weiss-Weinstein qui est la borne la plus précise dans la famille des bornes de Weiss-Weinstein a été considérée. Comme mentionné dans l'introduction,

la BWW est une borne Bayésienne, donc, elle est utile pour les trois zones d'opération des estimateurs. Elle peut capturer le décrochement de l'EQM obtenue par l'estimateur maximum a posteriori. La BWW a été beaucoup moins étudiée que la BCR du fait de sa complexité.

Encore une fois, nous allons étudier les deux modèles des signaux comme dans le chapitre précédent: le modèle stochastique et le modèle déterministe. Dans le contexte du traitement d'antenne, tandis que les expressions analytiques de la borne de Ziv-Zakai (plus précisément son extension proposée par Bell et. al. [BEV96a]) ont été proposées il y a environ 15 ans pour le modèle stochastique et les résultats concernant la BWW étaient généralement réalisés par des simulations. Concernant le modèle stochastique, dans [NH88], la BWW a été évaluée par des simulations, et ensuite comparée avec l'EQM obtenue par l'algorithme MUSIC et l'algorithme de formation des voies en utilisant un réseau de capteurs de 8×8 éléments. Dans [NV94], les auteurs ont introduit une comparaison numérique entre la BCR Bayésienne, la borne Ziv-Zakai, et la BWW pour le problème de l'estimation de la DDA. Dans [Ath01], des simulations numériques de la BWW pour optimiser la position des capteurs dans un réseau linéaire non-uniforme ont été proposées. Toujours concernant le modèle stochastique, dans [XBR04], les auteurs ont dérivé des expressions quasi-analytiques d'une version simplifiée de la BWW pour le problème de l'estimation de la DDA dans le contexte du traitement champ adapté. En effet, l'intégration sur la fonction de distribution *a priori* n'a pas été effectuée. Le modèle déterministe avec la séquence des signaux supposée connue, a été étudié seulement dans [Ren07], où les expressions analytiques de la BWW étaient données pour le cas de l'analyse spectrale.

Bien que l'objectif principal de ce chapitre soit de donner des expressions analytiques de la BWW pour le problème de l'estimation de la DDA d'une seule source en utilisant un réseau de capteurs planaire quelconque, et pour les modèles déterministe et stochastique, nous fournissons également des expressions quasi-analytiques de la borne qui pourraient être utiles pour d'autres problèmes.

- Premièrement, nous avons étudié le modèle général des observations Gaussiennes avec moyenne ou matrice de covariance paramétrée. En effet, pour ce modèle, l'un des succès de la BCR est dû à l'expression analytique de la matrice d'information de Fisher qui est appelée la formule de Slepian-Bang [Kay93]. Une telle formule n'avait pas été proposée pour la BWW.

- Deuxièmement, vu que l'un des objectif de cette partie est de fournir des formules qui pourraient être appliquées dans d'autres domaines, nous avons proposé quelques résultats pour le contexte de sources multiple sans avoir besoin de préciser la structure de la matrice directionnelle et de la matrice de covariance du bruit. Plus particulièrement, pour obtenir les expressions analytiques de la BWW, il faut calculer des intégrales sur les observations et sur les paramètres. Dans cette partie, l'intégration sur l'espace des observations a été proposée. Pour la deuxième intégration sur l'espace des paramètres, il a été nécessaire de détailler la structure de la matrice de covariance du bruit et de la matrice directionnelle afin d'obtenir des expressions analytiques.

- Ensuite, ces résultats ont été appliqués dans le cas particulier d'une seule source avec deux types de la géométrie du réseau: le réseau linéaire non-uniforme (estimer seulement l'angle d'élévation), et le réseau planaire (estimer l'angle azimut et l'angle d'élévation). Grâce à la structure exponentielle du vecteur directionnel, nous avons obtenu des expressions de la BWW plus compactes. En effet, nous avons trouvé que pour le cas d'une seule source, l'intégration sur les paramètres était obtenue directement. Il faut noter qu'une des particularité de cette contribution par rapport aux publications précédentes concernant la BWW est que nous n'avons pas utilisé l'hypothèse $s = 1/2$.

- Finalement, quelques simulations ont été présentées. Nous avons utilisé la BWW pour étudier la valeur optimal de l'angle d'ouverture de l'antenne en V mentionné précédemment. Nous avons montré que pour le modèle déterministe, cette valeur est égale à 90°.

Modèle des observations

Dans cette partie, nous nous limiterons au cas de l'estimation passive d'une DDA pour une source, située en champ lointain et dont le signal est supposé à bande étroite à partir d'un réseau linéaire (non-uniforme) constitué de N capteurs (les différentes généralisations présentées ci-dessus sont détaillées dans le chapitre 3). La position des capteurs dans le réseau est caractérisée par rapport à un réferentiel par le vecteur $\mathbf{d} = [d_1 \dots d_N]$. La réponse du i^{eme} capteur à l'instant t est un vecteur donné par : $y_i(t) = [\mathbf{a}(\varphi)]_i s(t) + \mathbf{b}_i(t), \quad t = 1, \dots, T,$. $s(t)$ est le signal de la source, T est le nombre des observations, et $[\mathbf{a}(\varphi)]_i = \exp\left(j\frac{2\pi}{\lambda} d_i \sin\varphi\right)$ est le i^{eme} élément du vecteur directionnel $\mathbf{a}(\varphi)$ où φ représente l'angle d'élévation. $\mathbf{b}_i(t)$ est un bruit additif supposé complexe, circulaire, gaussien de moyenne nulle et de covariance $\sigma^2\mathbf{I}$. Concernant le signal source, on considérera les deux modèles suivants :

- $\mathcal{M}_1$: Le modèle déterministe ou conditionnel où le signal est supposé connu [OVSN93].

- $\mathcal{M}_2$: Le modèle stochastique ou non-conditionnel où le signal est supposé aléatoire, complexe, circulaire, gaussien de moyenne nulle et de matrice de covariance $\sigma_s^2\mathbf{I}$ connue. Pour ce modèle, le signal est également supposé indépendant du bruit [OVSN93].

On considérera plus particulièrement l'estimation de l'angle électrique $\omega = \sin\varphi$. Cette étude de performance se déroulant dans le contexte Bayésien, on supposera que le paramètre ω est aléatoire avec une loi uniforme $\omega \sim \mathcal{U}[-1, 1]$ *a priori* :

$$p(\omega) = \left[\begin{array}{l} \frac{1}{2} \text{ si } -1 \leq \omega \leq 1, \\ 0 \text{ si non.} \end{array} \right. \tag{A.25}$$

Donc, le modèle des observations à l'instant t s'écrit

$$\mathbf{y}(t) = \mathbf{a}(\omega)s(t) + \mathbf{b}(t), \tag{A.26}$$

où $\mathbf{y}(t) = [y_1(t) \dots y_N(t)]^T$. A partir des hypothèses précédentes, la fonction de vraisemblance de toutes les observations, *i.e.*, du vecteur $\mathbf{y} = [\mathbf{y}^T(1) \dots \mathbf{y}^T(T)]^T$, pour le modèle $\mathcal{M}_1$ est donnée par

$$p(\mathbf{y}|\omega) = \frac{1}{(\pi\sigma^2)^{2NT}} e^{\left(-\frac{1}{\sigma^2}\sum_{t=1}^{T}\|\mathbf{y}(t)-\mathbf{a}(\omega)s(t)\|^2\right)}, \tag{A.27}$$

et la fonction de vraisemblance pour le modèle $\mathcal{M}_2$ est donnée par

$$p(\mathbf{y}|\omega) = \frac{1}{\pi^{2NT}\left|\mathbf{R}(\omega)\right|^T} e^{\left(-\sum_{t=1}^{T}\mathbf{y}(t)^H\mathbf{R}(\omega)^{-1}\mathbf{y}(t)\right)}, \tag{A.28}$$

où $\mathbf{R}(\omega) = \sigma_s^2\mathbf{a}(\omega)\mathbf{a}(\omega)^H + \sigma^2\mathbf{I}_{2N}$ représente la matrice de covariance pour le modèle $\mathcal{M}_2$. La BWW sera dérivée pour le modèle $\mathcal{M}_1$ et $\mathcal{M}_2$.

Borne de Weiss-Weinstein pour le réseau linéaire

La BWW est obtenue, en général, en cherchant le maximum d'une fonction sur un ensemble de points test et sur un ensemble de paramètres $s \in [0,1]$. Concernant le paramètre s, on utilise souvent l'hypothèse $s = 1/2$ [VRBM10a, XBR04, Ren07]. Ω et Θ représentent respectivement l'espace des observations et l'espace des paramètres, la BWW pour $s = 1/2$ s'écrit [WW88]:

$$\int_{\Theta}\int_{\Omega} (\hat{\omega}-\omega)^2 p(\mathbf{y},\omega) d\mathbf{y} d\omega \geq WWB = \sup_{h} \frac{h^2 \eta(h,0)\eta(0,h)}{2(\eta(h,h)-\eta(h,-h))} \tag{A.29}$$

où $\hat{\omega}$ est un estimateur de ω, où $p(\mathbf{y},.)$ représente la loi jointe entre le vecteur des observations et le paramètre (ou un point de test), et où h représente la différence entre le paramètre d'intérêt et un point de test appartenant à l'espace des paramètres (c'est-à-dire qu'il faut respecter $\omega + h \in \Theta$). On a défini

$$\eta(\alpha,\beta) = \int_{\Theta}\int_{\Omega} \sqrt{p(\mathbf{y},\omega+\alpha)p(\mathbf{y},\omega+\beta)} d\mathbf{y} d\omega = \int_{\Theta} \sqrt{p(\omega+\alpha)p(\omega+\beta)}\zeta(\omega,\alpha,\beta) d\omega \tag{A.30}$$

et $\zeta(\omega,\alpha,\beta) = \int_{\Omega} \sqrt{p(\mathbf{y}|\,\omega+\alpha)p(\mathbf{y}|\,\omega+\beta)} d\mathbf{y}$ où $p(.)$ représente la distribution *a priori* du paramètre.

Modèle déterministe $\mathcal{M}_1$

À partir de l'équation (A.59), l'expression de $\zeta(\alpha,\beta)$ est donnée par:

$$\zeta(\alpha,\beta) = \int_{\Omega} \frac{1}{(\pi\sigma^2)^{2NT}} \times e^{\left(-\frac{1}{2\sigma^2}\sum_{t=1}^{T}\left(\|\mathbf{y}(t)-\mathbf{a}(\omega+\alpha)s(t)\|^2+\|\mathbf{y}(t)-\mathbf{a}(\omega+\beta)s(t)\|^2\right)\right)} d\mathbf{y}. \tag{A.31}$$

Par le changement de variable

$$\mathbf{x}(t) = \mathbf{y}(t) - \frac{1}{2}\left(\mathbf{a}(\omega+\alpha)s(t) + \mathbf{a}(\omega+\beta)s(t)\right),$$

on obtient

$$\begin{aligned} &-\tfrac{1}{2\sigma^2}\sum_{t=1}^{T}\left(\|\mathbf{y}(t)-\mathbf{a}(\omega+\alpha)s(t)\|^2 + \|\mathbf{y}(t)-\mathbf{a}(\omega+\beta)s(t)\|^2\right) \\ &= -\tfrac{1}{\sigma^2}\sum_{t=1}^{T}\left(\|\mathbf{x}(t)\|^2 + \tfrac{1}{4}\|\mathbf{a}(\omega+\alpha)-\mathbf{a}(\omega+\beta)\|^2\right) \end{aligned} \tag{A.32}$$

Puisque

$$\int_{\Omega} \frac{1}{(\pi\sigma^2)^{2NT}} \exp\left(\sum_{t=1}^{T} -\frac{1}{\sigma^2}\|\mathbf{x}(t)\|^2\right) d\mathbf{x} = 1, \tag{A.33}$$

on a

$$\zeta(\alpha,\beta) = \exp\left(-\frac{\|\mathbf{s}\|^2}{4\sigma^2}\|\mathbf{a}(\omega+\alpha)-\mathbf{a}(\omega+\beta)\|^2\right). \tag{A.34}$$

Grâce à la structure du vecteur $\mathbf{a}(\omega)$, et sachant que les expression analytiques de $\|\mathbf{a}(\omega+\alpha)-\mathbf{a}(\omega+\beta)\|^2$ sont données par

$$\|\mathbf{a}(\omega+\alpha)\|^2 = \|\mathbf{a}(\omega+\beta)\|^2 = N, \tag{A.35}$$

$$\mathbf{a}(\omega+\alpha)^H\mathbf{a}(\omega+\beta)=\sum_{i=1}^{N}e^{\left(j\frac{2\pi}{\lambda}d_k(\beta-\alpha)\right)}, \tag{A.36}$$

et par

$$\mathbf{a}(\omega+\beta)^H\mathbf{a}(\omega+\alpha)=\sum_{i=1}^{N}e^{\left(j\frac{2\pi}{\lambda}d_k(\alpha-\beta)\right)}. \tag{A.37}$$

On trouve que les fonctions $\zeta(\alpha,\beta)$ ne dépendent plus du paramètre ω. Par conséquent, $\eta(\alpha,\beta)$ est donné par

$$\eta(\alpha,\beta)=\zeta(\alpha,\beta)\int_{\Theta}\sqrt{p(\omega+\alpha)p(\omega+\beta)}d\omega. \tag{A.38}$$

Sous l'hypothèse d'un distribution *a priori* uniforme, on obtient

$$\int_{\Theta}\sqrt{p(\omega+\alpha)p(\omega+\beta)}=1-\frac{|\alpha|+|\beta|}{2}. \tag{A.39}$$

À partir de (A.29), (A.35), (A.36), (A.37), (A.38) et (A.39), l'expression analytique de la BWW est donnée par (A.40).

$$BWW=\sup_h\frac{h^2\left(1-\frac{|h|}{2}\right)^2\exp\left(-\frac{\|\mathbf{s}\|^2}{\sigma^2}\left(N-\sum_{k=1}^{N}\cos\left(\frac{2\pi}{\lambda}d_kh\right)\right)\right)}{2\left(1-\frac{|h|}{2}\right)-2\left(1-|h|\right)\exp\left(-\frac{\|\mathbf{s}\|^2}{2\sigma^2}\left(N-\sum_{k=1}^{N}\cos\left(\frac{4\pi}{\lambda}d_kh\right)\right)\right)}. \tag{A.40}$$

Modèle stochastique $\mathcal{M}_2$

À partir de (A.28), l'expression analytique de $\zeta(\alpha,\beta)$ est donnée par:

$$\zeta(\alpha,\beta)=\int_{\Omega}\frac{1}{\pi^{2NT}\left|\mathbf{R}(\omega+\alpha)\right|^{T/2}\left|\mathbf{R}(\omega+\beta)\right|^{T/2}}e^{\left(-\sum_{t=1}^{T}\mathbf{y}(t)^H\left(\frac{\mathbf{R}(\omega+\alpha)^{-1}+\mathbf{R}(\omega+\beta)^{-1}}{2}\right)\mathbf{y}(t)\right)}d\mathbf{y} \tag{A.41}$$

En posant $\mathbf{\Gamma}^{-1}=\frac{\mathbf{R}(\omega+\alpha)^{-1}+\mathbf{R}(\omega+\beta)^{-1}}{2}$, on obtient, $|\mathbf{\Gamma}|=\frac{2^{2N}}{|\mathbf{R}(\omega+\alpha)^{-1}+\mathbf{R}(\omega+\beta)^{-1}|}$, ce qui donne

$$\zeta(\alpha,\beta)=\frac{|\mathbf{\Gamma}|^T}{\left|\mathbf{R}(\omega+\alpha)\right|^{T/2}\left|\mathbf{R}(\omega+\beta)\right|^{T/2}}\times\int_{\Omega}\frac{1}{\pi^{2NT}\left|\mathbf{\Gamma}\right|^T}\exp\left(-\sum_{t=1}^{T}\mathbf{y}(t)^H\mathbf{\Gamma}^{-1}\mathbf{y}(t)\right)d\mathbf{y}. \tag{A.42}$$

Puisque $\int_{\Omega}\frac{1}{\pi^{2NT}|\mathbf{\Gamma}|^T}\exp\left(-\sum_{t=1}^{T}\mathbf{y}(t)^H\mathbf{\Gamma}^{-1}\mathbf{y}(t)\right)d\mathbf{y}=1$, on a

$$\zeta(\alpha,\beta)=\frac{|\mathbf{\Gamma}|^T}{\left|\mathbf{R}(\omega+\alpha)\right|^{T/2}\left|\mathbf{R}(\omega+\beta)\right|^{T/2}}. \tag{A.43}$$

Grâce à la structure de la matrice $\mathbf{R}(\omega+\delta)=\sigma_s^2\mathbf{a}(\omega+\delta)\mathbf{a}(\omega+\delta)^H+\sigma^2\mathbf{I}_{2N}$, on a

$$\left|\mathbf{R}(\omega+\delta)\right|=\sigma^{4N}\left(1+\frac{\sigma_s^2}{\sigma^2}\left\|\mathbf{a}(\omega+\delta)\right\|^2\right). \tag{A.44}$$

En outre, par l'identité de Woodbury, on obtient

$$\mathbf{R}(\omega+\delta)^{-1} = \frac{1}{\sigma^2}\left(\mathbf{I}_{2N} - \frac{\sigma_s^2\mathbf{a}(\omega+\delta)\mathbf{a}(\omega+\delta)^H}{\sigma_s^2\left\|\mathbf{a}(\omega+\delta)\right\|^2+\sigma^2}\right), \tag{A.45}$$

donc,

$$\mathbf{R}(\omega+\alpha)^{-1}+\mathbf{R}(\omega+\beta)^{-1} = \frac{1}{\sigma^2}\left(2\mathbf{I}_{2N} - \frac{\sigma_s^2\mathbf{a}(\omega+\alpha)\mathbf{a}(\omega+\alpha)^H}{\sigma_s^2\left\|\mathbf{a}(\omega+\alpha)\right\|^2+\sigma^2} - \frac{\sigma_s^2\mathbf{a}(\omega+\beta)\mathbf{a}(\omega+\beta)^H}{\sigma_s^2\left\|\mathbf{a}(\omega+\beta)\right\|^2+\sigma^2}\right). \tag{A.46}$$

Le déterminant de la matrice $\mathbf{R}(\omega+\alpha)^{-1}+\mathbf{R}(\omega+\beta)^{-1}$ est obtenu par une analyse des valeurs propres. En particulier, il y a $2N-2$ valeurs propres qui sont égales à $2/\sigma^2$, et les vecteurs propres correspondant aux deux dernières valeurs propres forment une combinaison linéaire $\mathbf{a}(\omega+\alpha)+q\mathbf{a}(\omega+\beta)$. De plus, ces deux valeurs propres ν sont des solutions de l'équation suivante :

$$\left(\mathbf{R}(\omega+\alpha)^{-1}+\mathbf{R}(\omega+\beta)^{-1}\right)\left(\mathbf{a}(\omega+\alpha)+q\mathbf{a}(\omega+\beta)\right) = \nu\left(\mathbf{a}(\omega+\alpha)+q\mathbf{a}(\omega+\beta)\right), \tag{A.47}$$

ce qui se réduit à

$$\begin{aligned}&\mathbf{a}(\omega+\alpha)\left(\tfrac{1}{\sigma^2}\left(2-A\left\|\mathbf{a}(\omega+\alpha)\right\|^2-qAC\right)-\nu\right)\\&+\mathbf{a}(\omega+\beta)\left(\tfrac{1}{\sigma^2}\left(2q-Bq\left\|\mathbf{a}(\omega+\beta)\right\|^2-BC^H\right)-q\nu\right)=0,\end{aligned} \tag{A.48}$$

où $A=\frac{\sigma_s^2}{\sigma_s^2\|\mathbf{a}(\omega+\alpha)\|^2+\sigma^2}$, $B=\frac{\sigma_s^2}{\sigma_s^2\|\mathbf{a}(\omega+\beta)\|^2+\sigma^2}$ et $C=\mathbf{a}(\omega+\alpha)^H\mathbf{a}(\omega+\beta)$. On obtient l'équation

$$\begin{aligned}&\nu^2\sigma^4+\nu\sigma^2\left(2-A\left\|\mathbf{a}(\omega+\alpha)\right\|^2-2+B\left\|\mathbf{a}(\omega+\beta)\right\|^2\right)\\&-4+2A\left\|\mathbf{a}(\omega+\alpha)\right\|^2+2B\left\|\mathbf{a}(\omega+\beta)\right\|^2\\&-AB\left\|\mathbf{a}(\omega+\alpha)\right\|^2\left\|\mathbf{a}(\omega+\beta)\right\|^2+ABCC^H=0.\end{aligned} \tag{A.49}$$

En résolvant (A.49) pour ν, et vu que

$$\left\|\mathbf{a}(\omega+\alpha)\right\|^2=\left\|\mathbf{a}(\omega+\beta)\right\|^2=\left\|\mathbf{a}(\omega)\right\|^2,$$

on obtient

$$\left|\mathbf{R}(\omega+\alpha)^{-1}+\mathbf{R}(\omega+\beta)^{-1}\right| = \prod_{i=1}^{2N}\nu_i = \frac{2^{2N}}{\sigma^{4N}}\left(\frac{\sigma^2}{\left\|\mathbf{a}(\omega)\right\|^2\sigma_s^2+\sigma^2}+\frac{1}{4}\frac{\sigma_s^4\left(\left\|\mathbf{a}(\omega)\right\|^4-\|C\|^2\right)}{\left(\left\|\mathbf{a}(\omega)\right\|^2\sigma_s^2+\sigma^2\right)^2}\right). \tag{A.50}$$

Finalement, en remplaçant (A.44), (A.50) dans (A.43), on a

$$\zeta(\alpha,\beta) = \left(1+\frac{\sigma_s^2(\left\|\mathbf{a}(\omega)\right\|^4-\left|\mathbf{a}(\omega+\alpha)^H\mathbf{a}(\omega+\beta)\right|^2)}{4\sigma^2(\left\|\mathbf{a}(\omega)\right\|^2\sigma_s^2+\sigma^2)}\right)^{-T}. \tag{A.51}$$

Dans (A.35), (A.36), et (A.37), on trouve que $\zeta(\alpha,\beta)$ ne dépend pas du paramètre ω, comme dans le cas déterministe. Par conséquent, l'expression analytique de la BWW est donnée par (A.52).

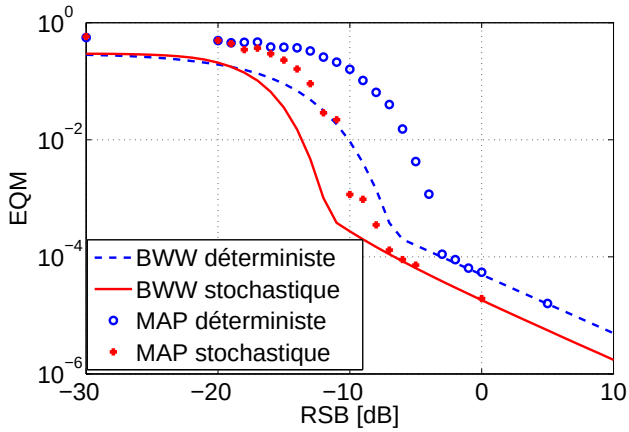

Figure A.5: MAP par rapport à la BWW.

$$BWW = \sup_{h} \frac{h^2 \left(1-\frac{|h|}{2}\right)^2 \left(1+\frac{\sigma_s^2\left(N^2-\left\|\sum_{k=1}^{N}\exp\left(j\frac{2\pi}{\lambda}d_k h\right)\right\|^2\right)}{4\sigma^2(N\sigma_s^2+\sigma^2)}\right)^{-2T}}{2\left(1-\frac{|h|}{2}\right)-2\left(1-|h|\right)\left(1+\frac{\sigma_s^2\left(N^2-\left\|\sum_{k=1}^{N}\exp\left(j\frac{4\pi}{\lambda}d_k h\right)\right\|^2\right)}{4\sigma^2(N\sigma_s^2+\sigma^2)}\right)^{-T}}. \quad \text{(A.52)}$$

Résultats de simulations

On considère un réseau linéaire uniforme composé de $N = 10$ capteurs avec une distance entre capteurs de $\lambda/2$. Le nombre des observations est égal à $T = 20$. Enfin, l'EQM empirique de l'estimateur du maximum *a posteriori* est réalisé à partir de 1000 tirages de Monte Carlo. La Fig. A.5 montre que la BWW donne une bonne approximation du décrochement de l'estimateur du maximum *a posteriori* pour les deux modèles de signaux considérés ici.

A.4 Le seuil statistique de résolution

En traitement d'antenne, le seuil statistique de la résolution (SSR) caractérise la séparation minimale entre les paramètres qui permet toujours de déterminer exactement le nombre des sources. L'application de la SSR concerne plusieurs domaines: traitement d'image, radar, astronomie, etc.

Dans la littérature, il y a trois approches principales pour obtenir le SSR :

(i) La première approche est basée sur la précision de l'estimation. Dans ce cas, on peut distinguer deux critères. Le premier critère introduit par Lee dans [Lee92] s'écrit de la manière suivante : *deux signaux sont résolus en fonction des paramètres d'intérêt θ_1 et θ_2, si l'écart-type de θ_1 et θ_2 est inférieur à la différence entre θ_1 et θ_2*. On peut trouver que le critère de Lee ignore le couplage entre les paramètres d'intérêt [EBRM10]. Pour tenir compte de cet effet, Smith a proposé le critère suivant [Smi05]: *Deux signaux sont résolus si la séparation entre les deux paramètres d'intérêt θ_1 et θ_2 est inférieure à l'écart-type de l'estimation de la séparation.* Par

conséquent, la SSR selon le critère de Smith est défini comme la séparation entre les paramètres d'intérêt θ_1 et θ_2, qui est égale à l'écart-type de la séparation des paramètres. Dans [EBRM10], l'extension de la SSR basée sur le critère de Smith était présentée pour le contexte de plusieurs paramètres par signal.

(ii) La deuxième approche est basée sur le concept de la moyenne de la valeur du pseudo-spectre [Cox73, SD95, AD08] et elle est pertinente seulement pour les algorithmes à haute résolution. Dans ce contexte, le critère de Cox [Cox73] spécifie que les deux sources sont résolues (en fonction d'un algorithme d'estimation à haute résolution considéré) si les moyennes des valeurs du pseudo-spectre aux points θ_1 et θ_2 sont inférieures à la moyenne de la valeur du pseudo-spectre au point $\frac{\theta_1+\theta_2}{2}$.

(iii) La troisième approche est basée sur le test d'hypothèses binaire [AW08, LN07, SM04, SM06]. Plus particulièrement, on considère l'hypothèse $\mathcal{H}_0$ qui représente le cas où les deux sources de signaux sont combinées en une seule source (c'est à dire $\theta_1 - \theta_2 = 0$), tandis que l'hypothèse $\mathcal{H}_1$ représente le cas où les deux sources sont résolues (c'est à dire $\theta_1 - \theta_2 \neq 0$). De cette manière, dans [AW08] Amar et Weiss ont dérivé la SSR basée sur le critère de probabilité d'erreur minimale (PEM) pour des signaux déterministes. Les auteurs ont utilisé le premier ordre du développement en série Taylor de la PEM pour dériver la SSR. Alors que dans [LN07], Liu et Nehorai ont défini la SSR en utilisant l'équivalence asymptotique du test du rapport de vraisemblance généralisé (TRVG). Dans [SM04] Sharman et Milanfar ont dérivé la SSR dans le contexte d'analyse spectrale en utilisant le TRVG. En outre, il faut noter que dans la littérature, il y a un lien entre le test des hypothèses binaire et la distance de Kullback-Leiber (DKL) entre les densités de probabilité sous les hypothèses $\mathcal{H}_1$ et $\mathcal{H}_0$. Dans ce sens, dans [SM06], Sharman et Milanfar ont dérivé la SSR pour le contexte du traitement d'image utilisant le test d'hypothèses binaire et la DKL.

En traitement d'antenne, il y a deux modèles concernant les paramètres d'intérêt : le modèle Bayésien et le modèle déterministe. L'approche déterministe fournit la SSR pour des valeurs des paramètres déterminées, c'est à dire, elle considère la SSR locale en fonction du paramètre d'intérêt. Tandis que l'approche Bayésienne considère la SSR sur l'ensemble des paramètres. Ce dernier modèle était moins étudié dans la littérature. Nous nous somme intéressés ici à l'approche de la SSR dans le contexte Bayésien. Par conséquent, les paramètres des sources sont supposés aléatoires avec des distributions *a priori* connues. Par contre, l'hypothèse de multi paramètres aléatoires rend le problème plus complexe. Pourtant, puisque nous étudions seulement le contexte où les paramètres des sources sont proches, et où, ces paramètres sont de même nature (c'est à dire de même type de distribution), donc, sans perte de généralité, nous supposons que la moyenne de ces paramètres est aléatoire avec le même distribution des paramètres. Cette hypothèse était présentée partiellement dans [AW08].

Dans ce chapitre, nous considérons l'approche de la SSR dans le context Bayésien basé sur la théorie de l'information et de la détection, plus particulièrement, basé sur le lemme de Stein [CT91] et sur le critère de décision Neyman-Pearson.

- Premièrement, nous avons introduit le modèle des observations linéarisé basé sur le développement en série Taylor. Ce modèle utilise également le critère de la probabilité d'erreur minimale (PEM) qui permet de déterminer les valeurs optimales des paramètres sous hypothèse $\mathcal{H}_0$ où les deux sources sont assimilées comme une seule source.

- À partir du modèle présenté, nous avons dérivé les expressions analytiques de la DKL en théorie de l'information, et de la probabilité d'erreur retirée du critère de décision Neyman-Pearson en théorie de détection. Nous avons ensuite déduit les expressions analytiques de la SSR Bayésienne pour ces approches.

- Les résultats obtenus étaient comparés avec d'autres approches Bayésiennes déjà exitantes dans la littérature. En particulier, nous avons considéré la méthode présenté dans [AW08] et une méthode empirique qui est le critère d'information de Akaike (CIA). Nous avons établi les rapports de la SSR entre les méthodes, et nous avons trouvé que ces rapports ne dépendent seulement que du taux de succès, ce qui veut dire que la performance relative de ces méthodes est invariant pour tous les contextes.
- Finalement, les simulations ont montré que la SSR obtenue par les méthodes théoriques et les méthodes numériques sont très proches.

Formulation du probléme

On considère le problème du seuil statistique de résolution limite basé sur un test d'hypothèses binaire. Sous l'hypothèse $\mathcal{H}_0$, le récepteur détecte seulement une seule source qui est la combinaison de deux sources, et sous l'hypothèse $\mathcal{H}_1$, les deux sources sont résolues. Ce test d'hypothèses peut s'écrire comme suit [AW08]:

$$\begin{cases} \mathcal{H}_0: & \mathbf{z}(t) = \mathbf{a}(\hat{\theta}(t))\hat{s}(t) + \mathbf{n}(t), \\ \mathcal{H}_1: & \mathbf{z}(t) = \mathbf{a}(\theta_1)s_1(t) + \mathbf{a}(\theta_2)s_2(t) + \mathbf{n}(t), \end{cases} \tag{A.53}$$

où $t = 1 \dots T$, avec T représentant le nombre des observations. $\mathbf{z}(t)$ représente le vecteur des observations. $\mathbf{a}(\theta)$ représente le vecteur directionnel de taille $N \times 1$, et sans perte de généralité, on suppose que $\|\mathbf{a}(\theta)\|^2 = N$. θ_i représente le paramètre d'intérêt de la $i^{ième}$ source tel que l'angle d'arrivée, la fréquence, etc. $s_i(t)$ représente l'amplitude du signal de la $i^{ième}$ source sous l'hypothèse $\mathcal{H}_1$. $\hat{s}(t)$ et $\hat{\theta}(t)$ représentent l'amplitude du signal et le paramètre d'intérêt sous $\mathcal{H}_0$, qui sont des combinaisons des amplitudes des signaux et des paramètres d'intérêt sous $\mathcal{H}_1$. Les signaux sources sont supposés déterministes et connus par le récepteur. Le vecteur $\mathbf{n}$ représente un bruit Gaussien de moyenne nulle et de matrice de covariance $\sigma^2\mathbf{I}$.

Principe des tests d'hypothèses à PEM

La probabilité d'erreur P_e est donnée par $P_e = p(\mathcal{H}_0)P_{fa} + p(\mathcal{H}_1)P_{nd} = 1 - \varpi$, où P_{fa}, P_{nd}, $p(\mathcal{H}_0)$, $p(\mathcal{H}_1)$ et ϖ représentent la probabilité de fausse alarme, la probabilité de non-détection, la probabilité *a priori* sous $\mathcal{H}_0$, la probabilité *a priori* sous $\mathcal{H}_1$ et le taux de succès, respectivement. Sans perte de généralité, on suppose que $p(\mathcal{H}_0) = p(\mathcal{H}_1) = 1/2$. On définit $\theta_c = \frac{\theta_1+\theta_2}{2}$. La SSR est donnée par $\delta = \theta_2 - \theta_1$. On suppose que θ_c est aléatoire avec une certaine distribution *a priori* notée $p(\theta_c)$. Les valeurs de $\hat{\theta}(t)$, et $\hat{s}(t)$ qui vérifient le principe de probabilité d'erreur minimale (PEM) sont données par [AW08] :

$$\hat{\theta}(t) = \theta_c + \gamma(t)\delta, \tag{A.54}$$

et

$$\hat{s}(t) = \frac{1}{N}\mathbf{a}^H(\hat{\theta}(t)) \left(\mathbf{a}(\theta_c - \frac{\delta}{2})s_1(t) + \mathbf{a}(\theta_c + \frac{\delta}{2})s_2(t) \right), \tag{A.55}$$

où on a défini

$$\gamma(t) = \frac{|s_2(t)|^2 - |s_1(t)|^2}{2\left(|s_2(t)|^2 + |s_1(t)|^2 + 2\Re\left\{s_1^*(t)s_2(t)\right\}\right)}. \tag{A.56}$$

Ainsi, les observations suivent une loi $\mathbb{C}\mathcal{N}(\boldsymbol{\mu}_i(t), \sigma^2\mathbf{I})$ avec

$$\begin{cases} \mathcal{H}_0: & \boldsymbol{\mu}_0(t) = \mathbf{a}(\hat{\theta}(t))\hat{s}(t), \\ \mathcal{H}_1: & \boldsymbol{\mu}_1(t) = \sum_{k=1}^{2} \mathbf{a}(\theta_k)s_k(t). \end{cases} \tag{A.57}$$

Par conséquent, les fonctions de distribution de probabilité sous $\mathcal{H}_0$ et $\mathcal{H}_1$ sont données par :

$$p(\mathbf{z};\mathcal{H}_0,\theta_c) = \frac{1}{(\pi\sigma^2)^{NT}} \exp\left(-\frac{1}{\sigma^2}\sum_{t=1}^{T}\|\mathbf{z}(t)-\boldsymbol{\mu}_0(t)\|^2\right), \tag{A.58}$$

$$p(\mathbf{z};\mathcal{H}_1,\theta_c) = \frac{1}{(\pi\sigma^2)^{NT}} \exp\left(-\frac{1}{\sigma^2}\sum_{t=1}^{T}\|\mathbf{z}(t)-\boldsymbol{\mu}_1(t)\|^2\right). \tag{A.59}$$

où $\mathbf{z} = \left[\mathbf{z}(1)^T \dots \mathbf{z}(T)^T\right]^T$.

Formulation du test d'hypothèses

Le développement en série de Taylor des vecteurs directionnels au voisinage du point θ_c est donné par:

$$\begin{aligned}
\mathbf{a}(\theta_1) &= \mathbf{a}(\theta_c) - \frac{\delta}{2}\dot{\mathbf{a}}(\theta_c) \ \text{ avec } \theta_1 = \theta_c - \tfrac{\delta}{2},\\
\mathbf{a}(\theta_2) &= \mathbf{a}(\theta_c) + \frac{\delta}{2}\dot{\mathbf{a}}(\theta_c) \ \text{ avec } \theta_2 = \theta_c + \tfrac{\delta}{2},\\
\mathbf{a}(\hat{\theta}(t)) &= \mathbf{a}(\theta_c) + \gamma(t)\delta\dot{\mathbf{a}}(\theta_c) \ \text{ avec } \hat{\theta}(t) = \theta_c + \gamma(t)\delta,
\end{aligned}$$

où la dérivation du premier ordre en fonction de θ_c du vecteur $\mathbf{a}(\theta_c)$ est donnée par $\dot{\mathbf{a}}(\theta_c)$. Ainsi, en utilisant (A.54) on obtient

$$\hat{s}(t) \cong p(t) + \frac{\delta}{2N}\kappa_c m(t), \tag{A.60}$$

où

$$p(t) = s_1(t) + s_2(t) \tag{A.61}$$

$$\kappa_c = \mathbf{a}^H(\theta_c)\dot{\mathbf{a}}(\theta_c), \tag{A.62}$$

$$\mathbf{m} = [m(1)\dots m(T)]^T = \mathbf{V}^T\mathbf{s}, \tag{A.63}$$

et où

$$\mathbf{s} = [s_1(1)\ s_2(1)\dots s_1(T)\ s_2(T)]^T$$

et

$$\mathbf{V} = \mathrm{Bdiag}\{\mathbf{v}(1),\dots,\mathbf{v}(T)\}$$

avec $\mathbf{v}(t) = [\gamma(t)+\frac{1}{2}\ \ \gamma(t)-\frac{1}{2}]^T$. On trouve que la valeur optimale du signal source $\hat{s}(t)$ est une approximation par une combinaison des sources $s_1(t)$ et $s_2(t)$. Par conséquent, en utilisant les expressions ci-dessus, le développement en série Taylor des moyennes sous $\mathcal{H}_0$ et $\mathcal{H}_1$ est donné par

$$\boldsymbol{\mu}_0(t) = \mathbf{a}(\hat{\theta}(t))\hat{s}(t) \cong \delta\boldsymbol{\nu}_0(t), \tag{A.64}$$

$$\boldsymbol{\mu}_1(t) = \sum_{k=1}^{2}\mathbf{a}(\theta_k)s_k(t) \cong \delta\boldsymbol{\nu}_1(t), \tag{A.65}$$

où

$$\boldsymbol{\nu}_0(t) = p(t)\gamma(t)\dot{\mathbf{a}}(\theta_c) + \left(\frac{\kappa_c m(t)}{2N}\right)\mathbf{a}(\theta_c), \tag{A.66}$$

$$\boldsymbol{\nu}_1(t) = \frac{q(t)}{2}\dot{\mathbf{a}}(\theta_c), \tag{A.67}$$

avec $q(t) = s_2(t) - s_1(t)$. Donc, le test d'hypothèses linéarisé est donné par

$$\begin{cases} \mathcal{H}_0 : & \mathbf{z} \cong \delta\boldsymbol{\nu}_0 + \mathbf{n}, \\ \mathcal{H}_1 : & \mathbf{z} \cong \delta\boldsymbol{\nu}_1 + \mathbf{n}, \end{cases} \tag{A.68}$$

où $\mathbf{n} = [\mathbf{n}(1)^T \dots \mathbf{n}(T)^T]^T$, $\boldsymbol{\nu}_0 = \left[\boldsymbol{\nu}_0^T(1) \dots \boldsymbol{\nu}_0^T(T)\right]^T$ et $\boldsymbol{\nu}_1 = \left[\boldsymbol{\nu}_1^T(1) \dots \boldsymbol{\nu}_1^T(T)\right]^T$.

SSR basée sur la théorie de l'information

Le lemme de Stein [CT91] stipule que pour une P_d maximisée et pour une $P_{fa} \leq \epsilon$ avec ϵ tendant lentement vers zéro, on a

$$\lim_{TN\to\infty} \ln P_{fa} = -\mathcal{D}(p(\mathbf{z}, \theta_c; \mathcal{H}_1) \| p(\mathbf{z}, \theta_c; \mathcal{H}_0)), \tag{A.69}$$

où $\mathcal{D}(p(\mathbf{z}, \theta_c; \mathcal{H}_1) \| p(\mathbf{y}, \theta_c; \mathcal{H}_0))$ désigne l'entropie relative entre deux distributions Gaussiennes à moyennes paramétrées, donnée par

$$\begin{aligned} \mathcal{D}(p(\mathbf{z}, \theta_c; \mathcal{H}_1) \| p(\mathbf{z}, \theta_c; \mathcal{H}_0)) &= \int_\Theta \int_\Omega p(\mathbf{z}, \theta_c; \mathcal{H}_1) \ln \left(\frac{p(\mathbf{z}, \theta_c; \mathcal{H}_1)}{p(\mathbf{z}, \theta_c; \mathcal{H}_0)} \right) d\mathbf{z} d\theta_c \\ &= \int_\Theta \frac{\delta^2}{\sigma^2} \sum_{t=1}^{T} \|\boldsymbol{\nu}_0(t) - \boldsymbol{\nu}_1(t)\|^2 \, p(\theta_c) d\theta_c \\ &= \mathbb{E}\left\{ \frac{\delta^2 ||\mathbf{m}||^2}{\sigma^2} \left\| \frac{\kappa_c}{N} \mathbf{a}(\theta_c) - \dot{\mathbf{a}}(\theta_c) \right\|^2 \right\} \\ &= \mathbb{E}\left\{ \frac{\delta^2 \|\mathbf{m}\|^2 \|\dot{\mathbf{a}}(\theta_c)\|^2}{\sigma^2} \cos^2(\Upsilon) \right\} \end{aligned} \tag{A.70}$$

où Θ et Ω représentent l'espace des paramètres et l'espace des observations et $\mathbb{E}$ représente l'opérateur d'espérance en fonction du paramètre θ_c. Υ représente l'angle canonique maximal entre $\mathbf{a}(\theta_c)$ et $\dot{\mathbf{a}}(\theta_c)$. Il est important de noter que l'entropie relative peut être approximée par une expression quadratique en δ. De plus, l'entropie relative est une fonction de la forme d'onde des signaux sources, de la distribution du réseau, de la variance du bruit et de la quantité géométrique que représente l'angle entre le vecteur directionnel et sa dérivée au premier ordre.

Pour une P_d maximale, $P_{fa} \approx 2P_e = 2(1 - \varpi)$, et donc, l'expression analytique de la SSR est donnée par

$$\delta \cong \frac{-\sigma\sqrt{\log(2) + \log(1 - \varpi)}}{\mathbb{E}\left\{ \|\mathbf{m}\| \, \|\dot{\mathbf{a}}(\theta_c)\| \cos(\Upsilon) \right\}} \tag{A.71}$$

où $\varpi > 1/2$, $\mu = \sqrt{\mathbf{s}^H \mathbf{V}\mathbf{V}^T \mathbf{s}}$, $\mathbf{V}\mathbf{V}^T = \text{Bdiag}\{\mathbf{G}(1) \dots \mathbf{G}(T)\}$ et $\mathbf{G}(t) = \begin{bmatrix} \left(\gamma(t) + \frac{1}{2}\right)^2 & \gamma^2(t) + \frac{1}{4} \\ \gamma^2(t) + \frac{1}{4} & \left(\gamma(t) - \frac{1}{2}\right)^2 \end{bmatrix}$.

SSR basée sur la théorie de la détection

Dans cette partie, on calcule la SSR basée sur la théorie de la détection, en particulier, basée sur le critère de Neyman-Pearson qui minimise la probabilité d'erreur P_e dans le contexte Bayésien (BNP).

On pose

$$\mathbf{z}' = \frac{\mathbf{z}}{\delta} - \boldsymbol{\nu}_0. \tag{A.72}$$

Par conséquent, en substituant (A.72) dans (A.68), on obtient :

$$\begin{cases} \mathcal{H}_0 : & \mathbf{z}' \cong \mathbf{n}', \\ \mathcal{H}_1 : & \mathbf{z}' \cong \boldsymbol{\zeta} + \mathbf{n}', \end{cases} \tag{A.73}$$

où $\boldsymbol{\zeta} = \boldsymbol{\nu}_1 - \boldsymbol{\nu}_0$ et $\mathbf{n}' \sim \mathbb{C}\mathcal{N}(\mathbf{0}, \frac{\sigma^2}{\delta^2}\mathbf{I})$. Par conséquent, on a

$$G_{NP}(\mathbf{z}') = \frac{p(\mathbf{z}'; \mathcal{H}_1, \theta_c)}{p(\mathbf{z}'; \mathcal{H}_0, \theta_c)} \underset{\mathcal{H}_0}{\overset{\mathcal{H}_1}{\gtrless}} \tau' = \frac{p(\mathcal{H}_0)}{p(\mathcal{H}_1)}, \tag{A.74}$$

posant $T_{NP}(\mathbf{z}') = \ln\left(G_{NP}(\mathbf{z}')\right)$ et $\tau = \ln(\tau')$, le test statistique est alors donné par

$$\begin{aligned} T_{NP}(\mathbf{z}') &= \ln\left(\frac{p(\mathbf{z}'; \mathcal{H}_1, \theta_c)}{p(\mathbf{z}'; \mathcal{H}_0, \theta_c)}\right) = \frac{\delta^2}{\sigma^2}\left(\left\|\mathbf{z}' - \boldsymbol{\zeta}\right\|^2 - \left\|\mathbf{z}'\right\|^2\right) \\ &= \frac{\delta^2}{\sigma^2}\left(\|\boldsymbol{\zeta}\|^2 - 2\Re\left\{\mathbf{a}^H\mathbf{z}'\right\}\right) \underset{\mathcal{H}_0}{\overset{\mathcal{H}_1}{\gtrless}} \tau. \end{aligned} \tag{A.75}$$

Puisqu'on a supposé que $p(\mathcal{H}_0) = p(\mathcal{H}_1) = 1/2$, on déduit

$$\begin{cases} \mathcal{H}_0 : & T_{NP}(\mathbf{z}') > 0, \\ \mathcal{H}_1 : & T_{NP}(\mathbf{z}') < 0. \end{cases} \tag{A.76}$$

En posant $L(\mathbf{z}') = \Re\left\{\boldsymbol{\zeta}^H\mathbf{z}'\right\}$, on obtient

$$\begin{cases} \mathcal{H}_0 : & L(\mathbf{z}') \sim \mathcal{N}(0, \varrho^2), \\ \mathcal{H}_1 : & L(\mathbf{z}') \sim \mathcal{N}(\|\boldsymbol{\zeta}\|^2, \varrho^2), \end{cases} \tag{A.77}$$

où

$$\varrho^2 = \frac{\sigma^2\|\boldsymbol{\zeta}\|^2}{2\delta^2}.$$

Donc, la probabilité d'erreur conditionnelle est donnée par [Kay98]:

$$P_e(\delta; \theta_c) = \frac{1}{2}\left(\left(1 - Q\left(\frac{-\|\boldsymbol{\zeta}\|^2}{2\sqrt{\varrho^2}}\right)\right) + Q\left(\frac{\|\boldsymbol{\zeta}\|^2}{2\sqrt{\varrho^2}}\right)\right), \tag{A.78}$$

où $Q(.)$ représente la surface de la queue de distribution à droite de la loi normale de moyenne nulle et de variance unité. Puisque $Q\left(\frac{-\|\boldsymbol{\zeta}\|^2}{2\sqrt{\varrho^2}}\right) = 1 - Q\left(\frac{\|\boldsymbol{\zeta}\|^2}{2\sqrt{\varrho^2}}\right)$, donc, on aura

$$P_e(\delta; \theta_c) = Q\left(\frac{\|\boldsymbol{\zeta}\|^2}{\sqrt{4\varrho^2}}\right). \tag{A.79}$$

Puisque la probabilité d'erreur marginale est :

$$P_e(\delta) = \int_{\Theta} P_e(\delta; \theta_c)p(\theta_c)d\theta_c = \mathbb{E}\left\{P_e(\delta; \theta_c)\right\}, \tag{A.80}$$

par conséquent, la SSR basée sur le critère NP est donnée par :

$$\delta \cong \frac{\sigma\sqrt{2}Q^{-1}(1 - \varpi)}{\mathbb{E}\left\{\|\mathbf{m}\|\,\|\dot{\mathbf{a}}(\theta_c)\|\cos(\Upsilon)\right\}} \tag{A.81}$$

où $Q^{-1}(.)$ représente la fonction Q inverse.

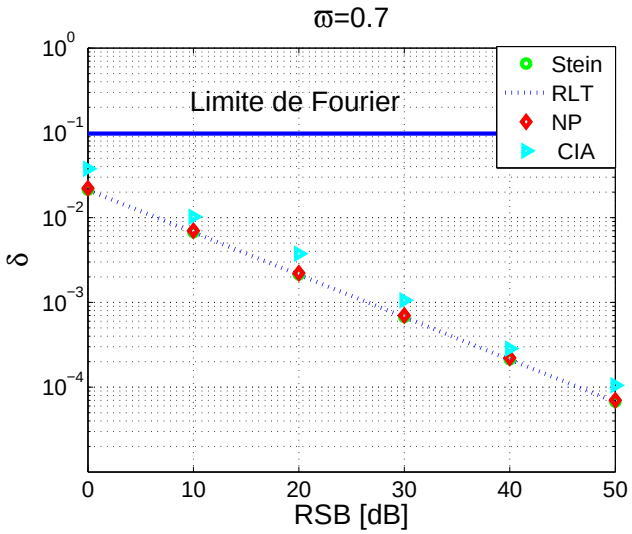

Figure A.6: SSR en fonction de RSB pour $\varpi = 0.7$.

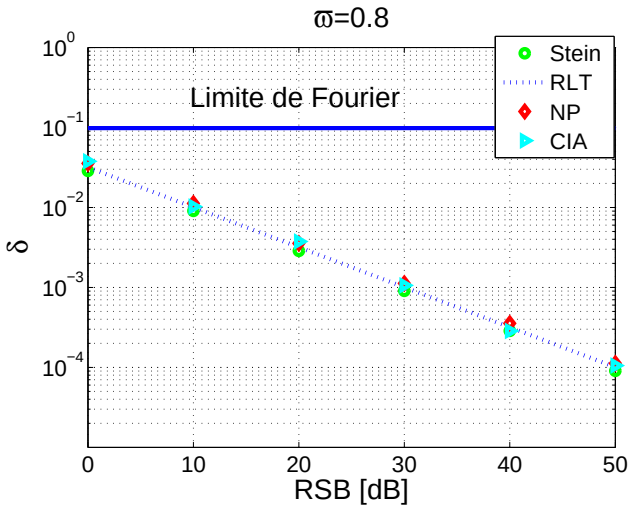

Figure A.7: SSR en fonction de RSB pour $\varpi = 0.8$.

Simulations

On considère le contexte d'analyse spectrale avec $T = 1$. Le vecteur $\mathbf{a}(\theta)$ a pour forme :

$$\mathbf{a}(\theta) = \left[1, e^{j\theta}, \ldots, e^{j(N-1)\theta}\right]^T,$$

où $N = 64$. Le rapport signal à bruit RSB est donné par $RSB = \frac{\left(\sum_{k=1}^{2} \|\mathbf{s}_k\|^2\right)}{(2T\sigma^2)}$. La valeur du taux de succès ϖ est prise dans l'intervalle $(0.5; 1]$. La valeur normalisée de la moyenne de la fréquence centrale θ_c est supposée uniforme aléatoire dans l'intervalle $[0; 1]$. On compare les deux méthodes présentées précédemment avec le méthode Bayésienne RLT [AW08] et avec la méthode numérique CIA [SSS95]. L'approche CIA est obtenue avec 200 tirages Monte Carlo et il faut

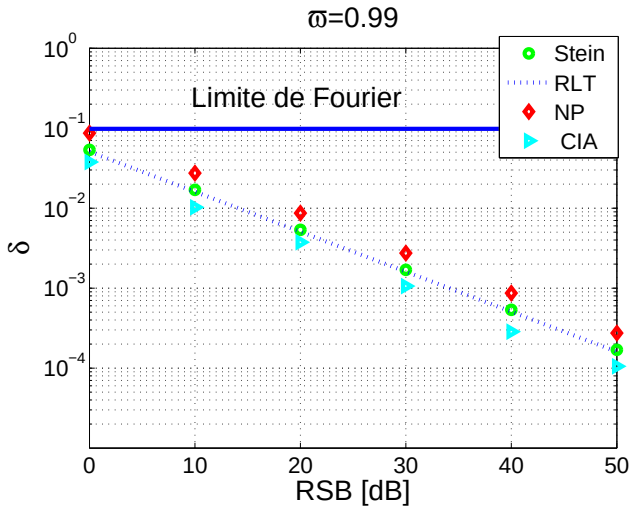

Figure A.8: SSR en fonction de RSB pour $\varpi = 0.99$.

noter que cette approche numérique est indépendante du taux de succès. Les Fig. (A.6), (A.7) et (A.8) montrent la SSR des approches en fonction du RSB pour des valeurs différentes de ϖ. La limite de Fourier est donnée par la séparation $\delta_F = 2\pi/(TN)$, en dessous de laquelle, les méthodes de faible résolution telles que le périodogramme ne peuvent pas résoudre les sources. On peut remarquer que les SSR en fonction du RSB au sens du lemme de Stein, du NP, d'Amar et Weiss [AW08] et même du CIA [SSS95] empirique sont très proches.

A.5 Conclusion et perspectives

L'objectif principal de cette thèse concerne le positionnement optimal des capteurs dans un réseau dans le contexte de la localisation de sources. Nous avons étudié les deux approches pour évaluer l'impact de la géométrie des réseaux de capteurs sur l'estimation de la DDA: l'approche basée sur les performances d'estimation et l'approche basée sur le seuil statistique de la résolution. Pour la première approche, deux types des bornes inférieures de l'EQM ont été étudiées: la borne de Cramér-Rao et la borne de Weiss-Weinstein. Pour la deuxième approche, nous avons considéré le test des hypothèses binaire pour caractériser le SSR. En outre, plusieurs modèles des paramètres et modèles des observations ont été étudiés. En particulier, concernant le modèle des paramètres, le modèle Bayésien qui suppose que les paramètres d'intérêt sont aléatoires, et le modèle des paramètres déterministes qui suppose que les paramètres sont déterministes. Concernant les modèles des observations, le modèle stochastique suppose que les signaux des sources sont aléatoires, tandis que le modèle déterministe suppose que les signaux sont déterministes.

Les contributions de cette thèse ont été présentées dans trois chapitres.

Dans le chapitre 2, nous avons considéré le positionnement optimal des capteurs dans un réseau basé sur les performance d'estimation pour le modèle des paramètres déterministe. Nous avons dérivé des expressions analytiques de la borne de Cramér-Rao pour les modèles des observations stochastique et déterministe. Ces expressions analytiques ont ensuite été utilisées pour étudier l'impact de la géométrie des réseaux de capteurs sur les performances d'estimation. En particulier, dans ce chapitre, nous avons considéré la géométrie 3D. Par rapport à la géométrie planaire classique, la géométrie 3D est moins étudiée dans la littérature, à cause de sa complexité. Nous avons étudié plusieurs types de réseaux de capteurs 3D constitués par des réseaux linéaires,

et les conditions d'isotropie et de découplage des réseaux ont été ensuite dérivées. À partir de ces conditions, nous avons trouvé que pour les modèles stochastique et déterministe, ces conditions ne sont pas les mêmes.

Dans le chapitre 3, le positionnement optimal des capteurs dans un réseau basé sur les performances d'estimation et pour le scénario Bayésien a été considéré. La borne de Weiss-Weinstein qui est la borne la plus précise dans la famille de Weiss-Weinstein a été étudiée avec les modèles déterministe et stochastique. Dans la littérature, la BWW a été moins étudiée à cause de sa complexité. Pour cette raison, la BWW a été seulement étudiée par simulation. Dans ce chapitre, nous avons calculé les expressions analytiques de la BWW pour un modèle d'observation Gaussien général à moyenne ou à covariance paramétrée. Bien que l'objectif principal de cette thèse est d'introduire la BWW comme un outil statistique pour étudier le traitement d'antenne, les expressions analytiques de la BWW que nous avons proposées peuvent-être appliquées également pour d'autres problèmes.

Dans le chapitre 4, nous avons considéré le problème du seuil statistique de résolution. Il y a plusieurs approches pour la SSR dans la littérature, mais la plupart des approches sont conduites dans le contexte de paramètres déterministes. Nous avons introduit, dans ce chapitre, le modèle Bayésien pour le problème de la SSR, où la moyenne des paramètres est supposée aléatoire avec une certaine distribution *a priori*. Les deux approches Bayésiennes basées sur la théorie de l'information et sur la théorie de la détection ont été introduites. Les résultats ont été ensuite comparés avec d'autres méthodes Bayésiennes et empiriques. Les simulations ont montré que les performances des méthodes théoriques et numériques sont très proches.

Les perspectives de cette thèse sont multiples:

- Les expressions analytiques de la BCR peuvent être utilisées pour étudier les réseaux lacunaires 3D. Par rapport aux réseaux classiques, les réseaux lacunaires peuvent atteindre les mêmes performances avec moins de capteurs.

- L'impact de la géométrie des réseaux de capteurs sur le problème d'ambiguïté peut être étudié en utilisant la géométrie différentielle.

- La SSR peut être étudiée par l'approche de la précision de l'estimation en utilisant la BCR. Cependant, la BCR est valable seulement dans le zone asymptotique. Par conséquent, les expressions analytiques de la BWW seront utiles pour considérer la SSR dans la zone non-asymptotique.

- La valeur optimale de la BWW est obtenue par l'optimisation sur l'ensemble des paramètres s. Dans le chapitre 3, nous avons montré que la valeur $s = 1/2$, qui est généralement utilisé dans la littérature pour simplifier les calculs, a donné la BWW optimale. Pour cette raison, chercher les conditions pour les quelles, $s = 1/2$ donnent la BWW optimale sera une perspective de cette thèse.

- Cette thèse n'a considéré que les modèles Gaussiens. Il est donc intéressant d'étudier les contextes non-Gaussiens tels que les distributions Gaussiennes composées.

Notations

Acronyms

- **ULA**: uniform linear array.
- **UCA**: uniform circular array.
- **UAA**: uniform angular array.
- **DOA**: direction of arrival.
- **CRB**: Cramér-Rao bound.
- **WWB**: Weiss-Weinstein bound.
- **MSE**: mean square error.
- **FIM**: Fisher information matrix.
- **SNR**: signal to noise ratio.
- **SRL**: statistical resolution limit.

General mathematical symbols

- $\mathbb{C}$ indicates the complex field.
- $\mathbb{R}$ indicates the real field.
- $\Re\{z\}$ indicates the real part of a complex number z.
- $\Im\{z\}$ indicates the imaginary part of a complex number z.
- The symbol * indicate the conjugate operator.

Matrix operators and symbols

- a, A, italic indicates a scalar quantity.
- $\mathbf{a}$, bold lower case indicates a vector.

- $\mathbf{A}$, bold upper case indicates a matrix.
- $\mathbf{A}^T$ is the transpose of $\mathbf{A}$.
- $\mathbf{A}^H$ is the transpose, and conjugate of $\mathbf{A}$.
- $\mathbf{I}_N$ denotes the $N \times N$ identity matrix.
- $|\mathbf{A}|$ indicates the matrix determinant.
- $\|.\|$ indicates the norm of a vector, or a complex scalar.
- $A_{i,j}$ denotes the element at the i^{th} row and j^{th} column of the matrix $\mathbf{A}$.
- $\otimes$ denotes the Kronecker product.

Relative symbols for probability

- $\mathcal{N}(\mathbf{m}, \mathbf{C})$ indicates a multivariate Gaussian law with $\mathbf{m}$ mean and $\mathbf{C}$ covariance matrix.
- $\Pr(.)$ indique une probabilité.
- $p(x)$ indicates a density distribution function.
- $p(x, y)$ indicates a joint density distribution function.
- $p(x|\, y)$ indicates a conditional density distribution function.
- $\mathbb{E}[.]$ indicates an expectation operator.
- $\mathbb{E}_{\mathbf{y},\theta}[.]$ indicates an expectation operator *w.r.t.* the joint distribution $p(\mathbf{y},\theta)$.
- $\mathbb{E}_{\mathbf{y}|\theta}[.]$ indicates an expectation operator *w.r.t.* the conditional distribution $p(\mathbf{y}|\,\theta)$.

List of Figures

List of Tables

Bibliography

[AD08] H. Abeida and J.-P. Delmas. Statistical performance of MUSIC-like algorithms in resolving noncircular sources. *IEEE Trans. Signal Processing*, 56(6):4317–4329, September 2008.

[Ath01] F. Athley. Optimization of element positions for direction finding with sparse arrays. In *Proc. IEEE Work. on Statistical Signal Processing*, volume 1, pages 516–519, 2001.

[AW08] A. Amar and A. J. Weiss. Fundamental limitations on the resolution of deterministic signals. *IEEE Trans. Signal Processing*, 56(11):5309–5318, November 2008.

[BE08] Z. Ben Haim and Y.C. Eldar. A comment on the Weiss-Weinstein bound for constrained parameter sets. 54(10):4682–4684, October 2008.

[BEV96a] K. L. Bell, Y. Ephraim, and H. L. Van Trees. Explicit Ziv-Zakaï lower bound for bearing estimation. 44(11):2810–2824, November 1996.

[BEV96b] K. L. Bell, Y. Ephraim, and H. L. Van Trees. Explicit Ziv-Zakaï lower bounds for bearing estimation using planar arrays. Lexington, MA, USA, March 1996. MIT Lincoln Laboratory.

[BM03] U. Baysal and R. L. Moses. On the geometry of isotropic arrays. *IEEE Trans. Signal Processing*, 51(6):1469–1477, June 2003.

[Bos94] A. Van Den Bos. A Cramer Rao lower bound for complex parameters. *IEEE Trans. Acoust., Speech, Signal Processing*, 42:2859, October 1994.

[Cho04a] Y. H. Choi. Unified approach to Cramer-Rao bounds in direction estimation with known signal structures. *Signal Processing*, 84(10):1875 – 1882, 2004.

[Cho04b] Y. H. Choi. Unified approach to Cramér-Rao bounds in direction estimation with known signal structures. 84(10):1875–1882, October 2004.

[CM97] M. Cedervall and R. L. Moses. Efficient maximum likelihood DOA estimation for signals with known waveforms in presence of multipath. *IEEE Trans. Signal Processing*, 45:808–811, March 1997.

[Cox73] H. Cox. Resolving power and sensitivity to mismatch of optimum array processors. *J. Acoust. Soc. Am*, 54(3):771–785, 1973.

[CT91] T.M. Cover and J. A. Thomas. *Elements of information theory*. Wiley, New York, 1991.

[EBRM12] M. N. El Korso, R. Boyer, A. Renaux, and S. Marcos. Statistical resolution limit for the multidimensional harmonic retrieval model: Hypothesis test and Cramér-Rao bound approaches. *EURASIP Journal on Advances in Signal Processing 2011*, 2011:12.

[EBRM10] M. N. El Korso, R. Boyer, A. Renaux, and S. Marcos. Statistical resolution limits for multiple parameters of interest and for multiple signals. In *Proc. IEEE Int. Conf. Acoust., Speech, Signal Processing*, pages 3602 – 3605, Dallas, TX, USA, March 2010.

[FC09] A. Ferréol and P. Chevalier. High resolution direction finding: from performance toward antenna array optimization -the mono-source case. In *Proc. European Signal Processing Conference*, pages 1973–1977, Glasgow, Scotland, August 2009.

[FT08] T. Filik and T. E. Tuncer. Uniform and nonuniform V-shaped isotropic planar arrays. In *Proc. IEEE Sensor Array and Multichannel Signal Processing Workshop*, pages 99–103, Darmstadt, Germany, July 2008.

[GAM09] H. Gazzah and K. Abed-Meraim. Optimum ambiguity free directional and omni directional planar antenna arrays for DOA estimation. *IEEE Trans. Signal Processing*, 57(10):3942–3953, October 2009.

[GC81] L. C. Godara and A. Cantoni. Uniqueness and linear independence of sterring vectors in array space. *J. Acoust. Soc. Amer.*, 70(2):467– 475, August 1981.

[GM06] H. Gazzah and S. Marcos. Cramér-Rao bounds for antenna array design. *IEEE Trans. Signal Processing*, 54(1):336–345, January 2006.

[GW91] M. Gavish and A. J. Weiss. Array geometry for ambiguity resolution in direction finding. *IEEE Trans. Antennas Propagat.*, 44(6):143– 146, February 1991.

[HRW91] X. Huang, J. P. Reilly, and M. Wong. Optimal design of linear array of sensors. In *Proc. IEEE Int. Conf. Acoust., Speech, Signal Processing*, volume 2, pages 1405–1408, Toronto, Ont., Canada, May 1991.

[HS91] Y. Hua and T. K. Sarkar. A note on the Cramér-Rao bound for 2-D direction finding based on 2-D array. *IEEE Trans. Signal Processing*, 39(5):1215– 1218, May 1991.

[HSW91] Y. Hua, T. K. Sarkar, and D. D. Weiner. An L-shaped array for estimating 2D directions of wave arrival. *IEEE Trans. Antennas Propagat.*, 39:143– 146, February 1991.

[Kay88] S. M. Kay. *Modern Spectral Estimation*. Prentice Hall, Englewood Cliffs, NJ, 1988.

[Kay93] S. M. Kay. *Fundamentals of Statistical Signal Processing*, volume 1. Prentice Hall, NJ, 1993.

[Kay98] S. M. Kay. *Fundamentals of Statistical Signal Processing*, volume 2. Prentice Hall, NJ, 1998.

[KV96] H. Krim and M. Viberg. Two decades of array signal processing research: the parametric approach. *IEEE Signal Processing Mag.*, 13(4):67–94, 1996.

[LC93] J. Li and R. T. Compton. Maximum likelihood angle estimation for signals with known waveforms. *IEEE Trans. Signal Processing*, 41:2850–2862, September 1993.

[Lee92] H. B. Lee. The Cramér-Rao bound on frequency estimates of signals closely spaced in frequency. *IEEE Trans. Signal Processing*, 40(6):1508–1517, June 1992.

[LHSV95] J. Li, B. Halder, P. Stoica, and M. Viberg. Computationally efficient angle estimation for signals with known waveforms. *IEEE Trans. Signal Processing*, 43:2154–2163, September 1995.

[LJ92] J. T. H. Lo and S. L. Marple. Jr. Observability conditions for multiple signal direction finding and array sensor localization. *IEEE Trans. Signal Processing*, 40(11):2641– 2650, November 1992.

[LN07] Z. Liu and A. Nehorai. Statistical angular resolution limit for point sources. *IEEE Trans. Signal Processing*, 55(11):5521–5527, November 2007.

[LRNM10] P. S. La Rosa, A. Renaux, A. Nehorai, and C. H. Muravchik. Barankin-type lower bound on multiple change-point estimation. 58(11):5534–5549, November 2010.

[LS09] K. W. K. Lui and H. C. So. A study of two-dmensional sensor placement using time-difference-of-arrival measurements. *Digital Signal Processing*, 19:650– 659, 2009.

[LvdV99] A. Leshem and A.-J. van der Veen. Direction-of-arrival estimation for constant modulus signals. *IEEE Trans. Signal Processing*, 47(11):3125 – 3129, November 1999.

[Man04] A. Manikas. *Differential Geometry in Array Processing.* Imperial College Press, 2004.

[Mof68] A. T. Moffet. Minimum redundancy linear arrays. *IEEE Trans. Antennas Propagat.*, 16:172–175, March 1968.

[MS91] A. Mirkin and L. H. Sibul. Cramér-Rao bounds on angle estimation with a two-dimensional array. *IEEE Trans. Signal Processing*, 39:515–517, February 1991.

[NH88] T. J. Nohara and S. Haykin. Application of the Weiss-Weinstein bound to a two dimensional antenna array. In *IEEE Trans. Acoust., Speech, Signal Processing*, volume 36, pages 1533–1534, September 1988.

[Nie94] R. O. Nielsen. Azimuth and elevation angle estimation with a three dimensional array. *IEEE J. Oceanic Eng.*, 19(1):84–86, January 1994.

[NV94] H. Nguyen and H. L. VanTrees. Comparison of performance bounds for DOA estimation. In *IEEE Seventh SP Workshop on Statistical Signal and Array Processing*, pages 313–316, 1994.

[OM05] U. Oktel and R. L. Moses. A Bayesian approach to array geometry design. *IEEE Trans. Signal Processing*, 53(5):1919– 1923, May 2005.

[OVSN93] B. Ottersten, M. Viberg, P. Stoica, and A. Nehorai. Exact and large sample maximum likelihood techniques for parameter estimation and detection in array processing. In S. Haykin, J. Litva, and T. J. Shepherd, editors, *Radar Array Processing*, chapter 4, pages 99–151. Springer-Verlag, Berlin, 1993.

[PF88] B. Porat and B. Friedlander. Analysis of the asymptotic relative efficiency of the MUSIC algorithm. *IEEE Trans. Acoust., Speech, Signal Processing*, 36(4):532–544, April 1988.

[RAFL07] A. Renaux, L. N. Atallah, P. Forster, and P. Larzabal. A useful form of the Abel bound and its application to estimator threshold prediction. 55(5, Part 2):2365–2369, May 2007.

[Ren07] A. Renaux. Weiss-Weinstein bound for data aided carrier estimation. *IEEE Signal Processing Lett.*, 14(4):283–286, April 2007.

[RFBL07] A. Renaux, P. Foster, E. Boyer, and P. Larzabal. Unconditional Maximum Likelihood performance at finite number of samples and high Signal-to-Noise Ratio. *IEEE Trans. Signal Processing*, 55(5):2358– 2364, May 2007.

[RFCL06] A. Renaux, P. Foster, E. Chaumette, and P. Larzabal. On the High-SNR Conditional Maximum-Likelihood estimator full statistical characterization. *IEEE Trans. Signal Processing*, 54(12):4840– 4843, December 2006.

[RFL+08] A. Renaux, P. Forster, P. Larzabal, C.D. Richmond, and A. Nehorai. A fresh look at the Bayesian bounds of the Weiss-Weinstein family. *IEEE Trans. Signal Processing*, 56(11):5334–5352, November 2008.

[RM95] I. Reuven and H. Messer. The use of the Barankin bound for determining the threshold SNR in estimating the bearing of a source in the presence of another. In *Proc. IEEE Int. Conf. Acoust., Speech, Signal Processing*, volume 3, pages 1645–1648, Detroit, USA, May 1995.

[RM97] I. Reuven and H. Messer. A Barankin-type lower bound on the estimation error of a hybrid parameter vector. *IEEE Trans. Inform. Theory*, 43(3):1084–1093, May 1997.

[SD95] K. Sharman and T. Durrani. Resolving power of signal subspace methods for fnite data lengths. In *Proc. IEEE Int. Conf. Acoust., Speech, Signal Processing*, pages 1501–1504, Florida, USA, 1995.

[SM04] M. Shahram and P. Milanfar. Imaging below the diffraction limit: A statistical analysis. *IEEE Trans. Image Processing*, 13(5):677–689, May 2004.

[SM05] P. Stoica and R.L. Moses. *Spectral Analysis of Signals*. Prentice Hall, NJ, 2005.

[SM06] M. Shahram and P. Milanfar. Statistical and information -theoric analysis of resolution in imaging. *IEEE Trans. Image Processing*, 52(8):3411–3437, August 2006.

[Smi05] S. T. Smith. Statistical resolution limits and the complexified Cramér-Rao bound. *IEEE Trans. Signal Processing*, 53(5):1597–1609, May 2005.

[SN89] P. Stoica and A. Nehorai. MUSIC, maximum likelihood and the Cramér-Rao bound. *IEEE Trans. Acoust., Speech, Signal Processing*, 37:720–741, May 1989.

[SN90a] P. Stoica and A. Nehorai. MUSIC, maximum likelihood and the Cramer Rao bound: further results and comparisons. *IEEE Trans. Acoust., Speech, Signal Processing*, 38:2140–2150, 1990.

[SN90b] P. Stoica and A. Nehorai. Performances study of conditional and unconditional direction of arrival estimation. *IEEE Trans. Acoust., Speech, Signal Processing*, 38:1783–1795, October 1990.

[SSL68] D. Sengupta, T. Smith, and R. Larson. Radiation characteristics of a spherical array of circularly polarized elements. *IEEE Trans. Antennas Propagat.*, 16(1):2–7, January 1968.

[SSS95] P. Stoica, V. Simonyte, and T. Soderstrom. On the resolution performance of spectral analysis. *Elsevier Signal Processing*, 44(2):153–161, January 1995.

[TGT96] K. C. Tan, S. S. Goh, and E. C. Tan. A study of the rank-ambiguilty issues in direction-of-arrival estimation. *IEEE Trans. Signal Processing*, 44(4):880– 887, April 1996.

[TK99] J. Tabrikian and J.L. Krolik. Barankin bounds for source localization in an uncertain ocean environment. *IEEE Trans. Signal Processing*, 47:2917–2927, November 1999.

[Van68] H. L. Van Trees. *Detection, Estimation and Modulation Theory*, volume 1. John Wiley & Sons, New-York, NY, USA, 1968.

[Van02a] H. L. Van Trees. *Detection, Estimation and Modulation theory: Optimum Array Processing*, volume 4. John Wiley & Sons, New-York, NY, USA, March 2002.

[Van02b] H. L. VanTrees. *Detection, Estimation and Modulation Theory: Optimum Array Processing*, volume 4. Wiley, New York, 2002.

[VB07] H. L. VanTrees and K. L. Bell. *Bayesian bounds for parameter estimation and nonlinear filtering/tracking*. Wiley, New York, 2007.

[VEB+11a] D. T. Vu, M. N. El Korso, R. Boyer, A. Renaux, and S. Marcos. Angular resolution limit for vector-sensor arrays: detection and information theory approaches. In *Proc. IEEE Work. on Statistical Signal Processing*, Nice, France, June 2011.

[VEB+11b] D. T. Vu, M. N. El Korso, R. Boyer, A. Renaux, and S. Marcos. Résolution limite angulaire : Appoches basées sur la théorie de l'information et sur la théorie de la détection. In *Proc. IEEE Work. on Statistical Signal Processing*, Bordeaux, France, September 2011.

[VEBM] D. T. Vu, M. N. El Korso, R. Boyer, and S. Marcos. Bayesian statistical resolution limit based on information and detection theories.

[VRB]

[VRBMa] D. T. Vu, A. Renaux, R. Boyer, and S. Marcos. Borne de Weiss-Weinstein pour la localisation de source polarisée l'aide d'un réseau de capteurs COLD. In *Proc. IEEE Work. on Statistical Signal Processing*, Bordeaux, France, September.

[VRBMb] D. T. Vu, A. Renaux, R. Boyer, and S. Marcos. A Cramér Rao bounds based analysis of 3d antenna array geometries made from ula branches. *Multidimensional Systems and Signal Processing*.

[VRBMc] D. T. Vu, A. Renaux, R. Boyer, and S. Marcos. Some results on the Weiss-Weinstein bound in array processing.

[VRBM10a] D. T. Vu, A. Renaux, R. Boyer, and S. Marcos. Closed-form expression of the Weiss-Weinstein bound for 3D source localization: the conditional case. In *Proc. IEEE Sensor Array and Multichannel Signal Processing Workshop*, Kibutz Ma'ale Hahamisha, Israel, October 2010.

[VRBM10b] D. T. Vu, A. Renaux, R. Boyer, and S. Marcos. Performance analysis of 2D and 3D antenna arrays for source localization. In *Proc. European Signal Processing Conference*, Aalborg, Denmark, August 2010.

[VRBM11] D. T. Vu, A. Renaux, R. Boyer, and S. Marcos. Wess-Weinstein bound and SNR threshold analysis for DOA estimation with a COLD array. In *Proc. IEEE Work. on Statistical Signal Processing*, Nice, France, June 2011.

[WW88] E. Weinstein and A. J. Weiss. A general class of lower bounds in parameter estimation. *IEEE Trans. Inform. Theory*, 34:338–342, March 1988.

[XBB04] W. Xu, A. B. Baggeroer, and K. Bell. A bound on mean-square estimation with background parameter mismatch. *IEEE Trans. Inform. Theory*, 50:621–632, April 2004.

[XBR04] W. Xu, A. B. Baggeroer, and C. D. Richmond. Bayesian bounds for matched-field parameter estimation. *IEEE Trans. Signal Processing*, 52:3293–3305, December 2004.

[YS05] B. Yang and J. Scheuing. Cramér-Rao bound and optimum sensor array for source localization from the differences of arrival. In *Proc. IEEE Int. Conf. Acoust., Speech, Signal Processing*, volume 4, pages 961–964, Philadenphia, USA, March 2005.